

**BRUNEL UNIVERSITY**

**The Mechanical and Resonant Behaviour of  
a Dry Coupled  
Thickness-Shear PZT Transducer used for  
Guided Wave Testing in Pipe Line**

by

**Bhavin Arun Engineer**

A thesis submitted to Brunel University for the degree of

**Doctor of Philosophy**

**School of Engineering and Design**

**September 2013**

## **Abstract**

The guided wave technique is an ultrasonic technique which is used to monitor large structures in a variety of industry sectors to safeguard against catastrophic failure. The guided wave technique for pipeline inspection has been commercially used since the early 2000s and this facilitates rapid inspection where from a single location over 100 metres of pipeline can be inspected. This technique is currently being used in pipeline infrastructure across the globe. For the technique to be successful it is highly dependent on a numerous of factors including, frequency selection, array designs and pipeline geometries. The transducers used on pipeline are dry coupled and the magnitude of the signal transmitted is dependent on the normal force applied to it. If this force is not controlled the signal being transmitted can degrade and lead to the difficult analysis of a complex signal. In this thesis studies have been undertaken to understand the relationship between dry force coupling of the transducer and the signal received, aligning this connection to classical contact theory. This is then further to extended to the influence surface contact conditions have on the transmission of signal from the transducer. Analysis of the results detected a peak in the operational frequency response which in turn initiated electrical impedance and structural resonance measurements to identify the presence of resonances which are induced by dry coupling. This behaviour was then modelled in FEA software and the validity of the FEA approach was tested against several prototype transducers. This thesis has been funded in joint collaboration between the Engineering Physics and Science Research Council and TWI ltd.

## Acknowledgements

First of all I would like to thank all mighty God for giving me the opportunity presented to me and the capability and intelligence needed to have reached this point. Secondly I would like to thank my parents for their love and support throughout my life and the push that was necessary. I would like to thank my beautiful partner Roshni for being patient with me over the past years and the love that she has shown me.

I would like to thank my supervisor Dr Joe Au for his continual support, guidance and supervision; he has always given me confidence and faith in the integrity of my work. Special praise should be reserved to two of my fellow colleagues and brothers, Alex Haig and Jeevan George Abraham. Not only have they technically supported me throughout they have given me mental strength and support to keep going, your contribution to this work cannot be overstated. The remainder of my research colleagues have to be mentioned, Keith Thornicroft, Kena Makaya, Billy Parthiphan, Matthew Deere, Ignacio Garcia de Carellan, Estafania Artigao, Juan Luis Ferrando, Balraj Ghatore, Shehan Lowe, Sina Fateri and Abbas Mohimi. The continual discussions and cross checking to build confidence in my ability has helped in developing the person I am today. When I was worn down at the most deepest darkest lowest crevices I could count on one of you to brighten my mood and pick up my spirit, so thank you. I have omitted Hugo Marques from the list because he deserves a note in his own right; the crux of my thesis is built around a piece of work Hugo helped me conduct. Prior to this happening I felt I was in a vast landscape and on a diverging path. With his help I managed to focus the scope of my PhD and comprehend the value of it. Thanks to all you guys, you guys are the best.

I would like to thank all my colleagues within Plant Integrity, with particular note to Angela Norrie for helping me with equipment, David Welsh for his assistance in carrying out empirical work and my industrial supervisor Peter Mudge.

I would like to thank Geraldine Durand, Dorothee Panggabean and Andy Wilson for being so generous in providing accommodation and their warm nature towards me during a critical period of time. I would like to thank CJ Engineer, Hina Engineer, Puish Engineer and Bianca Engineer for opening their house out to me in a bid to be close to University.

Finally I would like to thank the Engineering and Physical Sciences Research Board (EPSRC) and TWI Ltd for providing the funding for this research.

*Dedicated to Mum & Dad*

*This one was for you*

# Contents

Abstract.....	ii
Acknowledgements.....	iii
List of Figures.....	vii
List of Tables.....	ix
Abbreviations.....	x
1. Introduction.....	1
1.1 Application of Non-Destructive Testing.....	1
1.2 Motivation.....	1
1.3 Aim.....	6
1.4 Objectives.....	6
1.5 Structure of Thesis.....	7
1.6 Contribution to Knowledge.....	8
2. Guided Waves and Transduction Methods.....	9
2.1 Introduction to Guided Waves.....	9
2.2 Guided Waves in Plates.....	11
2.3 Guided Waves in Pipes.....	15
2.4 Transducers.....	17
2.4.1 Angle Probes.....	17
2.4.2 Comb transducers & Interdigital transducers.....	19
2.4.3 Piezoelectric Discs.....	20
2.4.4 Embedded piezoelectric transducers.....	22
2.4.5 Capacitive micromachined ultrasonic transducers (CMUTs).....	22
2.4.6 Electro Magnetic Acoustic Transducers (EMATs).....	23
2.4.7 Thickness-shear piezoelectric transducers (Shear PZTs) for Pipe Testing.....	24
2.4.8 Shear PZTs for high temperature plate testing.....	26
2.5 Commercial Guided Wave Pipe Testing Systems.....	28
2.6 Transmission Characterisation of GW & Ultrasonic Transducers.....	29
2.7 Resonant Characterisation of Ultrasonic Transducers.....	34
2.8 Resonant Modelling of Ultrasonic Transducers.....	36
2.9 Gap in Literature.....	40
3. Transmission Characteristics of a Shear PZT Dry Coupled Transducer.....	41
3.1 Introduction to Chapter 3.....	41
3.2 Hypothesis: Transmission Characteristic of a Shear PZT with Respect to a Variable Force.....	41
3.3 Transducer Test Rig.....	43
3.4 Waveguide Selection.....	45
3.5 Waveguide Preparation.....	50
3.6 Method to Measure Transmission Magnitude of Shear PZT Transducer against variable Clamping Forces.....	51

3.7	Procedure to Measure Transmission Magnitude of Shear PZT Transducer against variable Clamping Forces .....	52
3.8	Results: Measurement of Transmission Magnitude of Shear PZT Transducer against variable Clamping Forces .....	53
3.8.1	Time of Arrival Calculations for Fastest Wave Mode - L mode .....	53
3.8.2	Wave Mode Separation Calculations for L Mode and SH/SV Mode .....	58
3.8.3	Frequency Response of Transmitting Shear PZT with Respect to Variable Clamping Force	60
3.8.4	Transmission Output Magnitude of Shear PZT with Respect to Clamping Force.....	61
3.9	Method to Measure Transmission Magnitude of Shear PZT Transducer against variable Contact Area Surface Roughness.....	64
3.10	Procedure to Measure Transmission Magnitude of Shear PZT Transducer against variable Contact Area Surface Roughness.....	66
3.11	Results: Measurement of Transmission Magnitude of Shear PZT Transducer against variable Contact Area Surface Roughness.....	66
3.12	Discussion of the Transmission Characteristics of a Shear PZT Dry Coupled Transducer..	68
3.13	Contribution to Knowledge from Chapter 3 .....	70
4.	Resonance Characteristic of Shear PZT Transducer with Respect to Dry Coupling.....	71
4.1	Introduction to Chapter 4 .....	71
4.2	Method to Measure Electrical Impedance of Shear PZT Transducer under a Variable Coupling Force.....	71
4.3	Results: Measurement of Electrical Impedance of Shear PZT Transducer under a Variable Coupling Force.....	72
4.4	Measurement of Mechanical Resonance of Shear PZT Transducer under a Variable Coupling Force.....	76
4.5	Hypothesis: Mechanical Resonance of a Shear PZT Transducer with under a Variable Coupling Force.....	76
4.6	Method to Measure Mechanical Resonance of a Shear PZT Transducer under a Variable Coupling Force.....	79
4.7	Results: Measurement of Mechanical Resonance of a Shear PZT Transducer under a Variable Coupling Force.....	79
4.8	Discussion of the Resonance Characteristics of a Shear PZT Dry Coupled Transducer .....	85
4.9	Contribution to Knowledge from Chapter 4 .....	87
5.	FEA Model of Shear PZT Transducer to predict Dry Coupled Induced Resonances in Backing Mass .....	88
5.1	Introduction to Chapter 5 .....	88
5.2	2D Plane Stress FEA Model .....	88
5.3	3D Cuboid Backing Block FEA Model .....	90
5.4	Shear PZT FEA Transducer Model .....	92
5.5	Validation of FEA Model using Laser Vibrometry Measurements .....	95
5.6	A Parametric Study to Investigate the Effect of the Change in Backing Mass on the Resonance of the Shear PZT Transducer.....	99
5.7	Discussion of the FEA Models of Shear PZT Transducers to predict Dry Coupled Induced Resonances in Backing Mass.....	102

5.8	Contribution to Knowledge from Chapter 5 .....	103
6.	Conclusions and Further Work .....	105
6.1	Conclusions.....	105
6.1.1	Dry Coupled Transmission Behaviour of Shear PZT Transducer .....	105
6.1.2	Resonant Behaviour of Shear PZT Transducer.....	106
6.1.3	FEA Model of Shear PZT Transducer .....	107
6.2	Recommendations for Further Work .....	108
	References.....	110
	Appendix A – Technical Drawings of Transducers.....	115
	Appendix B – Contact Mechanics Literature.....	121
	Appendix C – Dispersion Curves and Wave Mode Displacements of 20mm <sup>2</sup> Rod Wave Guide .....	134
	Appendix D – Frequency Response & Transmission Amplitude vs Force Plots.....	139
	Appendix E – Waveguide Surface Roughness Optical Microscope Images .....	148
	Appendix F – Electrical Impedance versus Force Plots.....	151
	Appendix G – Laser Vibrometer Measurements of Mechanical Resonance in Transducer .....	161
	Appendix H – FEA Resonant Displacement Compared to Laser Vibrometer Measurement of Resonance in Transducers.....	170

## List of Figures

Figure 1.1: Jetty Line Inspection: - This area of corrosion under insulation was approximately 1 metre in length and 35% wall loss and was detected by Guided Waves. The cost of inspection would be significantly higher to inspect the length of this pipe using localised NDT methods due to scaffolding provisions for access and the unnecessary removal of protective insulation.....	4
Figure 1.2 Plant Integrity Guided Wave system for an 8” pipe.....	5
Figure 2.1: Phase velocity and group velocity dispersion curves of a 9mm steel plate generated by ABAQUS FEA software.....	11
Figure 2.2: S <sub>0</sub> displacement pattern (from Catton P, <i>Long Range Ultrasonic Guided Waves for the Quantitative Inspection of Pipelines</i> , PhD thesis, Brunel University, 2009).....	12
Figure 2.3: A <sub>0</sub> displacement pattern (from Catton P, <i>Long Range Ultrasonic Guided Waves for the Quantitative Inspection of Pipelines</i> , PhD thesis, Brunel University, 2009).....	13
Figure 2.4: Phase velocity dispersion curve of a 6” ASME schedule 40 steel pipe generated by Disperse software.....	15
Figure 2.5: ‘Teletest’ Transducer commercially available from Plant Integrity (Plant Integrity Ltd, 2013).....	24
Figure 2.6: Initial prototype design for shear PZT transducer (from Alleyne D.N. & Cawley P., <i>Journal of Nondestructive Evaluation</i> 15, 11-20, 1996).....	26
Figure 2.7: Inflatable Ring and Transducer Modules commercially available from Guided Ultrasonics Ltd.....	28
Figure 2.8: Amplitude output of dry coupled receiver versus clamping load (from Alleyne & Cawley, <i>Journal of Non-destructive Evaluation</i> , 15, pp 11-20) .....	30
Figure 2.9: Bulk wave reflection coefficient measurements from Perspex-Rubber interface with variation in normal load, surface roughness and concentration of dust (from Drinkwater et al., <i>Journal of Acoustical Society of America</i> 101, 970-981, 1997).....	31
Figure 2.10: Radius of the Hertzian contact formed between a fused quartz sphere of 100 pm radius and various planar samples (from Degertekin & Khuri-Yakhub, <i>IEEE Transactions on Ultrasonics, Ferroelectrics and Frequency Control</i> 44, 769-779, 1997).....	33

Figure 2.11: Schematic of transducer design (from TWI (1995) <i>Field implementation of a novel technique for detection of corrosion under insulation in oil and gas process pipework</i> . Cambridge, 8215/7/95, Fig. 2.10).....	38
Figure 3.1: Hertz contact of two half spheres. ....	42
Figure 3.2: Contact radius of steel half sphere under force. ....	43
Figure 3.3: (from left to right) CAD model of transducer test rig; transducer test rig.....	44
Figure 3.4: Simply supported beam under a point load. ....	44
Figure 3.5: Phase velocity dispersion curves for 20mm square steel bar generated by ABAQUS FEA software.....	46
Figure 3.6: Group velocity dispersion curves for 20mm square steel bar generate by ABAQUS FEA software.....	47
Figure 3.7: Displacement plot for wave mode ‘L’.....	48
Figure 3.8: Displacement plot for wave mode ‘SH/SV’.....	49
Figure 3.9: Displacement plot for wave mode ‘T’.....	49
Figure 3.10: PZT element adhered to wave guide. ....	50
Figure 3.11: Schematic of transmission characterisation set up.....	50
Figure 3.12: A scans for location A, D and H at 20 kHz for a transducer loading of 200N with anticipated L mode time of arrival indicated by red line envelopes plotted in MATLAB. ....	56
Figure 3.13: A scans for location A, D and H at 55 kHz for a transducer loading of 200N with anticipated L mode time of arrival indicated by red line envelopes plotted in MATLAB. ....	57
Figure 3.14: A scans for location A, D and H at 90 kHz for a transducer loading of 200N with anticipated L mode time of arrival indicated by red line envelopes plotted in MATLAB. ....	58
Figure 3.15: Average frequency response for Location G.....	60
Figure 3.16: Average frequency response for Location H.....	61
Figure 3.17: Average amplitude versus force for location G.....	62
Figure 3.18: Average amplitude versus force for location H.....	62
Figure 3.19: Percentage standard deviation for frequency response of repeated test. ....	63
Figure 3.20: Schematic of varied surface roughness test set up. ....	64
Figure 3.21: Average frequency response of Shear PZT transmitting through wave guide whilst in contact with varying surface roughness. ....	67
Figure 4.1: Impedance Magnitude of transducer for varying loading conditions on a steel bar.....	72
Figure 4.2: Impedance Phase of transducer for varying loading conditions on a steel bar.....	73
Figure 4.3: Impedance characteristics of transducer under 0N load on Steel bar.....	73
Figure 4.4: Impedance characteristics of transducer under 100N load on Steel bar.....	74
Figure 4.5: Impedance characteristics of transducer under 200N load on Steel bar.....	74
Figure 4.6: Impedance characteristics of transducer under 350N load on Steel bar.....	75
Figure 4.7: Isotropic view of transducer and indication of measured surface. ....	79
Figure 4.8: Frequency domain plot of transducer surface velocity for 0 to 450 kHz excited under varied load.....	80
Figure 4.9: Frequency domain plot of transducer surface velocity for 0 to 160 kHz excited under 0N load.....	81
Figure 4.10: Frequency domain plot of transducer surface velocity for 0 to 160 kHz excited under 100N load.....	81
Figure 4.11: Frequency domain plot of transducer surface velocity for 0 to 160 kHz excited under 200N load.....	82
Figure 4.12: Frequency domain plot of transducer surface velocity for 0 to 160 kHz excited under 350N load.....	82
Figure 4.13: Transducer surface velocity pattern over time at 21 kHz under a coupling force of 100N. ....	83
Figure 4.14: Transducer surface velocity pattern over time at 23 kHz under a coupling force of 200N. ....	84
Figure 4.15: Transducer surface velocity pattern over time at 25 kHz under a coupling force of 350N. ....	84
Figure 4.16: Transducer surface velocity pattern over time at 28 kHz under a coupling force of 350N. ....	85

Figure 4.17: Comparison between predicted contact resonance and measured.....	86
Figure 5.1: Plane stress model in ABAQUS.....	89
Figure 5.2: Resonant Displacement of Plane Stress Model at 135 kHz.....	90
Figure 5.3: FEA model of simplified transducer assembly with 6.4mm thickness. ....	90
Figure 5.4: Resonant displacement of FEA model of simplified transducer assembly with 6.4mm thickness at 72 kHz. ....	91
Figure 5.5: FEA model of simplified transducer assembly with 12.5mm thickness. ....	91
Figure 5.6: Resonant displacement of FEA model of simplified transducer assembly with 6.4mm thickness at 97 kHz. ....	91
Figure 5.7: FEA model of shear PZT transducer assembly. ....	92
Figure 5.8 : Resonant displacement of FEA model of shear PZT transducer at 83 kHz. ....	94
Figure 5.9: FEA model of shear PZT transducer attached to wave guide under coupling load.....	94
Figure 5.10: Resonant displacement of FEA model of shear PZT transducer attached to wave guide under coupling load at 19.6 kHz. ....	95
Figure 5.11: Resonant displacement of transducer in free air at 83 kHz in FEA ( <i>left</i> ) and 84 kHz by vibrometry ( <i>right</i> ). ....	97
Figure 5.12: Resonant displacement of transducer under 200N loading at 19.6 kHz in FEA ( <i>left</i> ) and 23 kHz by vibrometry ( <i>right</i> ).....	98
Figure 5.13: Displacement at 23 kHz in FEA model and measured displacement at resonance at 22.5 & 26 kHz for transducer backing mass with 10mm width.....	101
Figure 5.14: Displacement at 28.5 kHz in FEA model and measured displacement at resonance at 24.5, 30.5, 34.5, 37.5 & 41 kHz for transducer backing mass with 7.5mm width.....	101
Figure 5.15: Displacement at 32.5 kHz in FEA model and measured displacement at resonance at 22, 24, 31 & 35 kHz for transducer backing mass with 6mm width.....	102

## List of Tables

Table 2.1: FEA predictions of natural frequency for different parameters of transducer design. (data from TWI (1995) Field implementation of a novel technique for detection of corrosion under insulation in oil and gas process pipework. Cambridge, 8215/7/95, p.9). ....	39
Table 3.1: Properties of each test location on waveguide.....	51
Table 3.2: Arrival times of L mode at 20 kHz pulse at each location.....	54
Table 3.3: Arrival times of L mode at 55 kHz pulse at each location.....	55
Table 3.4: Arrival times of L mode at 90 kHz pulse at each location.....	55
Table 3.5: Separation frequencies at which wave modes will separate for each location. ....	59
Table 3.6: Grit blast media applied to steel waveguide and measurements of surface roughness on steel waveguide after treatment.....	65
Table 4.1: Predicted contact resonance between two steel half spheres. ....	77
Table 4.2: Predicted contact resonance between steel half sphere and alumina half sphere. ....	77
Table 5.1: Comparison of FEA predictions between Alleyne & Cawley (1995) and 2D plane stress model in ABAQUS .....	89
Table 5.2: Material properties used in FEA models. ....	93
Table 5.3: Comparison of FEA natural frequency predictions between different transducer models. .	95
Table 5.4: Comparison between detected natural frequencies of the shear PZT transducer in free air by the vibrometer and natural frequencies predicted by FEA model.....	97
Table 5.5: Comparison between detected natural frequencies of the transducer under 200N load by the vibrometer and natural frequencies predicted by FEA model.....	98
Table 5.6: List of predicted resonant frequencies for backing masses with varied width. ....	99
Table 5.7: List of measured resonant frequencies for backing masses with varied width.....	100

# **Abbreviations**

ASME – American Society of Mechanical Engineers

CMUTs – Capacitive Micromachined Ultrasonic Transducers

EMATs – Electro Magnetic Acoustic Transducers

FEA – Finite Element Analysis

GNP – Gross National Product

GW – Guided Waves

KLM model – Krimholtz, Leedom, and Matthaei model

NACE – National Association of Corrosion Engineers

NDT – Non-destructive testing

NOAA - National Oceanic and Atmospheric Administration

PVDF – Polyvinylidene Flouride

PZT – Lead Zirconate Titanate

# **1. Introduction**

This chapter will give an insight into the need for non-destructive testing. The application is highlighted and the repercussions to infrastructure without implementations of such systems are discussed. There is then a discussion about the merits of Guided Waves (GW) compared to competing technologies and the need to understand the transducer used in GW systems. The remainder of this chapter outlines the scope for the work conducted in this thesis, followed by structure and approach of this document and a summary of the contributions to knowledge.

## **1.1 Application of Non-Destructive Testing**

Ageing and contemporary infrastructure such as bridges, railways and pipeline are subjected to conditions including dynamic loads, thermal cycling and exposure to hazardous substances. These conditions can induce several mechanisms of damage where material loss will occur through cracking, pitting and oxidization. Non-volumetric damage can also occur through fracture, dislocations and delamination.

Non-destructive testing (NDT) is an integral part of the engineering industry and is implemented on a wide scale in a bid to tackle the issue of infrastructure integrity. Commonly periodic investigations are conducted to assess the condition and health of critical areas of interest in a structure.

## **1.2 Motivation**

The power generation industry is integral to providing a high standard of living to many societies across the world. In particular the oil and gas sector is the dominant supplier to all strands of society from households to industrial operations in an array of applications including automotive engines and heating.

The approximate total length of high pressure oil and gas transmission pipeline around the world is 3,500,000 km. With energy demands increasing an estimated 1.6% a year, there is an average increase of 40,000 km in high pressure onshore and offshore transmission pipeline each year to meet these demands (Hopkins, 2007). The construction and installation of pipeline infrastructure summates

to a cost of over £20 billion per annum. In the USA, 60% of Oil and Gas transmission lines are over 40 years old (NACE International, 2003).

Since 1988, it has been shown that there has been over 1000 significant incidents occurring in onshore and offshore pipeline contributing to 18% of all significant incidents in the USA (Baker, 2008). This equates to an average of over 50 significant incidents (defined as the occurrence of fatality or hospitalization and property damage) a year due to corrosion on a pipe line. This has led to an average annual cost of over \$25 million due to these incidents in the USA alone (Baker, 2008). In UK, the corrosion cost is estimated to be 4% of the Gross National Product (GNP) (Tems & Zahrani, 2006). The approximate UK GNP is £2 trillion; therefore the approximate cost of corrosion to the UK is £80 billion. The National Association of Corrosion Engineers International estimated that 5% of corrosion costs in the US occur in Oil & Gas transmission lines, which is comparable in the UK. Therefore the cost of corrosion in Oil & Gas pipelines in the UK is estimated as £4 billion. 50% of this cost will be operation and maintenance & 10% due to the cost of failures (Ahmad (2006)). This results in £200 million for the costs of failures in oil and gas pipeline in the UK alone. If there is a reduction of failures by 10% due to the improvement in technology, this saves operators £20 million a year in failure costs, solely in the UK.

The Prudhoe Bay oil spill is an example of catastrophic failure where BP had to expend \$500 million due to clean up, maintenance and litigation. In 2006, over two hundred thousand gallons of crude oil leaked from pipeline on to Prudhoe Bay in the Alaskan North slope (Associated Press, 2011). Subsequent investigation suspected corrosion areas at multiple locations on the pipeline as the fault. This resulted in a \$25 million US civil pay out and BP Exploration were ordered to install a system-wide pipeline safety management system as part of the court settlement.

Taking US data into account (Baker, 2008), there are on average 52 serious incidents involving oil and gas pipeline infrastructure per year due to corrosion. The consequences are on average a fatality and 5 injuries annually. Increasing inspection accuracy and coverage of pipelines will reduce the probability of incidents occurring and thus reduce the risk of death or serious injury.

In the event of an oil spill, toxic compounds can be ingested by animals directly, in their prey or by breathing or by preening and grooming. The consequences of this are difficult to measure; however as a case study, in 1989 the Exxon Valdez oil spill (BBC News, 2010) resulted in the death of 250,000 to 500,000 seabirds in addition to a large population of shore birds including bald eagles (NOAA Fisheries, 2014).

Even after clean-up operations, large quantities of oil can still be present and disruptive to fragile ecosystems for long periods of time. For instance the National Oceanic and Atmospheric Administration (NOAA) found 26,000 gallons of oil trapped in the Alaska shoreline due to the aforementioned Exxon Valdez oil spill 18 years later. This equated to a decaying rate of 4 per cent per year. The risk of incidents leading to environmental damage is significantly lowered with the capability of longer range rapid screening inspection of pipelines.

Corrosion can occur in inner and outer surfaces and this will reduce the wall thickness of a pipe thus compromising the integrity and safety of the pipe. It is standard practice to insulate pipeline which inhibits visual inspection for external corrosion. The removal of insulation over kilometres of pipeline is costly and time consuming and still does not provide insight on internal wall losses. Conventional ultrasonics, flash radiograph and eddy current can provide detailed wall loss measurements; however these techniques are slow, being single point acquisitions which render long range coverage (tens of meters) unfeasible (NDT Resource Centre, 2014). Pigging pipes is another method of inspection where an inspection tool flows downstream with the pipes contents enabling mass screening through continuous localised inspections. This requires shutdown which is costly and undesirable to the pipeline operator and this method is not viable in high pressure gas lines. Guided Waves can detect corrosion from a remote distance which is particularly advantageous needing only a keyhole access in the insulation to mount the transducers on the external pipe surface to inspect inaccessible or not visible areas and the inspection can take place in-situ (Figure 1.1). The larger wavelengths of guided waves in comparison to the resolution provided by conventional UT does not inhibit the detection of gross corrosion as the defect has a relatively large volumetric size particularly

compared to an open fatigue crack and guided waves are sensitive both to internal wall loss and external wall loss.



**Figure 1.1: Jetty Line Inspection: - This area of corrosion under insulation was approximately 1 metre in length and 35% wall loss and was detected by Guided Waves. The cost of inspection would be significantly higher to inspect the length of this pipe using localised NDT methods due to scaffolding provisions for access and the unnecessary removal of protective insulation.**

There are four commercial suppliers of Guided Wave inspection systems for pipeline testing, Plant Integrity Ltd in Cambridge UK, Guided Ultrasonic Ltd based in Chiswick UK, Guided Wave Analysis LLC founded in San Antonio USA and the multi-national Olympus. Plant Integrity and Guided Ultrasonic are currently market leaders (Esquerdo, 2012) who both exclusively have licence to the patent for pipeline Guided Wave testing (WO 96/12951). Current Guided Wave Ultrasonic Testing (GWUT) systems are portable and distribute transducers around a pipe at an accessible location (Figure 1.2). A clamping force with is applied to the transducers around the pipe. The transducer defined in the aforementioned patent is a thickness-shear PZT, where the thickness shear refers to the shear displacement produced upon piezoelectric actuation and PZT indicates the piezoelectric element being composed of Lead Zirconate Titanate.



**Figure 1.2 Plant Integrity Guided Wave system for an 8” pipe.**

The generic capability of GW systems is to detect a minimum 9% cross-sectional area wall loss with an average range of coverage of 30m from the systems location in both directions (Plant Integrity Ltd, 2004). The length of coverage is heavily dependent on the complexity of the pipe geometry, the contents of the pipeline and the insulating coating present on a pipeline. A Pipeline Research Council International report (2012) evaluating Guided Wave systems had concluded that it was desirable to have higher sensitivity over a longer tested volume. To service this requirement, the signal-to-noise of the GW system has to be improved to increase range and defect sensitivity. This requirement can be achieved by two fold; the magnitude of the signal being transmitted has to be increased by improving transduction efficiency and secondly the coherent noise generated has to be diminished by achieving a uniform ultrasonic output by each transducer in the array distributed around the pipe surface.

Since the patenting of pipeline GW testing in 1994 and the subsequent commercialisation there has been a dearth of published material investigating the behaviour of GW transducers.

### **1.3 Aim**

The aim of this work is to investigate a thickness-shear PZT transducer which is used in a system to implement Guided Wave Testing technique for the detection of corrosion in pipeline. The thesis investigates the mechanical response and resonant behaviour of the transducer under operational dry coupled conditions. The findings of this work are to be used in transducer design and array design decisions in future generation GW pipeline testing systems in order to improve signal-to-noise.

### **1.4 Objectives**

In order to achieve the aim of this thesis there are three main objectives:

- It is required to measure the relationship between the input of mechanical loading and the subsequent transmitted amplitude for a dry coupled guided wave transducer. This needs to be done for a variation of force and a range of operational frequencies. In addition surface roughness at the contact interface between the transducer and wave guide needs to be investigated to observe the effect on frequency response.
- The resonant behaviour of the transducer needs to be measured whilst under operational contact conditions to observe if any resonant characteristics have an effect on the ultrasonic behaviour of the transducer. This would be done by taking electrical impedance measurements and laser vibrometry structural resonant measurements of the transducer subjected to a range of physical forces.
- The final objective would be to develop an FEA model which would be able to predict the resonant behaviour of the transducer whilst simulated under approximate boundary contact conditions. This model should be able to highlight at what value a resonant frequency would exist and whether it would contribute to the operational frequency response of the transducer.

## 1.5 Structure of Thesis

The thesis begins with a chapter based on the concept of guided waves and the guided wave technique. The fundamental parameters and characteristics of guided waves in plates are described. The behaviour of guided waves in the alternative wave guides of a pipe is discussed. This is followed by a review of transduction methods and several types of transducers. Existing dry coupled guided wave sensors are reviewed as well as state-of-the-art transduction methods in pipes. This is then followed by a review of studies where conventional ultrasonic transmission with respect to mechanical loading has previously been investigated. This is followed by similar investigations regarding GW transducers. A review of previous resonance investigations of ultrasonic transducers is performed and a review of transducer resonant modelling is discussed. Previous FEA models of GW transducers are discussed and their assumptions which limited the accuracy of such models are highlighted. The gap in the literature regarding the characteristics and behaviour of the thickness-shear PZT transducer used for GW testing is stated.

Chapter 3 is the first technical chapter of the thesis and the objective is to measure the magnitude of the ultrasonic transmission with respect to clamping forces. A test rig setup used to collect the empirical data throughout the whole thesis is described. The method to assess the transmission output for a variable normal load on a transducer is specified and the results are displayed. This is followed by an investigation of the effect of surface roughness on transmission. The findings are discussed and the contribution to knowledge is pronounced.

Chapter 4 looks at resonances of the transducer. An electrical impedance measurement is taken under varying degrees of dry coupling and a second experiment to detect structural resonance of the transducer is performed. The subsequent results are discussed culminating in the contribution of knowledge from this package of work.

The final technical chapter, Chapter 5, is premised on modelling the resonances of the transducer. FEA models are created which replicate earlier work discussed in Chapter 2. An iteration of these models with appropriate geometries and boundary conditions is created with results compared to the

resonance data found in Chapter 4 which show correlation. A parametric study is performed in the FEA software and is subsequently validated by physical resonant measurements of fabricated prototypes.

The thesis is concluded in Chapter 6, which discusses further work generated by the work carried out in the thesis and suggests ways to overcome limitations in the work carried out.

## **1.6 Contribution to Knowledge**

There are three main contributions to knowledge in this thesis:

- The transmission relationship between a dry coupled shear PZT transducer used in pipeline inspection under varying pressure and surface roughness is demonstrated. It is shown that there is a relationship where ultrasonic output is proportional with the power of two-thirds to the loading force for a frequency range between 20 to 90 kHz. It is also shown that there is no effect on the ultrasonic output of the transducer when the surface condition of contact between  $R_a = 30$  micron and  $R_a = 90$  micron.
- A resonance induced by the dry coupled loading of the transducer has been measured between 20 and 30 kHz. This is a shear plane resonance which increases the magnitude of the ultrasonic frequency response at the resonant frequencies up to 8dB.
- A FEA model which possesses accurate geometries and boundary conditions of the transducer has been constructed to simulate the effectual dry coupled induced shear plane resonance at approximately 20 kHz. This model's capability to make predictions of resonance for alternative transducer backing mass has been proven.

## **2. Guided Waves and Transduction Methods**

### **2.1 Introduction to Guided Waves**

Conventional ultrasonic inspection uses bulk waves to inspect the material directly underneath where the probe is situated or within the adjacent area. In order to inspect a large volume of material the probe has to be incrementally moved to various locations, which is time consuming (Alleyne & Cawley, 1992).

Guided Waves propagate in a bounded area and are effective in structures such as rods, plates and tubes. Bulk longitudinal and shear waves propagate in a half space (a volume where there is only one boundary) or infinite space (a volume with no boundaries) without disturbance from a boundary. Guided waves are superimposed bulk waves which produce an interference pattern caused by the boundaries to allow it to propagate along a structure (Rose, 2000).

An alternative method of inspection is the use of guided waves. Guided Waves are waves which can propagate along the boundaries of a plate-like structure (Rose, 1999). Depending on the geometry, material and frequency of the wave, these waves can travel in the order of tens of metres along a line path of travel. There are two possible configurations to detect these waves; either there can be a receiver elsewhere on the structure at a distance from the transmitter which is referred to pitch-catch, or the transmitter itself can listen to echoes from a response generated by a feature, including a defect, of the structure which is referred to as pulse-echo. In the former, the integrity of the structure can be evaluated from the measurable properties, i.e. time-of-flight and amplitude, of the incident waves. An advantageous characteristic of using Guided Waves is that whilst propagating, stresses are produced throughout the thickness which means that defects can be detected regardless of location i.e. surface or internal of the body.

The other advantage of Guided Waves is that the rate of attenuation is lower than in bulk waves (Wilcox et al., 2001). The propagation of a bulk wave radiates in three dimensions and at a point source the amplitude will decrease inversely as a function of distance squared. Guided waves are

constrained within the boundaries with minimal lateral spreading which effectively propagates in one dimension along an axis. This in part explains the ability to propagate tens of metres still preserving signal integrity. This means for application guided waves can be used for inspection of structures at a point of remote access to investigate the integrity of structures under water or with restricted visibility due to coatings or insulation.

To predict wave propagation for any given structure with an infinite axial length, a system of homogenous equations can be derived using a governing wave equation, harmonic wave propagation solution, boundary conditions and theory of elasticity (Rose, 1999). A nontrivial solution to this set of equations can be provided by setting the determinant of the coefficient matrix to zero. The roots of the determinant of the characteristic equations can be plotted as a dispersion curve of phase or group velocity using a frequency thickness product. This dispersion curve characteristic of guided waves is discussed in the following section.

## 2.2 Guided Waves in Plates

Unlike bulk ultrasonic waves, guided waves have a tendency to vary in group velocity (the velocity at which the pulse propagates along the structure) and phase velocity (the velocity at which the sinusoidal signal within the pulse envelope propagates along the structure) with respect to frequency and thickness of the structure it is propagating in, known as the frequency-thickness product. This change in velocity across frequency is called dispersion. An example of dispersion curves generated by ABAQUS software FEA modelling for a 9mm thick steel plate which shows this relationship can be seen in Figure 2.1.

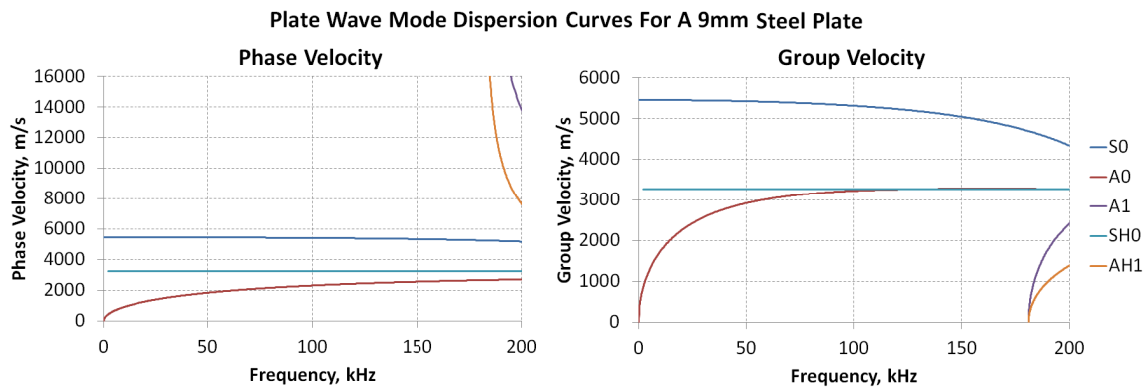


**Figure 2.1: Phase velocity and group velocity dispersion curves of a 9mm steel plate generated by ABAQUS FEA software.**

The repercussions of this dispersive characteristic are that a pulse with wide band frequency content could possess different velocity components which would cause the distortion and elongation of the pulse shape whilst travelling. It is important to control the frequency bandwidth of excitation in a bid to reduce the significance of dispersion. When comparing a tone burst signal to a windowed excitation signal Alleyne & Cawley (1992) demonstrated that using a Hann window with 5 cycles the side lobes in the frequency spectrum of a 1.2MHz signal were significantly eliminated. The use of windowed functions, in particular Hann window excitation, reduces the frequency band width around the centre frequency. It is desired to have a narrow band width around the centre frequency that is excited by a transducer in order to reduce dispersion and the associated effect of attenuation which

reduces signal-to-noise. This can be done by increasing the number of cycles, subsequently increasing the pulse duration and reducing the spatial resolution which makes it difficult to identify closely spaced features.

Another challenge with using guided waves can be observed by the presence of two fundamental wave modes (i.e. do not have a cut off frequency) in Figure 2.1. For a plate, the minimum number of wave modes that are generated at low frequency-thickness values are three, in this case defined as A0, S0 and SH0 (Catton, 2009). A0 and S0 contain asymmetric and symmetric displacement patterns about the geometric plane of symmetry observed in Figure 2.2 & Figure 2.3. SH0 propagates in a plate transversely to these two modes with a shear displacement through the plate and no out-of-plane displacement.

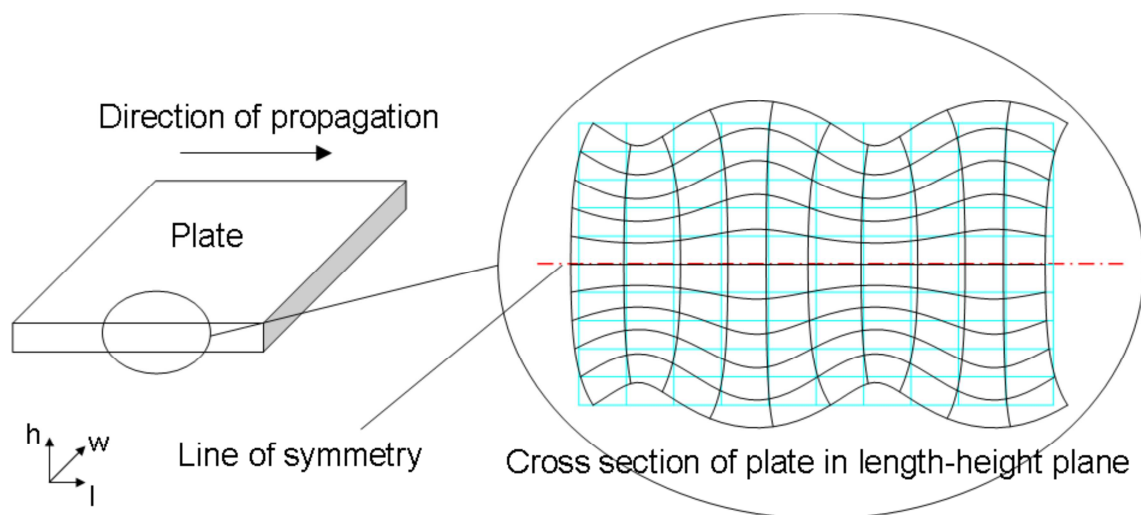


**Figure 2.2:**  $S_0$  displacement pattern (from Catton P, *Long Range Ultrasonic Guided Waves for the Quantitative Inspection of Pipelines*, PhD thesis, Brunel University, 2009)

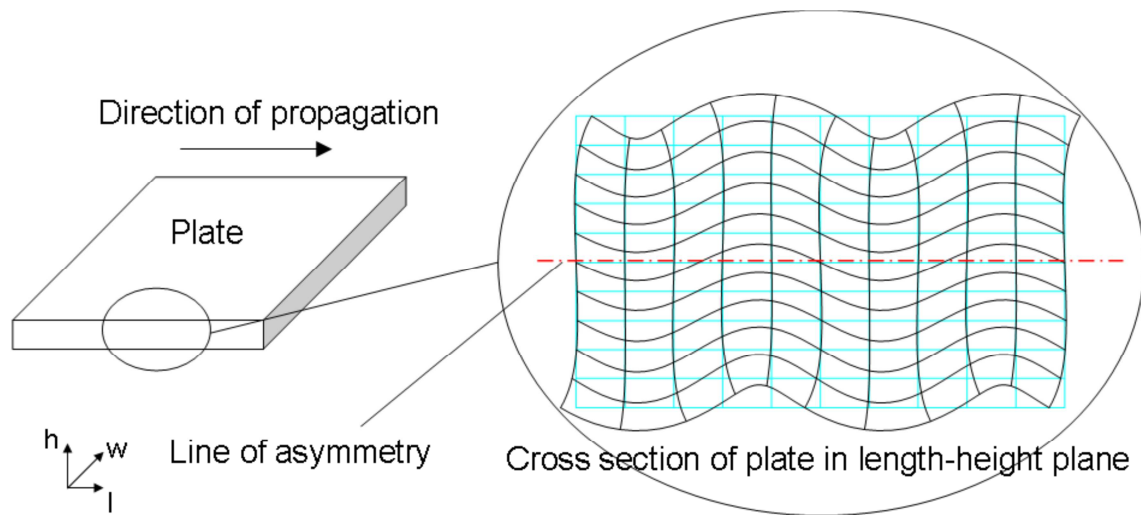


**Figure 2.3:**  $A_0$  displacement pattern (from Catton P, *Long Range Ultrasonic Guided Waves for the Quantitative Inspection of Pipelines*, PhD thesis, Brunel University, 2009)

At higher frequencies more modes exist in a plate with increasingly complicated displacement patterns.

It is desirable to excite a single mode which will eventually convert to another wave mode if it interacts with a structural feature such as a defect (Wilcox et al, 2001). If a single mode excitation is ensured it is possible to detect the presence of a defect by measuring a multi-mode signal.

With mode selection, it is recommended to use a non-dispersive frequency range otherwise the amplitude of the wave packet will reduce owing to distortion of the pulse shape and the transmitted signal will be undistinguishable from the noise floor (Rose, 2000). A non-dispersive frequency region occurs where the gradient of the dispersion curve tends towards zero, indicating the velocity is constant with a change in frequency, and the phase velocity and group velocity are approximately equal.

It is beneficial to pick maxima on the group velocity dispersion curves as the symmetric modes are higher than velocities of other modes which propagate at the same frequency. This aids signal interpretation as the modes are allowed to separate over time and a gate can be applied around a signal of interest (Cawley & Alleyne, 1996).

The selection of a mode should be decided by the feature of interest that is to be detected as the stresses through the thickness provided by a mode will be sensitively biased to a feature with a particular location through the thickness (Alleyne & Cawley, 1992).

The range a wave mode can travel depends on attenuation of material, the input power of the transducer (which in the case of a dry coupled GW transducer is the resultant of input voltage driving the transducer & the transduction efficiency through the clamping force) , the quality of the receiver and amplifiers and the uniformity of the cross-sectional geometry (Rose, 2000). This last factor makes guided waves ideal for pipes or rods as the wave will effectively propagate in one dimension along a transmission “line” and lateral beam spreading is minimized.

In general the sensitivity to a defect of a given mode will be increased as the wave length,  $\lambda$ , is reduced. As stated by Alleyne & Cawley (1992) this is due to the spatial resolution which is dictated by

$$\lambda = \frac{C_p}{f} \quad \text{Equation 2.1}$$

where  $f$  is frequency and  $C_p$  is phase velocity of the wave mode that is generated at this frequency. Wave length alone is not the only property that dictates the sensitivity to a defect. Different modes have different stress distributions through the thickness of the material and therefore a particular mode may have a biased sensitivity to a defect which may be located at a particular depth through the thickness of the material. For this reason, it may be desirable to select multiple modes to transmit. In general reducing the amount of modes present within a test aids the interpretation of the signal.

## 2.3 Guided Waves in Pipes

In pipe geometry for an arbitrary frequency many more modes exist than in a plate of similar thickness. An example of phase velocity dispersion curves of a pipe generated by commercially available software *Disperse* (Pavlakovic et al., 1997) can be seen in Figure 2.4.

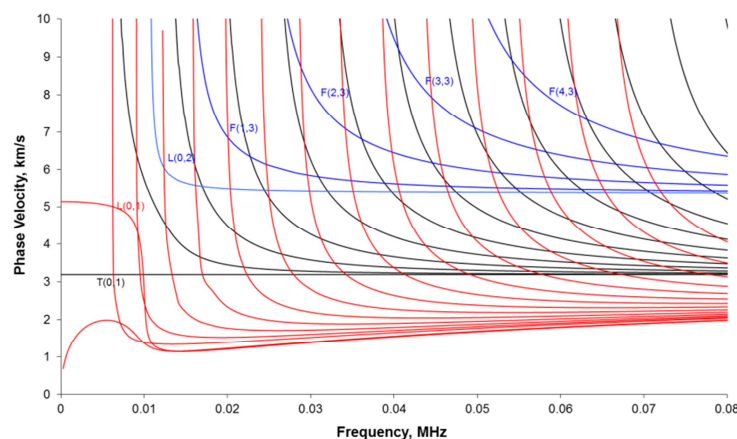


**Figure 2.4: Phase velocity dispersion curve of a 6" ASME schedule 40 steel pipe generated by *Disperse* software.**

Similar to a plate, a pipe will possess a minimum of three wave modes for any given frequency and the fundamental wave modes generate an axisymmetrical displacement. The naming conventions for wave modes present in a pipe have been developed by Meitzler (1961), Zemanek (1972) and Silk & Bainton (1979). The longitudinal wave mode  $L(0,1)$  has a uniformly radial displacement as it propagates axially through the pipe and is analogous to the  $A_0$  wave mode in a plate. The torsional wave mode  $T(0,1)$  has a uniform circumferential displacement as it propagates through the pipe with little radial displacement analogous to a  $SH_0$  in a plate. It is possible to generate flexural waves ( $F(m,n)$ ) at higher frequencies which possess displacement patterns related to a fundamental mode. It is possible to propagate higher order axisymmetric modes above a 'cut-off' frequency and at what value these frequencies occur is dependent on pipe geometry, mainly outer diameter and wall thickness. An axisymmetric mode commonly used in pipe inspection is  $L(0,2)$  due to its non-dispersive nature possessing a uniform radial displacement as the wave axially propagates; however through the thickness of the pipe a symmetric displacement on the outer and inner surface of the pipe occurs similar to  $S_0$  in a plate.

The importance of waveguide selection on wave mode separation can be demonstrated by comparing the complexity of multiple wave modes in a pipe and a plate. According to Figure 2.4 a 6" ASME schedule 40 steel pipe which possesses an approximate wall thickness of 7 mm, at 20 kHz can propagate three fundamental wave modes, L(0,1), F(1,1) and T(0,1) and in addition can have a higher order L(0,2) wave mode propagating through it. There are also a series of associated flexural wave modes that are capable of being propagated too. In comparison to dispersion curves of a thicker 9mm steel plate as seen in Figure 2.1, it can be seen there are similarly three fundamental modes however the higher order modes do not propagate within the plate until above 150 kHz. Hence it would be easier to discriminate wave modes at higher frequencies in a thicker plate than a thinner walled pipe.

## 2.4 Transducers

In the following sections several transduction methods of guided waves are reviewed and discussed.

### 2.4.1 Angle Probes

In early investigations by Alleyne & Cawley (1992) angle probe transducers were used for generating guided waves in a plate. Angle transducers contain standard bulk wave piezoelectric transducers and use the coincidence principle to propagate guided waves. The transducer will generate a nominal plane wave of wavelength  $\lambda_c$  in a coupling medium of water in an immersion tank or Perspex in a contact transducer. According to Alleyne & Cawley (1992) the wavelength of the plate wave is calculated by

$$\lambda_p = \frac{\lambda_c}{\sin \theta} \quad \text{Equation 2.2}$$

Taking into account  $\lambda_c = \frac{c}{f}$  for representing the wave length and velocity in the coupling medium and

$$\lambda = \frac{c_p}{f} \quad \text{Equation 2.1) the wave length and velocity in the plate structure with } f \text{ being the}$$

frequency,  $\lambda_p = \frac{\lambda_c}{\sin \theta}$  Equation 2.2 **Error! Reference source not found.** resolves to

$$\theta = \sin^{-1} \frac{c}{c_p} \quad \text{Equation 2.3}$$

Therefore Alleyne & Cawley (1992) showed it is possible to select a frequency which excites a specific mode according to the dispersion curve of the plate structure by varying the angle of transducer. The disadvantage is that only a constant wave velocity across a frequency range is generated which means there is a loss of wave mode control.

Alleyne & Cawley (1992) demonstrated that the use of variable angle probes allowed a change in angle which varied the frequency in a bid to select a particular set of modes. A compression piezoelectric element could be rotated around a Perspex body which was coupled to the metal substrate under inspection via a thin layer of liquid. It was stated that internal reflections from the Perspex degrade the signal and immersion testing under water provided better results. The use of immersion testing for inspection is appropriate for short range applications. However this is

unfeasible for long range applications and a suggested alternative was to place the transducer in a water column at the plate location. Again this would be a complicated setup for a pipe array solution.

Rose (2000) found that the diameter of a piezoelectric disc in angle probes had an effect on the bandwidth of the signal being sent. A larger diameter would produce a narrower bandwidth of excitation, which is desirable; however this may not be practical for low frequency application.

Wilcox et al. (2001) produced a transducer model to assess the suitability for a variable angled transducer to propagate asymmetric and symmetric modes in plates. The model simulated a transducer applying a spatially periodic distribution of surface tractions on the surface of the structure. It was concluded that for a steel plate a piezoelectric disc diameter 50 times the thickness of the plate would be needed to effectively propagate  $S_0$  with low attenuation and high excitability. Where this may be feasible for a plate with a thickness of 1mm, this would not be feasible for thicker plate applications. It was recommended that variable angled probes be restricted to inspecting liquid loaded plates as the high attenuation of  $A_0$  is an advantage to isolating the  $S_0$  for this specific case.

Cawley & Alleyne (1996) conducted a pitch catch test on a composite laminate plate using wedge piezoelectric transducer to generate  $S_0$ . Reverberations from the Perspex were found on the A-scan.

Angle probes and comb transducers have been used on pipe like structures (Rose, 2000). As seen in other work, angle probes have the limitation of selecting modes from a dispersion curve as they are restricted by the angle of incidence of the piezoelectric disc.

Both these angle probes and comb transducers were used for inspecting steam generator and heat exchange tubes (Rose et al., 1994) (Shin & Rose, 1998) (Rose & Shin, 1998). Tuning was required to select the mode of interest.

Ditri et al. (1993) developed a conical transducer that fits inside a heat exchanger tube which was accessed from an open end. The cone angle could be adjusted to select the desired mode using the coincidence principle. Standard compression transducers could excite an axially symmetric

longitudinal mode if placed on an open end, although practically it is not common to have such area of access.

## **2.4.2 Comb transducers & Interdigital transducers**

Comb transducers consist of a linear array of piezoelectric elements with a fixed spacing. The constraint of a comb transducer finger spacing means that only modes of a constant wavelength can be generated which again limits mode selection. This restriction could be bypassed by applying different phase of excitation to each element to excite several wave lengths; such is used in phased array systems. Interdigital guided wave transducers are a variant of comb transducers where electrode patterns of a particular spacing and orientation are specified to be optimised to generate a particular mode. They are generally comprised from piezoelectric polymer films such as PVDF (polyvinylidene fluoride). PVDF has the advantage of being low profile and flexible which lends itself for use on cambered surfaces. The pitfalls are that it is less sensitive than ceramics and it cannot be used at high temperatures. They are usually operated above 500 kHz and attached by surface bonding or being embedded and are predominantly used in plate applications for the aerospace sector (Monkhouse et al., 2000) (Capineri et al., 2002) (Giurgiutiu et al., 2002) (Bellan et al, 2005) (Na et al 2008). Jin et al. (2005) had used an interdigital transducer to detect cracks in aluminium plate by tuning the spacing for an A0 wave mode at 600 kHz. This transducer was double sided with electrodes to increase the magnitude of signal transmission and grease was used as a coupling medium to enable the transducer to be mobile. Manka et al. (2013) and Meyers et al. (2013) have also produced novel electrode patterns to optimise and increase the magnitude of transmission of target wave modes. Hay & Rose (2002) developed a PVDF comb transducer for pipe testing where a film was fabricated which wrapped round the entire surface of a stainless steel small diameter pipe (38mm outer diameter). This transducer was constrained onto the pipe by a pipe clamp but an applied pressure was not prescribed. The transducer operated in the higher frequency-thickness range and was successful at generating high order axisymmetric longitudinal wave modes L(0,3) and L(0,4). This work was further developed (Hay & Rose, 2006) by producing a pipe array and clamping multiple rings of PVDF transducer around a larger diameter pipe. The frequencies the pipe array was designed for ranges

within 190 kHz to 800 kHz which propagated higher order longitudinal modes. The comparative performance with respect to a piezoelectric pipe array showed that there was a 30 dB loss of sensitivity from a reflection instigated by a simulated defect therefore the transduction method was not deemed as effective for pipe inspection.

### **2.4.3 Piezoelectric Discs**

Piezoelectric discs are commonly polarised through the thickness of the disc (Gallego-Juarez, 1989). This results in producing a vibrational displacement normal to a waveguide surface and a radial displacement from the centre of the disc. Therefore piezoelectric discs are commonly used for generating guided waves in plates. Piezoelectric discs are commonly surface bonded. They are used for detecting defects, predominantly fatigue cracking, in aluminium plates (Leong et al., 2005) (Lee & Staszewski., 2007) (Fromme et al. 2006) and delamination in composite plates (Grondel et al., 2002) for applications in the aerospace industry. Hai-Yan & Jian-Bo (2011) used surface bonded PZT elements to help them derive a numerical and analytical model to predict the wave propagation of  $A_0$  and  $S_0$  in a homogeneous plate. The model would take different inputs into account including transducer geometry, the length and transducer position. The obvious disadvantage of surface bonding as a method of attachment is that this creates a permanent non-destructive system on a component under investigation which is undesirable for inspection systems with the requirements of being portable and temporary. A secondary disadvantage is that this will propagate both longitudinal and torsional modes in a pipe due to the radial displacements from the central source which is undesirable when the objective is to trying to excite a singular mode in a test.

Several contact transducers have been developed predominantly for plate testing using guided waves.

Degertekin & Khuri-Yakub (1996) fabricated Hertzian contact transducers to use surface traction to isolate the propagation of  $A_0$  and  $S_0$  in a 10mm thick aluminium plate.

Three types were fabricated which all consisted of a 3mm diameter 2mm thick PZT-5H disc which was bonded to the end of a quartz rod. The transducer was operational at 500 kHz centre frequency. A conical tip transducer with 100  $\mu\text{m}$  radius of curvature was used to generate normal traction at the

contact surface which was biased to transmitting and receiving an out of plane  $A_0$  mode. A straight grooved tip with a  $150^\circ$  angle was produced and brought into contact solely with the lower edge of a plate to generate shear traction and receive tangential particle motion. Similarly a straight grooved dual tip with both plate edges was also produced. The second configuration generated both  $A_0$  and  $S_0$  within the plate whereas the third configuration was biased to emitting  $S_0$  and suppressing  $A_0$ . The contact force was kept constant in this study and the relationship with varying contact pressure was not addressed. The transduction method was successful at producing shear wave modes in plate without a coupling medium or bonding but needed a free edge to accomplish this.

Lee & Kuo (2004) developed a transducer used for the investigation in the acoustoelastic effects on the wave propagation in the surface of a polymethylmethacrylate (PMMA). The transducer was constructed from two miniature conical (0.4mm tip diameter) PZT elements which acted as a point source and a point receiver. The transmitter would propagate a Rayleigh (surface) wave into the surface and the time of flight would be monitored across a short range distance of 7.10mm. The elements were backed with respective brass columns and copper housing. The centre frequency of operation for this transducer was 3.4MHz. The advantage of this transducer was that it could be dry coupled and it is portable.

Merheb et al. (2007) developed a pitch-catch guided wave inspection technique to detect fouling of closely spaced plate heat exchangers used in the food industry. Due to space constraints, hygienic considerations in addition to operating temperatures up to  $150^\circ\text{C}$  the system could not implement contacting transducers. It was found that frequencies above 100 kHz would attenuate heavily in the plates. A transmitter from one edge of the plate would transmit a mechanical pulse by an electromagnet pushrod striking the surface. The receiver attached to the opposite edge on the plate was constructed from composite materials with an embedded ferroelectric disc which was sensitive to low frequency acoustic waves and had low thermal conductivity. By assessing the amplitudes and the time of flights the gradual build-up of fouling on several plates were successfully monitored.

#### **2.4.4 Embedded piezoelectric transducers**

Tang et al. (2011) investigated the feasibility of embedding and surface mounting piezoelectric transducers into woven fiberglass/epoxy plates. The operational frequency was between 10 kHz and 50 kHz; however pitch-catch results were difficult to conventionally interpret. The other issue was the tendency for the piezoelectric element to break whilst subjected to the dynamic loading from an axial tensile test. Cement-based piezoelectric composites were developed and used as embedded transducers in concrete for damage detection (Qin et al., 2009). These were both used actively to monitor the integrity of concrete by generating conventional bulk waves with a broad frequency range (50 kHz to 1MHz). This sensor was also used as a passive sensor to facilitate acoustic emission.

#### **2.4.5 Capacitive micromachined ultrasonic transducers (CMUTs)**

Yaralioglu et al. (2001) devised an alternative to piezoelectric transducers to generate Guided Waves in silicon substrate used for integrated circuits. Capacitive micromachined ultrasonic transducers (CMUTs) were produced as they were stated to be appropriate for electronic integration and could be used to inspect integrated circuit fabrication processes. It was common to use CMUTs to produce ultrasound in an immersion medium. CMUTs consist of a metalized silicon nitride membrane supported by posts which is built on silicon wafer. An electrode on the silicon membrane and the silicon substrate form a parallel plate capacitor, which can be used to generate and detect ultrasonic waves in the immersion medium by applying a sinusoidal voltage. This voltage will cause the membrane to move towards and away from the substrate because of electrostatic forces. The resultant stresses and displacements cause ultrasonic waves in the surrounding immersion fluid. This behaviour also produces guided waves in the silicon substrate the transducer is micromachined on and guided waves can be propagated whilst the transducer and substrate is non-immersed. A pitch-catch configuration was used to demonstrate the reception of A0 at 1.8 MHz in silicon substrate. This transducer was suggested for the application of verifying circuit integrity.

## 2.4.6 Electro Magnetic Acoustic Transducers (EMATs)

Electro Magnetic Acoustic Transducers (EMATs) which use magnetic fields are relatively bulkier and heavier and produce a lower output compared to a piezoelectric transducer. EMATs are non-contact transducers however the performance of the EMAT is highly sensitive to lift off, i.e. the distance between the coil and the inspected substrate. There is an advantage that these can be used with the absence of liquid coupling or surface preparation which makes this transduction method attractive for inspecting high temperature components. An EMAT can be tuned to a particular mode and frequency where the coils are spaced at a specific wavelength. This constrains the choice of operational frequencies. For low frequencies, the wave lengths are large and therefore large lengths of coils would be needed. Furthermore EMATs are only viable on metallic structures.

An alternative method of application compared to early EMAT systems has been devised by Hirao & Ogi (1999) where an EMAT operating in pulse-echo was placed on the inner surface of a pipe and a wave mode is excited at 450 kHz which travels around the circumference. This EMAT device which used a periodic permanent magnet was mounted on wheels and travelled along the axis on the pipe, effectively taking a series of rapid localised scans of the circumference. In recent years, the feasibility of using electromagnetic principles for pipe testing has been advanced by the use of low profile magnetostrictive tape. Kannan et al. (2007) demonstrated the concept by generating T(0,1) in an aluminium pipe with a frequency range of 45 to 350 kHz. This method was also successful at detecting artificially grown defects. A similar configuration was produced by Cho et al. (2011) operating above 1MHz. Rather than using a continuous patch and coil around a pipe circumference, Kim et al. (2013) deployed segments of magnetostrictive patches acting as multiple transmitting transducers distributed around the circumference. These were used to generate T(0,1) at 500 kHz in a stainless steel pipe. This configuration successfully identified artificial axial and circumferential cracks in the pipe compared to a single piece EMAT which are conventionally used to sense axial cracks.

## 2.4.7 Thickness-shear piezoelectric transducers (Shear PZTs) for Pipe Testing

Thus far the transducers discussed to generate guided waves are predominantly applied by either surface bonding or with nominal contact and coupling gel or need access to a free edge of a structure. For a portable pipe testing system these methods of transduction are undesirable as they are either difficult to dismount the transducers, restrict the wave mode selection or are not able to generate wave mode purity without free edge access. The transducer investigated in this thesis is a shear mode transducer which is commercially available through Plant Integrity Ltd and commonly used in a pipe array for inspection of oil and gas pipeline (Figure 2.5).



**Figure 2.5: ‘Teletest’ Transducer commercially available from Plant Integrity (Plant Integrity Ltd, 2013).**

The transducer is an iteration of the transducer developed by Alleyne & Cawley (1996c) and this design and the pipe inspection technique has been patented (Cawley et al., 1994). The transducer uses a shear-polarised piezo-electric element (PZT 5A) of 0.5mm thickness, which imparts a tangential force or axial force at the surface of the pipe depending on the orientation. The element is protected by an adhesively bonded 0.1mm thick alumina wear plate which protects it from the hostile nature of the pipe surface as well as from fracture due to the hardness of steel. The element is bonded to a stainless steel backing mass with a cuboid geometry of 14mm (h) x 12.5mm (l) x 12.5mm (w). This mass is present to dampen the transducer in order to efficiently transmit sound into the pipe and secondly to be a buffer to withstand high pressures from a loading mechanism. The technical production drawing courtesy of Plant Integrity Ltd for this transducer can be found in Appendix A.

Thickness-shear piezoelectric transducers are polarised in the shear plane and are usually constructed from lead zirconate titanate. These will be referred to in the rest of the text as shear PZTs. Shear PZTs are normally dry coupled under load or surface bonded as shear waves would not propagate into a fluid because transverse loads are not supported in a perfect fluid. This is the reason conventional UT coupling gel is not used with shear PZTs.

Alleyne & Cawley (1996a) initially developed a Guided Wave inspection system for use on pipeline in a chemical plant that can detect a volume of corrosion which measures as  $3t \times 3t \times t/2$  where  $t$  is the original wall thickness. It was to be used on ASME 2- 12 inch diameter steel pipe with a minimum inspection range of 15m.  $L(0,2)$  was selected as the desirable wave mode as at 70 kHz it is non-dispersive and has the fastest velocity of all modes generated at this frequency. This allowed it to be separated from any other modes generated. The particle motion is axial and the strain displacement is uniform through the thickness which enables it to be sensitive to internal and external corrosion. Laboratory trials by Alleyne & Cawley (1996a) were conducted using surface bonded shear PZTs. These were 12.5mm in length by 3mm width and 0.5mm thickness. Sixteen elements were equally distributed around a circumference of a 3" pipe and in parallel acted as a transmitter. Eight elements were bonded around the circumference acting as receiver, listening to reflections from a pipe feature. A 70 kHz 10 cycle Hann windowed pulse was used with voltage output at 140V peak-to-peak and the receiver amplifier set to 20dB gain. They were able to show through these studies amplitude response reflections and mode conversion from various structural features of the pipe including butt welds, welded supports, flanges and a crescent shaped notch simulating corrosion. It was also shown that dry mineral wool insulation placed around the pipe had no attenuating effect on the tests.

In further a development to this initial work Alleyne & Cawley (1996b) defined criteria for a pipe inspection system to include the ability to mount and dismount from a pipe. The other criterion was to generate  $L(0,2)$  which is axisymmetric and has a major axial strain component. Therefore a shear PZT element could be used to generate this. The elements used in the development of this system are 12.5mm in length, with a 3mm width and 0.5mm thickness. The electrodes are on both faces with the bottom electrode extending over one end so both electrical connections can be made on the top face.

They conducted an investigation where sixteen circumferentially evenly distributed transmitting elements were initially bonded to a 3" schedule 40 (ASME Standard) pipe at a pipe end and eight receiving elements were bonded at a 1.26m distance from the pipe end. The arrays successfully showed the generation of L(0,2) and the suppression of flexural modes. The elements were said to be brittle and were at risk of fracturing upon attaching to the steel pipe surface. A protective shim made of brass was adhered to the piezoelectric face which engages the pipe. A tungsten loaded epoxy backing mass was used to increase flexural stiffness of the assembly. Tungsten loaded epoxy is commonly used as a high damping backing mass for conventional transducers. The assembly was contained in Tufnol housing Figure 2.6. There was no need to introduce any coupling medium at the surface where the transducer would be located.

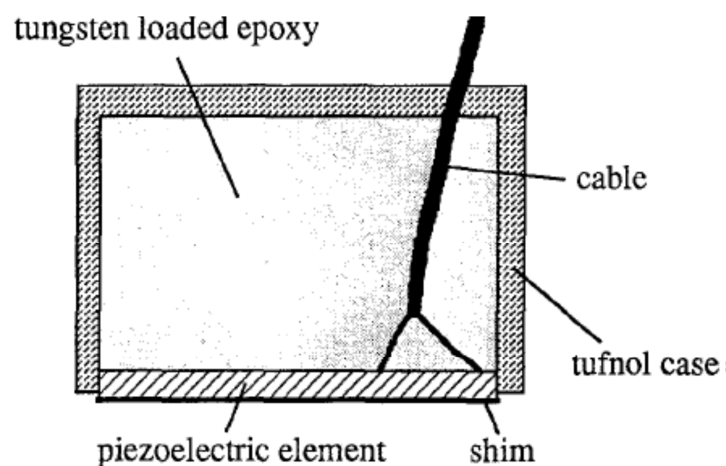


Figure 2.6: Initial prototype design for shear PZT transducer (from Alleyne D.N. & Cawley P., *Journal of Nondestructive Evaluation* 15, 11-20, 1996).

#### 2.4.8 Shear PZTs for high temperature plate testing

Atkinson & Hayward (1998) developed a lamb wave transducer using a shear PZT 5A element to excite longitudinal waves in wire fibres. These wire fibres were adhesively bonded onto the piezoelectric disc in a linear arrangement with periodic intervals in order to be tuned to excite A0 in a thin aluminium plate at a frequency of 267 kHz. The wires which acted like waveguides would transmit the propagating L(0,1) wave mode into the plate and act as multiple point sources which would mode convert the signal into A0 into the plate. This design was a form of comb transducer.

The concept was adapted for portability by gluing the wire fibres onto copper shim which could be moved around the plate rather than the wires being restricted by a permanent bond to the aluminium plate. This design successfully detected a through hole in the plate; however similar to the limitation of a comb transducer; a particular linear array would only be able to suitably generate a specific mode of choice. The concept to use fibres as a transmitter for guided waves was also applied to generating S0 at 250 kHz in carbon fibre reinforced composite plate by embedding the fibres into the plate (Atkinson & Hayward, 2001).

In a similar concept to Atkinson & Hayward (1998), Cegla et al. (2011) developed a dry-coupled ultrasonic transducer propagating waves remotely into an inspection material through the use of an attached waveguide. This transducer was being developed for use in petrochemical refinery plants, specifically to monitor the wall thickness of steel components which are subjected to accelerated corrosion due to elevated temperatures ( $>500^{\circ}\text{C}$ ). The construction of the transducer is a 12.5mm PZT element disc which was coupled with a shear coupling gel (honey) to a 15mm wide, 1mm thick and 300 mm long stainless steel strip acting as a waveguide. In turn, this waveguide is attached perpendicularly by brazing to a steel block acting as a sample under inspection. The alternative configuration was to clamp the transducer and waveguide into place onto the inspected block. A 2MHz Hann window was excited to generate an SH wave mode in the waveguide which subsequently generated an anti-plane shear bulk wave mode into the sample under inspection. It was found that the brazing attachment provided high noise due to the geometrical features of the fillet produced in the welding process. The dry clamping produced less noise, although when operated in pulse echo, the clamping junction was found to be too poor to generate high amplitude signal. However a pitch-catch dry clamped configuration was deemed to produce an acceptable signal-to-noise ratio. The devices collected data showing long term stability whilst the inspected structure was under thermal cycling. This form of transduction was viewed as permanently installed monitoring solution for a harsh environment.

## 2.5 Commercial Guided Wave Pipe Testing Systems

Currently there are two commercial products that facilitate the inspection of pipeline using guided waves with the use of the aforementioned patented transducer and technique. Both Plant Integrity Ltd and Guided Ultrasonics Ltd provide a portable dry coupled pipe array. The frequency range used for inspection is deemed as low frequency and is between 20 to 100 kHz. The Teletest system supplied by Plant Integrity Ltd distributes transducers circumferentially around a pipe with an axial orientation to generate axisymmetric longitudinal modes, specifically L(0,2) or a tangential orientation to generate an axisymmetric torsional mode T(0,1). A multiple of rings of transducers are mounted onto the pipe and the spacing of the rings are adjusted in order to use superposition principles to cancel the propagation of the slower more dispersive L(0,1) axisymmetric mode and control the directionality of the L(0,2) and T(0,1) mode. Mode purity and mode selection is improved by having each transducer outputting a uniform response. The reasons the transducers may not produce a uniform output are due to the manufacturing tolerance of the piezoelectric crystal and a variation in the pressure each transducer is applied under. The lack of uniformity in the array will propagate flexural modes and also degrade the effectiveness of wave mode cancellation ultimately increasing the presence of coherent noise, causing a reduction in signal-to-noise and decreasing diagnostic length/sensitivity. Guided Ultrasonics Ltd uses the same principles within the WaveScan system (Figure 2.7) (Lowe & Cawly, 2006).



**Figure 2.7: Inflatable Ring and Transducer Modules commercially available from Guided Ultrasonics Ltd.**

## **2.6 Transmission Characterisation of GW & Ultrasonic Transducers**

The shear PZT transducer that is investigated throughout this thesis is used in application by a dry coupled normal force. Ultrasonic energy can also be coupled efficiently to a sample through an elastic Hertzian contact formed between two solid bodies (Landau & Lifshitz, 1959). The effect of dry coupling on ultrasonic transmission has been researched by several authors.

Cawley & Alleyne (1996b) conducted tests to establish a shear PZT transducers (with a similar construction to the one tested in this chapter) response to a varying clamping force. A single transducer was placed on a steel 3" schedule 40 (ASME Standard) and subjected to differing dead weights. A transmission signal of 70 kHz from 16 bonded gauges was sent and the amplitude of the L(0,2) mode signal was measured. It was stated that the received amplitude settled above a clamping load of 50N and that this is an acceptable operational force as this provides a comparable response to bonded elements (Figure 2.8). The external surface roughness of the pipe was  $R_a=3\mu\text{m}$  with further tests conducted using the dry coupled transducers on chemical plant pipes which possessed an  $R_a$  of 8 -  $12\mu\text{m}$ . It was concluded that good signals were obtained with the dry coupled transducer system on this range of surfaces.

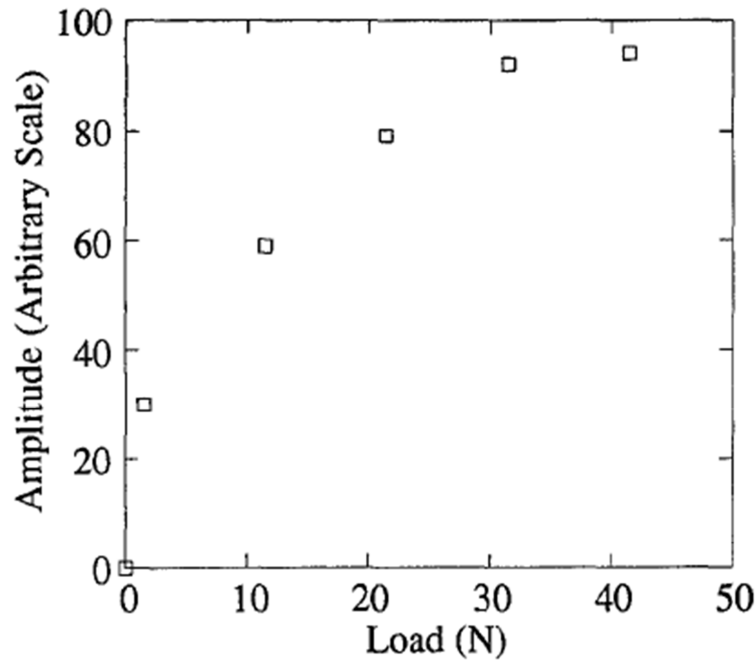


**Figure 2.8: Amplitude output of dry coupled receiver versus clamping load (from Alleyne & Cawley, *Journal of Non-destructive Evaluation*, 15, pp 11-20)**

Drinkwater et al. (1996) studied the effect of pressure between two interacting solid surfaces and the resultant transmission of ultrasound between the two bodies. This was in a bid to improve the performance of an ultrasonic wheel probe which contained a piezoelectric disc. This disc was housed within a rubber wheel which would be walked along a nominally flat surface for inspection. The probe was to transmit conventional bulk waves with a centre frequency of 4MHz. The method of investigation chosen was to place the transducer in a water bath which sat on a Perspex plate which in turn made contact with a rubber sheet. Increasing forces up to 60N were applied to the rubber sheet and the resultant reflection coefficient produced by the reflected signal at the boundary between the Perspex and the rubber meet was calculated. As the force applied was increased the reflection coefficient reduced non-linearly which implied that the transmission of sound across the boundary became more prominent. At lower loads the sound was reflecting back from the Perspex surface and the acoustic impedance mismatch with air allowed a greater reflection whereas with increasing contact the rubber would damp the sound. Various levels of surface roughness were introduced on a sample of Perspex by using emery paper and the resultant texture was measured using a stylus to

define the Ra and the correlation function for both height and lateral dimensional properties. It was shown that smoother roughness allowed the transmission of ultrasound through the boundary whereas the Perspex plates with greater Ra values produced higher reflection coefficients. An additional study was conducted to observe the effect the presence of dust and dirt had on the transmission of sound between the two surfaces. Particles consisting of silica, brass, iron, and diamond were used to simulate an unclean engineering surface on the Perspex. The resultant reflection coefficients were measured showing higher quantities of dust would inhibit the transmission of sound across the rubber-Perspex boundary. The graphs from these studies can be found in Figure 2.9.

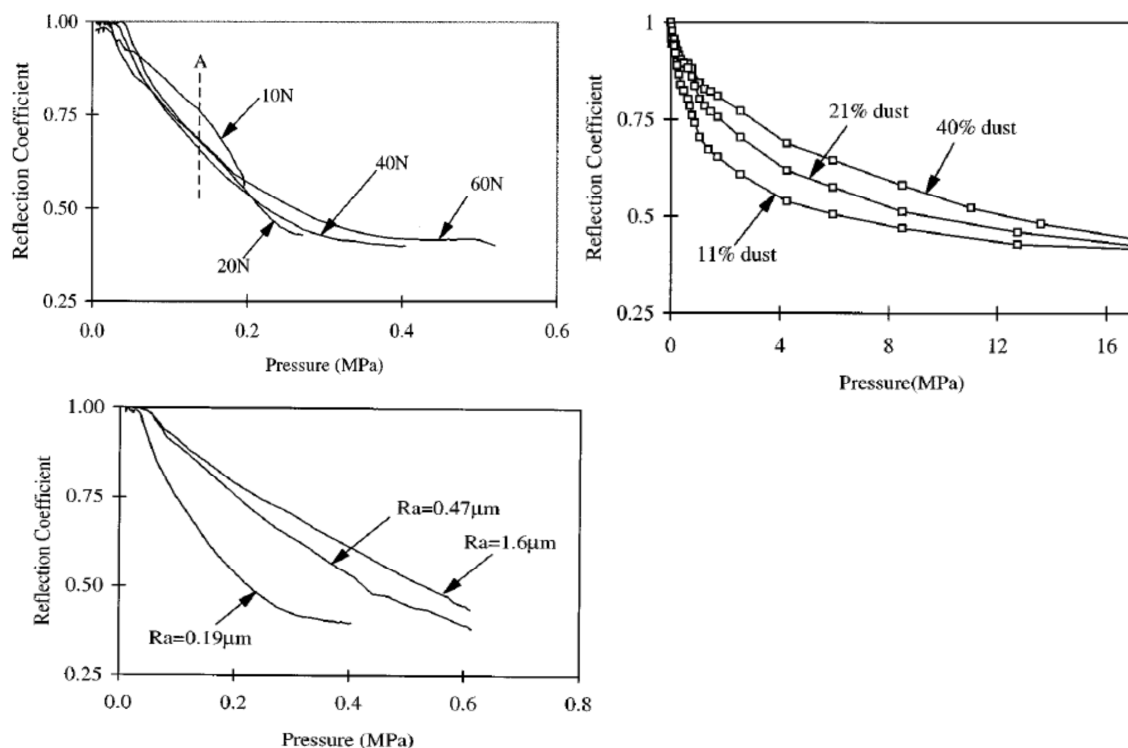


**Figure 2.9: Bulk wave reflection coefficient measurements from Perspex-Rubber interface with variation in normal load, surface roughness and concentration of dust (from Drinkwater et al., *Journal of Acoustical Society of America* 101, 970-981, 1997)**

As a follow on from a previous study (Drinkwater et al., 1996), Drinkwater et al. (2003) conducted an investigation where a piezoelectric angle probe was used to generate A0 at 300 kHz in a thin (approximately 4mm) glass plate waveguide. In the same study a piezoelectric contact transducer was

placed on a free edge of the plate in order to generate  $S_0$  at 120 kHz. A pitch-catch measurement was taken using a variable angle air coupled transducer at a remote distance on the plate. An elastomer plate was placed on the glass plate in between transmitting and receiving transducers and the elastomer plate was subjected to various uniformly distributed normal loads. The results showed that, for both modes, the velocity was unaffected whereas the transmission coefficient and calculated attenuation were strongly dependent on the applied load. The attenuation curves seemed to increase with respect to pressure with a proportion to the power of a third. Similarly the transmission coefficient with respect to load seemed to decrease inversely proportional to a third.

Further to work conducted by Drinkwater et al. (1996), a study was conducted by Thomas et al. (2004) at investigating the change in reflection coefficient from a conventional ultrasonic transducer emitting a longitudinal bulk wave into two interacting steel bodies. The interacting surfaces were grit blasted to produce a surface roughness of  $R_a=3.5\mu\text{m}$ . The surfaces were then subjected to an increasing normal load up to 45kN. This was done to imitate a closed fatigue crack within a steel structure. The transmitters used to propagate sound into the structure were coupled by a water bath. The frequency range excited was from 1MHz to 30MHz. The trend of the reflection coefficient with respect to increasing pressure agreed with earlier work for a particular frequency. However for various pressures the frequency responses of the reflection coefficient were distinguishable. In particular a higher pressure on the plates would reduce the reflection coefficient indicating a greater transmission of ultrasound through the structure. A study into the variation of surface roughness was not conducted.

Degertekin & Khuri-Yakhub (1996) produced a Hertzian contact transducer operating at 500 kHz using a piezoelectric cylinder bonded to a quartz buffer rod. The contact size depends on the geometry of the tip of the buffer rod, the applied force, and the material constants. Mode selection is achieved by the nature of excitation and the operating frequency. By spring loading, the transducers can be used on contoured samples. The criterion for the sensor was single mode operation to generate  $A_0$  and  $S_0$  in an anisotropic plate.

Degertekin & Khuri-Yakhub (2007) stated that the ultrasonic energy is coupled through the Hertzian contact at transducer-plate interface, and subsequently the contact size determined the aperture of the source of the sound (or receiver). For two spherical isotropic solids with radii  $R_1$  and  $R_2$ , the contact is circular with radius  $a$

$$a = F^{1/3} \left[ \frac{DR_1R_2}{(R_1+R_2)} \right]^{1/3} \quad \text{Equation 2.4}$$

where

$$D = \frac{3}{4} \left( \frac{1-\nu_1^2}{E_1} + \frac{1-\nu_2^2}{E_2} \right) \quad \text{Equation 2.5}$$

and  $E_1$  and  $E_2$  are Young's moduli, and  $\nu_1$  and  $\nu_2$  are Poisson's ratios of the two media, respectively, and  $F$  is the force applied to the contact. Subsequently a graph is plotted between the contact transducer's contact area with various anisotropic samples under different loading showing a relationship where the contact radius is to a power of a third to the force exerted on the transducer (Figure 2.10).

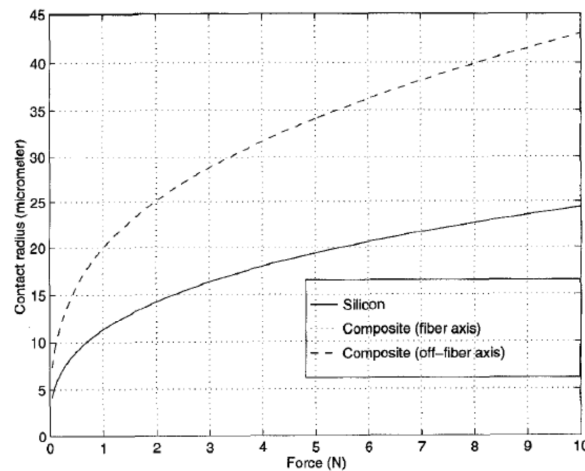


**Figure 2.10: Radius of the Hertzian contact formed between a fused quartz sphere of 100  $\mu\text{m}$  radius and various planar samples (from Degertekin & Khuri-Yakhub, *IEEE Transactions on Ultrasonics, Ferroelectrics and Frequency Control* 44, 769-779, 1997).**

## 2.7 Resonant Characterisation of Ultrasonic Transducers

It is conventional to use an ultrasonic transducers at a centre frequency for which the transducer design would have been optimised for (Nakamura, 2012). The transducer would be designed to resonate at a centre frequency to provide the maximum displacement output into the inspected structure in order to provide a heightened signal-to-noise. A method to characterise the resonant frequency of a transducer is to measure the electrical impedance of the transducer. This method has been followed by several authors.

Further to Atkinson & Hayward (1998) on the development of a guided wave transducer using wire fibres, an optimization process began to improve the signal-to-noise performance (Atkinson & Hayward, 2001). Initially the piezoelectric elements electrical impedance was modelled using FEA software. A wave propagation model was then created to investigate the displacement spectrum in the fibres when subjected to excitation frequencies up to 1MHz.

“In general, such impedance minima (electrical resonant frequencies) are associated with the maximum displacements of the transducer and, consequently, the optimum frequencies for transmission purposes.” (Atkinson & Hayward, 2001, pg. 1046)

Atkinson & Hayward (2001) found from the analysis of the models that there was a large shear mode displacement in the element at 265 kHz which coincided with a maximum frequency response peak in the fibre waveguide. A series of optimization models were run to demonstrate that the conical geometry of the bond line between the piezoelectric element and the emitting fibre wave guide had a significant effect on the transmission amplitude of L(0,1) at resonant frequency. A transducer with a single fibre was constructed using bond line geometry from the models. This sensor demonstrated experimentally that a 25dB level of improvement was achieved by implementing the design recommendations.

Nassar & Nongaillard (2000) developed an ultrasonic transducer using a piezoelectric element to monitor the gelation process in milk production. The technique was used to detect changes of the ambient temperature and the mechanical resistance of the medium. The geometrical shape of the

transducer was triangular with the tip acting as a point source in comparison to the wavelengths generated under a 100 kHz. A study was conducted where the sensor was analysed by using FEA analysis to calculate the resonant modes of the structure under 120 kHz when in free air. In addition the electrical impedance of the transducer was measured once the transducer was fully constructed with housing to identify resonances which corresponded to the model. Sixty kHz was identified as the resonant frequency at which the longitudinal extension of the element would occur and this was chosen as the operating frequency. This transducer was successful at being able to detect changes in time of flight of the signal under different stages of the milk gelation process.

Bhalla & Soh (2004) developed numerical models to investigate the effect bond line characteristics have on the electrical impedance of surface bonded PZTs. In contrast to active wave propagating transducers, conventional compression piezoelectric elements are attached to surfaces of a structure under investigation and the electromechanical impedance is measured. Damage to the structure will subsequently change the impedance trace measured. The application of PZTs for this technique is also discussed in Naidu & Soh (2004). The electrical impedance and the change in resonant frequencies with a frequency range up to 250 kHz were simulated for a change in the shear lag of the adhesive, the bond line thickness and the area of the bond. These models were validated empirically using 10mm<sup>2</sup> PZT patches adhered to an aluminium block. All the resonances detected by the impedance traces were found above 100 kHz.

Zhu & Rizzo (2012) developed a technique which combined the use of electromechanical impedance measurement and active guided wave propagation by using bonded PZTs on aluminium plate. A frequency of 200 kHz was employed to generate A<sub>0</sub> and S<sub>0</sub> and amplitude data was correlated against impedance traces to analyse a progressive damage scenario.

An impedance simulation of both the bare element used in the shear PZT transducer being investigated in this thesis and the fully built transducer was produced by modelling the transducer as an electrical circuit using a KLM model first developed by Krimholtz et al. (1970) (T. Phartipan et al, 2011a & 2011b). A Solatron SII260 impedance analyser was used to measure the practical

impedance. The impedance curves seemed to have good agreement for the frequency range of 20-100 kHz. It was measured that the resonant frequency occurs at 1.7 MHz in free air i.e. no contact with a wave guide surface.

Predominantly in the literature, authors are measuring electrical impedance to observe the natural resonant frequency of a transducer. However there is a mechanical resonance which can occur within a transducer due to contacting with another body.

This can be predicted by taking into account equations from K.L. Johnson (1987). It was stated, that if the equation to predict relative displacement,  $\delta$ , between two elastic half spheres in contact is taken into consideration, it can be interpreted as:

$$P = K\delta^{3/2} \quad \text{Equation 2.6}$$

where K is a constant which is derived from geometrical and elastic properties and P is the normal force applied. Making an assumption that the normal load on the half sphere produces a uniformly distributed pressure throughout the body the effective stiffness can be calculated by:

$$s = \frac{dP}{d\delta} = \frac{3}{2}(K^2P)^{1/3} \quad \text{Equation 2.7}$$

Given the two elastic spheres are attributed mass,  $m_1$  and  $m_2$  and are freely supported; the frequency of contact resonance can be given by the following:

$$\omega^2 = \frac{s(m_1+m_2)}{m_1m_2} \quad \text{Equation 2.8}$$

where  $\omega$  is the angular frequency of contact resonance.

## 2.8 Resonant Modelling of Ultrasonic Transducers

FEA modelling simulation of the geometry and backing material of ultrasonic transducers used to generate compression waves and guided wave has been conducted by several authors. The main objective from the authors discussed in this section has to been to predict the mechanical resonant frequency due to the structural geometry and material properties of the transducer assembly.

Allin & Cawley (2003) developed a bulk wave ultrasonic transducer which was housed in a wheel probe (Drinkwater & Cawley, 1995) (Drinkwater & Cawley, 1997) and was dry coupled in order to inspect bonded aluminium joints for the automotive industry. The technique used for inspection was to time gate the trailing signal after initial pulsed received signal to assess any changes to the frequency spectrum. In order to perform this type of technique it is important to avoid the transducer generating a resonant frequency within its operating range. A resonant frequency would provide ringing in the signal which would make the signal opaque. The operating frequency was chosen to be 350 kHz and due to environmental constraints the transducer had to be housed within 15mm<sup>3</sup> dimensions and be waterproof. In a bid to achieve this, FEA analysis was performed on a cube of PZT with varying lengths to establish the resonant frequencies. The PZT was modelled as an isotropic material and it was found that this simplification gave accurate results. The first resonance in air of a 2mm<sup>3</sup> element was predicted to be 645 kHz and this was found to be 600 kHz experimentally. On this premise, an air backed transducer was constructed and which was adhesively bonded to a waterproof membrane. This membrane was the engaging surface with immersion fluid and the surface under investigation. The transducer was found to successfully operate in an immersion tank between 200 – 500 kHz with the resonant effect of the transducer being minimal after low pass filtering starting from 450 kHz with the response decreasing to zero at 550 kHz.

Clark et al. (2009) developed a guided wave transducer using a piezoelectric element disc to generate A<sub>0</sub> in aluminium plate. It was desirable to alter the through thickness resonance of the transducer to a frequency between 20 and 40 kHz. It was also stated that softer interfacial layers between the disc and plate would suppress in plane displacements and hence suppress S<sub>0</sub> propagating. An FEA model of axisymmetric geometry of the transducer was constructed. It consisted of cylindrical steel backing mass, a piezoelectric disc and silicon carbide foam interlayer, with all parts joined by a nominal epoxy bond line. In addition the aluminium waveguide was modelled too and the transducer assembly was modelled as being surface bonded with a nominal bond line rather than a dry coupled approach. It was found that a small change in the bond line thickness had minimal effect on the results. A parametric study was conducted by investigating various backing mass lengths, transducer diameters,

and front layer thicknesses. The model indicated that an increase in height of the backing mass would lower the resonant frequency characteristic of the transducer. Similarly it was also found that increasing the interlayer thickness resulted in lowering the resonant frequency. Although it was predicted that waveguide plate thickness has an effect on the resonant frequency of the sensor too, it was shown that above a 4mm thickness the resonant value asymptotes to a stable value. However as the plates become thinner not only does the resonant frequency rise in value but the response becomes broader around the centre frequency. The model predictions were partially validated using a 2-mm thick PZT disc with a 6-mm long backing mass and a 2-mm thick silicon carbide foam front layer which had a measured resonant frequency of 22 kHz. Using the transducer for this operational mode it was shown that a signal-to-noise ratio of above 35dB between A0 and S0 generated signals could be achieved and hence biasing the sensor effectively to select an A0 mode.

In 1995 (Alleyne & Cawley, 1995) the refinement and optimisation process of a shear PZT transducer was performed. As stated in Section 2.4.7, the main criteria of the backing mass were to mount and protect the PZT element as well as to dampen any resonant modes of the transmitter out of the operating frequency (20 to 100 kHz). A schematic of the design can be seen in Figure 2.11. The shim and the two bond lines possessed a thickness of 0.1mm and the PZT has a thickness of 0.5mm.

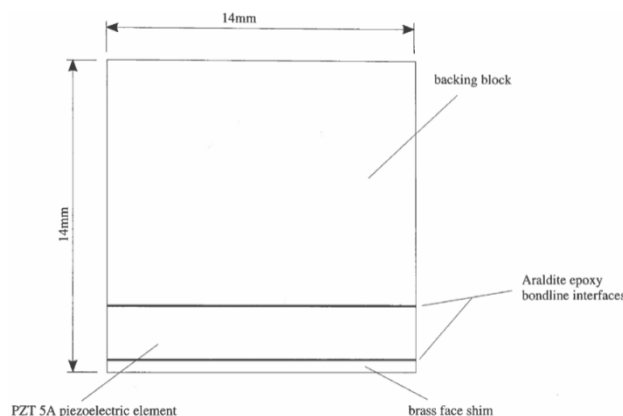


**Figure 2.11: Schematic of transducer design (from TWI (1995) *Field implementation of a novel technique for detection of corrosion under insulation in oil and gas process pipework*. Cambridge, 8215/7/95, Fig. 2.10)**

An FEA model was constructed to predict the lowest natural resonant mode. This was a plane strain model and is completely unconstrained on any external edges. The model was iterated several times where the material properties of the backing mass were changed. A second parameter was investigated where the thickness of the bond line between the backing mass and PZT was altered (Table 2.1).

Backing Material	Backing/PZT bond line thickness (mm)	Lowest Natural Frequency (kHz)
Steel	0.1	140
Aluminium	0.1	123
Brass	0.1	97
Tungsten Epoxy	0.1	83
Backing Material	Backing/PZT bond line thickness (mm)	Lowest Natural Frequency (kHz)
Steel	0.1	140
Steel	0.25	130
Steel	3	52

**Table 2.1: FEA predictions of natural frequency for different parameters of transducer design. (data from TWI (1995) Field implementation of a novel technique for detection of corrosion under insulation in oil and gas process pipework. Cambridge, 8215/7/95, p.9).**

Experimental measurements found a steel backed transducer with a width of 6.4mm and a nominal bond line of 0.1mm had the lowest resonant frequency of 152 kHz. This work was the foundation for the current transducer commercially sold by Plant Integrity Ltd & Guided Ultrasonics Ltd.

A 3D FEA model of the transducer used in the Plant Integrity system was later developed (Chaston, 2008). Again this model assumed that there were no contact conditions with a waveguide and resultantly predicted a resonant frequency at 150 kHz. This prediction was verified by measuring the transducer's electrical impedance phase in free air.

## 2.9 Gap in Literature

The majority of guided wave transducer investigations have been conducted in a high frequency range (above 100 kHz). A dry coupled shear PZT transducer low frequency transmission response under varied load has not been analysed prior to the work stated in this thesis. The receive characteristics for a singular frequency from a transmitting array had been assessed on a pipe waveguide; however the response above a 50N load has not been observed as it was said that the receive amplitude reached an asymptote (Alleyne & Cawley, 1996b). Additionally the effect of surface roughness at the area of contact on the transmission of a dry coupled shear PZT transducer has not been conducted.

Additionally the resonant frequency of a dry coupled shear PZT transducer has only been measured in the literature by electrical impedance measurements (T. Phartipan et al, 2011a & 2011b). The measurements found an electrical resonance at 1.2 MHz whilst the transducer was unconstrained in free air. The effect of mechanical/structural resonance due to contact with a wave guide has never been investigated prior to this thesis.

Similarly FEA models to predict the resonance of a dry coupled shear PZT transducer have only taken into account free air conditions and simplistic 2D geometrical properties which predict structural resonances of the transducer above the conventional operational frequency range GW pipe testing (100 kHz). FEA models which take into account the contact resonance induced by a wave guide and 3D geometrical features have not been published in the literature neither has there been empirical validation of the mechanical resonance of the transducer.

## **3. Transmission Characteristics of a Shear PZT Dry Coupled Transducer**

### **3.1 Introduction to Chapter 3**

As discussed in Section 2.6, the magnitude of amplitude output with respect to a variable clamping force on a shear PZT transducer has only been investigated in the literature by Alleyne & Cawley (1996b). This investigation only varied the force on a receiving transducer whilst a surface bonded transmitter transmitted a single frequency of 70 kHz. The conclusion was that there was a maxima of receive amplitude above a clamping force of 50N. The limitation of the published literature does not address a variable clamping force on a transmitting transducer neither is there diligence on frequency dependency. The result from this work contradicted a continuous rise in received amplitude expected through classic Hertzian contact theory discussed by Degertekin & Khuri-Yakhub (2007). In addition there is no investigation in the literature which studies the effect of surface roughness at the contact area between a shear PZT transducer and a wave guide and the resultant effect on the frequency response. In this Chapter, a design of experiments has been conducted to address these gaps in the literature, to understand the relationship between the transmission output of a dry coupled shear PZT transducer with respect to variable clamping force as well as varying contact area surface roughness.

### **3.2 Hypothesis: Transmission Characteristic of a Shear PZT with Respect to a Variable Force**

A flat surface can be modelled as a large asperity of half-sphere geometry consisting of multiple smaller asperities on the surface (see Appendix B). The contact between the nominally flat transducer alumina wear plate and the nominally flat steel waveguide can be approached by Hertzian contact theory similarly to the work stated by Degertekin & Khuri-Yakhub (2007). The flat surfaces can be assumed to be large single asperities coming into contact. Hertz contact theory was used to calculate the expected contact area between two steel half spheres under varying normal forces with an absence of an adhesive force. The transducer and the wave guide in contact can be represented by two steel half spheres (Figure 3.1).

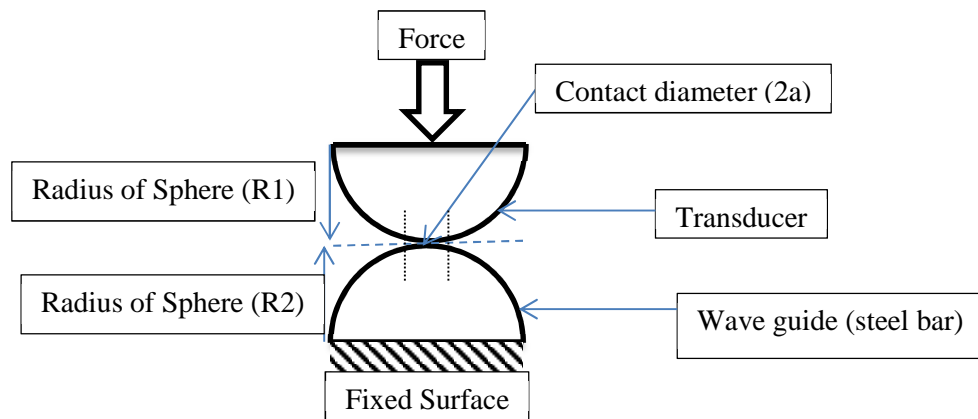


Figure 3.1: Hertz contact of two half spheres.

The material properties of steel were defined by a Young's Modulus of 210 GPa and a Poisson's Ratio of 0.3. The radii of the half spheres were taken as 14mm, which represent the height of the transducer according to Appendix A and an approximated wave guide of 14mm thickness. The equation used by Degertekin & Khuri-Yakhub (2007) to predict contact area between their contact dependent transducer and inspection substrate was used to calculate the predicted contact radius and area of the two bodies whilst subjected to a load of 0N load to 400N. This equation is

$$\frac{1}{R_1} + \frac{1}{R_2} = \frac{1}{R_{1+2}} \quad \text{Equation 2.4.}$$

The relationship between force and contact radius derived from this equation is graphically demonstrated in Figure 3.2.

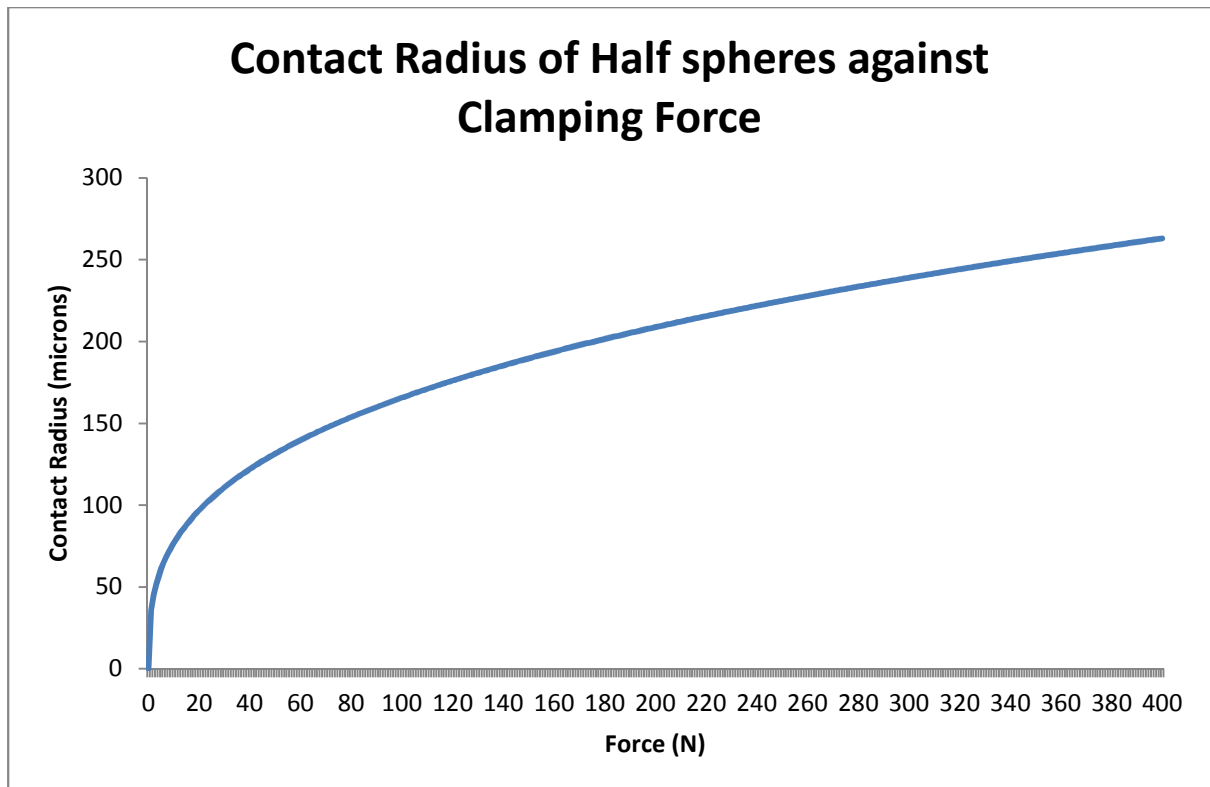


Figure 3.2: Contact radius of steel half sphere under force.

It is expected that the transmission output amplitude of the transducer under a normal force will exhibit a similar non-linear relationship and continue to increase beyond 50N loading. It is postulated that this will occur for every frequency excited.

### 3.3 Transducer Test Rig

A test rig was designed to mount commercially available shear PZT transducers and accommodate waveguides of various lengths to test on (Figure 3.3). The purpose of the rig was to apply a normal force onto the transducer. The force applied had to be controlled and varied. In addition the rig had to house and to support a selection of waveguides which could possess a variety of geometric dimensions. There is a limitation to accommodate wave guides within the following space envelope; the cross sectional width would be no longer than 38mm and the axial length would be no longer than 6000mm. The test rig accommodates the wave guide cross section width of 20mm used in the investigations for this thesis. The test rig is able to perform pitch-catch tests if there is a receiver on the wave guide and/or pulse echo tests. The test rig has been designed with the intention to

accommodate other wave guides for future research and development by Plant Integrity ltd beyond the scope of this thesis.

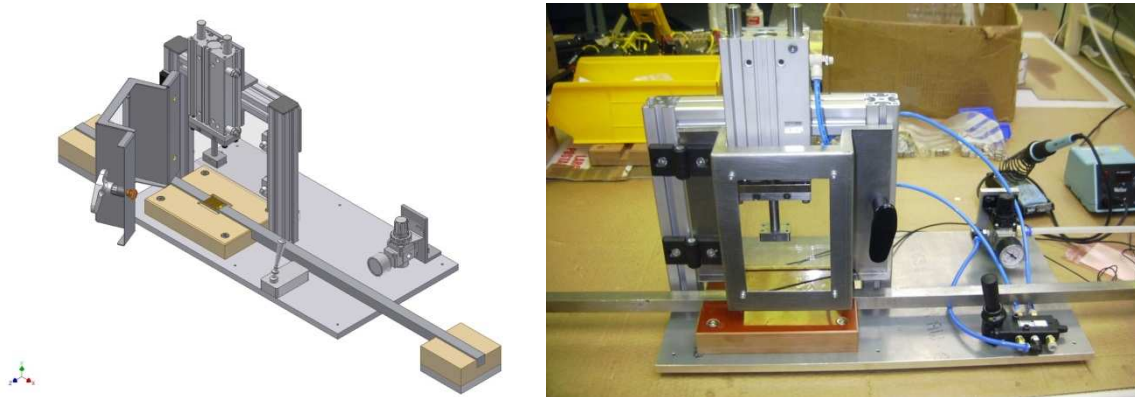


**Figure 3.3: (from left to right) CAD model of transducer test rig; transducer test rig.**

This test rig would be used for collection of data in subsequent investigations (Chapter 4 & Chapter 5). The premise of the rig was based on a supported beam subjected to a point load (Figure 3.4).

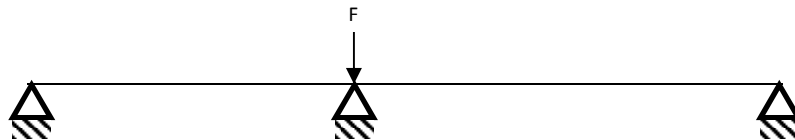


**Figure 3.4: Simply supported beam under a point load.**

As can be seen in Figure 3.4 the middle fulcrum is where the dry coupling of the transducer would occur. A pneumatically driven ram is used to apply a force. The ram is bolted onto an aluminium truss. The ram contains an extended shaft that houses the transducer and accurately positions the transducer repeatedly. There was provision within this shaft head for a male MCX connector and coaxial cable to allow an electrical connection to a signal generator in order to drive the transducer. The shaft head has been produced by injection moulding of glass bead filled nylon 6-6. This material has been specified as to provide acoustic insulation from the transducer into the ram and supporting

structure. An anti-vibration mount has been placed between the shaft and the shaft head with the purpose of adjusting to allow nominal flat-to-flat contact in the event of a slight parallel misalignment between the transducer wear plate surface and the inspection surface. When the transducer is placed within the rig the piezoelectric element is oriented in the axial direction of the waveguide. The force applied is varied by an air pressure regulator with a gauge indicating the pressure supplied to the ram. A toggle switch has been implemented to actuate and retract the ram in order to safely mount and dismount the transducer.

Negating the self-weight of the beam, any force applied on the middle fulcrum will create an equal but opposite reaction force at this location on the beam. This principle was used to measure the force being exerted on the transducer by the pneumatic ram. A load cell sensitive to compression forces is placed directly underneath the waveguide at the location where the transducer is in contact with the waveguide. With the waveguide sitting on the load cell, a reaction force reading can be taken when an external force is applied to the waveguide. The load cell is sat within a pocket and slightly protrudes out of a Tufnol base block.

The supports on the extremities of the beam correspond to the Tufnol blocks which prop the waveguide. These Tufnol blocks can be appropriately placed remotely from the jig assembly which provides the force. The Tufnol blocks throughout the assembly have been dimensioned with a height to allow the waveguide to sit nominally flat. Tufnol material has been used because it has excellent machinability properties to provide a smooth flat surface for the waveguide to be positioned on.

### **3.4 Waveguide Selection**

For investigations presented in this thesis 20mm square cross section carbon steel bars of 5850mm length have been used as the waveguide. A waveguide of this geometry was chosen for several reasons; the flat surface geometry allowed repeatable nominal flat-to-flat contact with the flat transducer wear plate surface. Additionally, relatively long extruded lengths of non-square cross section steel profiles are difficult to manufacture to a high degree of straightness and welding of profiles have to be performed to extend an axial length of a waveguide. This type of cross section

was available in 6m lengths which would allow sufficient distance to perform pitch-catch tests with mode separation. Finally as will be seen below and in Hayashi et al. (2003), this cross-sectional geometry allows large bandwidths on a low frequency spectrum where modes are non-dispersive.

Dispersion curves were computed for a 20mm square cross section carbon steel bar. The assumed material properties were Young's Modulus,  $E = 210\text{GPa}$ , Poisson's Ratio  $\nu = 0.3$  and density,  $\rho = 7860\text{ kg/m}^3$ . The curves were derived analytically with ABAQUS software by using Eigen-mode analysis. Figure 3.5 & Figure 3.6 shows the wave modes present at an excitation frequency spectrum within the bar from 10 kHz to 100 kHz and the corresponding phase and group velocities.

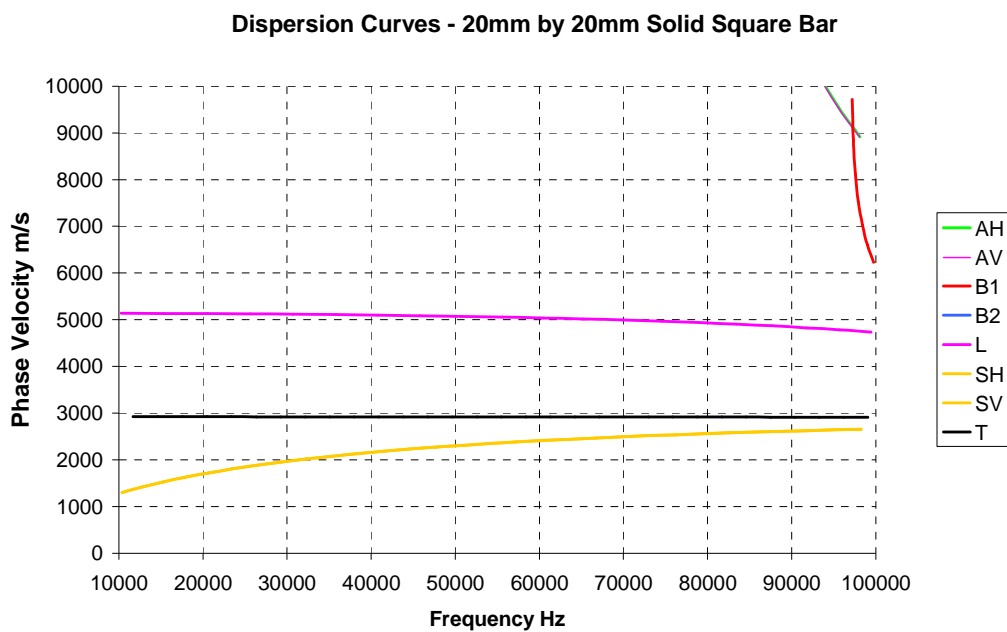
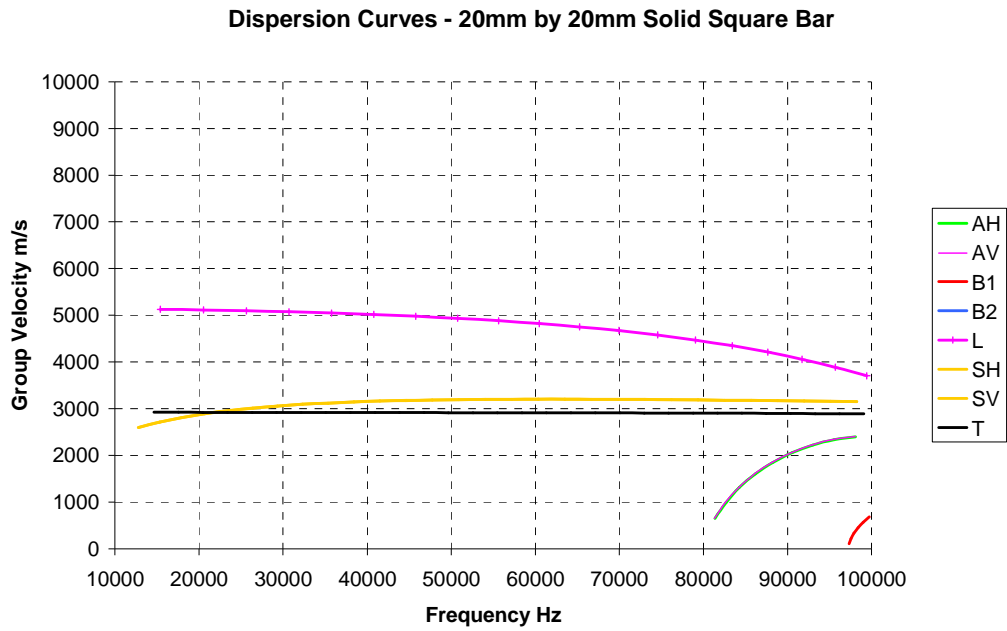
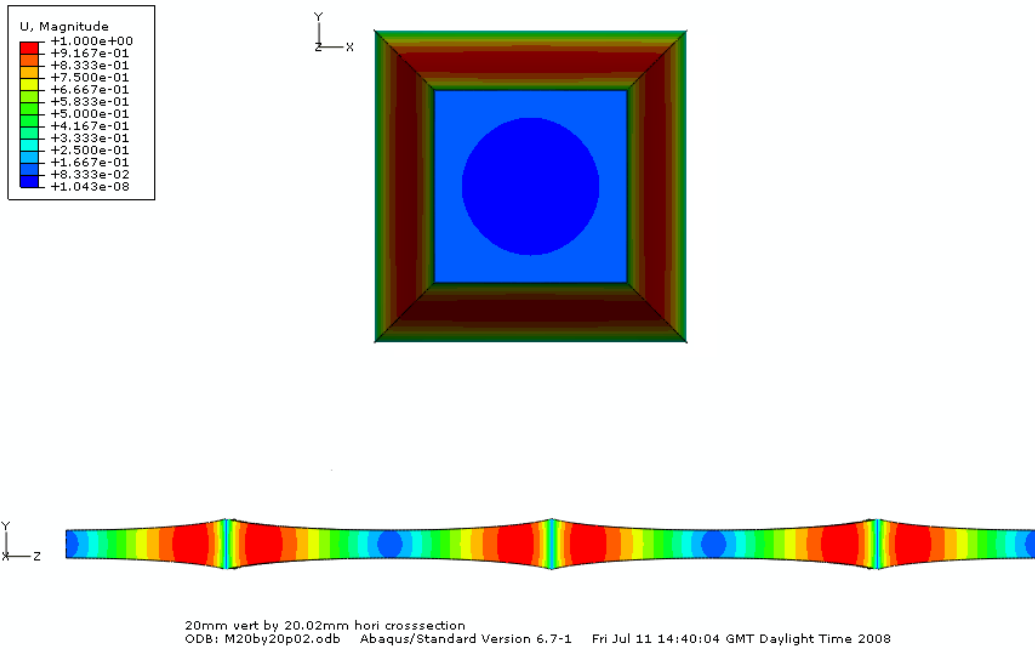


Figure 3.5: Phase velocity dispersion curves for 20mm square steel bar generated by ABAQUS FEA software.



**Figure 3.6: Group velocity dispersion curves for 20mm square steel bar generate by ABAQUS FEA software.**

It can be seen that the fastest wave mode throughout the frequency range is a fundamental wave mode and has an approximate phase and group velocity of 5000m/s. Unlike for plates and pipes, there is currently no conventional nomenclature to wave modes in square rods, therefore the wave modes present are described. The displacement pattern of this wave mode through the thickness of the bar can be found in Figure 3.7 and is symmetric around the neutral axis (called here as L) which can be analogous to S0 in plates and L(0,2) in pipes.



**Figure 3.7: Displacement plot for wave mode 'L'.**

This wave mode is non-dispersive (i.e. has a constant phase and group velocity and approximate 0 gradient) up until 80 kHz. The importance of this observation is that the fastest wave mode generated in the inspection structure can be predictably received using Equation 2.1. There are two other fundamental wave modes present and calculations were made to assess whether the second fastest wave mode present in the inspection structure would interfere with the desired wave mode being received at the distances being inspected. The slower wave modes correspond to an asymmetric displacement (called here as SH/SV) pattern analogous to A0 in plates (Figure 3.8), and L(0,1) in pipes and to a torsional displacement (called here as T) which can be corresponded to SH in plates at low frequency (Figure 3.9).

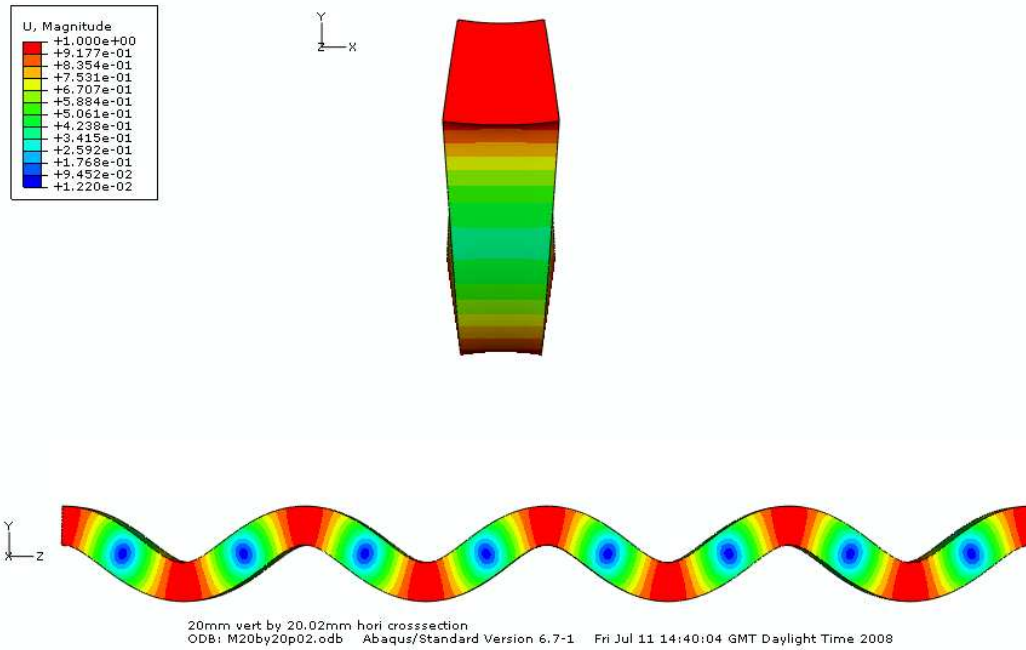


Figure 3.8: Displacement plot for wave mode ‘SH/SV’.

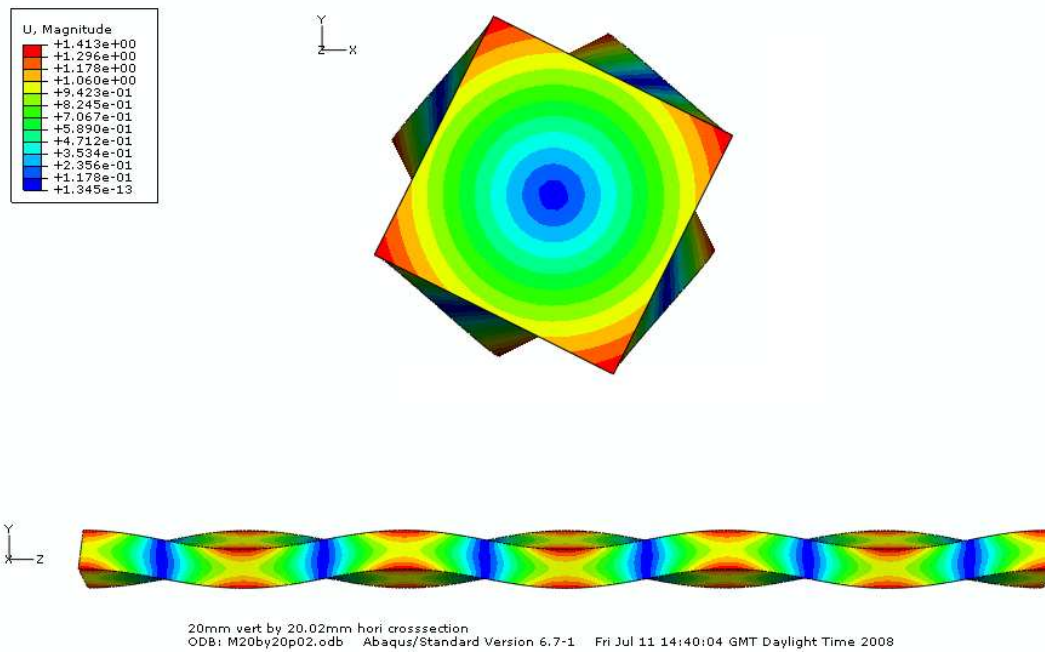


Figure 3.9: Displacement plot for wave mode ‘T’.

Above 80 kHz the group velocity of the L wave mode slows down and becomes slightly dispersive. Approximately between 80 – 85 kHz higher order wave modes, which are highly dispersive and possess more complicated displacement patterns (Appendix C), are generated within the structure at a faster phase velocity than the fundamental modes. Therefore the signal measured after 80 kHz was

expected to arrive outside the expected time window and there would be degradation in the peak-to-peak amplitude.

### 3.5 Waveguide Preparation

The bar was polished clean with a hand held polishing tool at locations A-H stated in Table 3.1. The tool was applied in steps of polishing pads from 60 grit, 120 grit, to 240 grit. Superglue was used to bond PZT elements axially to the locations A-H to act as receivers. These locations were chosen as to observe whether any inferences made from the investigation were independent of distance between transmitter and receiver. The PZT elements were adhered in an axial orientation in order to be sensitive to the displacement pattern of fastest wave mode being propagated. At each location, the PZT element was attached to a MCX cable by soldering (Figure 3.10). The PZT elements were not calibrated to possess an equally sensitivity hence comment could not be made on the rate of attenuation within the wave guide. The schematic of the test set up can be observed in Figure 3.11.

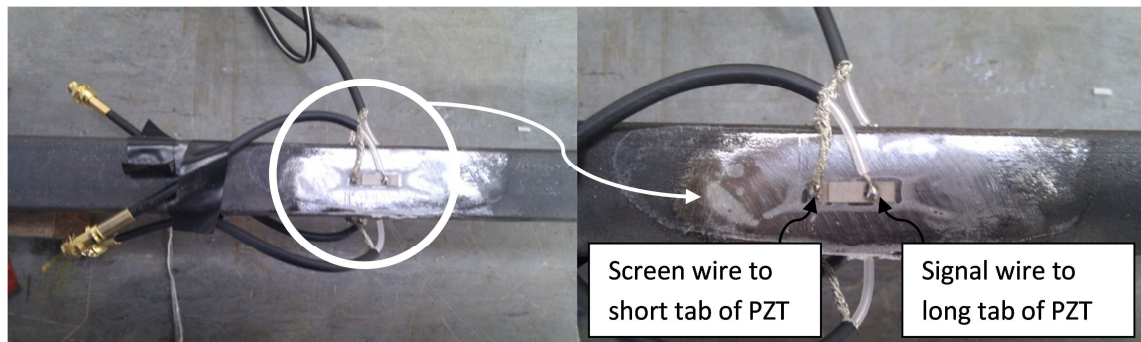


Figure 3.10: PZT element adhered to wave guide.



Figure 3.11: Schematic of transmission characterisation set up

Location Identity	Tx	A	B	C	D	E	F	G	H
Transducer Type	Commercial Shear Mode Transducer	PZT Element							
Attachment	Dry Coupled	Adhered							
Transducer Mode	Transmit	Receive							
Distance from face end (mm)	1200	2350	2850	3350	3850	4350	4850	5350	5850

**Table 3.1: Properties of each test location on waveguide.**

### **3.6 Method to Measure Transmission Magnitude of Shear PZT Transducer against variable Clamping Forces**

A pitch-catch test was conducted where a shear PZT transducer was dry coupled to a steel square cross section bar and varying forces were exerted to the transducer whilst transmitting a 10 cycle Hann window pulse at different frequencies. In positions located at several distances axially away from the transmitting transducer, there were eight independent bonded PZT elements to receive and measure the signals transmitted. The assumption is made that the receive transducers are independent of one another and do not possess the same sensitivity. Thus without any preliminary calibration set-up, any measurements made were not robust enough to comment on and quantify the attenuation of wave modes generated in the bar. The transmitting transducer was connected to a Teletest Focus<sup>+</sup> signal generator (commercially available through Plant Integrity Ltd) which is an arbitrary wave form signal generator which provides 3V peak to peak to the electrical signal transducer. The signal

transmission to the transducer was delivered by using commercially available Teletest WaveScan research software (provided by Plant Integrity Ltd) which excited the transducer with a signal of 10 cycles in a Hann window envelope for a frequency range between 20 kHz and 90 kHz. The adhesively bonded PZT elements were connected to the signal generator and the receive signal was recorded by the WaveScan software as ASCII files.

### **3.7 Procedure to Measure Transmission Magnitude of Shear PZT Transducer against variable Clamping Forces**

The transmit transducer is mounted on the transducer test rig. It is excited at a frequency range from 20 kHz to 90 kHz (with 1 kHz steps) whilst not being in contact with the inspection structure and data is collected.

The transmit transducer is then brought into contact by activating the switch of the pneumatic mounting rig and adjusting the connected air pressure supply through a regulator until the load cell reading is 25N. The transmit transducer is excited at a frequency range from 20 kHz to 90 kHz (with 1 kHz steps) and data is collected.

The pressure is then subsequently adjusted to provide 50N, 75N, 100N, 125N, 150N, 175N, 200N, 225N, 250N, 275N, 300N, 325N and 350N. Data collection is taken for a frequency range from 20 kHz to 90 kHz for each load cell reading.

This procedure is repeated four more times.

### 3.8 Results: Measurement of Transmission Magnitude of Shear PZT Transducer against variable Clamping Forces

To observe the transmission magnitude of the shear PZT transducer with respect to clamping force, a frequency response plot needs to be derived for each clamping force. A frequency response is the peak-to-peak magnitude (i.e. maximum amplitude *minus* minimum amplitude) of a separated wave mode for every frequency transmitted. Wave mode separation can be achieved by measuring the fastest wave mode travelling in the wave guide, fully separating from slower trailing wave modes.

#### 3.8.1 Time of Arrival Calculations for Fastest Wave Mode - L mode

The A-scans for each frequency under each load were imported into MATLAB for processing. The time of arrival of the fastest mode, which according to the dispersion curves in Figure 3.5 & Figure 3.6 would be the 'L' mode propagating through the wave guide, was calculated using Equation 2.1 to find the leading edge of the pulse:

$$\lambda = \frac{c_p}{f} \quad \text{Equation 2.1)}$$

The trailing edge of the pulse is calculated by:

$$\text{Time of arrival} + \text{Pulse Length} = \frac{\text{Distance}}{\text{Wave speed}} \quad \text{Equation 3.1}$$

where Pulse Length is number of cycles divided by the centre frequency of the pulse.

$$\text{Time of leading edge of pulse} = 1.15\text{m}/5000\text{ms}^{-1}$$

$$= 2.3 \times 10^{-4}\text{s}$$

The longest pulse length can be calculated by taking the lowest frequency to be excited 20 kHz with a 10 cycle Hann window pulse = 10/20000 Hz

$$= 5 \times 10^{-4}\text{s}$$

Hence the first pulse for the fastest wave mode (L mode) generated at 20 kHz will arrive at 230  $\mu\text{s}$  and the tail will end at 730  $\mu\text{s}$ .

The time of arrival of the L wave mode at the lowest frequency 20 kHz for each location is displayed in Table 3.2.

Location	Distance (m)	Time of Arrival ( $\mu\text{s}$ )	End of pulse ( $\mu\text{s}$ )
A	1.15	230	730
B	1.65	330	830
C	2.15	430	930
D	2.65	530	1030
E	3.15	630	1130
F	3.65	730	1230
G	4.15	830	1330
H	4.65	930	1430

**Table 3.2: Arrival times of L mode at 20 kHz pulse at each location.**

The calculated anticipated arrival time for a 55 kHz and 90 kHz pulse are displayed in Table 3.3 and Table 3.4 respectively. The time of arrivals for these two frequencies have been displayed as 55 kHz is the mid-point value of the frequency range and 90 kHz is the upper limit of the frequency range collected.

Location	Distance (m)	Time of Arrival ( $\mu\text{s}$ )	End of pulse ( $\mu\text{s}$ )
A	1.15	230	411
B	1.65	330	511
C	2.15	430	611
D	2.65	530	711
E	3.15	630	811
F	3.65	730	911
G	4.15	830	1011
H	4.65	930	1111

**Table 3.3: Arrival times of L mode at 55 kHz pulse at each location.**

Location	Distance (m)	Time of Arrival ( $\mu\text{s}$ )	End of pulse ( $\mu\text{s}$ )
A	1.15	230	341
B	1.65	330	441
C	2.15	430	541
D	2.65	530	641
E	3.15	630	741
F	3.65	730	841
G	4.15	830	941
H	4.65	930	1041

**Table 3.4: Arrival times of L mode at 90 kHz pulse at each location.**

Based on the predictive calculations made from Equation 2.1 and Equation 3.1 for each frequency the first pulse received at each location was measured with the window of measurement being adjusted for each frequency excited. Sample A-scan of the signals received at 20 kHz for a transducer under 200N can be seen in.

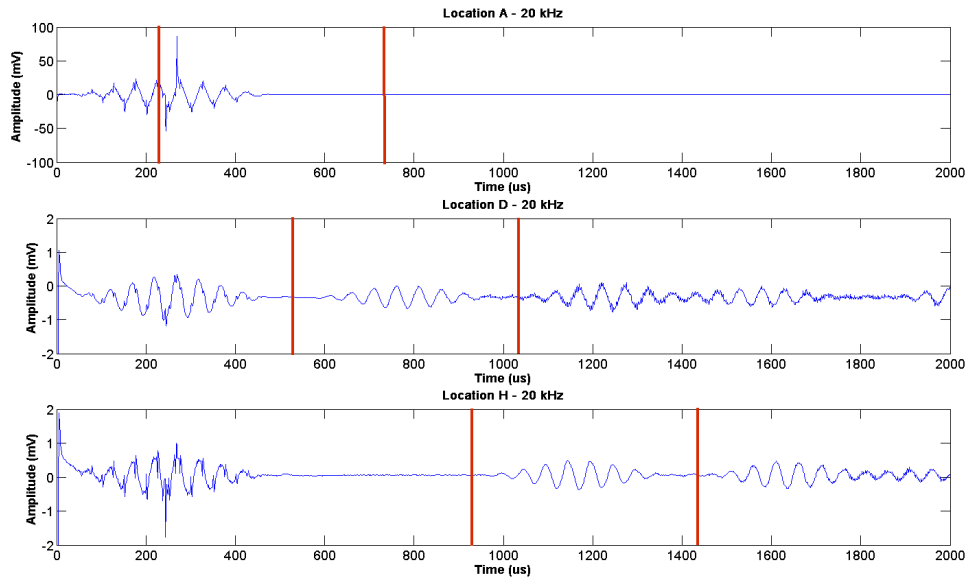


**Figure 3.12: A scans for location A, D and H at 20 kHz for a transducer loading of 200N with anticipated L mode time of arrival indicated by red line envelopes plotted in MATLAB.**

The initial pulse observed on the scans up to 400  $\mu\text{s}$  is an electrical switch on spike which occurs when the signal generator is transitioning from transmit to receive. It can be seen that the signal expected to arrive at location A is interfered by the switch on spike. However there is a pulse shape arriving in the time of arrival gates at location D and location H as expected. The signals trailing this gate are either slower wave modes or reflections from the free ends of the wave guide.

It can be seen from the A-scans at these locations at the mid-point of the frequency range, 55 kHz, in Figure 3.13 that there is nominal receive signal at location A, but a pulse envelope at the expected time of arrival at location D and location H. Again slower arriving pulses attributed to slower wave modes and reflections can be observed after the time of arrival of the L mode pulse.

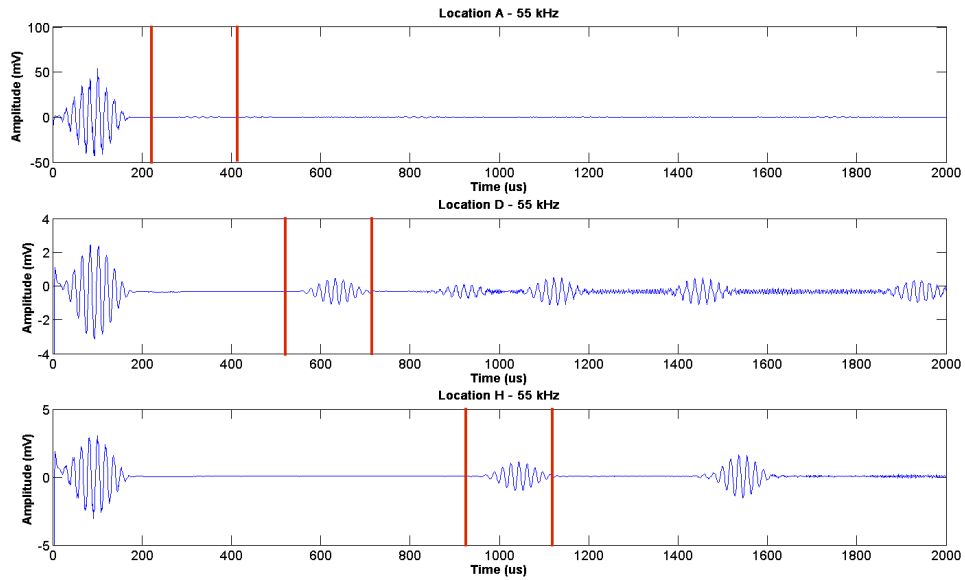


**Figure 3.13: A scans for location A, D and H at 55 kHz for a transducer loading of 200N with anticipated L mode time of arrival indicated by red line envelopes plotted in MATLAB.**

However in Figure 3.14, it is observed that the pulse of arrival on the A-scan at location D and location H for 90 kHz arrive at a later time than expected calculations. This is attributed to dispersion of the L mode at frequencies above 70 kHz which can be observed on the dispersion curves in Figure 3.5 and Figure 3.6. At location A there is still a nominal receive signal.

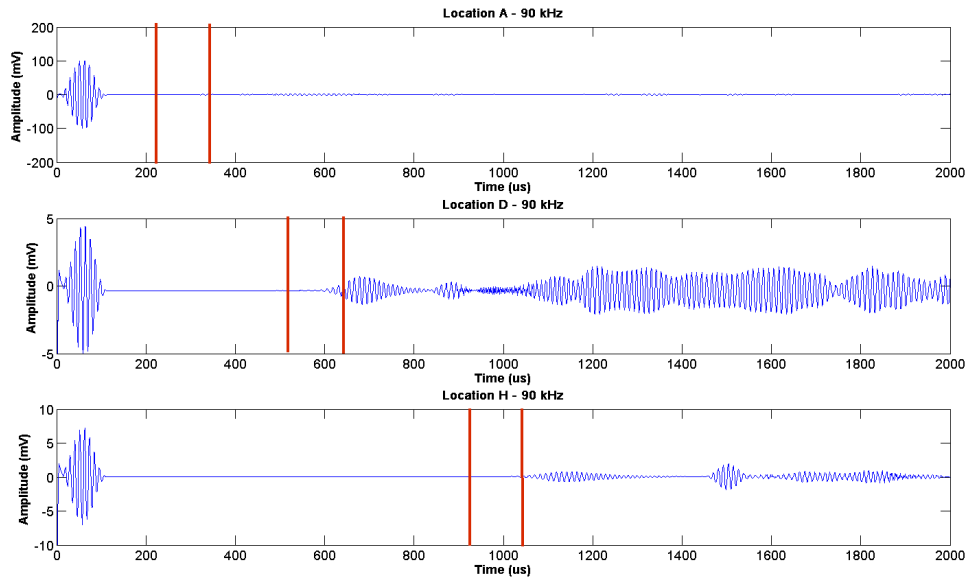


**Figure 3.14: A scans for location A, D and H at 90 kHz for a transducer loading of 200N with anticipated L mode time of arrival indicated by red line envelopes plotted in MATLAB.**

### **3.8.2 Wave Mode Separation Calculations for L Mode and SH/SV Mode**

There is a possibility that the receivers are placed within a close proximity of the source of the guided wave, as to not allow separation between the fastest fundamental L mode and second fastest SH/SV mode. This creates interference of the wave modes and potentially distorts the shape of the measured pulse. The frequency at which separation between the wave modes occurs can be calculated for a given distance. If location A is taken as an example; the arrival time of the leading edge of the pulse is assumed to be 230  $\mu\text{s}$ . Assuming the second fastest fundamental wave mode (SH/SV mode) has a phase velocity of  $3000\text{ms}^{-1}$ , the time it arrives at location A will be;

$$1.15\text{m} / 3000\text{ms}^{-1}$$

$$= 3.8 \times 10^{-4}\text{s}$$

The pulse length (in terms of time) for the fastest wave mode to be separated can now be calculated;

$$3.8 \times 10^{-4}\text{s} - 2.3 \times 10^{-4}\text{s}$$

$$= 1.5 \times 10^{-4} \text{ s}$$

Hence the frequency for this pulse can be calculated assuming a 10 cycle Hann window excitation is being transmitted;

$$\text{Frequency} = \frac{\text{Cycles}}{\text{Time}} \quad \text{Equation 3.2}$$

$$10 / 1.5 \times 10^{-4} \text{ s}$$

$$= 65217 \text{ Hz}$$

Thus at location A, two wave modes will be present when the first pulse is received if the excitation frequency transmitted is below 65 kHz. Above an excitation of 65 kHz, the wave modes will separate and the measured pulse will be free from interference. The frequency threshold where the wave modes are separated for each location of measurement is displayed in Table 3.5.

Location	Separation Frequency (kHz)
A	65
B	45
C	35
D	28
E	24
F	21
G	18
H	16

**Table 3.5: Separation frequencies at which wave modes will separate for each location.**

Therefore at locations G and H a frequency response can be plotted for all frequencies between 20 kHz and 90 kHz ensuring that the L mode pulse is not distorted by superposition with a slower wave mode pulse and a peak-to-peak amplitude measurement can be correctly made for this single mode.

### 3.8.3 Frequency Response of Transmitting Shear PZT with Respect to Variable Clamping Force

For location G and H the peak-to-peak amplitude of the measured pulse of the fastest wave mode, L-mode, is measured for each A-scan at each clamping force. This data processing was conducted using MATLAB script. These measurements are plotted as a frequency response line graph where the frequency is on the x axis and amplitude is plotted on the y axis. Each line on the graph represents a different force that the transducer was under. Figure 3.15 & Figure 3.16 display the average frequency response for both locations. The frequency plots for all locations can found in Appendix D.

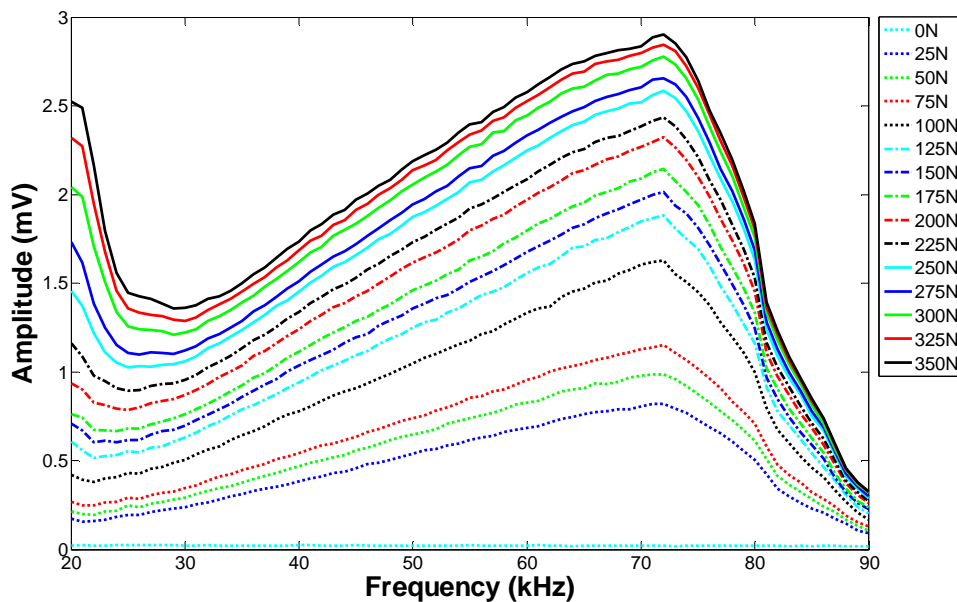


Figure 3.15: Average frequency response for Location G.

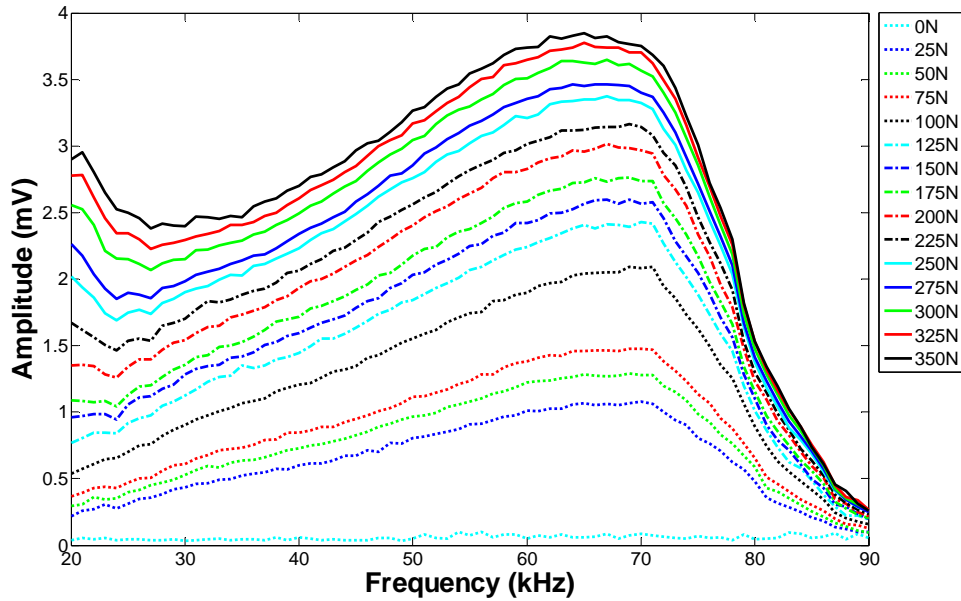


Figure 3.16: Average frequency response for Location H.

As can be seen in both these figure that there is a local peak of amplitude occurring at 20 kHz as the clamping force is increased. Above 30 kHz there is a linear increase in amplitude as frequency increases until a drop in amplitude after 70 kHz. This drop in amplitude is attributed to dispersion where the pulse begins to elongate above 70 kHz due to the discrepancy between group and phase velocity and the later time of arrival which has not been accounted for when calculating the time gates to plot the frequency response.

### 3.8.4 Transmission Output Magnitude of Shear PZT with Respect to Clamping Force

To demonstrate the relationship between transducer transmission amplitude and clamping force Figure 3.17 and Figure 3.18 have been generated in MATLAB. These two figures use the peak-to-peak amplitude of the fastest arriving L mode from the A-scans received at location G and location H. For clarity, only 8 frequencies have been displayed; 20, 30, 40, 50, 60, 70, 80 and 90 kHz. These plots for all locations can be observed in Appendix D.

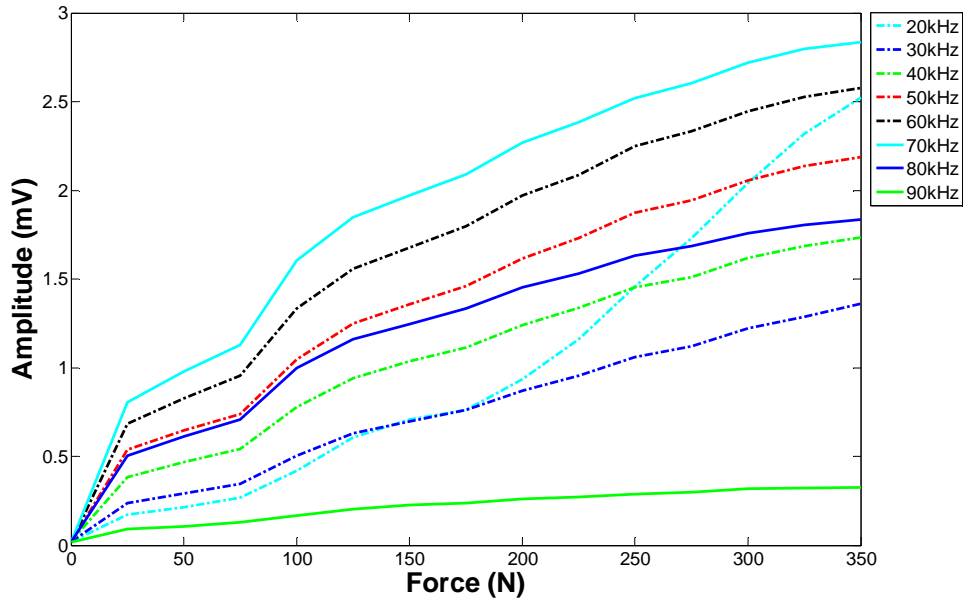


Figure 3.17: Average amplitude versus force for location G.

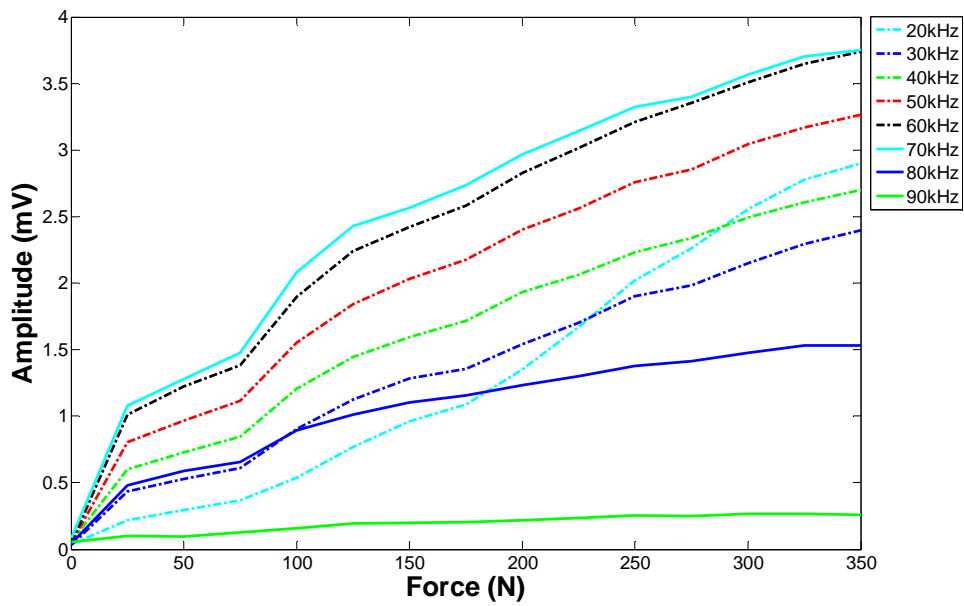
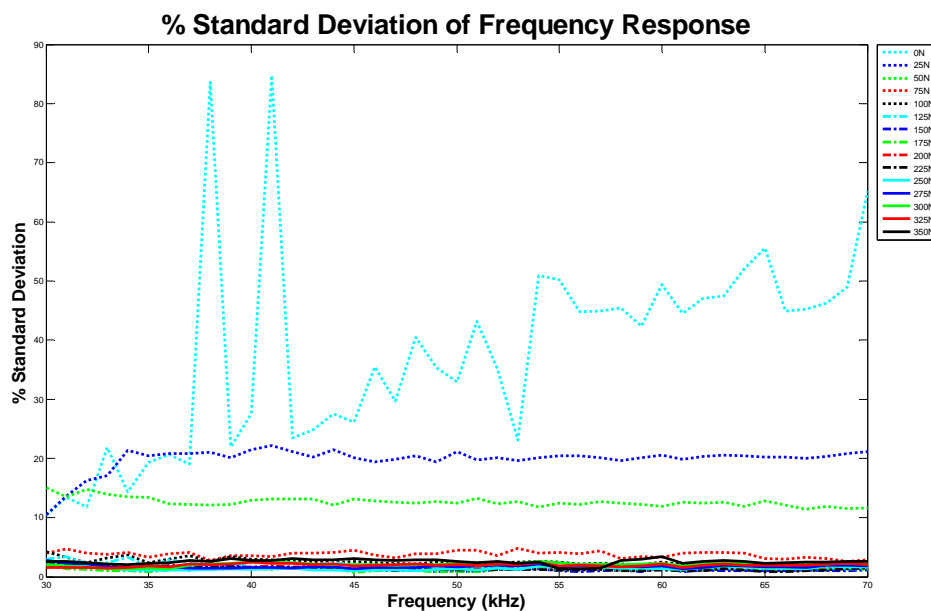


Figure 3.18: Average amplitude versus force for location H.

It can be seen that similarly to Alleyne & Cawley (1996b), Degertekin & Khuri-Yakhub (2007) and the hypothesised contact radius due to increasing force observed in Figure 3.2 that there is a nonlinear relationship between transmitted amplitude of a shear PZT and clamping force. However in contrast to Alleyne & Cawley (1996b), the magnitude of amplitude increases above a transducer clamping

force of 50 N and this is true for all frequencies including when the pulse suffers distortion due to dispersion at higher frequencies. Aside from frequencies between 20 kHz and 25 kHz the trend of amplitude with respect to clamping force follows Hertzian classic contact theory where the contact radius (and ultimately contact area) is proportional to the force applied to the power of a third. It can be concluded that the increase in contact area between transducer and wave guide will increase the amplitude of the transmitted signal.

The standard deviations of the five tests collected at location G were calculated using MATLAB script; these were then calculated as a percentage of the mean value and plotted (Figure 3.19).



**Figure 3.19: Percentage standard deviation for frequency response of repeated test.**

According to Figure 3.19, when the shear PZT transducer is clamped with a force higher than 75N, there is less than a deviation of amplitude magnitude of 5%, however for clamping forces of 25N and 50N there is less repeatability, which may be due to the lack of strong contact junctions between the transducer and the wave guide.

### 3.9 Method to Measure Transmission Magnitude of Shear PZT Transducer against variable Contact Area Surface Roughness

A study of the effect of surface roughness at the contacting location between the transducer and the waveguide and the resultant transmission response has not been conducted. An investigation to study this was performed. As stated by Alleyne & Cawley (1996b) the typical measured Ra of bare pipeline in chemical plants are between 8-12 $\mu\text{m}$ , however it is common industry practice to prepare oil and gas pipeline to grit blast the surface prior to applying adhesives or protective coatings. The approximate roughness range produced by the grit blasting for these tests is between 30 $\mu\text{m}$  and 90 $\mu\text{m}$ .

A pitch-catch test was conducted where the transducer was dry coupled to a steel square 20mm x20mm cross section bar with a grit blasted surface 2350mm from a face end. A 200N load was exerted to the transducer whilst transmitting a 10 cycle Hann window pulse at different frequencies. A schematic of the test setup can be seen in Figure 3.20.

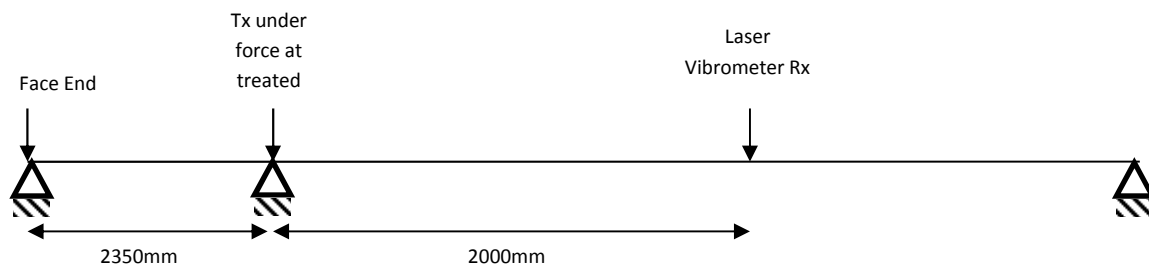


Figure 3.20: Schematic of varied surface roughness test set up.

Five bars were subjected to grit blasting and a sample of each grit blasted process was optically inspected and measured under an Olympus LEXT microscope. An image of each surface can be found in Appendix E. The type of treatment and the resultant surface roughness can be observed in Table 3.6.

Grit blast media	Surface Roughness (Ra)
Alumina 100	29.37 $\mu$ m
Alumina 36	42.38 $\mu$ m
Alumina 12	52.62 $\mu$ m
Alumina 20	58.96 $\mu$ m
Rough Iron G55	87.40 $\mu$ m

**Table 3.6: Grit blast media applied to steel waveguide and measurements of surface roughness on steel waveguide after treatment.**

In a position located at 2000mm axially away from the transmitting transducer, a laser vibrometer measured the out of plane displacement generated by the transducer over time. As seen from calculations in Section 3.8.2 above this distance is sufficient to provide wave mode separation. A non-contact laser vibrometer (Polytec PSV400) was adopted in a bid to control all other variables apart from the surface roughness where the transducer was sat. Adhesively bond PZTs would introduce variation from the integrity of the bond line in addition to the manufacturing tolerance of the element itself. The laser vibrometer uses a precision optical transducer to determine vibration velocity and displacement at a point of interest. It uses the Doppler-effect by transmitting a laser beam and sensing the frequency shift of back scattered light from a moving surface. To be able to determine the velocity of an object, the received signal is measured against a reference laser signal to calculate the Doppler frequency. This is done in the vibrometer by using a laser interferometer (Polytec GmbH, 2011).

### **3.10 Procedure to Measure Transmission Magnitude of Shear PZT Transducer against variable Contact Area Surface Roughness**

A transmit shear PZT transducer is mounted on the transducer test rig and connected to a Teletest Focus<sup>+</sup> signal generator. A wave guide is placed in the test rig. The transmit transducer is then brought into contact by activating the switch of the pneumatic mounting rig and adjusting the connected air pressure supply until the load cell reading is 200N. The transmit transducer is excited by Teletest WaveScan research software at a frequency range from 30 kHz to 70 kHz (with 5 kHz steps) and received signal is collected in the time domain by Polytec PSV Scanning Vibrometer Software in the form of txt files. This frequency range is chosen as this region creates a linear frequency response for transmission on the waveguide on the evidence found in Section 3.8.3.

The transducer is then dismantled and the test bar is substituted by a test bar treated with an alternative grit blasted surface. The process is repeated until all test bars have been inspected.

This procedure is repeated two more times.

### **3.11 Results: Measurement of Transmission Magnitude of Shear PZT Transducer against variable Contact Area Surface Roughness**

The raw A-scans collected from each bar were subjected to the same time gating and peak-to-peak calculation as seen in Section 3.8.1 and 3.8.2. The average frequency response for each waveguide is found in Figure 3.21.

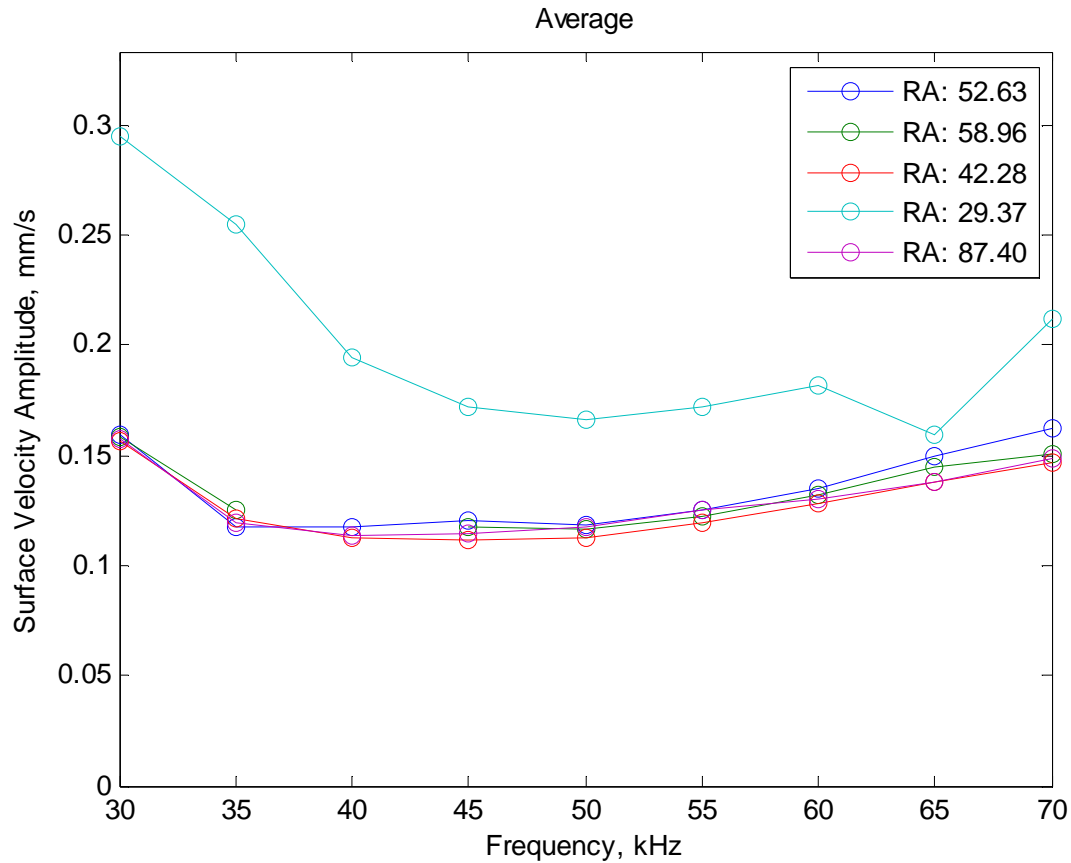


**Figure 3.21: Average frequency response of Shear PZT transmitting through wave guide whilst in contact with varying surface roughness.**

The frequency response in Figure 3.21 is measured in terms of surface velocity (mm/s) in contrast to voltage seen in Section 3.8.3 as the laser vibrometer used in these set of experiments is sensitive to surface displacements rather than PZTs which convert displacement to voltage. The surface velocity measurement is indicative of the displacement generated at the point of receive. The frequency response for the wave guides that contain an Ra of 42 to 87 have a linear frequency response between 35 kHz and 70 kHz which correlates to frequency responses seen in Section 3.8.3. There is a local peak of amplitude at 30 kHz which again correlates to a local peak that is generated at 20 kHz on the frequency response plot in Section 3.8.3. Between a contact surface roughness of Ra 42 and 87 the frequency response produced for each wave guide is within 10% of a mean frequency response. The waveguide that possessed the smoothest surface roughness of Ra 29 produced an outlier frequency response. The maximum discrepancy between this outlier frequency response and the other responses occurs at 30 kHz where there is a signal-to-noise difference of 6 dB. The general difference between

the frequency responses for the remaining frequencies is approximately 3 dB apart from at 65 kHz where the received values are nominally the same.

### **3.12 Discussion of the Transmission Characteristics of a Shear PZT Dry Coupled Transducer**

As can be seen in Figure 3.17 and Figure 3.18 the relationship between the forces applied on the transducer and peak-to-peak amplitude output is non-linear as predicted by Hertzian contact theory discussed in Section 3.2. The trend applies to all frequencies being excited apart from at 20 kHz. The data gathered correlates to the power-law of a two-thirds proportionality between normal forces upon a body and the resultant real contact radius discussed earlier in Section 3.2.

However, with respect to the absolute values of amplitude produced and frequency excited, the output is heavily frequency dependent which can be seen in Figure 3.15 and Figure 3.16. As discussed previously in Section 3.4 the signal excited between 20 and 70 kHz is expected to be non-dispersive in nature. Generally the relationship between the frequency and the transmitted amplitude is linear. Although the frequency response in the range of 20-30 kHz is of interest as there is a local peak of output, which becomes more pronounced as an increase in force is applied to the transducer. This local peak of amplitude at the lower frequency range due to the force is significant. For instance, if the linear line of best fit for the frequency response between 30 and 70 kHz at 350N at location G (Figure 3.15) is derived, this would approximate an intersect of 1mV at 20 kHz. The actual measure value is approximately 2.5 mV, which indicates a signal-to-noise gain of 8dB.

The heightened amplitude output of the transducer at 20 kHz due to the increase in clamping force indicates that there is an additional function present in the system aside from the increase in contact area which enables the transducer to excite a larger amplitude output within this lower frequency spectrum.

The frequency response after 70 kHz shows a reduction in amplitude recorded and this can be attributed to the dispersive nature of the signal where the pulse becomes elongated, losing its shape. In addition the pulse is arriving at a slower time than expected, which can be seen in Figure 3.14. As

a result of this, it can be seen in Figure 3.17 and Figure 3.18 that the effects of higher force on the sensor at higher frequencies is greatly reduced.

When using multiple shear PZT transducers as part of a pipe array for inspection, it is desirable to inspect as long a distance of pipeline as feasible from one location. This is achieved by increasing the signal-to-noise of the tool and the signal, which preferably would be a non-dispersive axisymmetric mode (i.e. T(0,1) or L(0,2)). It has been shown in Figure 3.17 and Figure 3.18 that when operating a transducer under a 350N clamping force in contrast to a 100N force a non-dispersive symmetric mode signal can be increased up to 9 dB. This can be translated to bare steel pipeline where attenuation is 1dB/metre which means operating at clamping forces of 350N in contrast 100N would achieve additional inspection range of 9m as long as the coherent noise level is a constant. In contrast the signal increase between operating at clamping 200N and 350N is approximately 4 dB, which would yield an extra 4m inspection length. This would indicate that in the design of GW tools for pipe inspection, to increase inspection range it is desired to increase the force within a safe practical limit.

It can be seen by the percentage standard deviation of the tests that the variability of the data collected is below 10% when the transducer is subjected to a load higher than 75N (Figure 3.19). Under a load of 75N, the unpredictability of nominal contact and the junctions formed leads to a fluctuation in the transmitted output which has a greater effect due to the weak strength of the signal. It can be seen that the inherent noise of the system (whilst the transducer is under 0N) has a tendency to vary, however the absolute magnitude of the noise is negligible in comparison to collected signals. In general the repeatability demonstrated by this statistical analysis instils confidence in the results and the subsequent deductions made.

The effect of surface roughness on the frequency response of the transducer showed that for surfaces rougher than Ra of 42µm there was very little influence. The smoothest surface with Ra of 29 µm showed a slight increase in measured amplitude with a signal-to-noise increase of approximately 3 to 6dB. This somewhat correlates to similar work carried out with bulk wave transducers having an

improved transmission through smoother surfaces. The effect may also be due to the smoothest surface possessing the cleanest surface with the removal of dust and dirt. The other mechanism may be due to the fact that the asperities at the contacting surface may deform within an elastic region due to smooth polished surfaces having a low plasticity index (Appendix B).

### **3.13 Contribution to Knowledge from Chapter 3**

A relationship between a shear PZT transducer transmission amplitude and dry coupling force has been demonstrated to be proportional to the power of two-thirds up to a clamping force of 350N. Furthermore it has been shown that this trend correlates to classical elastic contact theory and that this is the mechanism behind transmission of ultrasound between the transducer and the wave guide. This relationship between transmission output and coupling force is true for a frequency range of 20 to 90 kHz. It has been shown that there is an additional function at 20 kHz due to clamping forces above 100N which creates a rise in transmission magnitude which is not related to an increase in contact area. It has also been shown that for a contact area surface roughness between the wave guide and the transducer which ranges between Ra 40 and 90 there is no discernible change in transmission output.

## **4. Resonance Characteristic of Shear PZT Transducer with Respect to Dry Coupling**

### **4.1 Introduction to Chapter 4**

In Chapter 0, it was observed that there was a local peak in transmission of a shear PZT transducer approximately at 20 kHz as the transducer was constrained by increasing force. It was concluded, that in contrast to frequencies above 20 kHz there was additional mechanism which increased the transmission magnitude aside from the increase in contact area between the transducer and the waveguide. It has been assumed that the electrical impedance/admittance and resonant characteristics of the transducer would remain the same despite the change in coupling force. As discussed in Section 2.7 the electrical resonance of the transducer has been recorded at 1.2 MHz in free air conditions. However there is no literature that considers the onset of a mechanical resonance which is deduced by the contact of the shear PZT transducer with the waveguide. The initial investigation in this chapter was to use electrical impedance measurements to detect additional resonances due to coupling of the transducer within the operating frequency (20 to 100 kHz).

### **4.2 Method to Measure Electrical Impedance of Shear PZT Transducer under a Variable Coupling Force**

The transducer is mounted in the transducer testing rig (Section 3.3). The MCX connector of the transducer is connected to an impedance analyser (Solatron SII260). The impedance magnitude and phase of the transducer is measured whilst it is being excited with a frequency from 1 Hz to 32 MHz whilst in free air conditions (out of contact with the steel bar).

The transmit transducer is then brought into contact by activating the switch of the test rig and adjusting the connected air pressure supply until the load cell reading is 25N. The transducer is excited with a frequency ranging from 1 Hz to 32 MHz and impedance data is collected as a TXT file.

The pressure is then subsequently adjusted to 50N, 75N, 100N, 125N, 150N, 175N, 200N, 225N, 250N, 275N, 300N, 325N and 350N. Impedance data collection is taken for each load cell reading.

### 4.3 Results: Measurement of Electrical Impedance of Shear PZT Transducer under a Variable Coupling Force

The TXT files for the impedance magnitude and impedance phase for each clamping force were imported into MATLAB and plotted for all frequencies. These can be seen in Figure 4.1 and Figure 4.2.

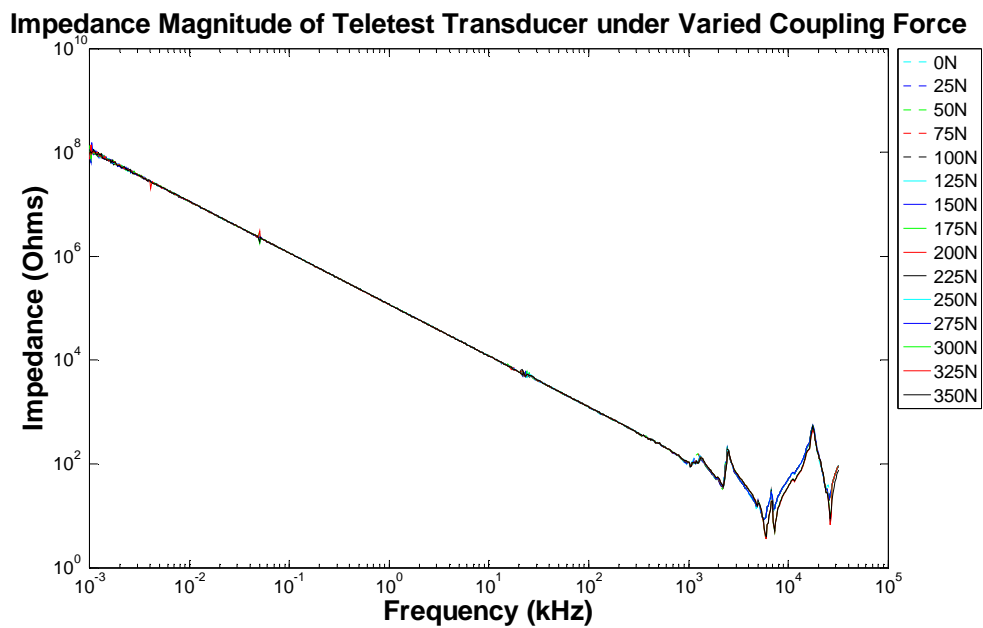


Figure 4.1: Impedance Magnitude of transducer for varying loading conditions on a steel bar.

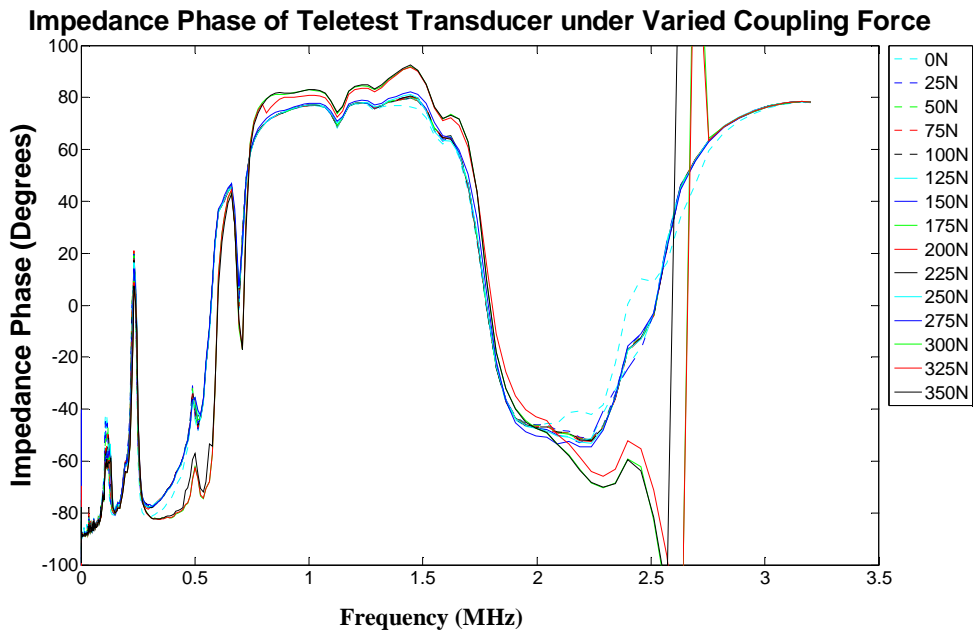


Figure 4.2: Impedance Phase of transducer for varying loading conditions on a steel bar.

It can be seen in Figure 4.1 that for all transducer coupling forces the macroscopic impedance magnitude peaks occur above 1 MHz which agrees with the literature. When the impedance trace is magnified to the frequency range of interest (20 to 100 kHz) it is found that the transducer in free air conditions does not produce any impedance peaks (Figure 4.3).

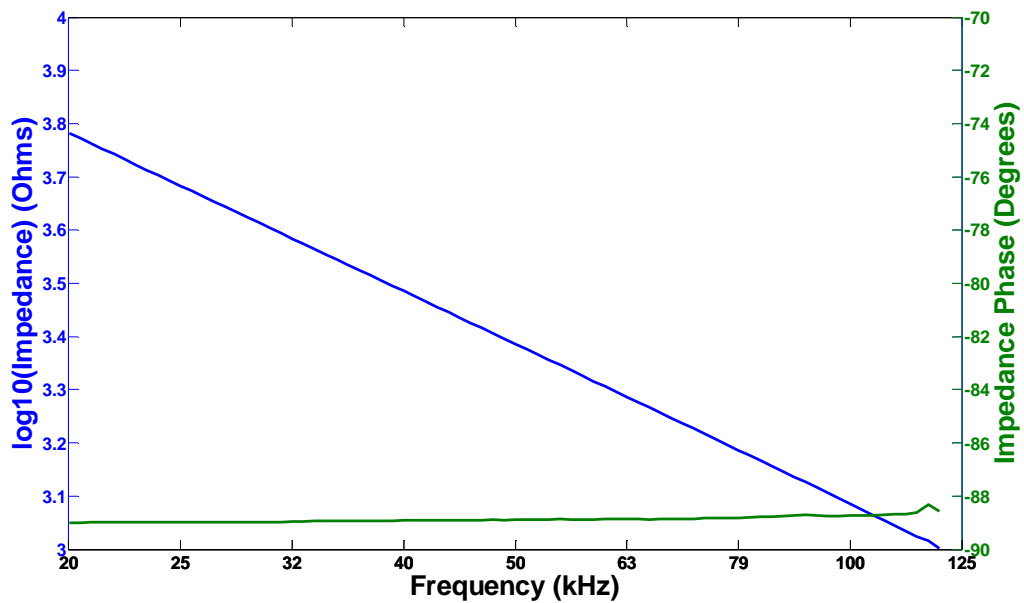


Figure 4.3: Impedance characteristics of transducer under 0N load on Steel bar.

However as the force on the transducer increases, an impedance peak begins to develop at 20 kHz which can be observed in Figure 4.4

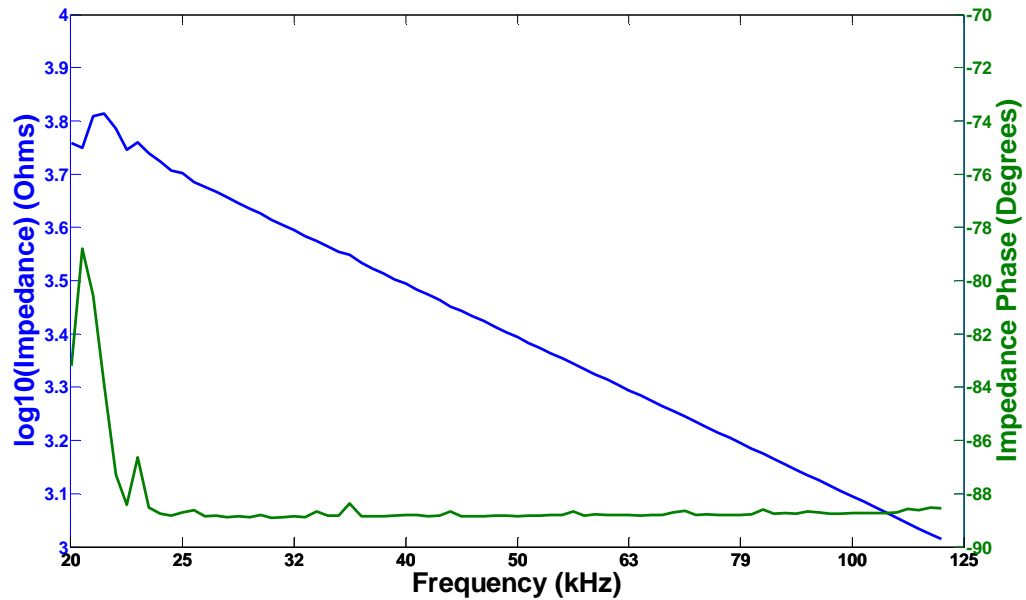


Figure 4.4: Impedance characteristics of transducer under 100N load on Steel bar.

As the force is increased to 200N this then develops into two distinct resonances at a higher frequency of 23 and 25 kHz.

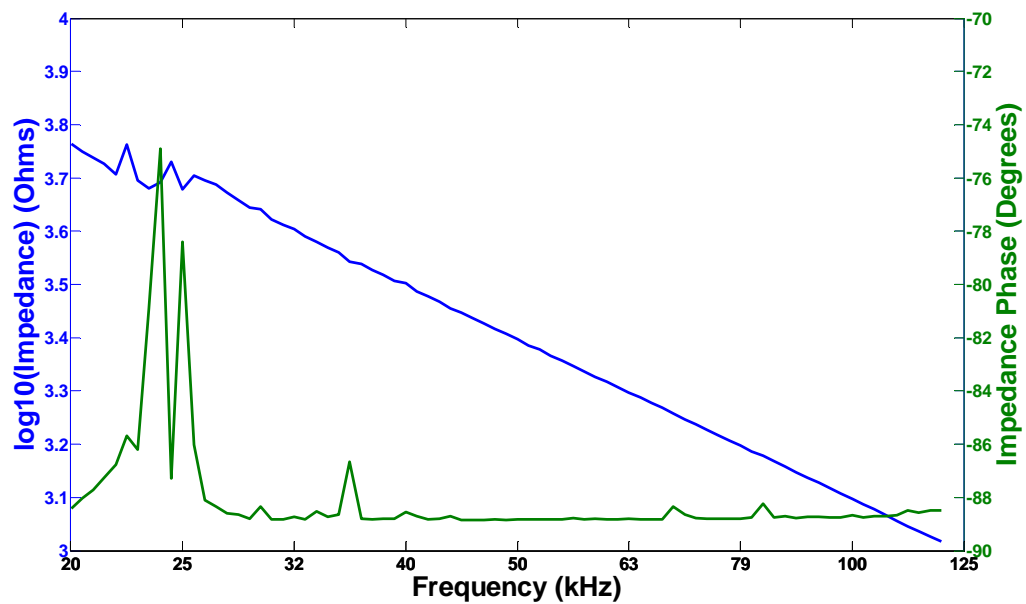
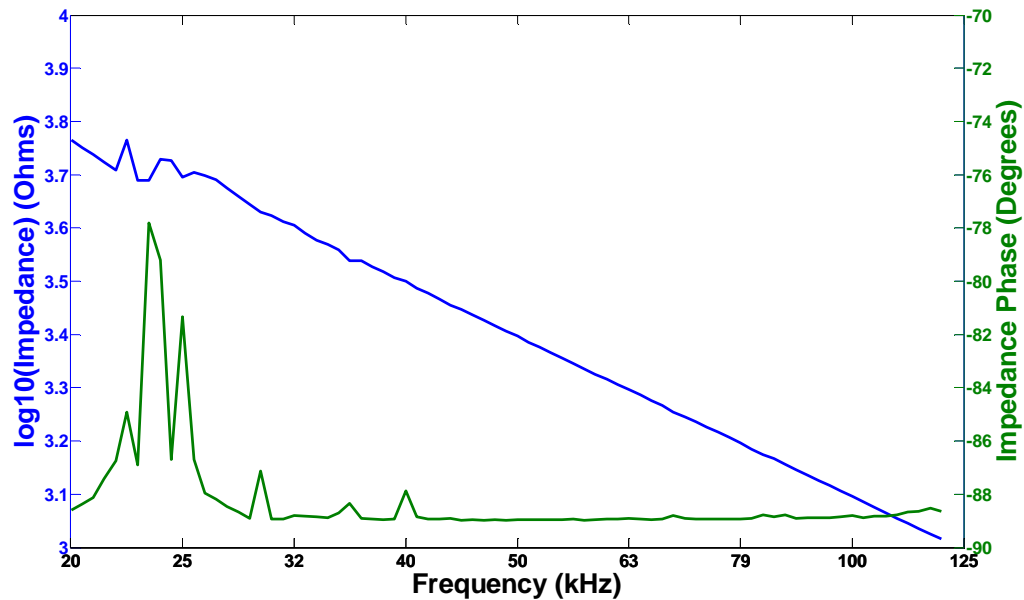


Figure 4.5: Impedance characteristics of transducer under 200N load on Steel bar.

This localised forced dependent electrical resonance begins to become broader when the transducer is under the maximum load of 350N. The broadness of the resonances are centred around 23 kHz, spanning between 20 kHz and 30 kHz as can be seen Figure 4.6.



**Figure 4.6: Impedance characteristics of transducer under 350N load on Steel bar.**

The impedance traces for all load conditions can be found in Appendix F. The phase of the transducer changes from a capacitive state and tends more towards to an inductive state between 20 and 40 kHz as load increases, although the transducer never reaches inductance. This implies that the power efficiency of the transducer is rising within this frequency range as the applied force is increased. This correlates to the behaviour observed in ultrasonic frequency responses prior in Section 3.8.

#### **4.4 Measurement of Mechanical Resonance of Shear PZT Transducer under a Variable Coupling Force**

The conventional method in the literature to detect resonance of ultrasonic transducers has been conducted by measuring electrical impedance. It has been detected that there is a local resonance which correlates to an increase in ultrasonic transmission output which is force dependent but not attributed to the increase in contact area. The investigation in this section conducts laser vibrometry analysis of the transducer structure whilst excited in the operating frequency range under varying coupling forces to obtain the resonances formed by contact present in the backing mass and changes in the resonant behaviour. The purpose was to distinguish whether there is any mechanical/structural design effect contributing to the increase in power efficiency.

#### **4.5 Hypothesis: Mechanical Resonance of a Shear PZT Transducer with under a Variable Coupling Force**

It is postulated that as the behaviour is related to an increase in force and particularly there is a power efficiency effect that the introduction of force induces a natural resonance in the transducer. This can be predicted by taking into account Equation 2.8 from K.L. Johnson (1987):

$$\omega^2 = \frac{s}{m_1 + m_2} \frac{m_1 m_2}{r} \quad \text{Equation 2.8}$$

If the transducer is assumed to be a steel half sphere with a radius of 14mm analogous to the height and the surface of the waveguide where the transducer is loaded onto is also approximated as a steel half sphere with a radius of 14mm, the predicted natural contact resonance can be found in Table 4.1.

Load (N)	Frequency (kHz)
0	0
25	7.965
50	8.941
75	9.566
100	10.036
125	10.416
150	10.737
175	11.017
200	11.265
225	11.488
250	11.692
275	11.879
300	12.052
325	12.214
350	12.366
375	12.509
400	12.644

**Table 4.1: Predicted contact resonance between two steel half spheres.**

Alternatively the transducer can be assumed to be a harder alumina half sphere to accommodate the properties of the alumina wear plate which is the contact face of the transducer that engages the waveguide. The contact resonance predictions for this alternative can be found in Table 4.2.

Load (N)	Frequency (kHz)
0	0
25	10.492
50	11.777
75	12.601
100	13.219
125	13.720
150	14.144
175	14.512
200	14.838
225	15.133
250	15.401
275	15.647
300	15.876
325	16.089
350	16.289
375	16.477
400	16.656

**Table 4.2: Predicted contact resonance between steel half sphere and alumina half sphere.**

It can be seen in Table 4.1 and Table 4.2 that a contact resonance can be predicted when two bodies of similar masses to the transducer and the interfacing section of the wave guide exhibiting the same material properties. Furthermore at which frequency this resonance is induced is dependent on

normal force applied on these bodies. The resonant frequencies predicted are between the 8 kHz and 17 kHz range.

The purpose of the following investigation was to empirically detect the presence of a contact resonance occurring within the transducer. In addition this would determine if the source of the increase in performance of the transducer ultrasonically and electrically is due to a natural frequency of the system.

## 4.6 Method to Measure Mechanical Resonance of a Shear PZT Transducer under a Variable Coupling Force

A transducer was mounted in a pneumatically driven test rig (Section 3.3). A laser vibrometer was used to measure the surface velocity normal to the transducer backing mass face (Figure 4.7). This face had been adhesively coated with a layer of retro reflective glass beads (45 to 63 microns diameter) to ensure the laser was adequately reflected for detection. The laser vibrometer measure points on a 45 x 45 square grid on this surface. The transducer was excited with a chirp broad band signal which excites a frequency of 10 kHz to 450 kHz. Measurements were initially taken whilst the transducer was out of contact with the wave guide. Subsequently the transducer was brought into contact with a 20mm squared steel bar and measurements were taken at incremental steps of applied force of 25N until reaching a maximum load cell reading of 350N.

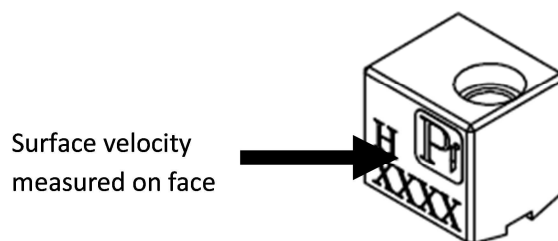
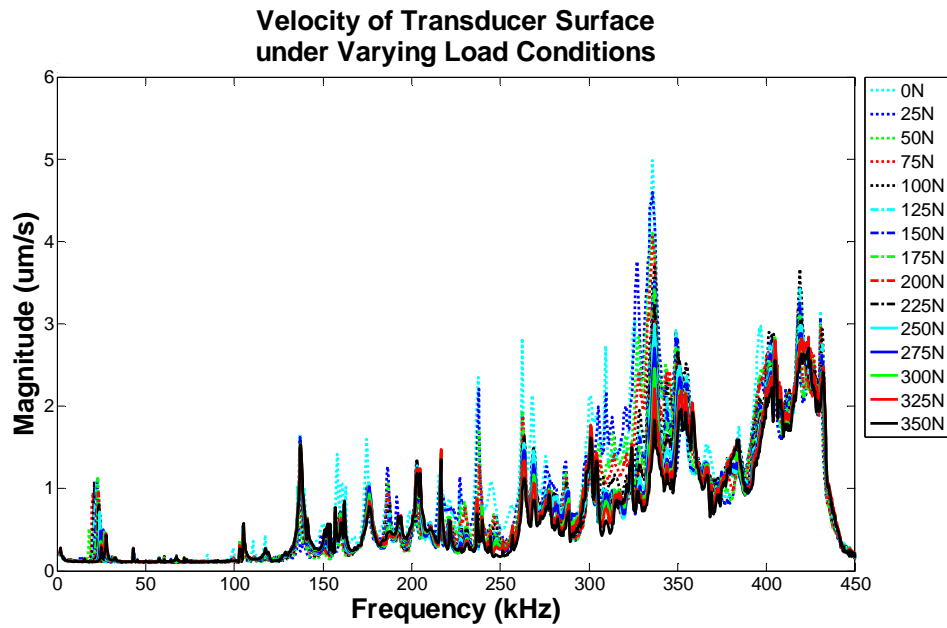


Figure 4.7: Isotropic view of transducer and indication of measured surface.

## 4.7 Results: Measurement of Mechanical Resonance of a Shear PZT Transducer under a Variable Coupling Force

Using the surface velocity measurements in the time domain for each measured point on the transducer surface the Polytec PSV Scanning Vibrometer Software was able to produce a Fourier Transform plot which indicated the frequencies where there was significant coherent displacement in the transducer. These frequency domain plots were exported as TXT files and plotted in MATLAB. The frequency domain plot for the broadband excitation up to 450 kHz can be observed in figure Figure 4.8.



**Figure 4.8: Frequency domain plot of transducer surface velocity for 0 to 450 kHz excited under varied load.**

It is seen in Figure 4.8 that there are many displacements in the transducer backing mass above 100 kHz independent of the coupling force applied on the transducer. However within the frequency range of 0 to 100 kHz it is observed that there are different magnitudes of surface velocity depending on the force applied to the transducer. In Figure 4.9, there is nominal displacement within the block in free air conditions between 0 to 100 kHz. However there is a displacement within the transducer at 140 kHz which coincide with the findings by Alleyne & Cawley (1995) and Chaston (2008).

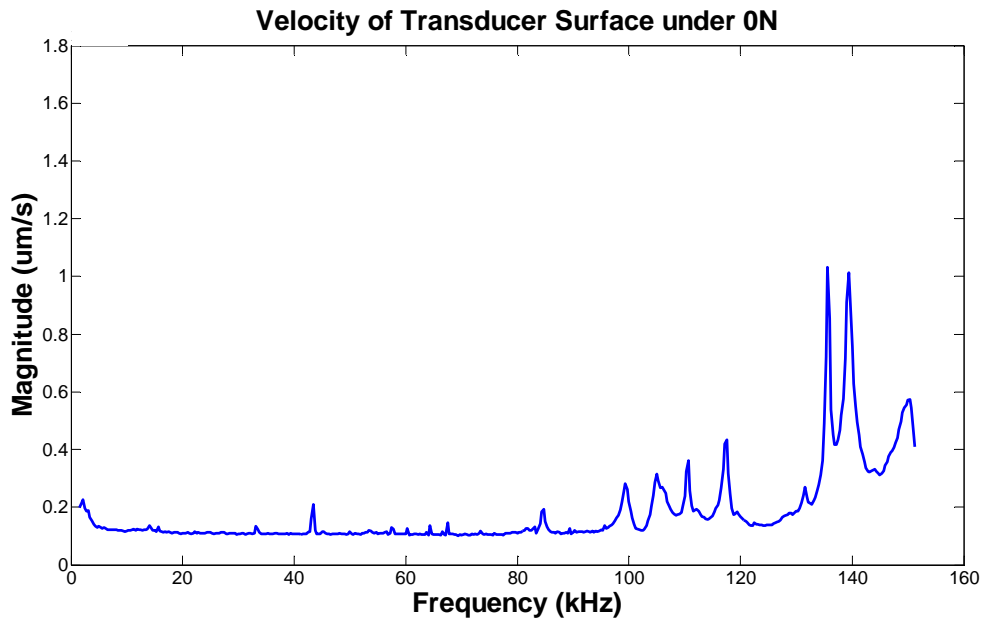


Figure 4.9: Frequency domain plot of transducer surface velocity for 0 to 160 kHz excited under 0N load.

As the coupling force is increased to 100N onto the transducer a peak at 21 kHz is produced indicating a displacement in the block (Figure 4.10).

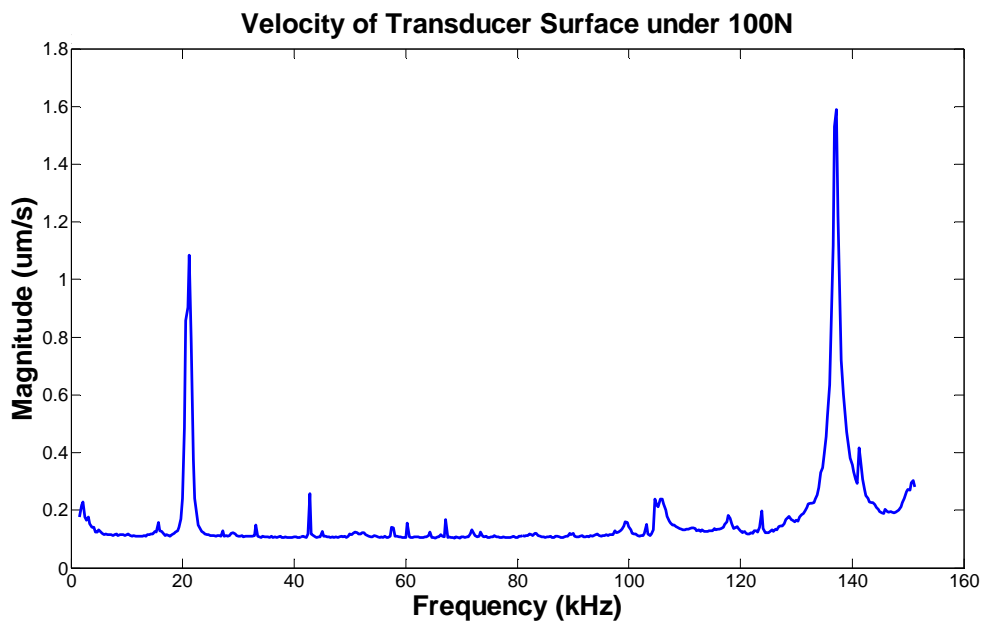
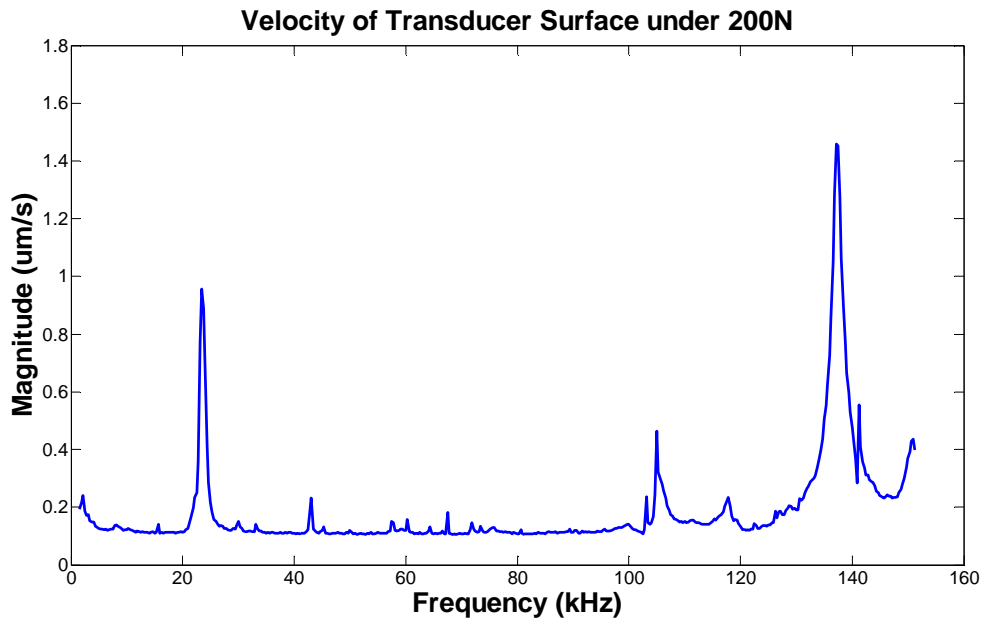


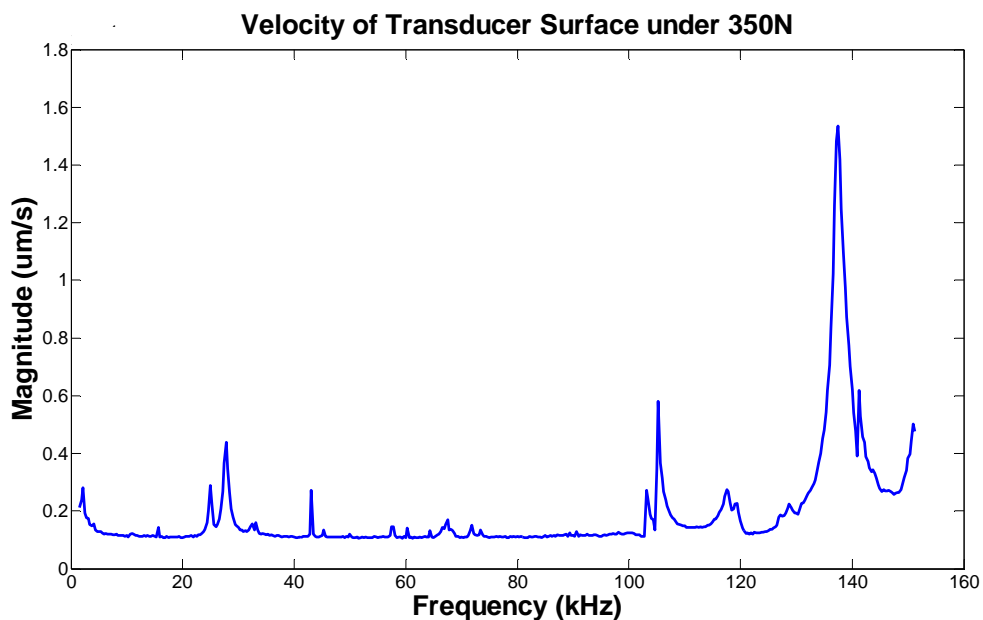
Figure 4.10: Frequency domain plot of transducer surface velocity for 0 to 160 kHz excited under 100N load.

This peak begins to move up the frequency range as the load increases, where under a 200N loading the frequency where the displacement in the block occurs is at 23 kHz (Figure 4.11).



**Figure 4.11: Frequency domain plot of transducer surface velocity for 0 to 160 kHz excited under 200N load.**

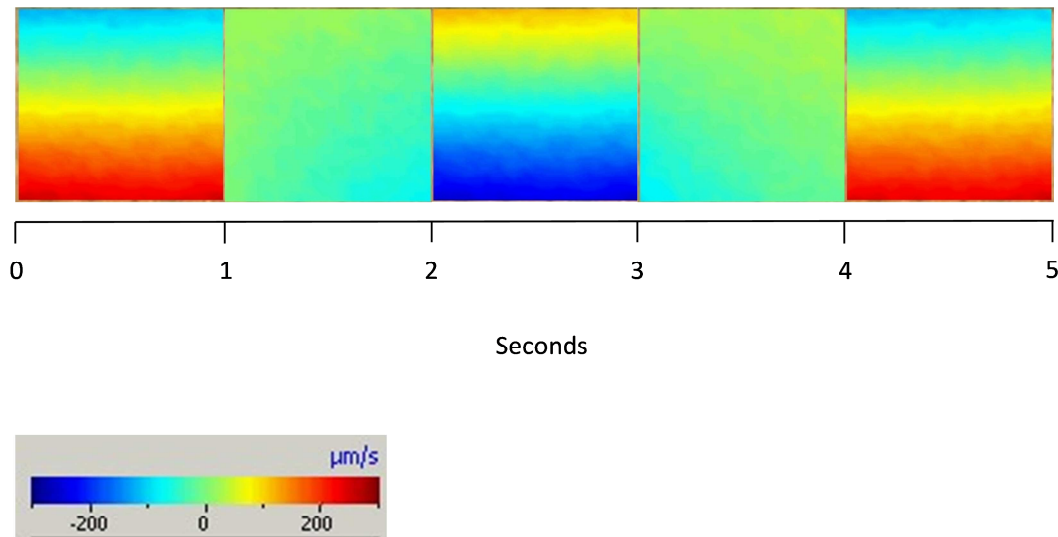
At a maximum coupling force of 350N, the frequency domain plot shows that this peak is split into two distinct peaks which move to 25 kHz and 28 kHz and broaden out to span between 23 kHz and 30 kHz (Figure 4.12).



**Figure 4.12: Frequency domain plot of transducer surface velocity for 0 to 160 kHz excited under 350N load.**

Frequency domain plots between 0 to 160 kHz for all coupling forces can be found in Appendix G.

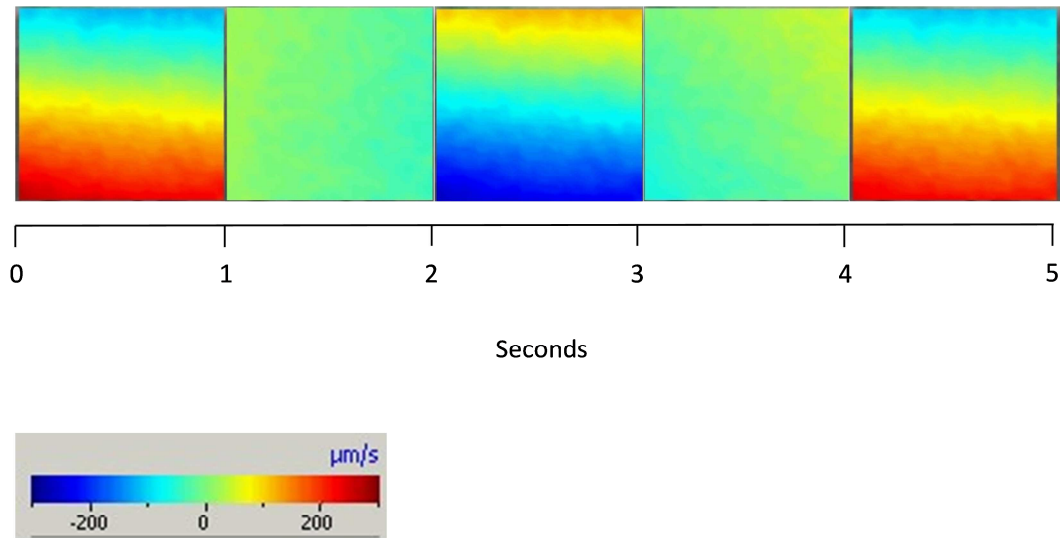
The surface velocity plots of the face at the frequencies that the peaks occurred due to the force coupling were observed in the time domain in order to understand the motion of the displacement within the transducer backing mass (Figure 4.13).



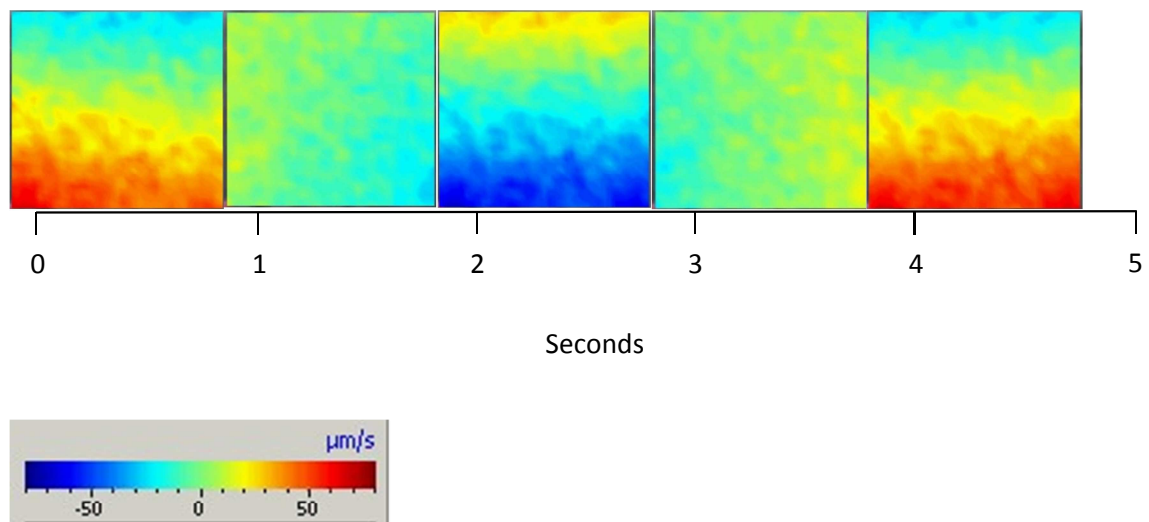
**Figure 4.13: Transducer surface velocity pattern over time at 21 kHz under a coupling force of 100N.**

Figure 4.13 shows that there is a motion in the backing block of the transducer which is in the shear plane of the transducer. The transducer backing block has high displacement on the lower edge of the transducer block (where the PZT is located) moving normal to the transducer face, whilst the upper edge of the transducer block is displacing equally but in the opposite direction. The block then oscillates over time around a plane located at the mid-point of the height of the transducer and the upper edge of the transducer block has displaced in the opposite direction in addition to the lower edge displacing in its respective counter direction.

This velocity pattern can also be observed in the frequency domain peak which moves from 21 kHz to 23 kHz with an increase load of 200N (Figure 4.14) and also can be seen at 25 kHz when the transducer is loaded with 350N (Figure 4.15).



**Figure 4.14: Transducer surface velocity pattern over time at 23 kHz under a coupling force of 200N.**



**Figure 4.15: Transducer surface velocity pattern over time at 25 kHz under a coupling force of 350N.**

The second peak developed at 28 kHz under a transducer coupling force of 350N has a shear plane motion too (Figure 4.16). At this frequency the transducer backing block has high displacement on the right hand edge of the transducer block moving normal to the transducer face, whilst the left hand edge of the transducer block is displacing equally but in the opposite direction. The block then oscillates over time around a plane located at the mid-point of the length of the transducer and the left edge of the transduce block has displaced in the opposite direction in addition to the right edge

displacing in its respective counter direction. This is analogous to the same motion observed in the frequency peaks at lower loadings however the oscillation rotates around a different mid plane.

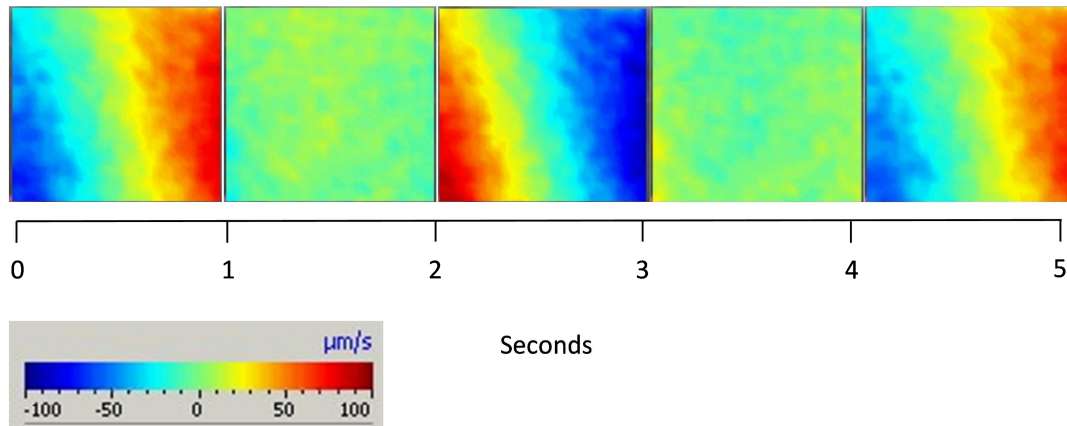


**Figure 4.16:** Transducer surface velocity pattern over time at 28 kHz under a coupling force of 350N.

## **4.8 Discussion of the Resonance Characteristics of a Shear PZT Dry Coupled Transducer**

The main electrical impedance peak of the shear PZT transducer in free air has been recorded at 1.2MHz which indicates that the main resonance of the transducer occurs at this frequency which agrees with the literature discussed in Section Resonant Characterisation of Ultrasonic Transducers2.7. However, there is an impedance change in the operating frequency range of the transducer (20 kHz to 100 kHz), when a force above 100N is applied to the transducer. There is a local fluctuation of impedance demonstrating a resonance in the transducer between 20 and 40 kHz. This local fluctuation of impedance is increasingly present with increasing load. The impedance phase of the transducer changes from a capacitive state and tends more towards an inductive state implying that the power efficiency of the transducer is rising within this frequency range as the applied force is increased. The frequency at which the local impedance peak occurs seems to shift to a higher frequency with higher load which leads to a conclusion that this resonance is force dependent. The efficiency of the transducer at 20 kHz correlates to results found in Section 3.8.4 which shows an increase in transmission amplitude at 20 kHz due to loading but independent on the increase in contact between the transducer and the wave guide.

It has been shown through laser vibrometer measurements that a coherent shearing motion, which is not detectable whilst the transducer is in free air, becomes prominent at 20 kHz when the transducer is subjected to a normal force above 100N. This indicates towards a natural resonant frequency occurring in the transducer backing block due the contact between the transducer and the wave guide. Furthermore, the frequency at which this velocity pattern exists is dependent on the magnitude of the force that is applied on the transducer which agrees with the hypothesis in Section 4.5. This force dependent resonance increases from 13 kHz at a 25N loading to 25 kHz at a 350N loading (Appendix G). After a load of 250N, this resonance separates into two related coherent velocity patterns and continuously shifts higher in frequency as a greater load is applied on the transducer. The correlation between the numerical predictions and the empirical data can be seen in Figure 4.41.

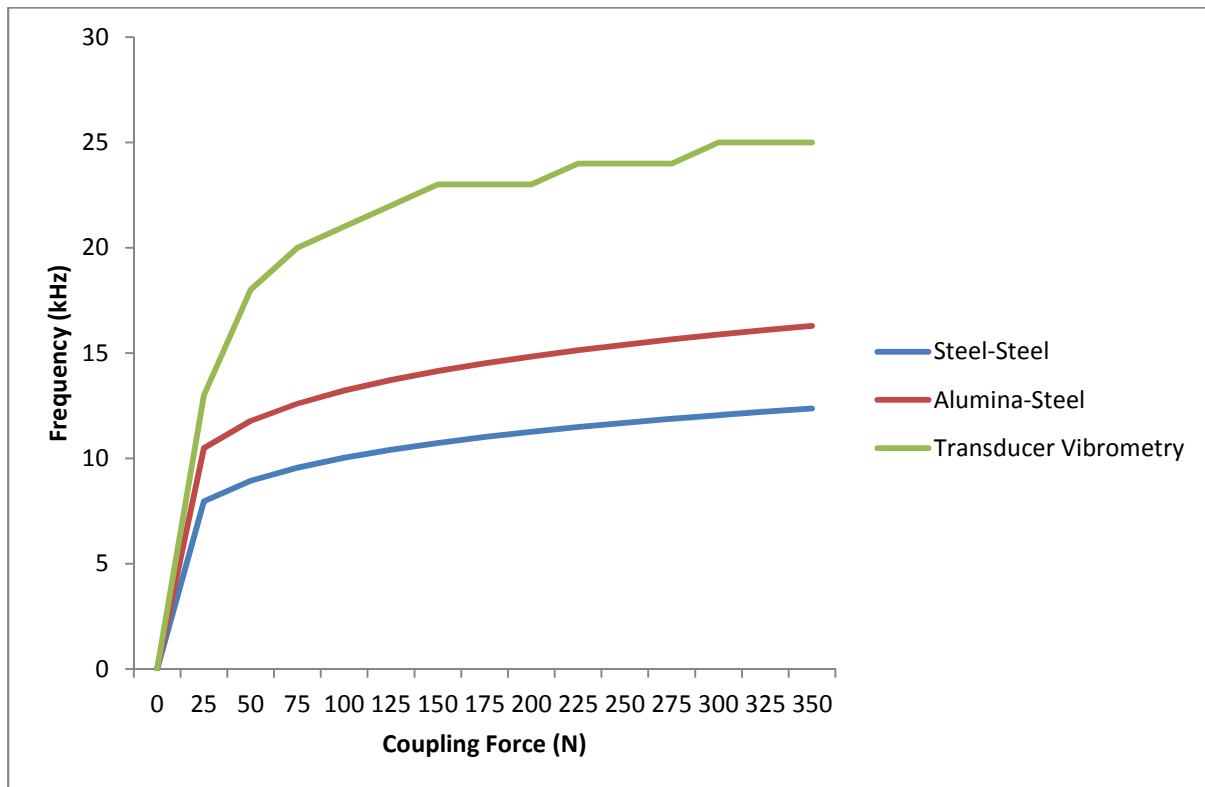


**Figure 4.17: Comparison between predicted contact resonance and measured.**

The coupled induced resonant behaviour of the transducer found in this Chapter coincides with the increase in amplitude transmission of the transducer at 20 kHz. It has been shown through laser vibrometer measurements that this is because the resonance developed in the transducer due to contact

is of a shearing motion which amplifies the motion of the transducer whilst propagating guided waves.

With the findings reported in this chapter, an operator may wish to use a frequency range 20 – 40 kHz when using a single source shear mode transducer for achieving a high signal-to-noise ratio. In addition the operator may want to design their array spacing accordingly for 25 kHz (assuming controlled coupling force of 350N) to benefit from the efficiency in output. The disadvantage is that due to the relatively longer wavelength there may be a loss in defect sensitivity and that the near zone is extended due to the lack of wave mode separation.

It is advised to avoid using 20 to 30 kHz frequency range for pipe inspection with the current transducer design when the operator is trying to ascertain wave mode control for superposition particularly when dry coupled and there is a lack of control of clamping force around the pipe circumference. This is because any variation in force distribution across the array can lead to a non-uniform output from each transducer hence compromising the superposition effects of wave mode cancellation, establishing directionality and diminishing signal-to-noise.

## **4.9 Contribution to Knowledge from Chapter 4**

It has been empirically demonstrated that there is a resonant effect for a shear PZT transducer between 20 kHz and 40 kHz which is both electrical in the PZT element and structural in the transducer backing mass and is induced by a normal load above 100N impinging on the transducer. Furthermore this resonance creates a shearing displacement in the backing mass and contributes to a local peak in the frequency response output in the transmission of a guided wave. This has not been stated in the literature prior to this investigation.

## **5. FEA Model of Shear PZT Transducer to predict Dry Coupled Induced Resonances in Backing Mass**

### **5.1 Introduction to Chapter 5**

In Chapter 4 a dry coupled dependent resonance had been found in the transducer between 20 and 30 kHz. This resonance had a shear plane motion which contributed to the amplification of transmission by the transducer which is observed in Chapter 0. In this chapter a model has been devised to simulate this and a parametric study was conducted to demonstrate the value of the model which could be used as an optimization design tool. The model developed in this Chapter has been empirically validated by the use of laser vibrometry with the same procedure found in Section 4.6. As discussed in Section 2.8, the development work of the transducer conducted by Alleyne & Cawley (1995) predicted a resonance of the backing block at 140 kHz using a 2D plane stress model. Chaston (2008) developed an FEA model of the transducer using 3D geometry which similarly predicted a resonance of the transducer backing block at 150 kHz. The predictions from these authors agree with data in Section 4.7 which observe a high displacement in the backing block between 140 and 150 kHz whilst the transducer is in free air.

### **5.2 2D Plane Stress FEA Model**

An initial plane stress model (Figure 5.1) was created within ABAQUS/CAE software in order to replicate the predictions made by Alleyne & Cawley (1995). The lowest natural frequency yielded from the model and the comparative results predicted by Alleyne & Cawley (1995) are displayed in Table 5.1.

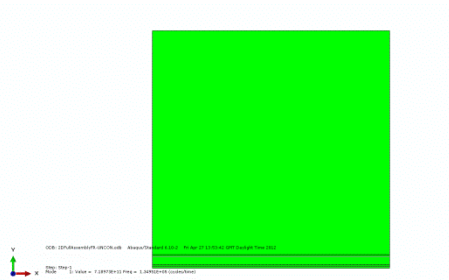


**Figure 5.1: Plane stress model in ABAQUS**

Backing Material	Backing/PZT bond line thickness (mm)	Alleyne and Cawley Lowest Natural Frequency	ABAQUS Lowest Natural Frequency (kHz)
Steel	0.1	140	135
Aluminium	0.1	123	122
Brass	0.1	97	100
Tungsten Epoxy	0.1	83	35
Steel	0.1	140	135
Steel	0.25	130	102
Steel	3	52	30

**Table 5.1: Comparison of FEA predictions between Alleyne & Cawley (1995) and 2D plane stress model in ABAQUS**

The results from the 2D plane stress showed agreement with the predictions made from Alleyne & Cawley (1995). The largest discrepancy was the model which consisted of Tungsten Epoxy backing mass and this is probably due to the material properties used being different. Tungsten Epoxy is a composite material and the ratio between Tungsten and Epoxy can significantly affect the density and elasticity of the material. The other discrepancy between the models was where the bond line thickness was 3mm. This is probably because the ABAQUS algorithm to model cohesive elements is different to the modelling method implemented by Alleyne & Cawley. The displacement of the 2D plane stress model with steel backing block and 0.1mm bond line thickness is seen in Figure 5.2.

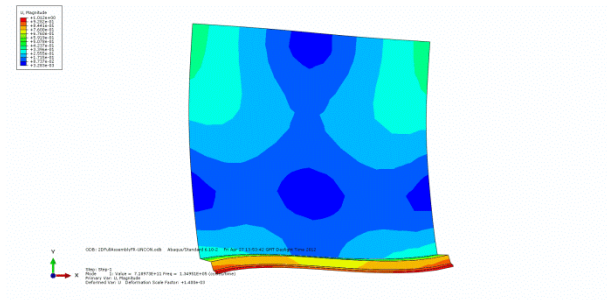


**Figure 5.2: Resonant Displacement of Plane Stress Model at 135 kHz.**

It can be seen that most of the displacement at this resonant frequency occurs within the faceplate, bondline and PZT element layers.

### **5.3 3D Cuboid Backing Block FEA Model**

The 2D plane stress model was iterated and a finite thickness was assigned to the transducer design consisting of a 14mm x 14mm steel backing mass with a 0.1 mm bond line thickness (Figure 5.3). The thickness given was 6.4mm in order to be consistent with the transducer design stated in the experimental work that validated the 2D plane stress models by Alleyne & Cawley (1995). This yielded a lowest natural frequency of 72 kHz (Figure 5.4).

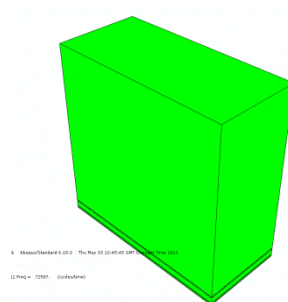


**Figure 5.3: FEA model of simplified transducer assembly with 6.4mm thickness.**

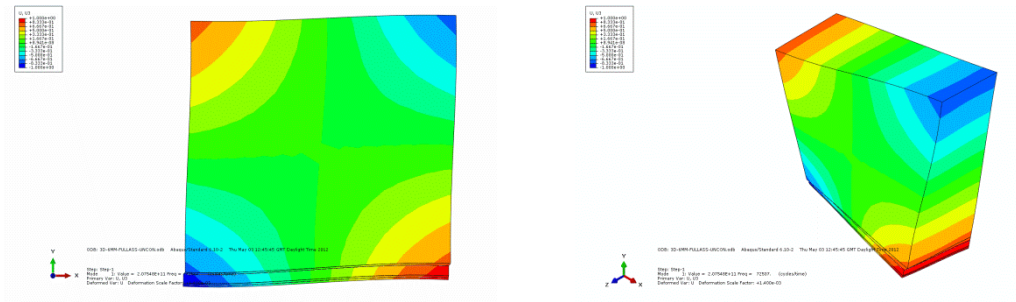


**Figure 5.4: Resonant displacement of FEA model of simplified transducer assembly with 6.4mm thickness at 72 kHz.**

The lowest natural resonant occurred at a lower frequency when the model consists of a finite body and the displacements at 72 kHz occurred at the corners edges of the cube.

The current transducer backing mass design possesses a thickness of 12.5mm and hence the model was altered to mirror this feature (Figure 5.5). This had the effect of increasing the natural frequency to 97 kHz (Figure 5.6).

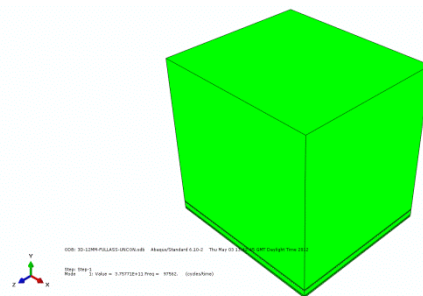


**Figure 5.5: FEA model of simplified transducer assembly with 12.5mm thickness.**

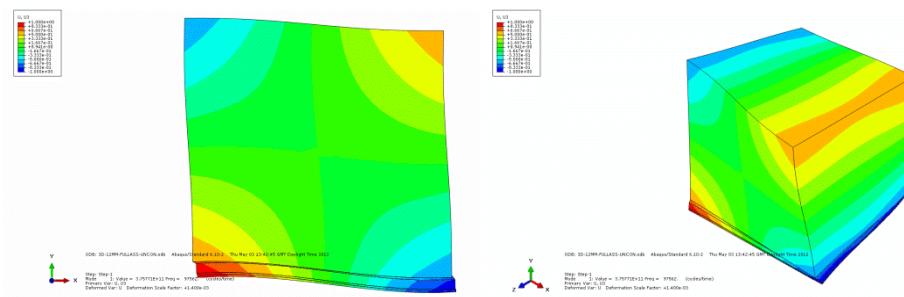


**Figure 5.6: Resonant displacement of FEA model of simplified transducer assembly with 6.4mm thickness at 97 kHz.**



Material	Steel	PZT	Epoxy	Alumina
Density ( $\text{kgm}^{-3}$ )	7850	7600	752	3960
Young's Modulus (GPa)	210	76	1.47	370
Poisson's Ratio	0.3	0.31	0.4082	0.22

**Table 5.2: Material properties used in FEA models.**

The backing block, PZT element and wear plate were assigned solid homogeneous sections. The bond lines were modelled using cohesive sections.

The interacting faces between the backing mass, bond lines, PZT element and wear plate were all constrained using the tie constraint algorithm, which constrains each of the nodes present on an interfacing surface to have the same motion as the point on the connected interface to which it is closest.

Initially all boundary conditions were omitted and the transducer was effectively allowed to move in free air with all degrees of freedom.

Due to the relative complexity of the backing block with geometrical features including chamfers and a varying diameter through hole, a continuum linear tetrahedral element was used to mesh this part. The PZT element and wear plate were meshed with a continuum linear brick element. Finally the bond lines were assigned cohesive elements.

A natural frequency analysis was performed on the model to establish the natural resonances between frequencies of 5 kHz and 200 kHz. This model predicted a lowest natural frequency of 83 kHz (Figure 5.8).

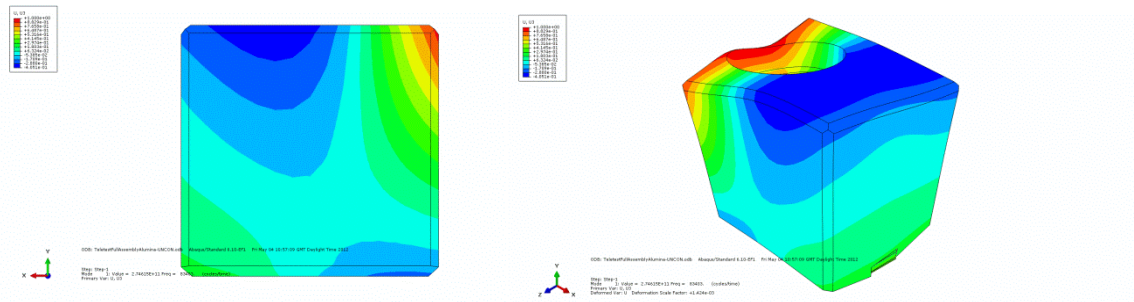


**Figure 5.8 : Resonant displacement of FEA model of shear PZT transducer at 83 kHz.**

It can be seen that at the lowest natural frequency of 83 kHz the transducer backing mass displaces the most at the thin walled region where the hole for the MCX connector is.

The final iteration of the model was to tie constrain the transducer wear plate to a wave guide which was simulated by a 16mm<sup>3</sup> steel block. This steel block was assigned zero degrees of freedom as the resonance of the block was not of interest. A uniformly distributed normal load of 200N was applied to the load bearing face situated on top.

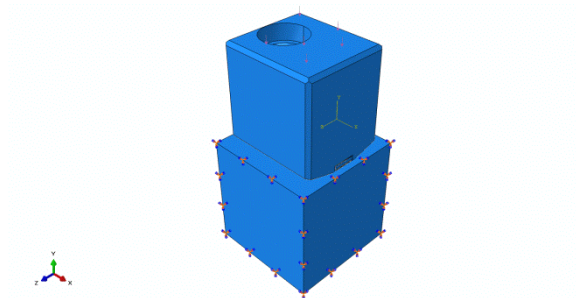


**Figure 5.9: FEA model of shear PZT transducer attached to wave guide under coupling load.**

The lowest natural frequency of the transducer under these conditions was 19.6 kHz (Figure 5.10).

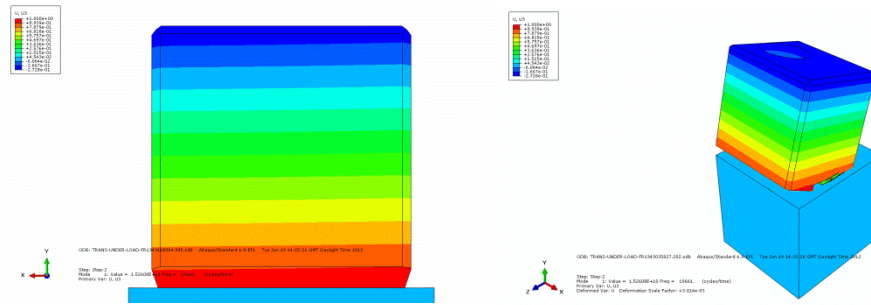


**Figure 5.10: Resonant displacement of FEA model of shear PZT transducer attached to wave guide under coupling load at 19.6 kHz.**

In comparison to the transducer resonance displacement whilst in free air, the resonant displacement of the transducer under constraint indicates a shearing motion, where the transducer rotates about the XY plane.

## 5.5 Validation of FEA Model using Laser Vibrometry Measurements

A summary of the predicted lowest natural frequency for each model is found in Table 5.3.

Model	Lowest Natural Frequency (kHz)
Alleyne and Cawley Plane Stress Model	140
ABAQUS Plane Stress Model	135
3D Transducer Block Assembly – 6.4mm width	72
3D Transducer Block Assembly – 12.5mm width	97
Current Transducer Assembly (Free Air)	83
Current Transducer Assembly (Constrained)	19.6

**Table 5.3: Comparison of FEA natural frequency predictions between different transducer models.**

It is observed that as the FEA model is resolved to include geometrical features of the backing block and constraints are implemented to attach the transducer to the wave guide, the natural resonant

frequency decreases lower down the frequency spectrum. Furthermore the type of displacements generated by the natural resonance change from the contortion of geometric features on the backing mass to a shearing motion of the whole backing block.

Comparisons between the displacement patterns observed in the laser vibrometry work package referred to in Section 4.7 and the predicted natural resonances in this Chapter have been made in order to validate the model. First the transducer in free air conditions is observed (Table 5.4).

Resonance detected by Laser Vibrometer (kHz)	Resonance predicted by FEA (kHz)
84	83
99	103
111	112
118	132
139	136

**Table 5.4: Comparison between detected natural frequencies of the shear PZT transducer in free air by the vibrometer and natural frequencies predicted by FEA model.**

It can be seen that the displacement pattern detected by the laser vibrometer at 84 kHz indicates a displacement in the thin wall region where the hole for MCX connector is situated.

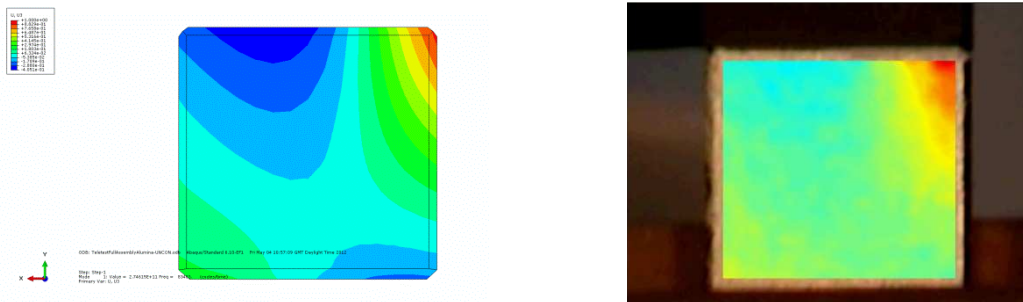


**Figure 5.11: Resonant displacement of transducer in free air at 83 kHz in FEA (left) and 84 kHz by vibrometry (right).**

The remaining resonance comparisons can be found in Appendix H. The comparison between the FEA model where the transducer is constrained and the resonances detected by the vibrometer are found in Table 5.5.

Resonance detected by Laser Vibrometer (kHz)	Resonance predicted by FEA (kHz)
23	19.6
105	105
137	141

**Table 5.5: Comparison between detected natural frequencies of the transducer under 200N load by the vibrometer and natural frequencies predicted by FEA model.**

The resonance detected by electrical impedance and laser vibrometry measurements in Chapter 4 due to the contact between the transducer and wave guide has been simulated in FEA by using the boundary conditions discussed in this Chapter.

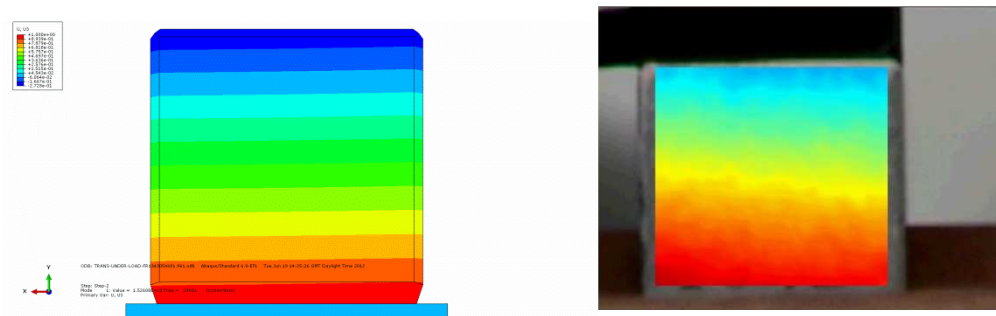


**Figure 5.12: Resonant displacement of transducer under 200N loading at 19.6 kHz in FEA (left) and 23 kHz by vibrometry (right).**

It can be seen in Figure 5.12 that the shear plane motion generated in the transducer block which contributes to an increase in transmission amplitude has been replicated in the FEA model. The remaining resonance comparisons for this model can be found in Appendix H.

## 5.6 A Parametric Study to Investigate the Effect of the Change in Backing Mass on the Resonance of the Shear PZT Transducer

As discussed in Section 4.2 the resonant frequency produced by two bodies in contact is dependent on the stiffness of the system, which is a function of material properties and forces in the system, in addition to the mass of the bodies. The model developed in this Chapter was used to predict the resonant characteristic of several backing mass geometries. The height (14mm) and the axial length (12.5mm) of the transducers were unaltered whereas the width of the backing mass had been altered. The width of the backing mass had been changed to 10, 7.5 and 6mm. The same approach for FEA modelling had been taken as prior where the backing mass was created in CAD and imported into ABAQUS FEA software. The material properties, type of interactions and mesh elements were also consistent with the earlier model. This produced a list of resonant frequencies up to a 100 kHz for each transducer (Table 5.6).

Predicted resonant frequencies (kHz) 10mm width backing mass	Predicted resonant frequencies (kHz) 7.5mm width backing mass	Predicted resonant frequencies (kHz) 6mm width backing mass
11	14	16.5
23	28	32.5
80	69	54
	93	80

**Table 5.6: List of predicted resonant frequencies for backing masses with varied width.**

Three transducers were then fabricated by taking the existing transducer backing mass and cutting down to the desired width using a hot wire cutter. The manufacturing drawings for these three prototype backing masses can be found in Appendix A. The transducers together with the PZT and the wear plate were assembled with the production manufacturing process used to construct commercially available transducers for Plant Integrity Ltd. These transducers were then mounted in the transducer test rig and the method of measurement used to identify structural resonances of the

backing block in Chapter 4 was employed. The resonant frequencies for each block within 100 kHz range are displayed in Table 5.7.

Measured resonant frequencies (kHz) 10mm width backing mass	Measured resonant frequencies (kHz) 7.5mm width backing mass	Measured resonant frequencies (kHz) 6mm width backing mass
10	15	16.5
22.5	24.5	22
26	30.5	24
77	33	31
90	34.5	35.5
97	37.5	58.5
	41	61.5
	63	76.5
	69	87.5
	86	

**Table 5.7: List of measured resonant frequencies for backing masses with varied width.**

The comparison between the FEA model and the laser vibrometer measurements for the contact induced natural frequency for the different transducers are found in Figure 5.13, Figure 5.14 and Figure 5.15.

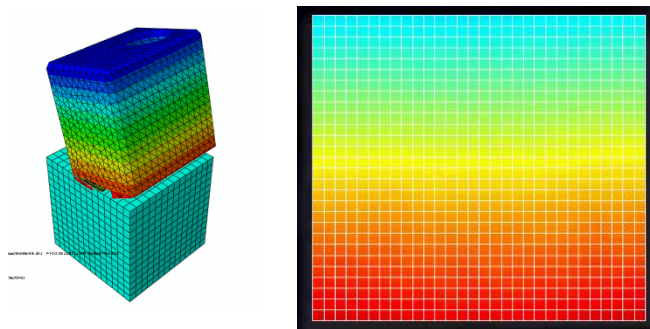


**Figure 5.13: Displacement at 23 kHz in FEA model and measured displacement at resonance at 22.5 & 26 kHz for transducer backing mass with 10mm width.**

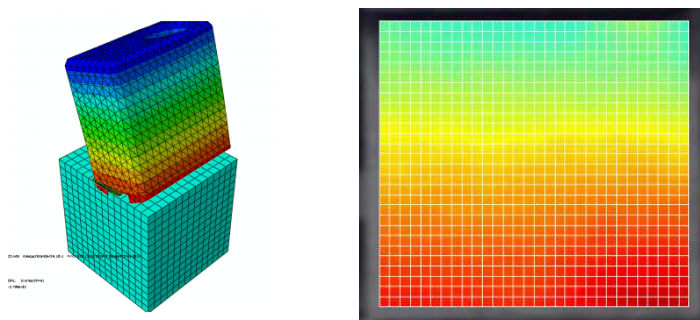


**Figure 5.14: Displacement at 28.5 kHz in FEA model and measured displacement at resonance at 24.5, 30.5, 34.5, 37.5 & 41 kHz for transducer backing mass with 7.5mm width.**

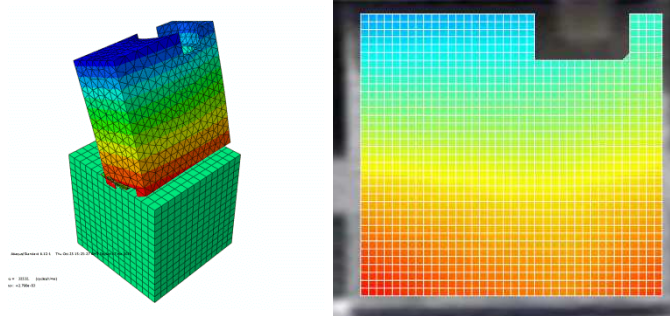


**Figure 5.15: Displacement at 32.5 kHz in FEA model and measured displacement at resonance at 22, 24, 31 & 35 kHz for transducer backing mass with 6mm width.**

It can be seen that the shearing motion in the transducer is identified for each prototype backing mass and the frequency at which this occurs has been predicted by the FEA model. The findings also agree with the equation to predict resonance due to contact where according to:

$$\omega^2 = \frac{s(m_1+m_2)}{m_1m_2} \quad (\text{Equation 2.8})$$

Where a larger mass will produce a lower natural resonant frequency providing the stiffness is kept constant.

## **5.7 Discussion of the FEA Models of Shear PZT Transducers to predict Dry Coupled Induced Resonances in Backing Mass**

The initial plane strain FEA models used to predict the natural resonance of simplified transducer geometry had predicted the lowest natural frequency above 100 kHz. A model that consisted of the full transducer geometry was created to assess the natural frequencies in the absence of boundary conditions. This provided solutions for natural resonances occurring below 100 kHz, which were not predicted by the work of Alleyne & Cawley (1995) and Chaston (2008). The predictions made in this FEA model were verified by comparative Fast Fourier Transform analysis of the surface velocity measurements made on the transducer backing mass under laser Vibrometry.

The FEA model was developed to include the boundary condition where the transducer is in contact with the wave guide. This predicted a natural resonance at 19.6 kHz. This has also been observed by

laser vibrometry while the transducer is under load. With the resonance occurring approximately at this frequency, it is of a shear nature and has shown a local efficiency of the transducer increasing the transmitted ultrasonic amplitude at this frequency.

From the parametric study it can be observed that a thinning of the width and a reduction of the mass raise the frequency of the contact dependent resonance into the operating frequency range. From observing the measured vibrometry data the other effect that occurs is that the bandwidth of each resonance broadens, meaning the natural resonance is more dominant over a greater frequency spectrum. This seems to agree with work conducted by Clarke et al. (2009). This shows that the modelling approach complete with geometry and boundary conditions taken can accurately estimate the natural resonances of a shear wave mode transducer. This model has been partially validated for several transducer backing masses and therefore a prospective designer can implement a transducer backing mass geometry and constraint to output whether a coupled induced resonance will occur in frequency response of the transducer.

## **5.8 Contribution to Knowledge from Chapter 5**

The work conducted by Alleyne & Cawley (1995) to develop the shear PZT transducer used for pipe testing disregarded the effect of dry coupling on the resonant characteristic of the transducer and thus FEA models predicted resonances of the transducer above the operational frequency limit of 100 kHz. This seemed to be incorrect when taking empirical measurements of the resonant behaviour of the transducer which showed a resonance at approximately 20 kHz. In this Chapter an FEA model has been produced which implemented 3D geometrical features of the transducer backing mass and boundary conditions which simulated contact with a wave guide which was previously ignored. This model accurately predicted natural frequencies in agreement with the experimentally measured resonances of the transducer. The model was able to identify a resonant motion in the shear plane which contributes to a localised peak frequency response of the transducer transmission output. This modelling approach was taken for several other transducer backing mass geometries and the results were validated by measuring resonances of fabricated prototypes. This model is robust enough to be used as an isolated approach to predicting resonant effectual frequencies of prototype shear PZT

transducers or could be further incorporated into a holistic model to ascertain a transmission output frequency response.

## **6. Conclusions and Further Work**

### **6.1 Conclusions**

#### **6.1.1 Dry Coupled Transmission Behaviour of Shear PZT Transducer**

In section 2.6, it was demonstrated that there is a dearth of literature which investigates the relationship between dry coupling force on a thickness shear guided wave transducer and the resultant transmission amplitude produced. Previous work concerning dry coupled transducers was based around the use of conventional ultrasonic sensors propagating bulk waves to characterise coupled boundary interfaces. Literature aligning itself to dry coupled guided wave transducers was predominantly centred on piezoelectric discs for the use of plate testing. The ability of a single thickness shear transducer, used for pipe testing, to receive had been conducted (Alleyne & Cawley, 1996b) and it was shown that there was a plateau of received amplitude for a singular frequency after being subjected to a normal load of 50N. The capability of a pipe testing thickness shear transducer to transmit amplitude with respect to dry coupled force across a broadband of frequencies had not been established.

The investigation carried out in Chapter 0 managed to fill this gap in the knowledge. It was shown that as the normal force used to impinge the transducer on the wave guide increased the corresponding transmission amplitude increased in magnitude at a non-linear rate across the frequency spectrum of excitation. Furthermore there was an absence of a plateau characteristic above 50N loading; in contrast there was a continual rise up to the normal load of 350N which was the practical limitation of the experiment. This behaviour has been prescribed by classical elastic contact theory as the mechanism and the trend found in section 3.2. Hertzian contact theory states that the contact area produced between two surfaces is proportional to the normal load applied to the impinging surfaces to the power law of  $\frac{1}{3}$ . The non-linear relationship between the magnitude of the amplitude transmitted and the normal force used to dry couple the transducer showed the same power law relationship of a  $\frac{1}{3}$  for all frequencies tested apart from 20 kHz where an additional mechanism caused the transmission magnitude to rise.

A secondary investigation was conducted to observe the effect of surface roughness at the contact area between transducer and waveguide on the subsequent transmitted amplitude whilst the transducer is subjected to a constant force. This had only been investigated for pipe surfaces with the roughness  $R_a$  range of 8 – 12  $\mu\text{m}$  prior. The investigation conducted in section 0 widened the roughness range studied to be between approximately 30 and 90  $\mu\text{m}$ . It was found for this roughness range no discernible effect was produced on the frequency response from the transducer.

### **6.1.2 Resonant Behaviour of Shear PZT Transducer**

Observations made from the frequency responses found in section 3.8.3 showed that there was a local peak of amplitude emerging at the lower end of the operational frequency range as the transducer was subjected to an increase in force. In section 2.7 it can be seen that most recent work regarding piezoelectric transducers electrical impedance and natural resonant behaviour has been for the use of modal analysis of a structure for damage detection. The frequencies concerned in these applications were above 100 kHz and the method of attachment was typically not of a dry coupled elastic nature.

An electrical impedance model of the transducer studied in this thesis had been previously constructed and validated whilst the transducer was in free air conditions. The prediction and measurements showed a natural resonance in the MHz range. The resonant behaviour within the operational frequency spectrum of a thickness shear transducer whilst under a dry coupled load had not been conducted. In section 4.2, the electrical impedance of the transducer was measured under varying loading conditions and it was found to show resonant behaviour developed approximately at 20 kHz when the transducer was subjected to a load above 100N. As the load increased above 100N the frequency of resonance increased.

The natural resonance of the backing mass of the transducer was measured using a laser Doppler vibrometer whilst the load on the transducer was varied. The presence of structural resonances was not detected in the backing mass of the transducer whilst in free air until a 140 kHz. However when the transducer was impinged onto a substrate a resonant frequency began to be observed in the

backing mass approximately at the 20 kHz value. Similarly the value of the frequency where this would occur shifted higher as the load was increased.

Both electrical impedance and structural resonance measurements coincided with local peaks of amplitude produced in the operational frequency response of the transducer in Chapter 3. Furthermore, the behaviour recorded correlated to theoretical contact resonance equations which predicted for the approximate mass and stiffness of the transducer and waveguide a natural resonance would occur just under 20 kHz.

### **6.1.3 FEA Model of Shear PZT Transducer**

In section 2.8 previous FEA modelling for a shear PZT transducer used for pipe testing was discussed. Previous models that have been constructed excluded the effect of dry coupling on the resonant characteristic of a thickness-shear PZT transducer. These models would provide solutions of resonant behaviour for the transducer above the operational frequency limit of 100 kHz. This clearly contradicts the measurements displayed in Chapter 4.

In section 5.4 an FEA model was produced with appropriate loading boundary conditions and geometrical features which was able to predict natural frequencies which were experimentally confirmed in Chapter 4. The model was able to identify a resonant motion approximately at 20 kHz in the shear plane which contributes to a localised peak frequency response of the transducer transmission output observed in Chapter 3.

The ability of the model to predict natural resonances of prospective transducer designs were demonstrated by modelling several transducer backing mass geometries and empirically measuring the resultant resonances of fabricated prototypes. The model was able to predict the effectual resonant frequency of prototype shear PZT transducers.

## 6.2 Recommendations for Further Work

There are several limitations of the investigation conducted in Chapter 3. The maximum force applied to the transducer was 350N. Therefore any conclusions made from the data are only valid up until this application of force. A higher force was not achieved due to the absence of higher air pressure supply lines and the safety concerns associated with working at these pressures. It is postulated that the amplitude generated from the transducer will increase with increasing force application until the performance of the transducer degrades due to one of two effects. One of the mechanisms will be a fracture caused in the PZT element or alumina wear plate due to excessive loading causing a sharp decline in output. The other mechanism will be the over-damping of the transducer, restricting the PZT element from resonating and hence producing a drop in output. A repeat of the investigation achieving higher forces on the transducer would need to be conducted to observe whether and at what force magnitude these failure mechanisms would occur. However, there is an aspect of feasibility and safety of attaining post-350N loading “on-site” applications and the data gathered is of value for current practical implementation.

The wave mode measured only refers to the ‘longitudinal’ displacements produced within the bar. The investigation could be repeated with the orientation of the transducer placed as to produce a ‘torsional’ wave mode. It would then be observed as to whether the signals collected expressed the same pattern of frequency response and force-amplitude output. The lack of dispersion would indicate the transducers behaviour at higher frequencies, although higher modes and the presence of a faster ‘shear horizontal’ mode could potentially interfere with the received signal.

The transducer characteristics observed are only applicable to steel. It would be of use to conduct a similar test set-up using other engineering materials for the wave guide, for instance copper which is used commonly for piping or carbon fibre composite where the parameter of anisotropic properties has to be accounted for.

An investigation should be conducted with the alteration of transmitting on a surface bonded PZT and the transducer receiving under loads of a similar range in Chapter 3. This would verify or contradict

earlier work that has been conducted. If the receive characteristic of the transducer has a similar trend to the transmit characteristic then this would imply that there would be a squared effect of increasing the force on the transducer whilst under pulse-echo operation.

The transmission effect from varying surface roughness in the secondary investigation was widely inconclusive of a distinct trend. It may have been too limited in range and it is recommended that surfaces should be produced with a wider variety of surface finishes.

As existing electrical impedance graphs of the shear mode transducer exist and an exercise should be conducted where a model of the electrical impedance behaviour of the transducer using an equivalent R-L-C circuit (i.e. KLM model) incorporates the low frequency resonant effects with respect to a force parameter in order to trace the curves empirically observed.

A limitation to the transducer Vibrometry setup was that access to all six faces of the transducer was limited, thus the complete transducer displacement behaviour is still unknown and resonances that occur in other planes of motion may have been undetected. It is recommended that the procedure outlined in Chapter 4 & 5 should be repeated taking 3D measurements within a jig that allows appropriate access to the transducer geometry.

At present the resonance of the transducer predicted at 19.6 kHz in the FEA model is independent of a change in the applied load. A user defined relationship between pressure and stiffness needs to be calculated and integrated into the FEA model to replicate identically the load dependent nature of this resonating frequency. An additional iteration to the model would be to implement piezoelectric constants to the material properties of the element rather than modelling it as a isotropic homogeneous part.

The test conducted in Chapter 3 where the frequency response is measured on a pitch catch test with the prototypes fabricated in Chapter 5 needs to be repeated to ascertain the effect that thinning the transducer width has on the broadness of the ultrasonic frequency response peaks.

## References

- Ahmad Z. (2006) *Principles of Corrosion Engineering and Corrosion Control*, Butterworth-Heinemann.
- Alleyne D. & Cawley P. (1992) 'Optimization of Lamb wave inspection techniques', *NDT & E International* **25** (1), pp. 11-22.
- Alleyne D. & Cawley P. (1995) –TWI report (1995) Field implementation of a novel technique for detection of corrosion under insulation in oil and gas process pipework. Cambridge, 8215/7/95.
- Alleyne D. & Cawley P. (1996a) 'The effect of discontinuities on the long-range propagation of Lamb waves in pipes', *Proceedings of the Institution of Mechanical Engineers, Part E: Journal of Process Mechanical Engineering*, pp. 217-226.
- Alleyne D. & Cawley P. (1996b) 'The Excitation of Lamb Waves in Pipes Using Dry-Coupled Piezoelectric Transducers', *Journal of Nondestructive Evaluation*, **15** (1), pp. 11-20.
- Allin J.M. & Cawley P. (2003) 'Design and construction of a low frequency wide band non-resonant transducer', *Ultrasonics*, **41**, pp. 147–155.
- Assosicated Press (2011) Guardian: Environment: Oil Spills. Available at:
- Atkinson D. & Hayward G. (1998) 'Fibre waveguide transducers for lamb wave NDE', *IEE Proceedings of Scientific Measurement Technology*, **145** (5), pp. 260-268.
- Atkinson D. & Hayward G. (2001) 'The Generation and Detection of Longitudinal Guided Waves in Thin Fibers Using a Conical Transformer', *IEEE transactions on ultrasonics, ferroelectrics, and frequency control*, **48** (4), pp. 1046-1053.
- Baker M. (2008) 'Pipeline Corrosion', *US Department of Transportation*, DTRS56-02-D-70036.
- BBC News (2010) Available at: <http://www.bbc.co.uk/news/10324021>
- Bellan F., Bulletti A., Capineri L., Masotti L., Yaralioglu G. G., Degertekin F. L., Khuri-Yakub B.T., Guasti F. & Rosi, E. (2005) 'A new design and manufacturing process for embedded Lamb waves interdigital transducers based on piezopolymer film', *Sensors and Actuators A*, **123–124**, pp. 379–387.
- Bhalla S. & Soh C.K. (2004) 'Electromechanical Impedance Modeling for Adhesively Bonded Piezo-transducers', *Journal of Intelligent Material Systems and Structures*, **15**, pp. 955-972.
- Bhushan B., Wyant J. C. & Meiling J., *Wear* **122**, pp. 301-312.
- Blevins R.D. (1995) *Formulas for Natural Frequency and Mode shape*, Malabar Florida: Krieger Publishing.
- Capineri L., Gallai A. and Masotti L. & Materassi M. (2002), 'Design Criteria And Manufacturing Technology Of Piezo-Polymer Transducer Arrays For Acoustic Guided Waves Detection', *IEEE Ultrasonics Symposium*, pp. 857-860.
- Catton P. 'Long Range Ultrasonic Guided Waves for the Quantitative Inspection of Pipelines', PhD thesis, Brunel University, (2009).
- Cawley P. & Alleyne D (1996) 'The use of Lamb waves for the long range inspection of large structures', *Ultrasonics*, **34**, pp. 287-290.
- Cawley, P., Alleyne, D.N. & Chan, C.W. (1994) 'Inspection of pipes', WO 96/12951, priority date 20-10-1994.

- Cegla F.B., Cawley P., Allin J. & Davies J. (2011) 'High-Temperature (>500°C) Wall Thickness Monitoring Using Dry-Coupled Ultrasonic Waveguide Transducers', *IEEE Transactions on Ultrasonics, Ferroelectrics, and Frequency Control*, **58** (1), pp. 156-167.
- Chaston A. 'Development of a transducer to be used in Long Range Ultrasonic Testing', PhD thesis, Cardiff University, (2008).
- Cho S.H., Kim H.W. & Kim Y.Y. (2011) 'Megahertz-Range Guided Pure Torsional Wave Transduction and Experiments Using a Magnetostrictive Transducer', *IEEE transactions on ultrasonics, ferroelectrics, and frequency control*, **57** (5), pp. 1225-1229.
- Clarke T. 'Guided wave health monitoring of complex structures', PhD thesis, Imperial College London, (2009).
- Clarke T., Simonetti F., Rohlin S. & Cawley P. (2009) 'Development of a Low-Frequency High Purity  $A_0$  Mode Transducer for SHM Applications', *IEEE Transactions on Ultrasonics, Ferroelectrics, and Frequency Control*, **56** (7), pp. 1457-1468.
- Degertekin F.L. & Khuri-Yakhub B.T. (1996) 'Single mode Lamb wave excitation in thin plates by Hertzian contacts', *Applied Physics Letters*, **69** (2), pp. 146-148.
- Degertekin F.L. & Khuri-Yakhub B.T. (1997) 'Lamb wave Excitation by Hertzian Contacts with Applications in NDE', *IEEE transactions on ultrasonics, ferroelectrics, and frequency control*, **44** (4), pp. 769-779.
- Ditri J., Rose J., & Pilarski A. (1993) 'Generation of guided waves in hollow cylinders by wedge and comb type transducers', *Proceeding of the QNDE Conference*, **12A**, pp. 211–218.
- Drinkwater B. & Cawley P. (1995) 'An ultrasonic wheel probe alternative to liquid coupling', *Review of Progress in Quantitative NDE*, pp. 983–989.
- Drinkwater B. & Cawley P. (1997) 'Practical application of solid coupled ultrasonic transducers', *Materials Evaluation*, **55** (3), pp. 401–406.
- Drinkwater B., Castaings M. & Hosten B. (2003) 'The measurement of  $A_0$  and  $S_0$  Lamb wave attenuation to determine the normal and shear stiffnesses of a compressively loaded interface', *Journal of Acoustical Society of America*, **113** (6), pp. 3161-3170.
- Drinkwater B., Dwyer-Joyce R. & Cawley P. (1996) 'A study of the transmission of ultrasound across solid–rubber interfaces', *Journal of Acoustical Society of America*, **101** (2), pp. 970-981.
- Esquerdo A. C. 'Market analysis for a long range ultrasonic inspection program of the enterprise AREVA', Master's thesis, Hamburg University of Applied Sciences (2012)
- Fromme P., Wilcox, P.D., Lowe M.J.S. & Cawley P. (2006) 'On the Development and Testing of a Guided Ultrasonic Wave Array for Structural Integrity Monitoring', *IEEE transactions on ultrasonics, ferroelectrics, and frequency control*, **53** (4), pp. 777-785.
- Gallego-Juarez J. A. (1989) 'Piezoelectric ceramics and ultrasonic transducers', *Journal of Physics and Scientific Instrumentation*, **22**, pp. 2804–816.
- Giurgiutiu V., Zagari A. & Bao J. J. (2002), 'Piezoelectric Wafer Embedded Active Sensors for Aging Aircraft Structural Health Monitoring', *Structural Health Monitoring* **1** (1), pp. 41-61.
- Greenwood J. A. & Williamson J. B. P. (1966) 'Contact of nominally flat surfaces', *Proceedings of the Royal Society of London*, **A295** (1442), pp. 300-319.

Grondel S., Paget C., Delebarre D., Assaadet J. & Levin K. (2002) 'Design of optimal configuration for generating A0 Lamb mode in a composite plate using piezoceramic transducers', *Journal of Acoustical Society of America*, **112** (1), pp. 84-90.

Guided Ultrasonics Limited (2013) Available at: <http://www.guided-ultrasonics.com/> [ Accessed 28 May 2013]

Hai-Yan Z. & Jian-Bo Y. (2011) 'Piezoelectric transducer parameter selection for exciting a single mode from multiple modes of Lamb waves', *Chinese Physical Society*, **20**, (9), pp. 094301-1 - 094301-9.

Hay T. R. & Rose J. L. (2002) 'Flexible PVDF comb transducers for excitation of axisymmetric guided waves in pipe', *Sensors and Actuators A*, **100**, pp. 18–23.

Hay T. R. & Rose J. L. (2006) 'Flexible Piezopolymer Ultrasonic Guided Wave Arrays', *IEEE transactions on ultrasonics, ferroelectrics, and frequency control*, **53** (6), pp. 1212-1217.

Hayashi T., Song W & Rose J. L. (2003) 'Guided wave dispersion curves for a bar with an arbitrary cross-section, a rod and rail example', *Ultrasonics*, **41**, pp. 175–183.

Hertz H. (1881) 'On the fixed contact of elastic bodies', *Journal of Pure and Applied Mathematics*, **92**, pp. 156-171.

Hirao M. & Ogi H. (1999) 'An SH-wave EMAT technique for gas pipeline inspection', *NDT&E International*, **32**, pp. 127–132

Hopkins P. (2007) 'OIL AND GAS PIPELINES: Yesterday and Today', *American Society of Mechanical Engineers*.

The Guardian (2011) <http://www.theguardian.com/environment/2011/may/04/bp-25m-north-slope-oil-spill> [Accessed 21 April 2013]

Hutchings I. M. (1992) *Friction and Wear of Engineering Materials*, Edward Arnold.

Jin J., Quek S.T. & Wang Q. (2005), 'Design of interdigital transducers for crack detection in plates', *Ultrasonics*, **43**, pp. 481–493.

Johnson K.L. (1987) *Contact Mechanics*, Cambridge University Press.

Kannan E., Maxfield B.W. & Balasubramaniam K. (2007) 'SHM of pipes using torsional waves generated by in situ magnetostrictive tapes', *Smart Materials & Structures*, **16**, pp. 2505–2515.

Kim H.W., Kwon Y.E, Cho S.H., & Kim Y.Y. (2013) 'Shear-Horizontal Wave-Based Pipe Damage Inspection by Arrays of Segmented Magnetostrictive Patches', *IEEE transactions on ultrasonics, ferroelectrics, and frequency control*, **58** (12), pp. 2689-2698.

Krimholtz, R, Leedom, D.A & Matthaei, G.L (1970) 'New equivalent circuits for elementary piezoelectric transducers', *Electronic Letters*, **6** (13), pp. 398-339.

Landau L. & Lifshitz E. M. (1959) 'Theory of Elasticity', New York: Pergamon.

Lee B.C. & Staszewski W.J. (2007) 'Lamb wave propagation modelling for damage detection II – Damage monitoring strategy', *Smart Materials and Structures*, **16** (2), pp. 260 – 274.

Lee Y.C. & Kuo S.H. (2004) 'A New Point Contact Surface Acoustic Wave Transducer for Measurement of Acoustoelastic Effect of Polymethylmethacrylate', *IEEE transactions on ultrasonics, ferroelectrics, and frequency control*, **51** (1), pp. 114-120.

- Leong W. H., Staszewski W. J., Lee B. C. & Scarpa F. (2005) 'Structural health monitoring using scanning laser vibrometry III: Lamb waves for fatigue crack detection', *Smart Materials and Structures*, **14** (6) pp. 1387 – 1395.
- Lowe M.J.S. & Cawley P. (2006) 'Long Range Guided Wave Inspection Usage – Current Commercial Capabilities and Research Directions', Imperial College London.
- Lowe M.J.S., Alleyne D.N. & Cawley P. (1998) 'Defect detection in pipes using guided waves', *Ultrasonics*, **36**, pp. 147-154.
- Mańka1 M., Rosiek M., Martowicz A., Stepinski T., & Uhl T. (2013), 'Lamb wave transducers made of piezoelectric macro-fiber composite', *Structural Control Health Monitoring*. **20**, pp. 1138–1158.
- Meitzler A H. (1961) 'Determination of Elastic Constants of Isotropic Materials at Megacycle Frequencies', *Journal of the Acoustical Society of America*, **33** (435).
- Merheb B., Nassar G. , Nongaillard B. , Delaplace G. & Leuliet J.C. (2007) 'Design and performance of a low-frequency non-intrusive acoustic technique for monitoring fouling in plate heat exchangers', *Journal of Food Engineering*, **82**, pp. 518–527.
- Meyers F.N, Loh K. J., Dodds J.S. & Baltazar A. (2013), 'Active sensing and damage detection using piezoelectric zinc oxide-based nanocomposites', *Nanotechnology*, **24**, 185501 (10pp) .
- Monkhouse R. S. C., Wilcox P. W., Lowe M. J. S., Dalton R. P. & Cawley P. (2000) 'The rapid monitoring of structures using interdigital Lamb wave transducers', *Smart Material Structures*, **9**, pp. 304–309.
- Naa J. K., Blackshireb J. L. & Kuhra S. (2008), 'Design, fabrication, and characterization of single-element interdigital transducers for NDT applications', *Sensors and Actuators A*, **148**, pp. 359–365.
- NACE International, The Corrosion Society (2003) 'The United States Cost of Corrosion Study'. Houston, USA.
- Naidu A.S.K. & Soh C.K. (2004) 'Identifying Damage Location with Admittance Signatures of Smart Piezo-transducers', *Journal of Intelligent Material Systems and Structures*, **15**, pp. 627-642.
- Nakamura K. (2012) *Ultrasonic Transducers: Materials & Designs for Sensors, Actuators and Medical Applications*, Elsevier.
- Nassar G. & Nongaillard B. (2000) 'Optimization of a low-frequency ultrasonic technique to monitor the change in physical states in viscoelastic media: Gelation process', *Journal of Acoustical Society of America*, **107** (5), pp. 2735-2743.
- NDT Resource Centre (2014) Available at: [http://www.ndt-ed.org/index\\_flash.htm](http://www.ndt-ed.org/index_flash.htm)
- NOAA Fisheries (2014) Available at: <http://alaskafisheries.noaa.gov/oil/>
- Pavlakovic, B, Lowe, M, Alleyne, D, & Cawley, P. (1997). *Disperse: a general purpose program for creating dispersion curves*.
- Phartipan T. et al. (2011a) 'Power estimation by system modelling for reliable structural integrity monitoring', *Proceedings of the 2011 conference for the engineering doctorate programmes in environmental technology & sustainability for engineering & energy systems – University of Surrey* 21 & 22 June 2011.
- Phartipan T. et al. (2011b) 'Design and Analysis of ultrasonic NDT instrumentation through system modelling', *International Journal of Modern Engineering*, **12** (1), pp. 88-97.
- Polytec Scanning Vibrometer Hardware Manual PSV400*, Polytec GmbH, 2011.

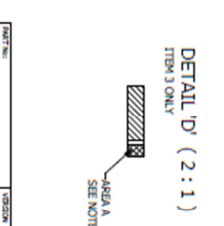
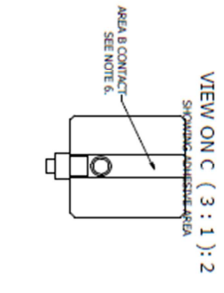
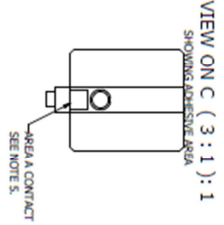
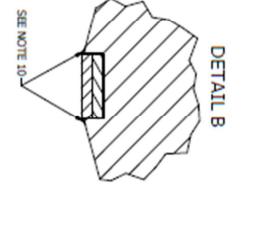
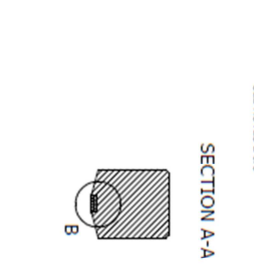
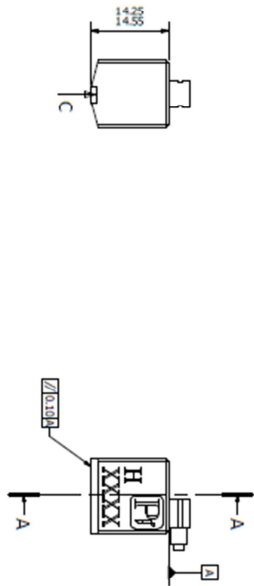
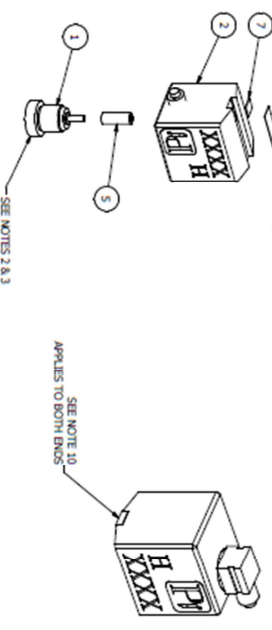
- Qin L., Huang S., Cheng X., Lu Y. & Li Z. (2009) 'The application of 1–3 cement-based piezoelectric transducers in active and passive health monitoring for concrete structures', *Smart Materials and Structures*, **18**, 095018 (8pp).
- Rose J. L. & Shin H. J. (1998) 'Ultrasonic guided waves for finned tubing evaluation', *7th Annual Research Symposium, ASNT Spring Conference*, Anaheim, CA, pp. 265–267.
- Rose J. L. (2000) 'Guided Wave Nuances for Ultrasonic Nondestructive Evaluation', *IEEE transactions of ultrasonics, ferroelectrics and frequency control*, **47** (3), pp. 575-582
- Rose J. L., Rajana K., & Carr F. T. (1994), 'Ultrasonic guided wave inspection concepts for steam generator tubing', *Journal of Materials Evaluation*, **52**, (2) pp. 307–311, Feb. 1994.
- Rose J.L. (1999) *Ultrasonic Waves in Solid Media*, Cambridge University Press.
- Sayles R. S. & Thomast T. R., *J. Phys. E: Sci. Instrum.* **9**, pp. 855-861.
- Shin H. J. & Rose J. L. (1998) 'Guided wave tuning principles for defect detection in tubing', *Journal of Nondestructive Evaluation*, **17**, (1) pp. 27–36.
- Simulai Dassault Systems, 2012. *ABAQUS/CAE manual*.
- Tabor D. (1972) 'Friction, lubrication and wear, in Matijevic E (Ed)', *Surface and Colloid Science*, **5**, pp. 245-312.
- Tang H.Y., Winkelmann C., Lestari W. & La Saponara V. (2011) 'Composite Structural Health Monitoring Through Use of Embedded PZT Sensors', *Journal of Intelligent Material Systems and Structures*, **22**, pp. 739-755
- Teletest Operator Training Course notes*, Plant Integrity Ltd, 2004.
- Tems R. & Al Zahrani A. M. (2006) 'Cost of corrosion in oil production and refining', *Saudi Aramco Journal of Technology*, **summer 2006**, pp.1-14
- Thomas R., Drinkwater B.D. & Laiptsis D. (2004) 'The reflection of ultrasound from partially contacting rough surfaces', *Journal of Acoustical Society of America*, **117** (2), pp. 638-645.
- Watson W. King T. G. & Spedding T. A. & Stout K. J., *Wear* **57**, pp. 195-205.
- Wilcox P.D., Lowe M. J. S. & Cawley P. (2001) 'Mode and transducer selection for long range lamb wave inspection', *Journal of Intelligent Material Systems and Structures*, **12** pp. 553-565
- Yaralioglu G. G., Badi M. H., Ergun A. S., Cheng C. H., Khuri-Yakub B. T. & Degertekin F. L. (2001) 'Lamb wave devices using capacitive micromachined ultrasonic transducers', *Applied Physics Letters*, **78** (1), pp. 111-113.
- Zhu X. & Rizzo P. (2012) 'A unified approach for the structural health monitoring of waveguides', *Structural Health Monitoring*, **11** (6), pp. 629–642.

## **Appendix A – Technical Drawings of Transducers**

ITEM #	QTY	PART NUMBER	DESCRIPTION	SHOW ON DWG
1	1	MEC-3000-0104	CONNECTOR - KEY RELEASED	DWG-3000-0104
2	1	MEC-3000-0102	COATED TILTEST TRANSDUCER	DWG-3000-0102
3	1	MEC-3000-0012	TRANSDUCER PZEO ELEMENT	DWG-3000-0012
4	1	MEC-3000-0014	ALUMINA FACE PLATE	DWG-3000-0014
5	1	MEC-3000-0918	INSULATION	N/A
6	1	MEC-3000-0919	INSULATIVE EPOXY	N/A
7	1	MEC-3000-0921	CONDUCTIVE EPOXY	N/A
8	1	MEC-3000-0922	POLYURETHANE SEALANT - WHITE	N/A
9	1	WR-3000-0920	0.09MM 99.99M WIRE (ALLOY 200) TO DINGSONG (05-IN-10290-1-0)	N/A
20	1	CON-3000-0157	CONNECTOR - FIBERS SNIFFER	N/A

REV	DESCRIPTION	DATE	EN	CHK
1	RELEASED FOR PRODUCTION	26/04/2010	AJF	CBM

REVISION HISTORY	DATE	EN	CHK
1	26/04/2010	AJF	CBM



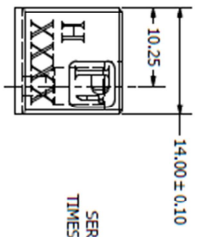
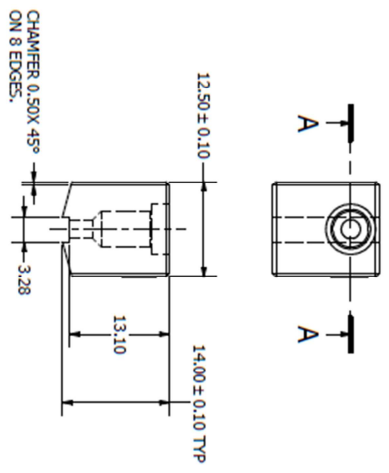
- NOTES:
1. ENSURE ITEM 3 TO BE THOROUGHLY DEGREASED AND FREE FROM MACHINING SWarf PRIOR TO ASSEMBLY.
  2. ITEM 1 TO BE FLUSH OR SCRAPED TO TOP SURFACE OF ITEM 2.
  3. ITEM 1 MINIMUM PULL-OUT FORCE FROM ITEM 2: 50N.
  4. ENSURE ITEM 5 IS USED TO CENTRALISE ITEM 3 WIRE IN HOLE.
  5. SUFFICIENT QTY OF ITEM 7 MUST BE USED TO ENSURE CONDUCTIVITY TO ITEM 3.
  6. SUFFICIENT QTY OF ITEM 6 MUST BE USED.
  7. ADEQUATE QUANTITY OF ITEM 8 MUST BE USED.
  8. TRANSDUCER TO SHOW >20MΩ RESISTANCE AT 500DC.
  9. TRANSDUCER TO SHOW >20MΩ RESISTANCE AT 500DC.
  10. OBSERVE ITEM 8 TO SEAL EXPOSED ENDS.

DESIGNED BY AJF	CHECKED BY MJB	DATE 26/04/2010	SCALE 1/1
ISSUED BY AJF	REVISION A	PROJECT TRANSDUCER-ASSEMBLY	DWG NO. DWG-3000-0045
TITLE TRANSDUCER-ASSEMBLY		PART NO. V0522M	
SHEET NO. 21		PART NO. A	
TOTAL SHEETS 21		PART NO. A	
TOL. LIMIT DIM. 0.15		PART NO. A	
TOL. LIMIT FITS 1.5		PART NO. A	
TOL. LIMIT SURF. 0.1		PART NO. A	

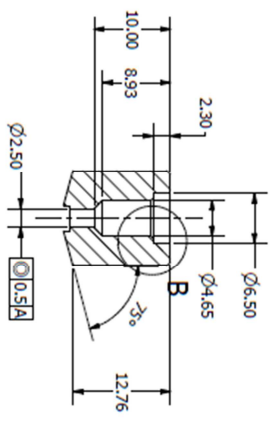
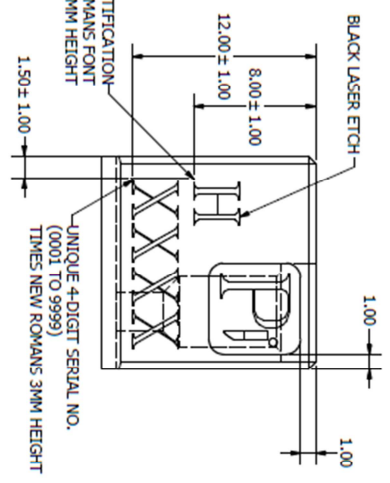
REVISION HISTORY					
REV	DESCRIPTION	DATE	EQN	ORG	CHK
1	RELEASED FOR PROTOTYPE	13/12/2009	---	GJB	SCD
2	13.10 WAS 13.15	22/02/2010	---	GJB	AJF
3	PRINT MARKING DETAILS ADDED	23/02/2010	---	GJB	AJF



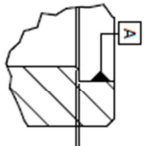
ISO VIEW



PART MARKING DETAIL ( 4 : 1 )



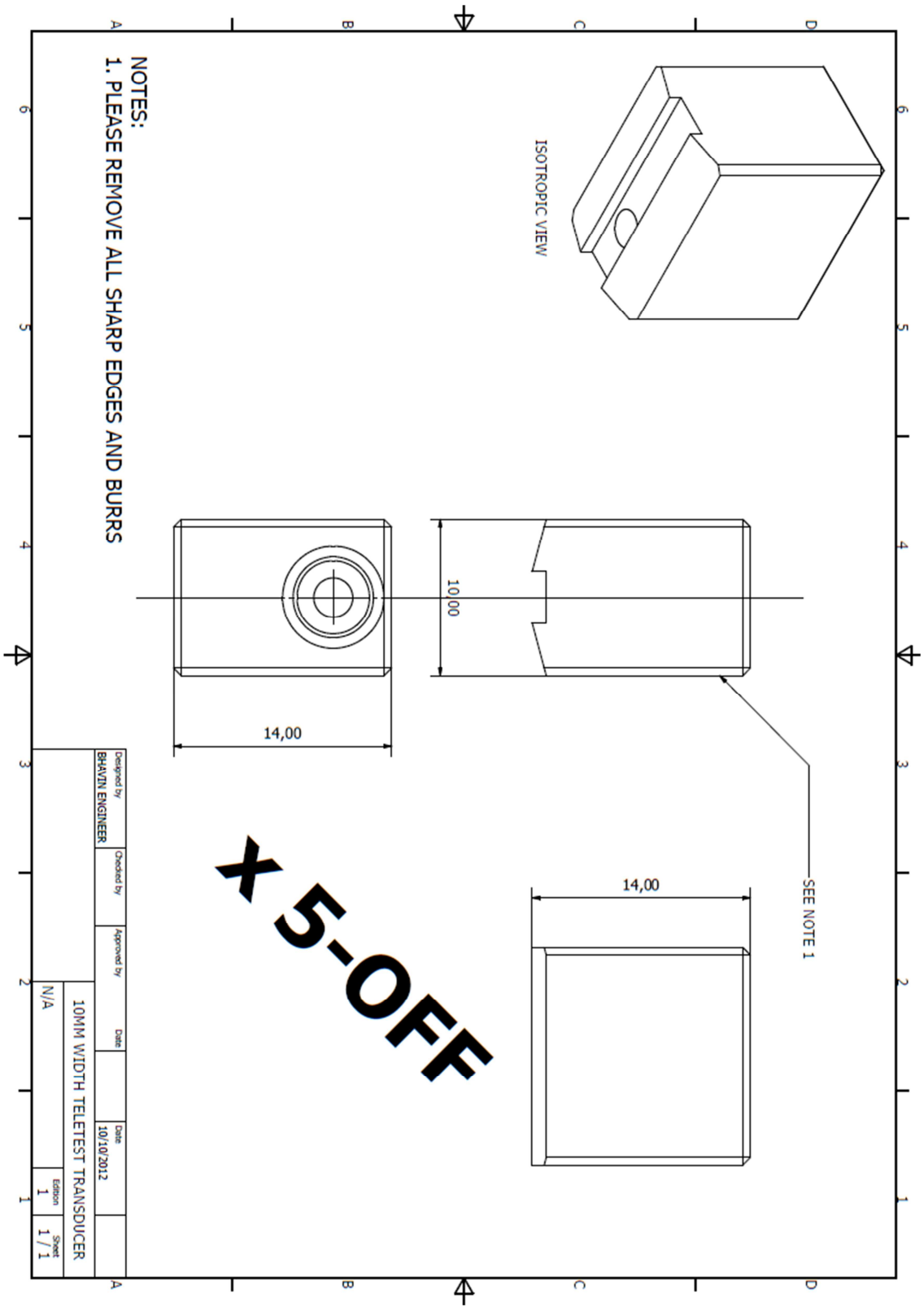
SECTION A-A

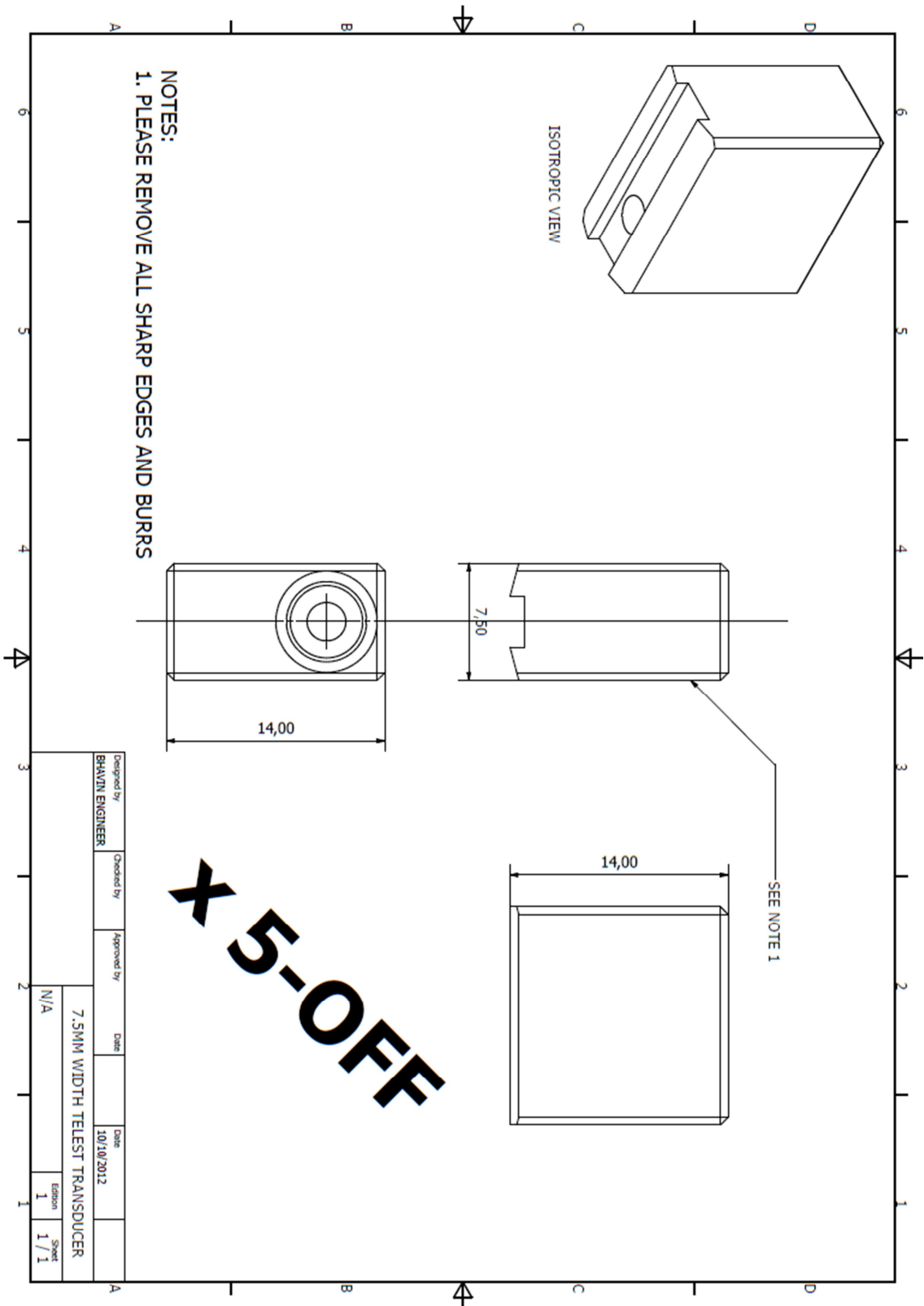


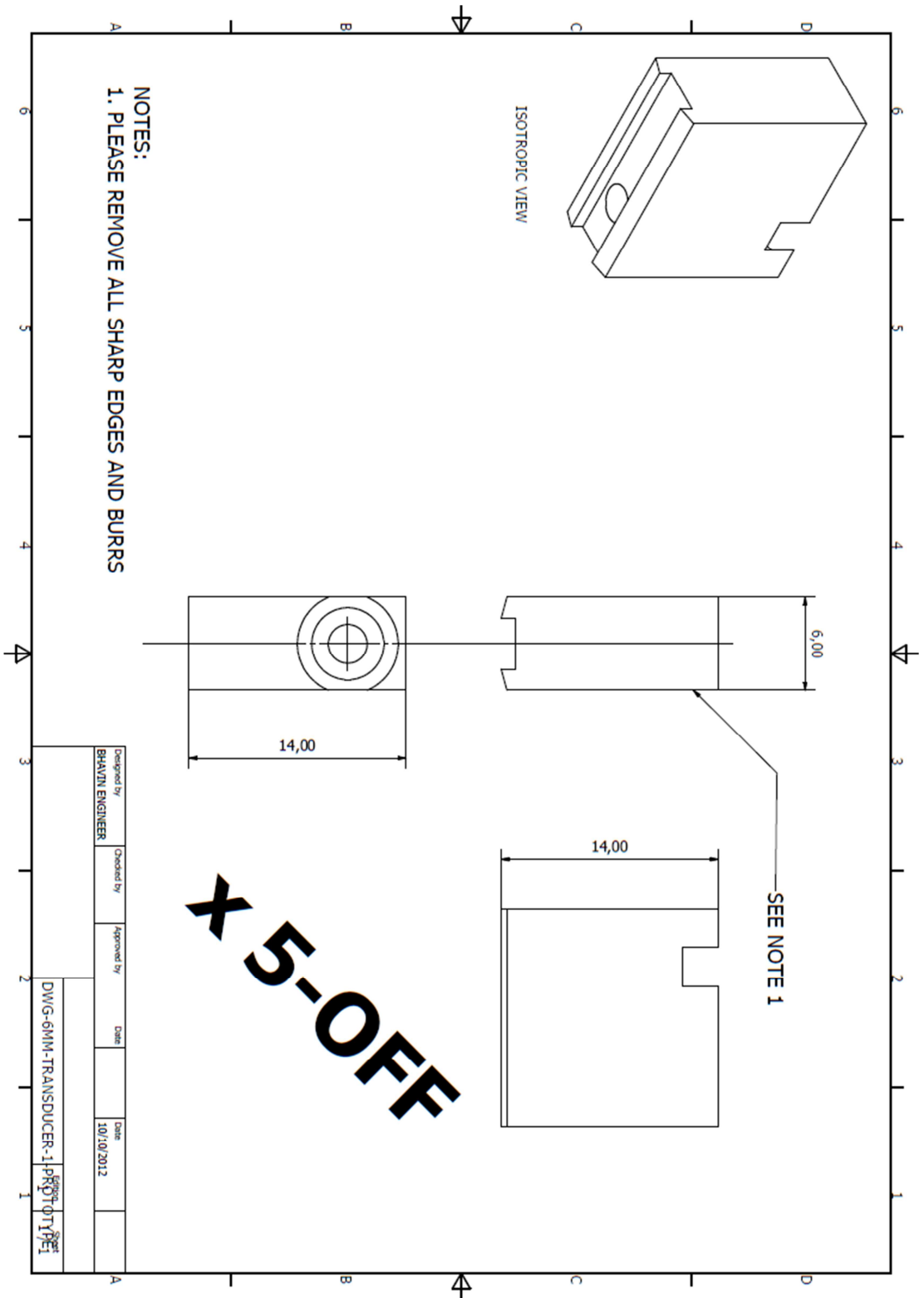
DETAIL B

- NOTES:
1. THOROUGHLY DEGREASE COMPONENT AFTER MACHINING.
  2. ENSURE ALL SWarfs REMOVED FROM HOLE.
  3. REMOVE ALL BURRS AND SHARP EDGES.

UNLESS OTHERWISE SPECIFIED, DIMENSIONS ARE IN MILLIMETERS. DIMENSIONS OF HOLES AND TOLERANCES TO BE SHOWN TO 3 SIG FIGS. UNLESS OTHERWISE SPECIFIED, DIMENSIONS ARE IN MILLIMETERS. DIMENSIONS OF HOLES AND TOLERANCES TO BE SHOWN TO 3 SIG FIGS. UNLESS OTHERWISE SPECIFIED, DIMENSIONS ARE IN MILLIMETERS. DIMENSIONS OF HOLES AND TOLERANCES TO BE SHOWN TO 3 SIG FIGS.	DESIGNED BY AJ FRANCE	CHECKED BY BJ ELBORN	THIRD ANGLE PROJECTION	DRAWING NO. DWG-3000-0043	REVISION 3	DRAWING STATUS PROTOTYPE
TOL. LENGTH DIM ± 0.05	DRAWING SCALE 2:1	DATE 25/03/2009		PART NO. MEC-3000-0043	VERSION B	
TOL. RADIUS DIM ± 0.05	SHEET SIZE A3			MATERIAL STAINLESS STEEL: GRADE 303; BS10088 PART 3; 2005		
TOL. ANGULAR DIM ± 0.2°				FINISH GROUND		
INDEX BEND RADIUS ± 1.0				TREATMENT N/A		







## **Appendix B – Contact Mechanics Literature**

## Theories and models of contact between surfaces

If two parallel planes come into gentle contact, contact will only occur at a small amount of asperities. As the normal load applied onto these surfaces is increased than a higher number of asperities come into contact. These points of contact support the load and are the sources of friction between the surfaces.

### Deformation of a single asperity

In a bid to understand contact between multiple asperities of two surfaces, it is sensible to break down and simplify the model for the contact of one asperity. As discussed before, asperities have a very shallow gradient (less than  $10^\circ$ ) and hence are blunt objects. It is convenient to model them with a smooth spherical geometry. The simplest scenario that can be set is a deformable sphere, acting as the asperity, normally loaded onto a non-deformable rigid flat plane surface. After understanding this case, this model can be developed into something more sophisticated.

#### Elastic deformation

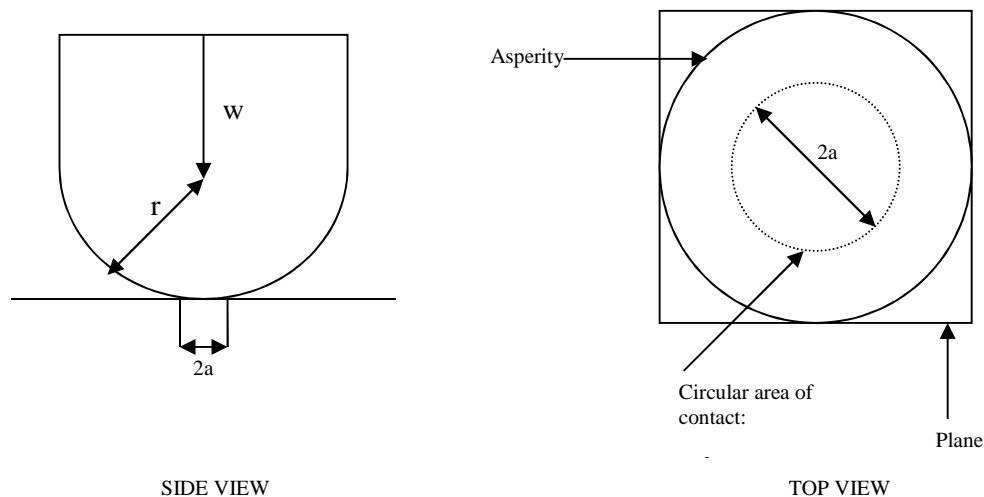


Figure B.1: Elastic deformation upon single asperity contact.

When a sphere made out of elastic material is normally loaded onto a plane with a load  $w$ , a circular area of contact will occur with a radius of  $a$ . This can be summarized in a relationship by Hertz theory of elastic deformation (1881):

$$a = \left( \frac{3wr}{4E} \right)^{1/3} \quad (\text{Equation B.1})$$

Where  $r$  is radius of the sphere and  $E$  is the elastic modulus. This elastic modulus can be calculated by the Young Modulus of the sphere and the plane,  $E_1$  and  $E_2$  and the Poisson's ratio of the sphere and the plane,  $\nu_1$  and  $\nu_2$ :

$$\frac{1}{E} = \frac{(1-\nu_1^2)}{E_1} + \frac{(1-\nu_2^2)}{E_2} \quad (\text{Equation B.2})$$

The area of contact can thus be calculated by:

$$\pi a^2 = 0.83\pi \left( \frac{wr}{E} \right)^{2/3} \quad (\text{Equation B.3})$$

In a pure elastic system the deformation is proportional to  $w^{2/3}$ .

To find the mean pressure (normal stress), the concept of  $P = \frac{F}{A}$  is applied where:

$P_{mean}$  over the contact area  $= \frac{W}{\pi a^2}$  and the driving factor for this value is  $w^{1/3}$ . This will not be a uniformly distributed pressure and will have a maximum pressure at the centre of the circular contact area and will recede to a minimum at the edge of the circular contact area, as shown in Figure L.

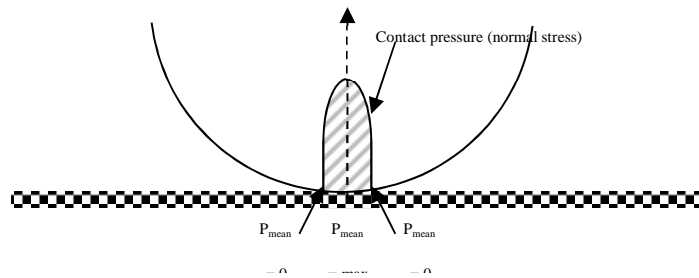


**Figure B.2: Distribution of normal stress (contact pressure) in a simple asperity under elastic deformation.**

The maximum pressure in the contact circle  $P_{max}$  will be  $3/2$  times greater than the mean pressure:

$$P_{max} = \frac{3}{2} P_{mean} \text{ (Equation B.4)}$$

### **Plastic Deformation**

After a critical load is applied the contact will extend from elastic behaviour to elements that deform plastically. Applying this behaviour to the single asperity model previously discussed, two situations are possible; the sphere is rigid and the plate will exhibit plastic flow and the second situation where conversely the plate stays rigid and the sphere plastically deforms.

Both these scenarios have a simplified relationship to indentation hardness testing. Hertz investigated the indentation between a plastic half-space and a rigid sphere. Whilst analysing physical re-enactments he found the elastic stress field to show that the maximum shear stress occurs at a depth of  $0.47a$  beneath the indenter.

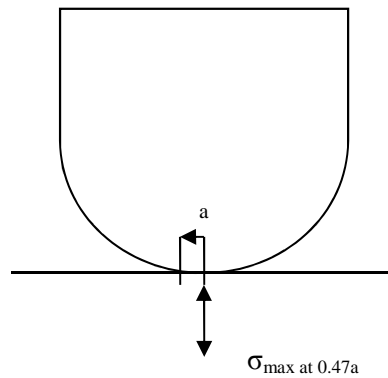


**Figure B.3: Point of maximum shear stress under indenter discovered by Hertz.**

Plastic flow begins to happen at this point dependent on the yield criterion. If the Tresca criterion is valid, then the maximum shear stress is equal to  $\frac{Y}{2}$  where  $Y$  is the uni-axial yield stress of the material:

$$\sigma_{\max} = \frac{Y}{2} \text{ (Equation B.5)}$$

If the material possesses a Poisson's ratio of approximately 0.3, then the shear stress at a depth of  $0.47a$  underneath the sphere is 0.47 times the mean contact pressure,  $P_{\text{mean}}$ :

$$\sigma_{\max} = 0.47 P_{\text{mean}}$$

Hence

$$\sigma_{\max} = \frac{Y}{2} = 0.47P_{\text{mean}} \quad (\text{Equation B.6})$$

$$\frac{Y}{2} \div 0.47 = P_{\text{mean}}$$

$$\frac{Y}{2} \times \frac{1}{0.47} = Y \times \frac{1}{0.94} \approx 1.1Y = P_{\text{mean}}$$

Plastic deformation occurs when a mean contact pressure is  $1.1Y$ . Once this method of loading for initiating plastic flow has been surpassed, additional loading will extend the zone of plastic deformation from beneath the indenter (at  $0.47a$ ) upwards to the surface. When this happens, the load applied for metallic materials can be 50 - 100 times greater than the load applied initially to instigate plastic flow. The contact area will still be very small, approximately a radius ( $a$ ) that is less than 1% of the radius of the sphere ( $r$ ). The mean pressure ( $P_{\text{mean}}$ ) on the area of contact by this stage will have risen to  $3Y$  and that will be the maximum for any subsequent loading:

$$P_{\text{mean}}(\text{max}) = 3Y. \quad (\text{Equation B.7})$$

This means once full plasticity has been achieved the mean contact pressure is independent of the load. What's more the pressure is directly related to the yield stress of the material and this,  $Y$ , is a defining factor.

This test and these relationships are the basis for indentation hardness testing. When these tests are conducted inversely, i.e. a soft sphere is pressed against a rigid plane, similar results are established providing the loading is not too large to produce fracture.

‘...it does not much matter which component yields; the mean pressure over the contact area will always be of the order of three times the uniaxial yield stress of the softer material. More important, the area of contact should be directly proportional to the load...’ (from Hutchings I M, Friction and Wear of Engineering Materials, Edward Arnold, 1992).

## Simple theory of multiple asperity contact

The theory for a single asperity contact can be extrapolated to serve a theory for multiple asperity contact. A statistical approach would be more apt for investigating a more realistic scenario however a simple theory can give some insight and estimation of what is expected.

The problem is simplified to contact between a row of spherical asperities representing a rough surface and a rigid frictionless plate. Here it is assumed each asperity deforms independently of one another. Each asperity will have the same radius and same height.

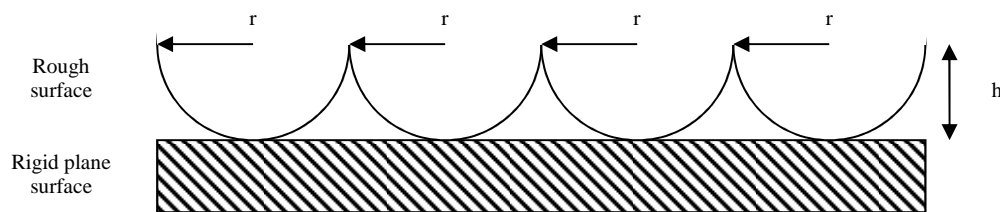


Figure B.4: Elastic deformation upon simple multiple asperity contact.

In this scenario, upon contact each asperity will distribute the load equally and consequently display the same total area of contact. The same relationship will occur as discussed previously when all the contact and loading is summed up to show that in a pure elastic case

$$A \propto W^{2/3}$$

And for perfect plastic behaviour

$$A \propto W$$

In reality, true surface geometry will have non-uniform asperities with a variety of radii and heights. These will be statistically distributed. To gain a truer reflection of multiple asperities contacting, statistical theories are used to investigate behaviour.

## Statistical theories of multiple asperity contact

A widely accepted statistical theory for contact of rough surfaces is from Greenwood and Williamson 'Contact of nominally flat rough surfaces' (1966).

In this model, the following assumptions are made:

All contacting asperities have a spherical geometry with a constant radius  $r$ . They all deform elastically under load according to Hertz's equation.

There is a graphical demonstration of the model taken into account: contact between a rough surface and a rigid plane.

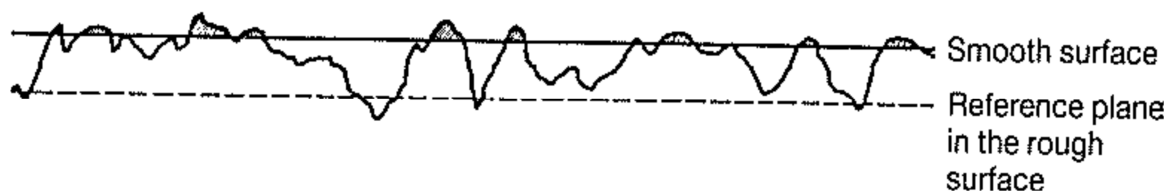


Figure B.5: Model for contact between a rough surface and a smooth rigid plane (from Greenwood J A and Williamson J B P, Proc. Roy. Soc. Lond. A295, 300-319, 1966).

The height from the peak of an asperity to the reference plane is  $z$ . The separation distance between the reference plane in the rough surface and the flat surface is  $d$ . If  $d$  is less than  $z$  then the asperity will compress elastically and a load will be supported,  $w$ , which is calculated by Hertzian theory.

$$w = \frac{4}{3} Er^{1/2} (z - d)^{3/2} \quad (\text{Equation B.8})$$



Figure B.6: Example of statistical model for contact between a rough surface and a smooth rigid plane.

I.e.:

$$z = 50\mu\text{m}$$

$$d = 30\mu\text{m}$$

If  $d < z$  elastic deformation will occur.

$30\mu\text{m} < 50\mu\text{m}$  hence elastic deformation occurs at a load  $w$ , where  $w = \frac{4}{3}Er^{1/2}(z-d)^{3/2}$ .

The heights of the asperities will be statistically distributed. The probability of an asperity having a height between  $z$  and  $z+\delta z$  is  $\phi(z)\delta z$  where  $\phi(z)$  is a probability density function which describes the distribution of asperity heights. This function is different to  $p(y)$  (amplitude density function) as it concerns identifying individual asperities.

The probability of an asperity making contact with the rigid surface would be the same as the probability that its height  $z$  is greater than the plane separation,  $d$ .

$$\text{prob}(z > d) = \int_d^{\infty} \phi(z) dz \quad (\text{Equation B.9})$$

If the total asperities on the surface is  $N$ , then the predicted number of contacts will be  $n$ :

$$n = N \int_d^{\infty} \phi(z) dz \quad (\text{Equation B.10})$$

If each contact deforms elastically to carry a load  $W$ , then the total load  $W$  will be

$$W = \frac{4}{3} NEr^{1/2} \int_d^{\infty} (z-d)^{3/2} \phi(z) dz \quad (\text{Equation B.11})$$

$$[W = \underbrace{w}_{\text{Load per contact}} \cdot \underbrace{n}_{\text{Number of contacts}}]$$

Greenwood and Williamson applied their theory to two different types of distribution of asperity heights. The first was an exponential distribution. In this case equation 18 can be analytically integrated. This solves to show that the total load  $W$  is linearly proportional to the total true area of contact. When the load is increased, each asperity contact spot increases, but more asperities come into contact which in turn means the average size of each asperity contact becomes the same.

An exponential distribution of most surfaces is an adequate description; however a Gaussian (normal) distribution is a better description. This has been validated experimentally.

In this case equation 18 is numerically integrated. The results do not seem to majorly vary from an exponential distribution. The true area of contact is not exactly proportional to the load but it will almost be linear. It also shows that the true area of contact is not dependent on the apparent area of contact.

The theory was set for a purely elastic system, although plastic flow can be predicted. The proportion of asperity contacts that occur when there is plastic flow is dependent on the plasticity index  $\psi$ .

$$\psi = \frac{E}{H} \left( \frac{\sigma^*}{r} \right)^{1/2} \quad (\text{Equation B.12})$$

E is the elastic modulus. H is the indentation hardness of a rough surface (the plastic flow stress at

contact points) and  $\sigma^*$  is the standard deviation of asperity heights.  $\left(\frac{\sigma^*}{r}\right)^{1/2}$  is the average gradient of the asperities.

In theory, the plasticity index and the nominal pressure define the proportion of asperity contact points that exhibit plastic flow. In reality it is the plasticity index that is the influencing factor.

When  $\psi < 0.6$  plastic flow occurs at very high nominal pressures. At  $\psi > 1$ , plastic deformation occurs at light loads. In engineering metal surfaces  $\psi$  ranges from 0.1 to 100. Only finely polished surfaces will retain elastic deformation. In ceramics and polymers elastic contact is more likely than plastic

because the material properties that define  $\frac{E}{H}$  are smaller than metals (up to a tenth) thus reducing the value of  $\psi$ .

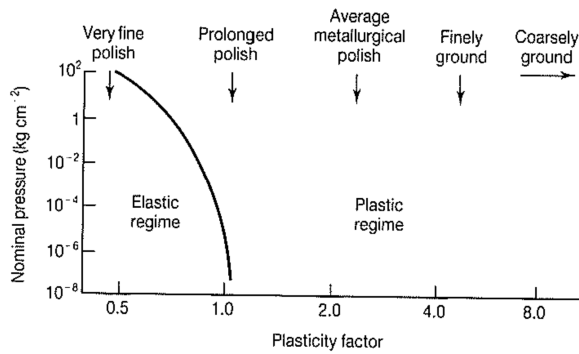


**Figure B.7: The dependence of asperity deformation mode on plasticity index  $\psi$  for aluminium surfaces with different roughnesses (from Tabor D, Friction, lubrication and wear, in Matijevic E (Ed), Surface and Colloid Science vol. 5, John Wiley, 1972, pp. 245-312).**

In summary, it is expected in the majority of cases that plastic deformation will occur between metal surfaces in contact in practical applications. The load supported on each contact is proportional to the normal load regardless of distribution of asperity heights. Elastic contact occurs for materials with

low ratios of  $\frac{E}{H}$  which are observed in ceramics, polymer and extremely smooth metals.

In elastic contact, it still stands true that the total real area of contact is proportional to the load because the number of peaks that contact increases but the mean area for each contact area stays constant.

## **Appendix C – Dispersion Curves and Wave Mode Displacements of 20mm<sup>2</sup> Rod Wave Guide**

Dispersion Curves - 20mm by 20mm Solid Square Bar

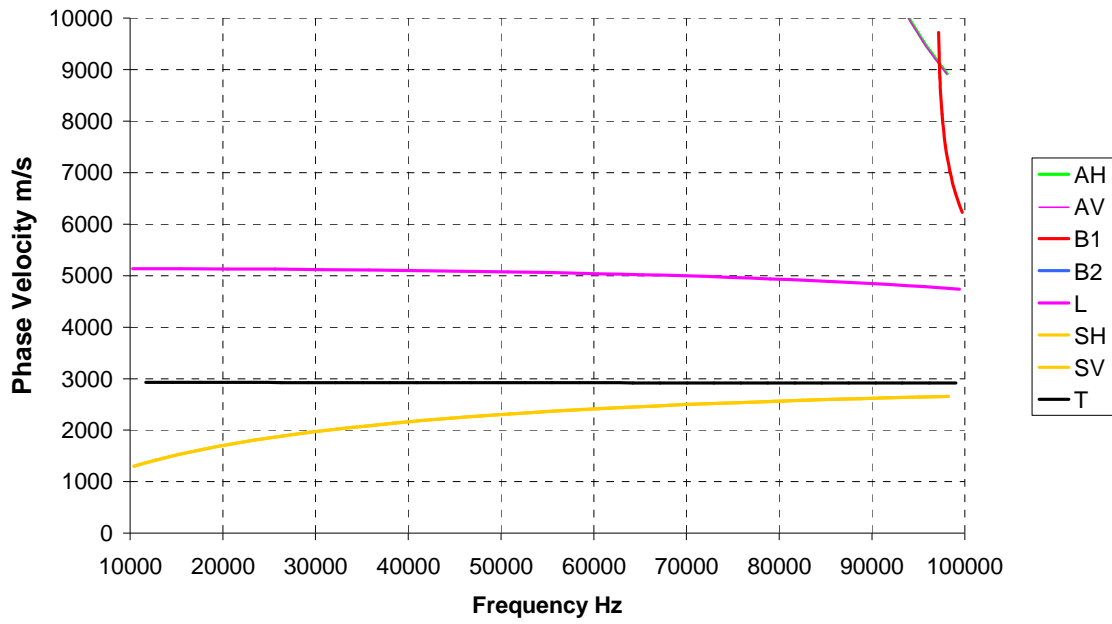


Figure C1: Phase velocity dispersion curves for 20mm square steel bar.

Dispersion Curves - 20mm by 20mm Solid Square Bar

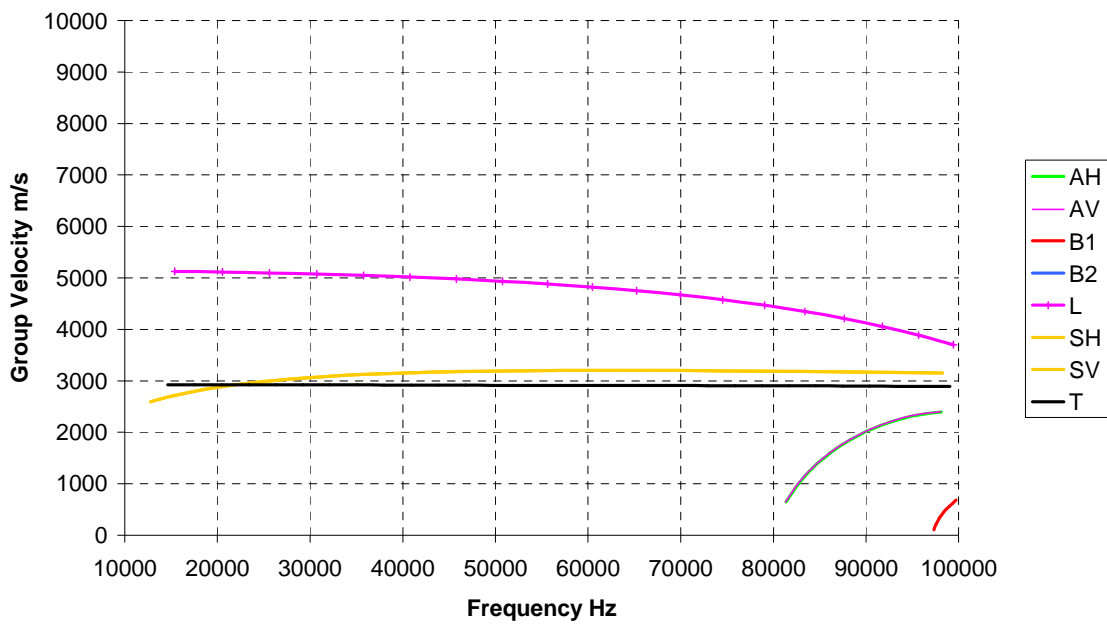


Figure C2: Group velocity dispersion curves for 20mm square steel bar.

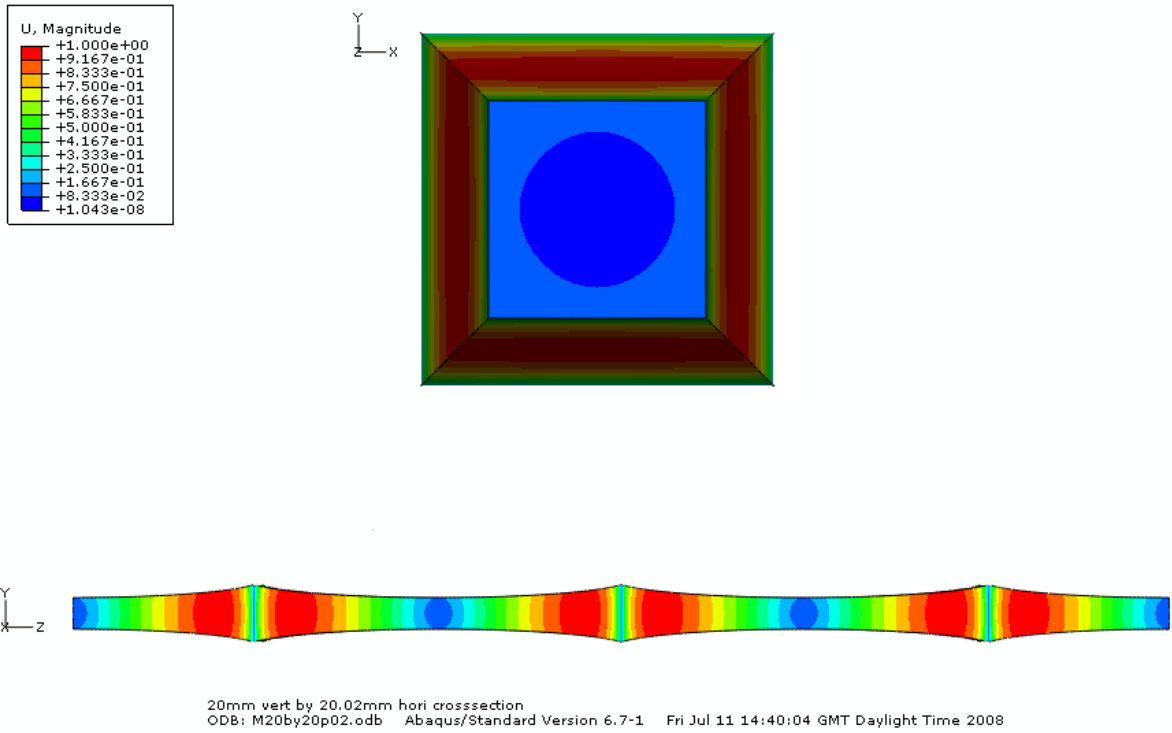


Figure C3: Displacement for wave mode 'L'.

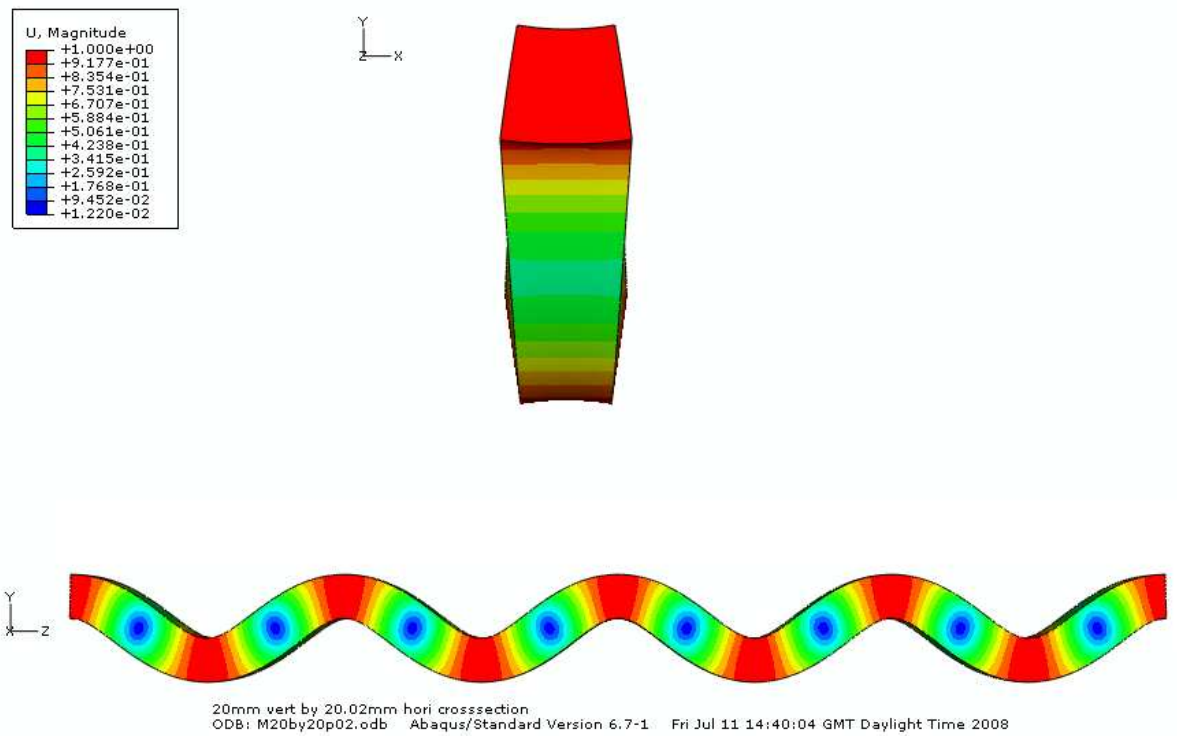


Figure C4: Displacement for wave mode 'SH/SV'.

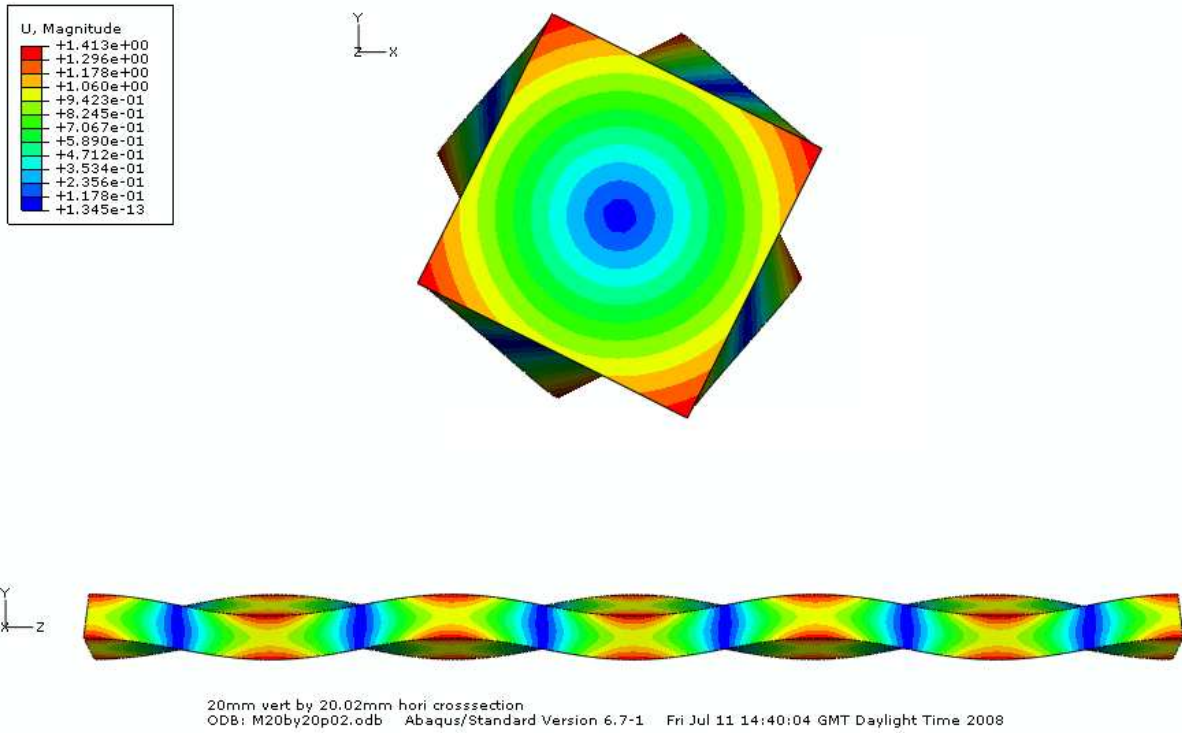


Figure C5: Displacement for wave mode 'T'.

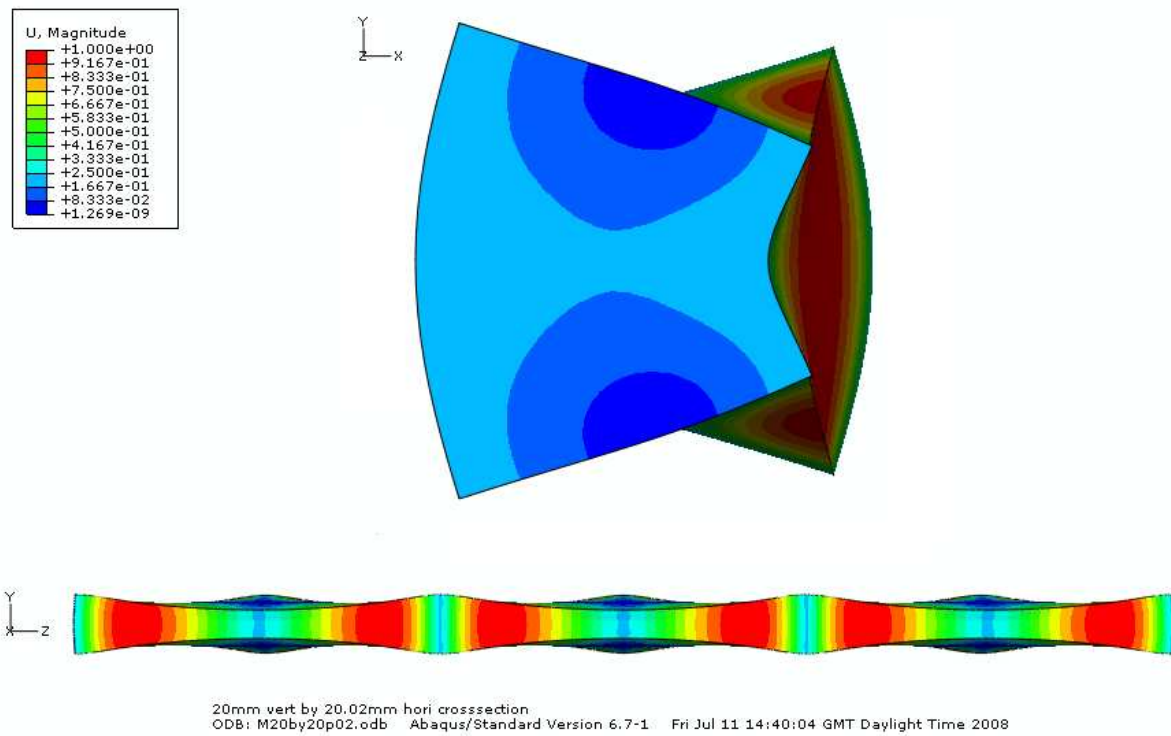
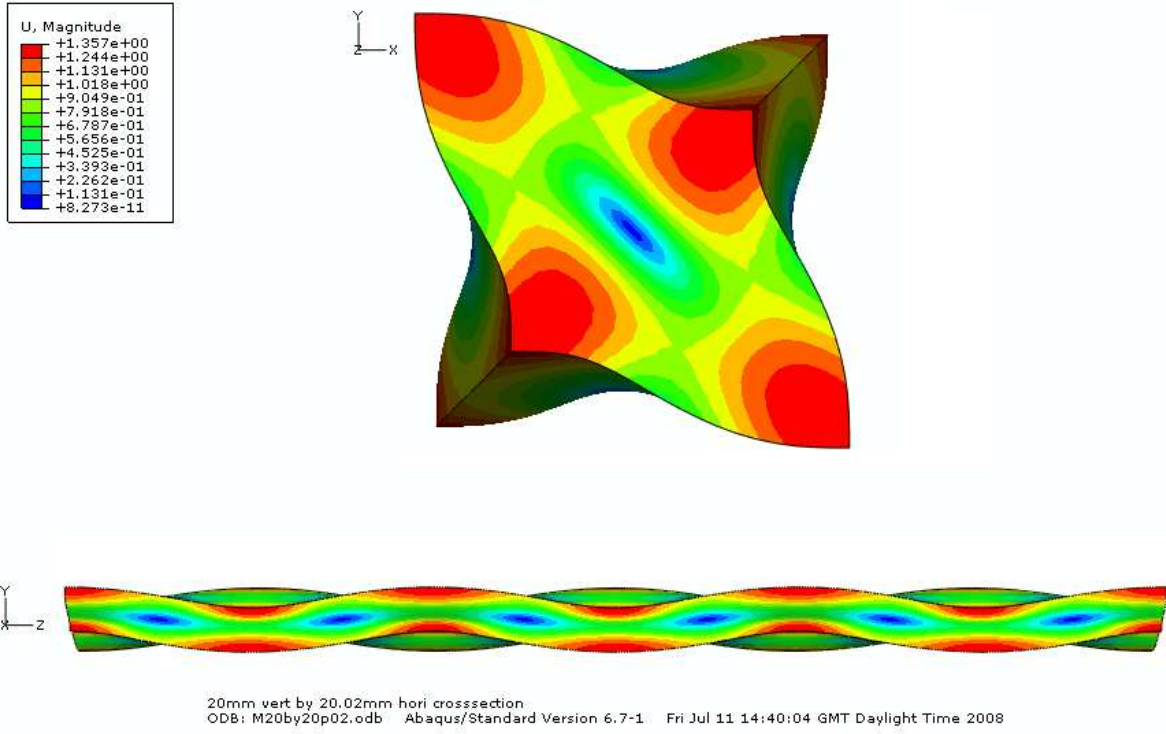


Figure C.6: Displacement for wave mode 'AV'.



**Figure C7: Displacement for wave mode 'B'.**

## **Appendix D – Frequency Response & Transmission Amplitude vs Force Plots**

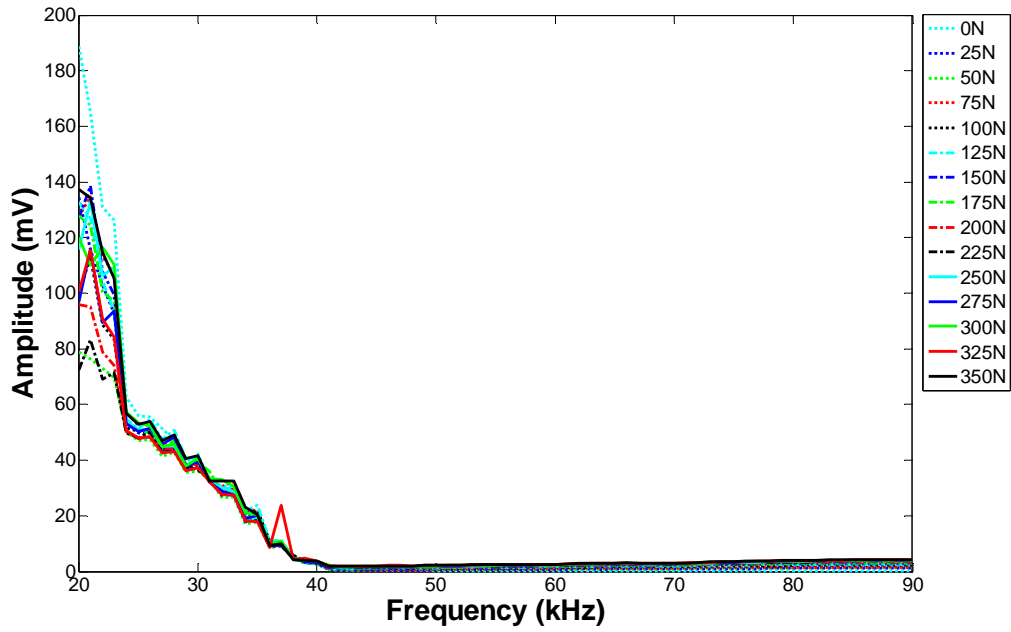


Figure D.1: Average frequency response for location A.

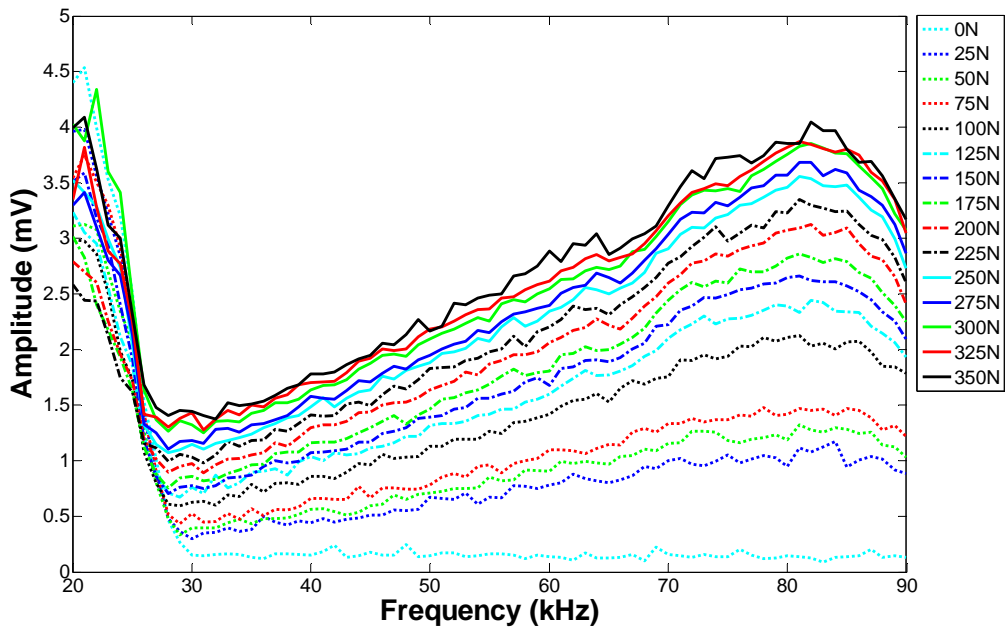


Figure D.2: Average frequency response for location B.

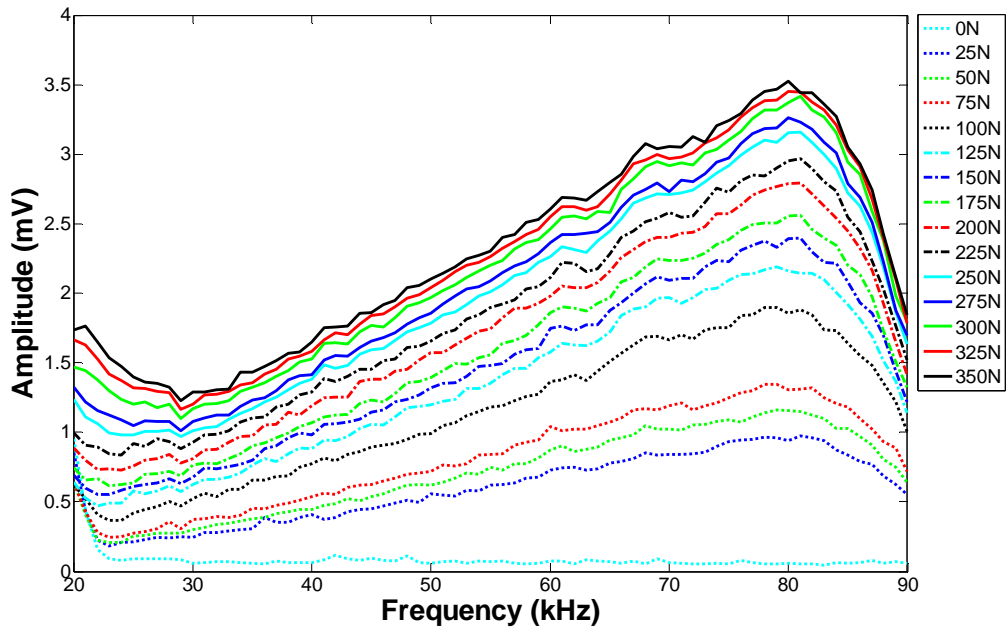


Figure D.3: Average frequency response for location C.

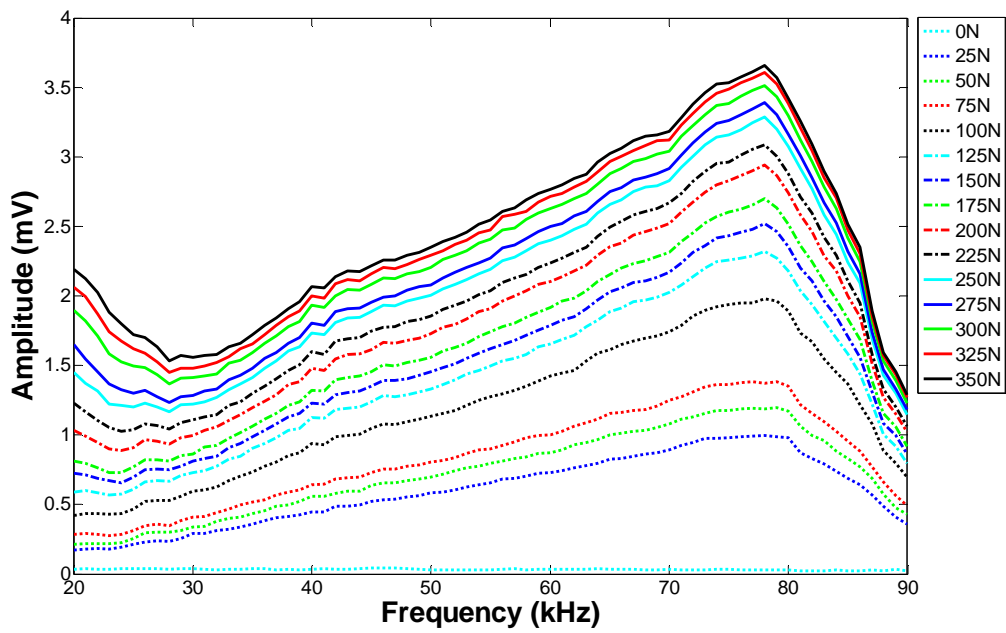


Figure D.4: Average frequency response for location D.

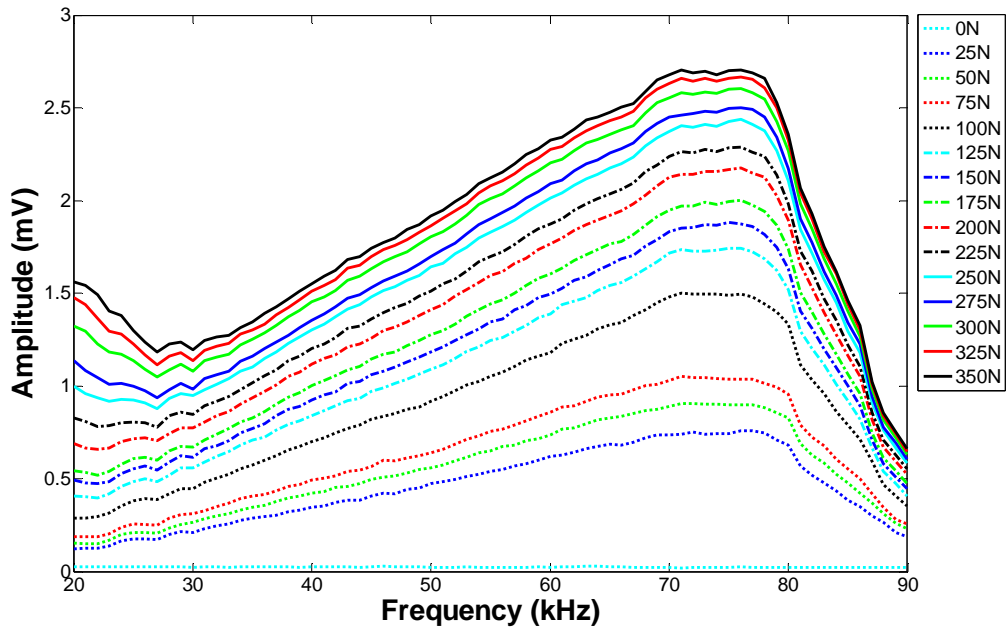


Figure D.5: Average frequency response for location E.

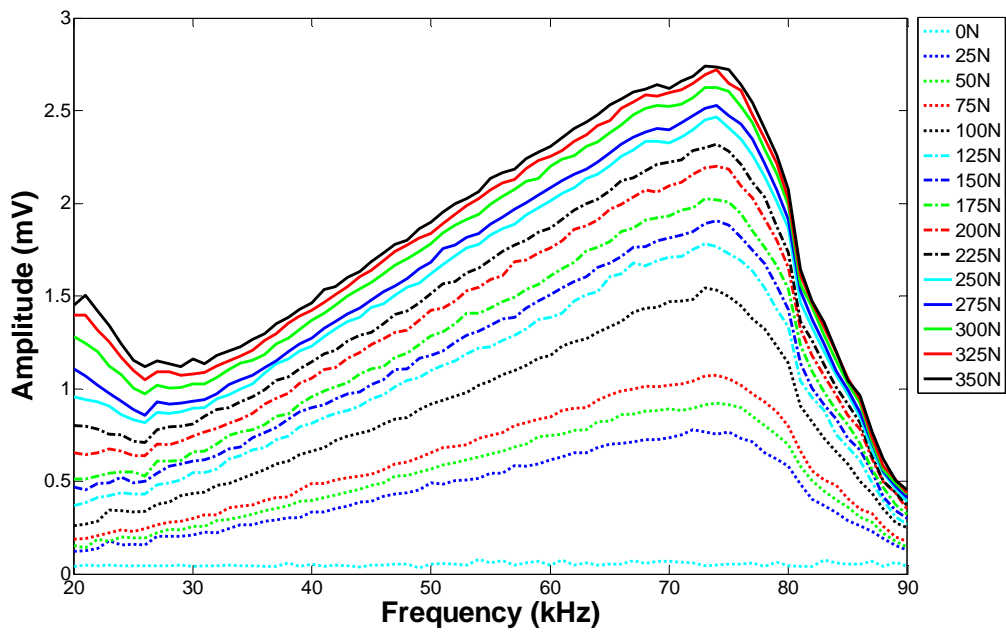


Figure D.6: Average frequency response for location F.

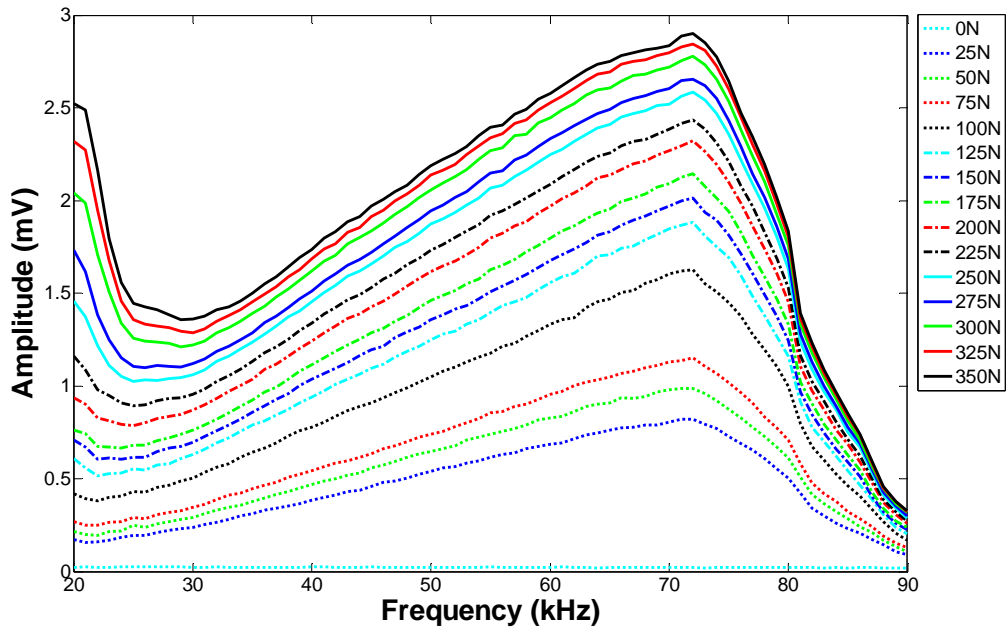


Figure D.7: Average frequency response for location G.

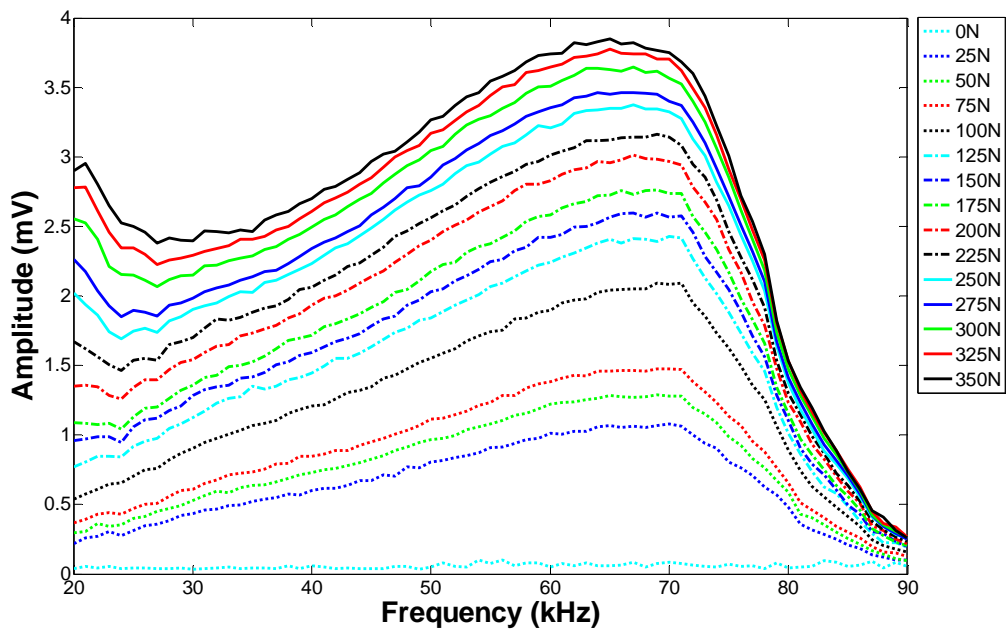


Figure D.8: Average frequency response for location H.

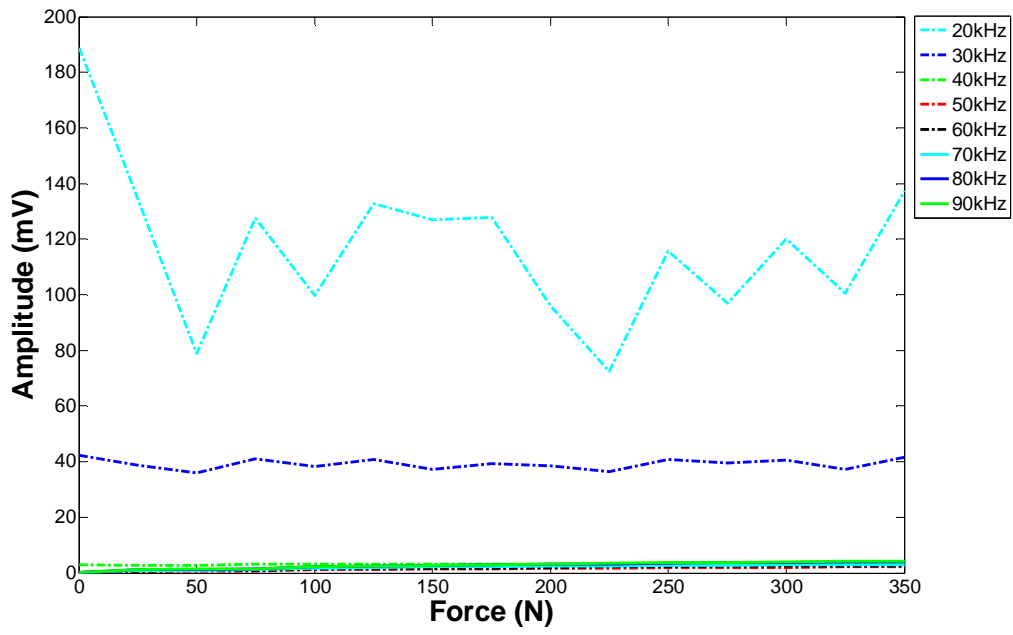


Figure D.8: Average amplitude versus force for location A.

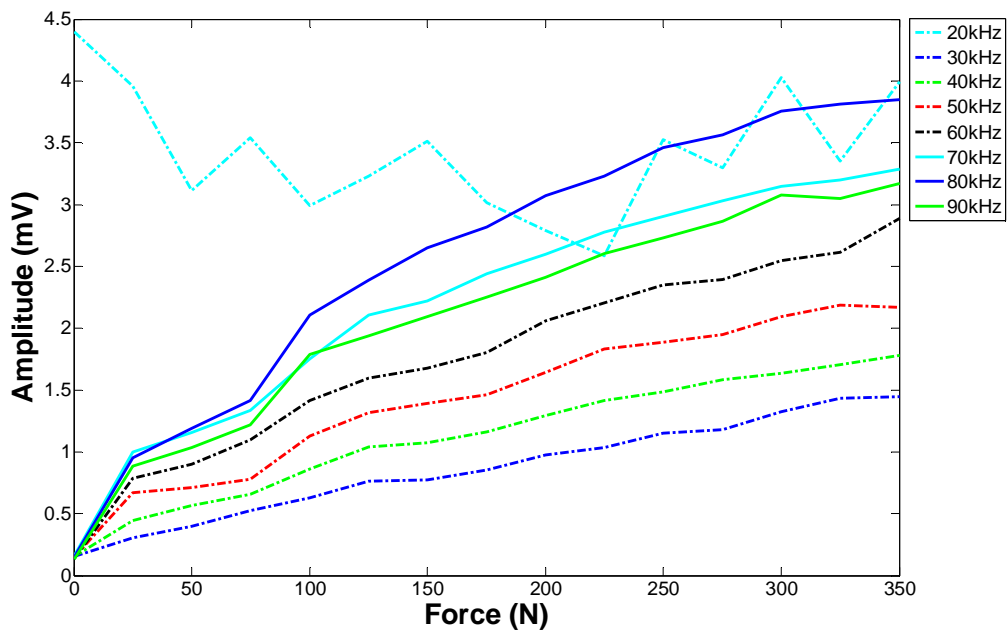


Figure D.9: Average amplitude versus force for location B.

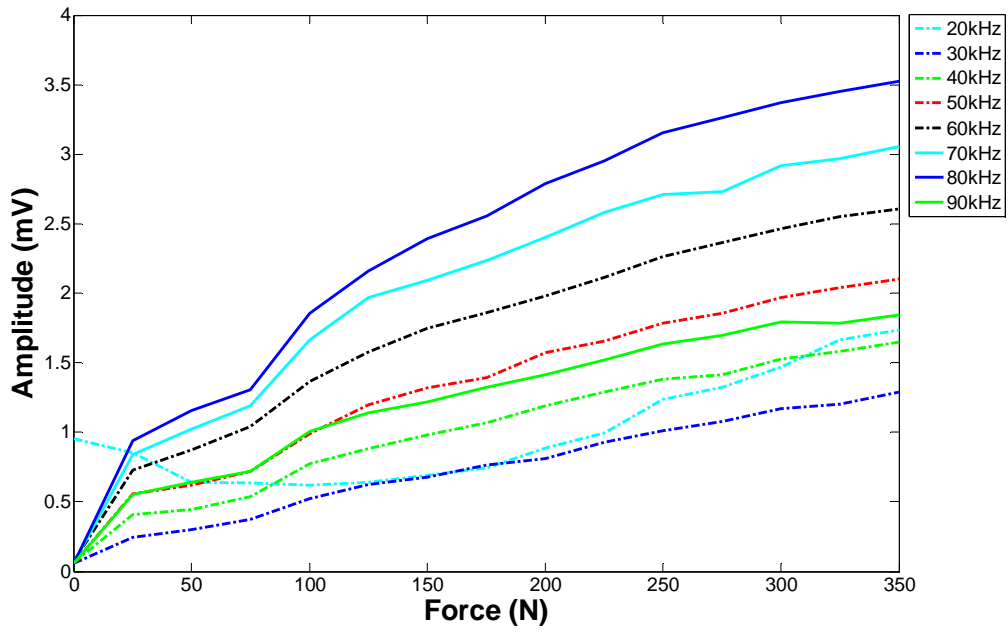


Figure D.10: Average amplitude versus force for location C.

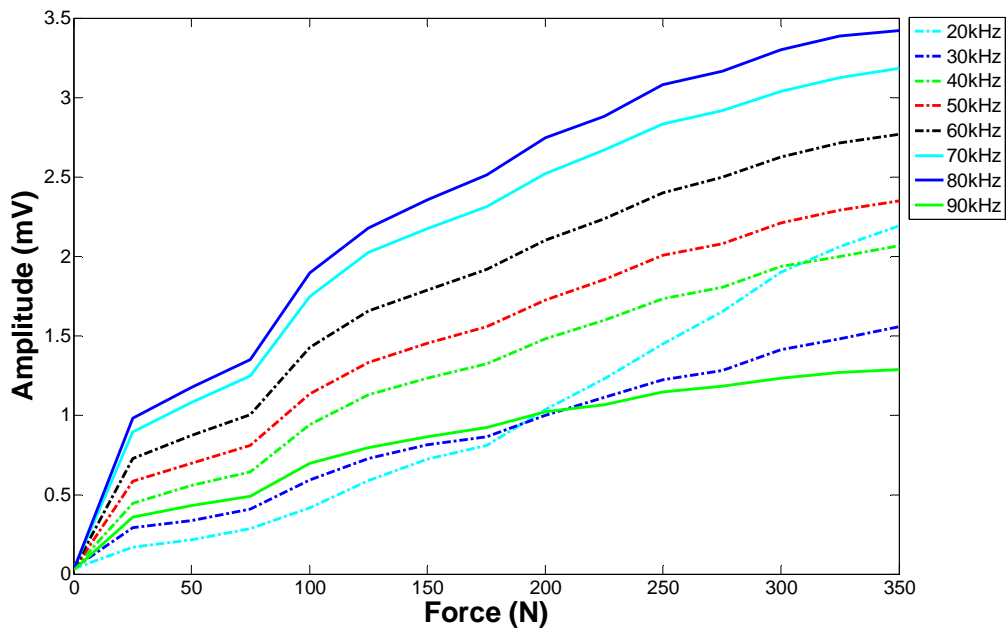


Figure D.11: Average amplitude versus force for location D.

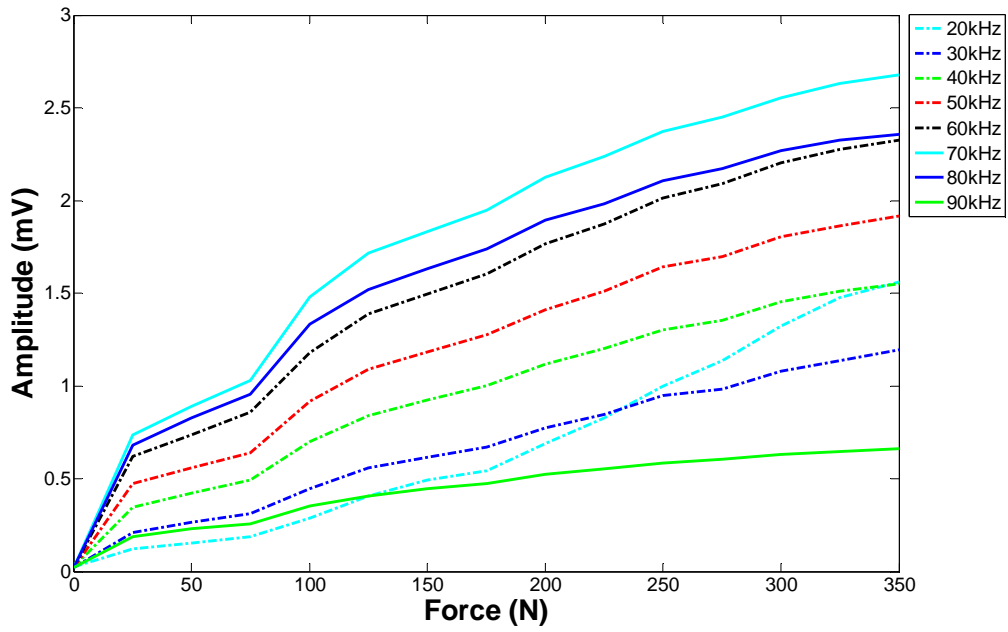


Figure D.12: Average amplitude versus force for location E.

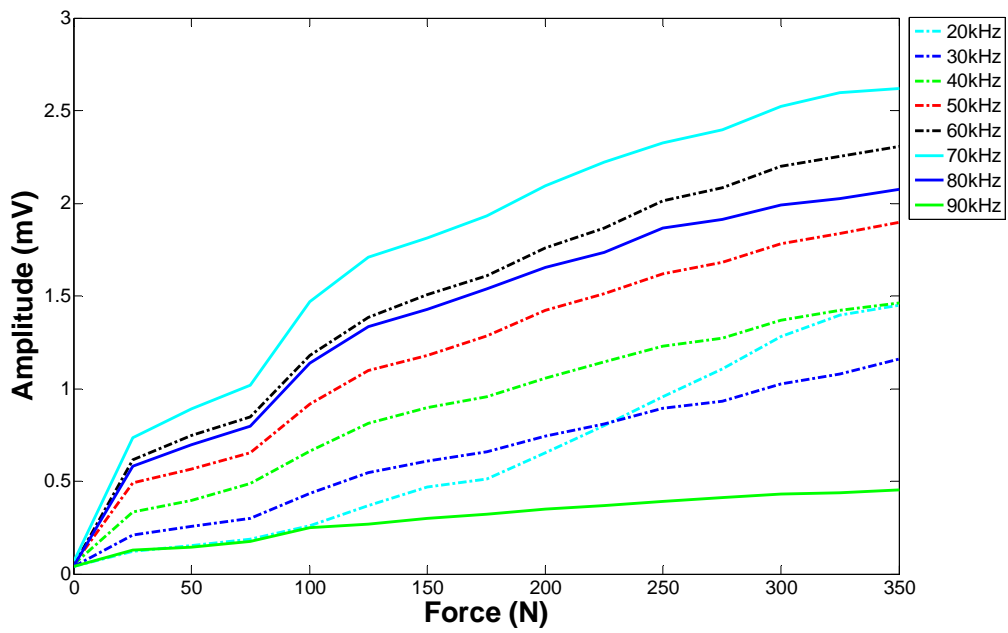


Figure D.13: Average amplitude versus force for location F.

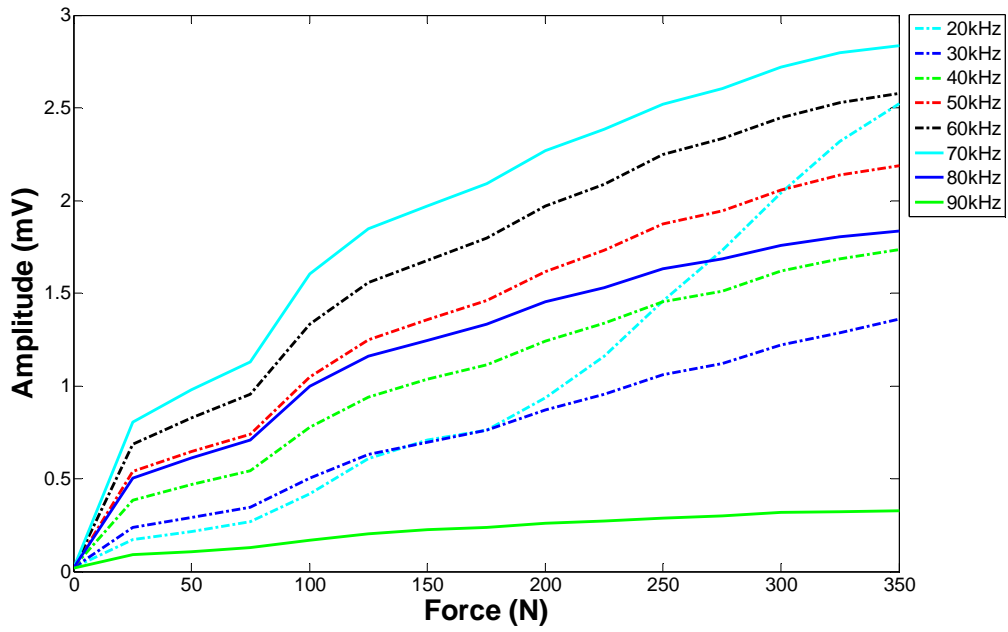


Figure D.14: Average amplitude versus force for location G.

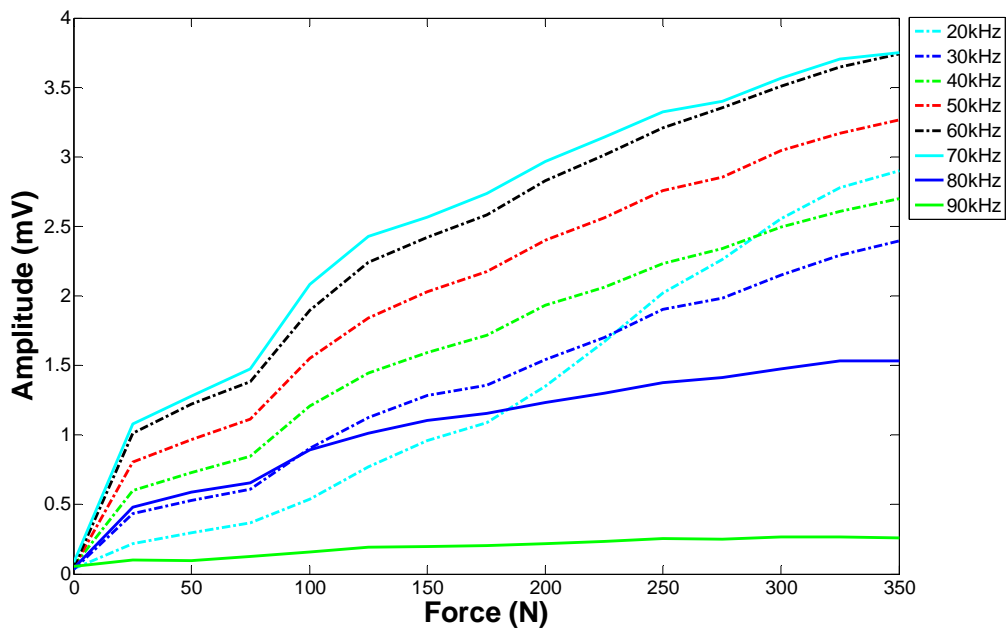
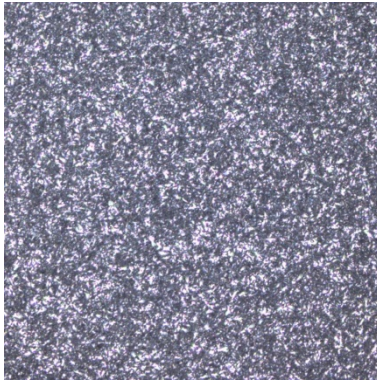
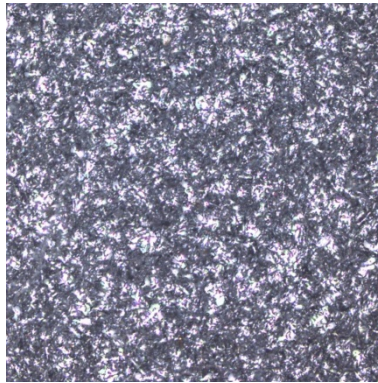


Figure D.15: Average amplitude versus force for location H.

## **Appendix E – Waveguide Surface Roughness Optical Microscope Images**



**Figure E.1: 2.6mm x 2.6mm optical microscope image (x 10) of Steel wave guide surface after grit blasting by Alumina 100.**



**Figure E.2: 2.6mm x 2.6mm optical microscope image (x 10) of Steel wave guide surface after grit blasting by Alumina 36.**

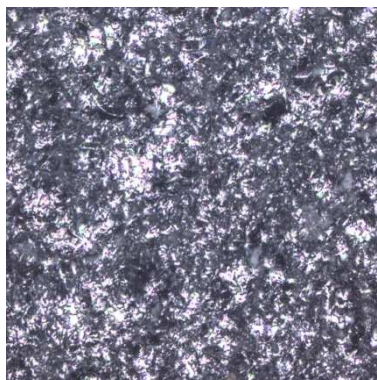


**Figure E.3: 2.6mm x 2.6mm optical microscope image (x 10) of Steel wave guide surface after grit blasting by Alumina 12.**

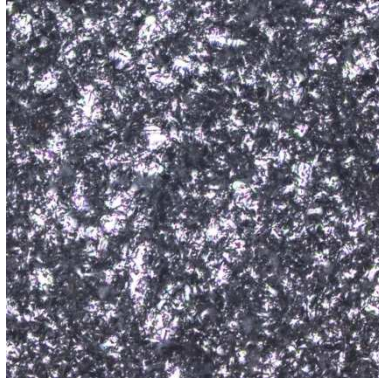


**Figure E.4: 2.6mm x 2.6mm optical microscope image (x 10) of Steel wave guide surface after grit blasting by Alumina 20.**

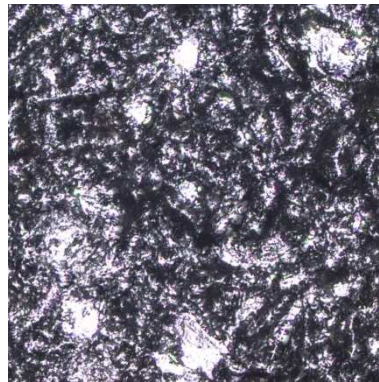


**Figure E.5: 2.6mm x 2.6mm optical microscope image (x 10) of Steel wave guide surface after grit blasting by Rough Iron G55.**

## **Appendix F – Electrical Impedance versus Force Plots**

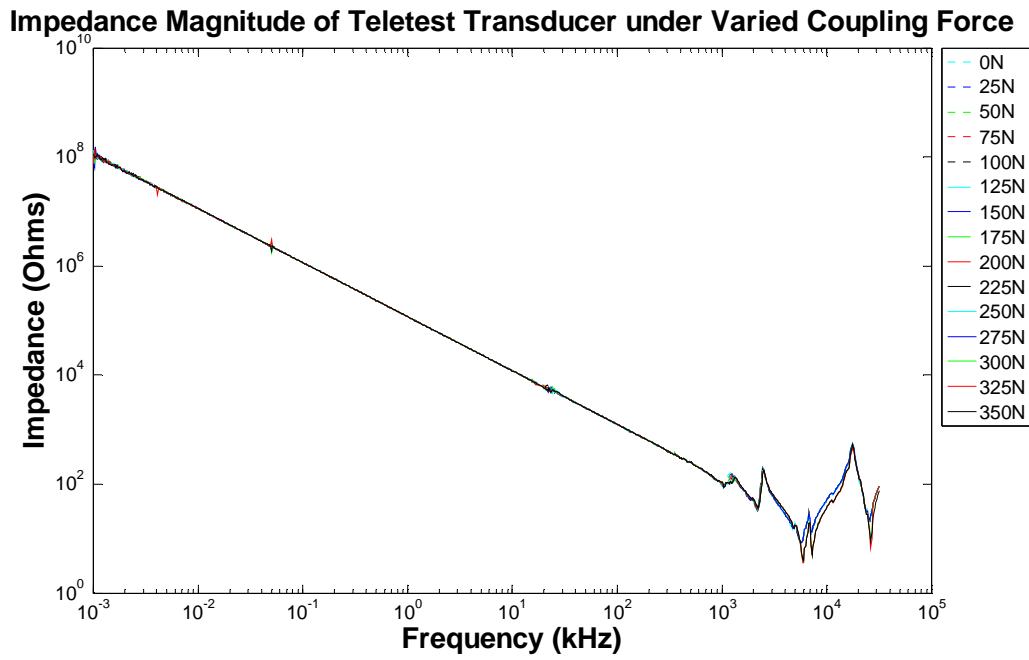


Figure F.1: Impedance Magnitude of transducer for varying loading conditions on a steel bar.

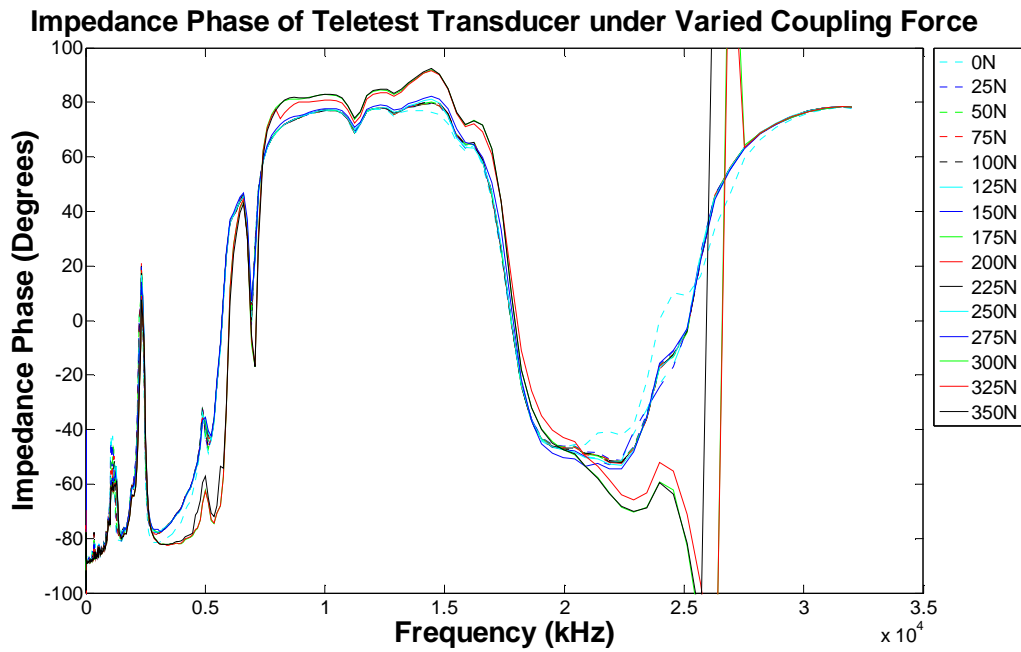


Figure F.2: Impedance Phase of transducer for varying loading conditions on a steel bar.

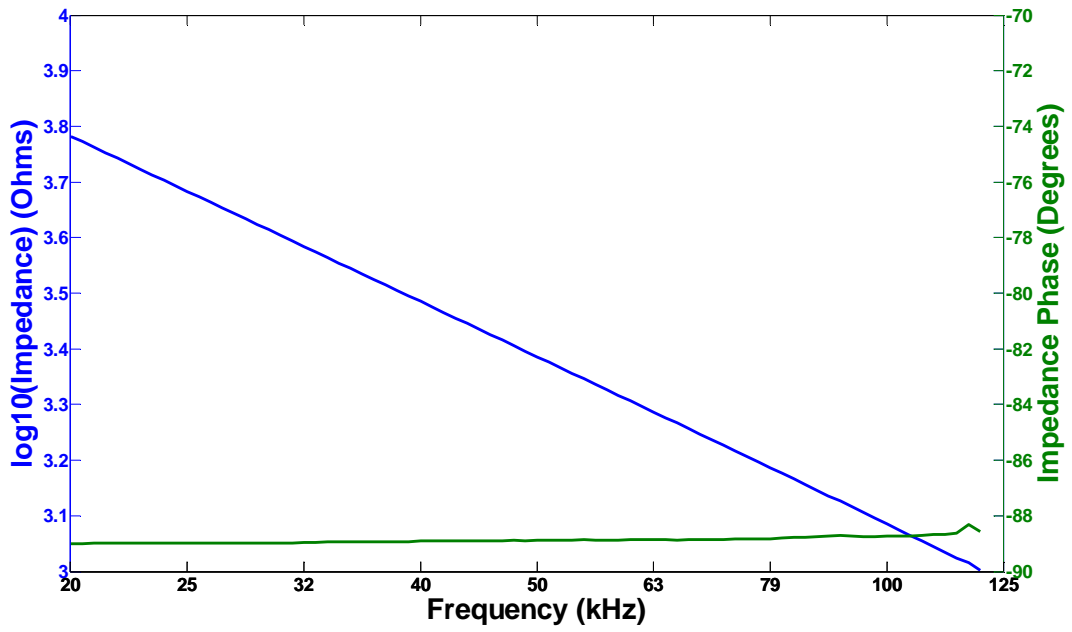


Figure F.3: Impedance characteristics of transducer under 0N load on Steel bar.

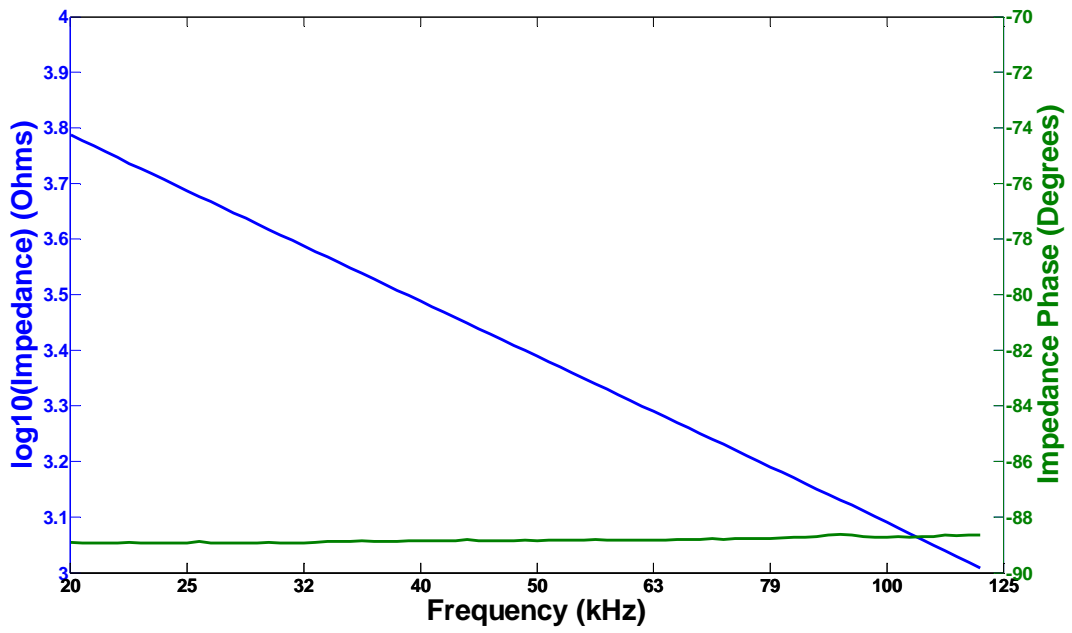


Figure F.4: Impedance characteristics of transducer under 25N load on Steel bar.

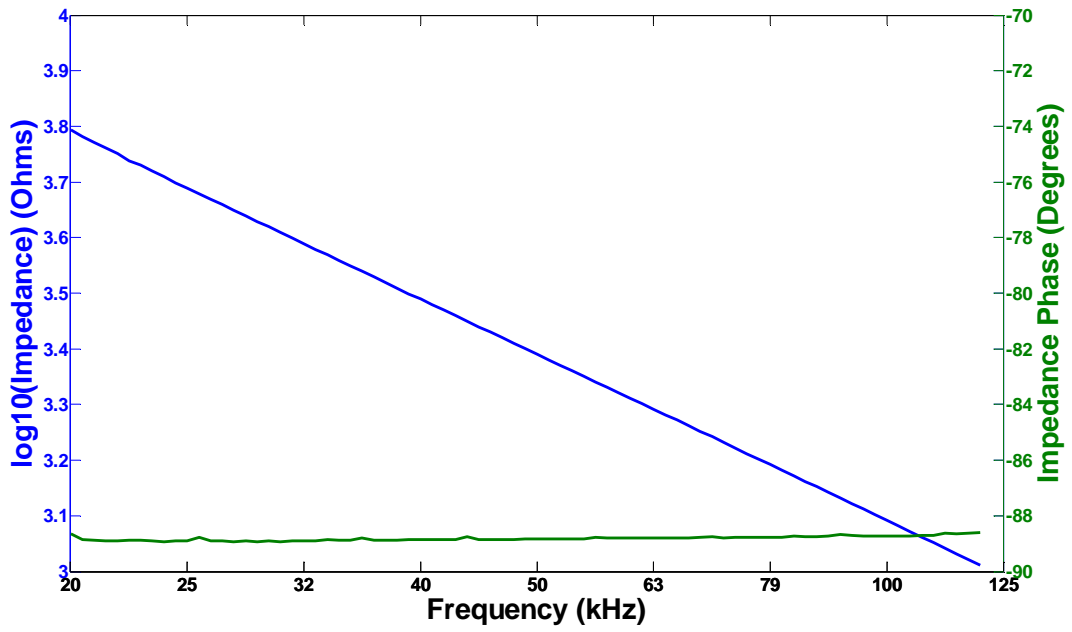


Figure F.5: Impedance characteristics of transducer under 50N load on Steel bar.

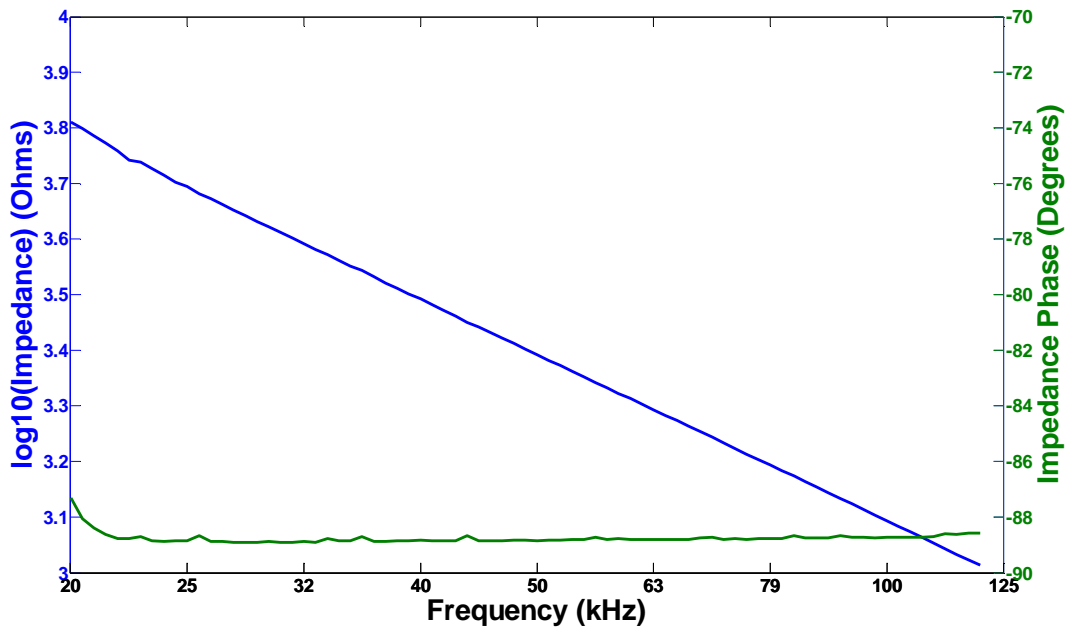


Figure F.6: Impedance characteristics of transducer under 75N load on Steel bar.

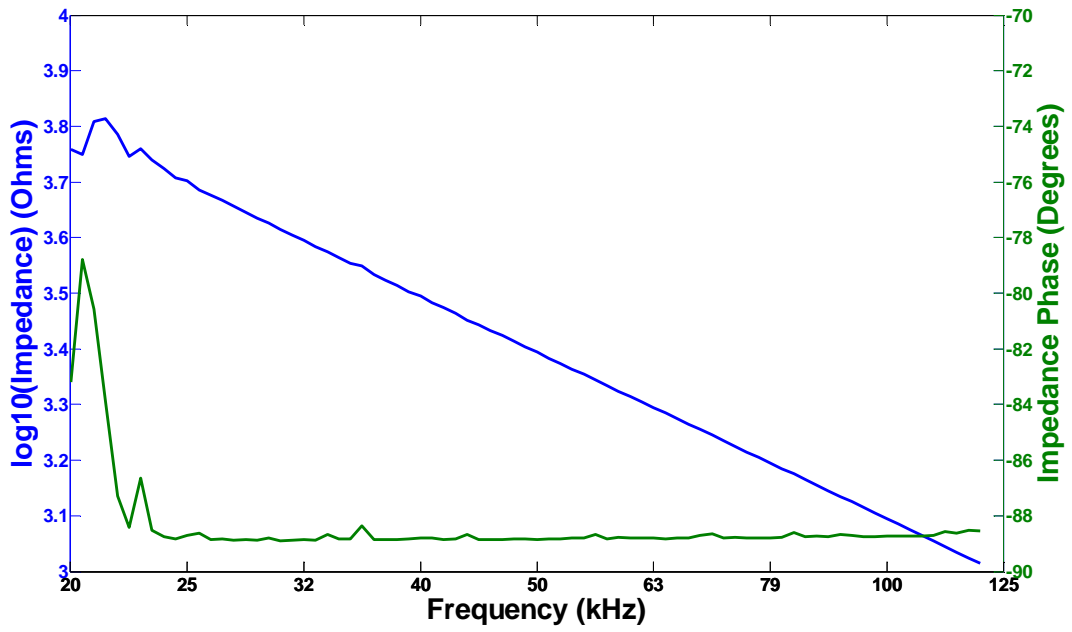


Figure F.7: Impedance characteristics of transducer under 100N load on Steel bar.

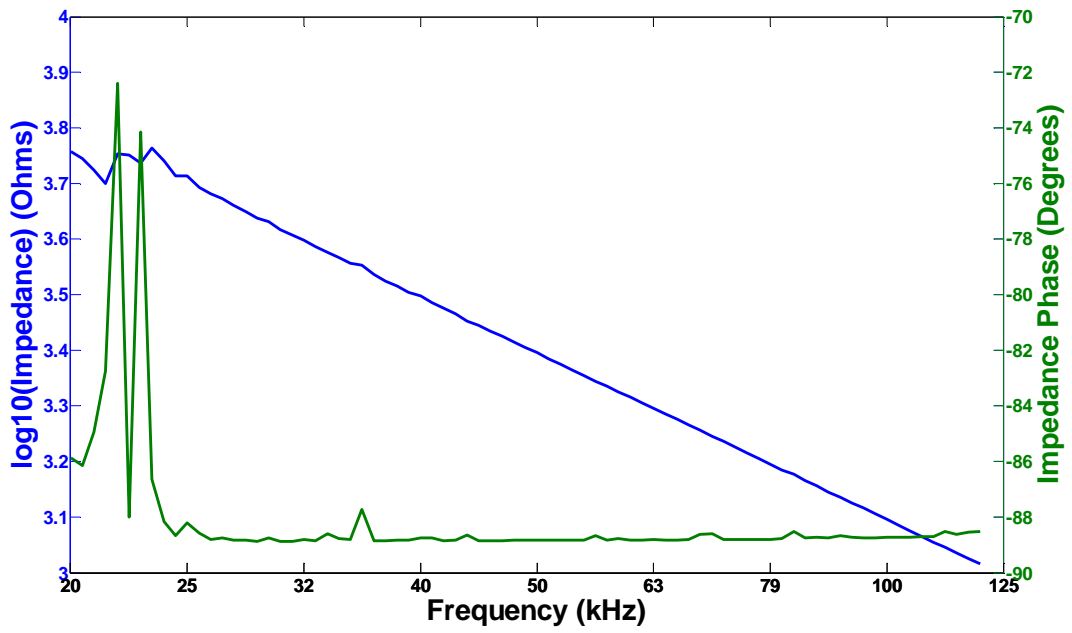


Figure F.8: Impedance characteristics of transducer under 125N load on Steel bar.

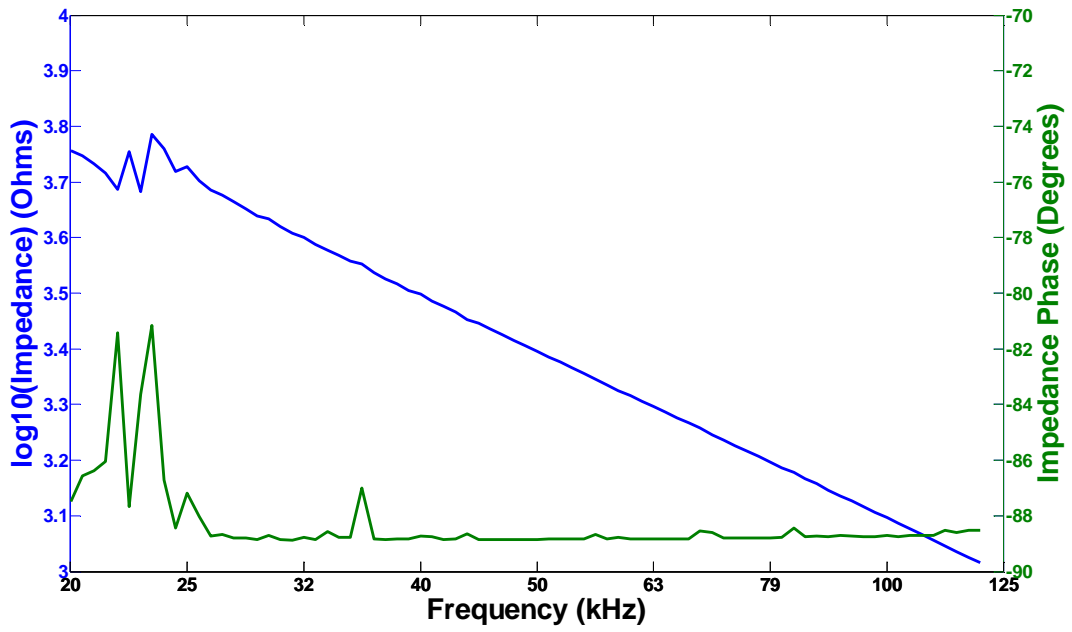


Figure F.9: Impedance characteristics of transducer under 150N load on Steel bar.

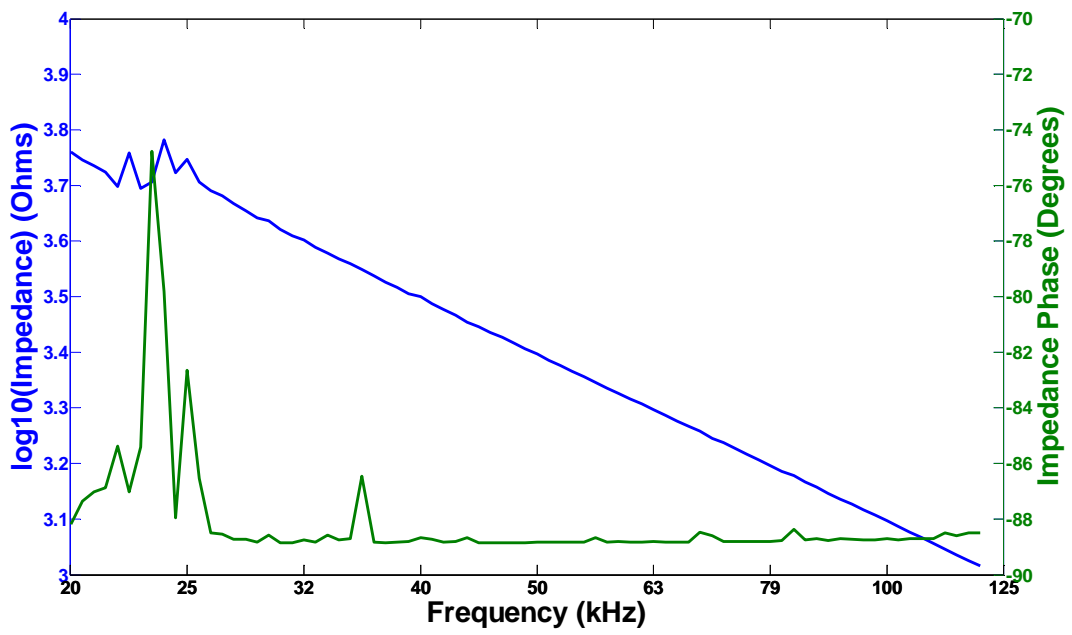


Figure F.10: Impedance characteristics of transducer under 175N load on Steel bar.

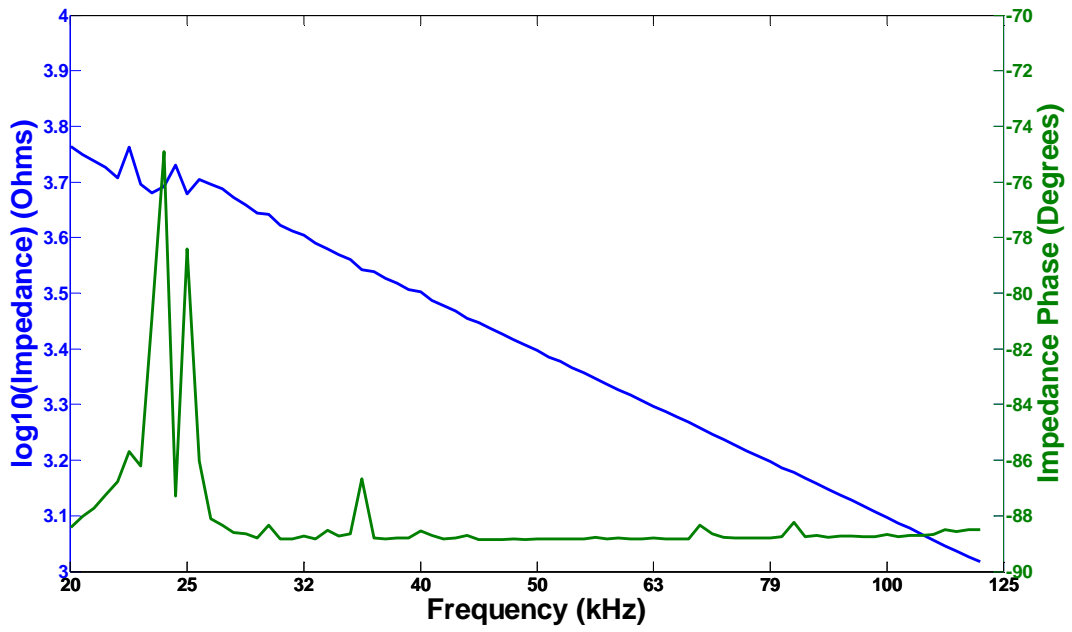


Figure F.11: Impedance characteristics of transducer under 200N load on Steel bar.

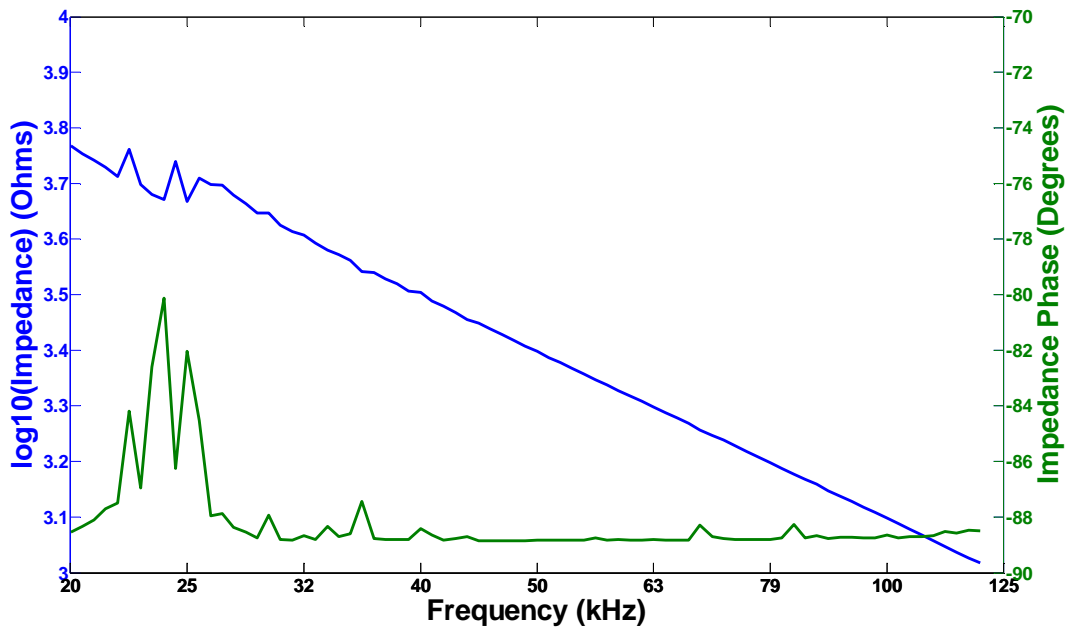


Figure F.12: Impedance characteristics of transducer under 225N load on Steel bar.

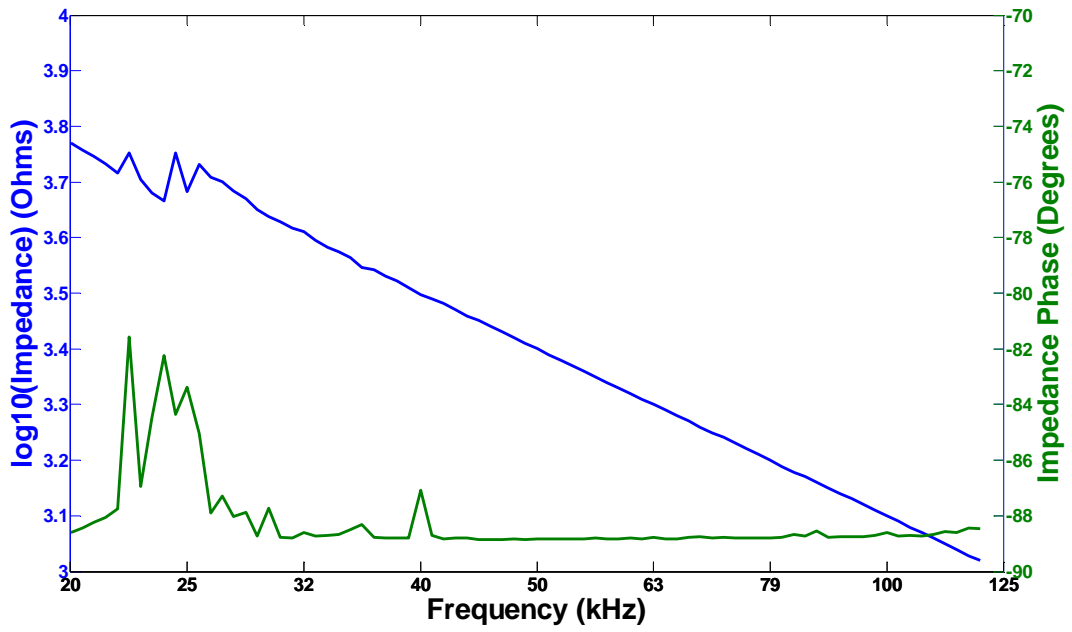


Figure F.13: Impedance characteristics of transducer under 250N load on Steel bar.

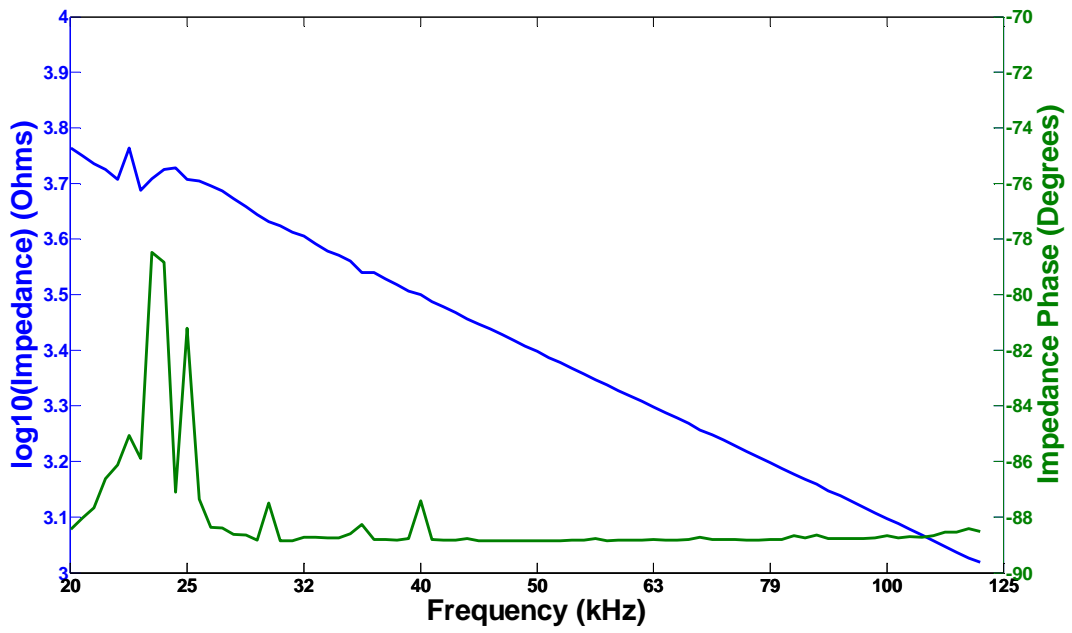


Figure F.14: Impedance characteristics of transducer under 275N load on Steel bar.

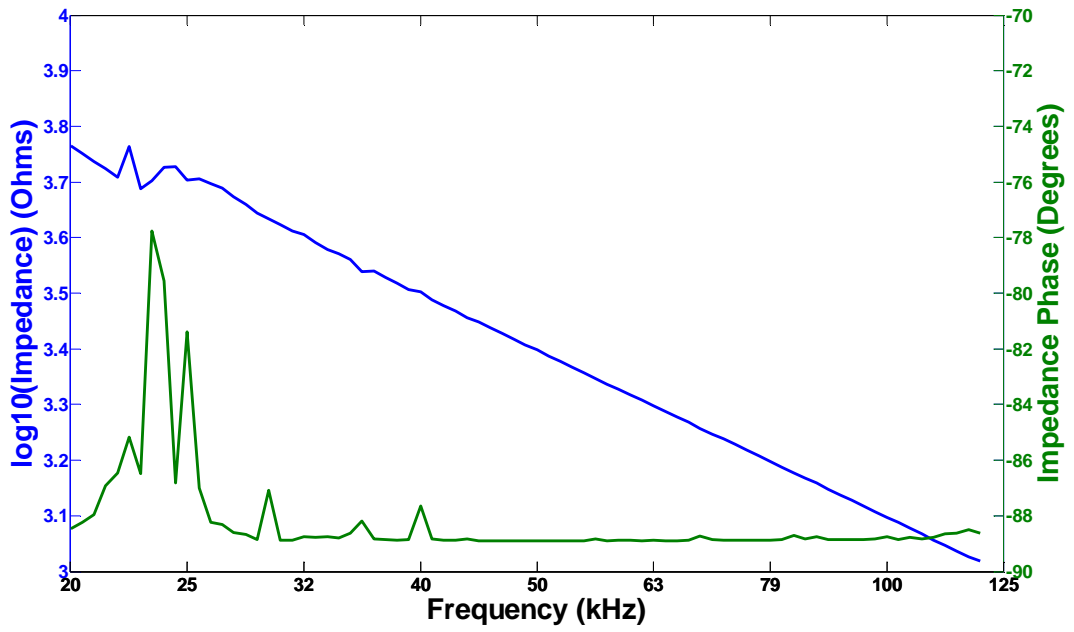


Figure F.15: Impedance characteristics of transducer under 300N load on Steel bar.

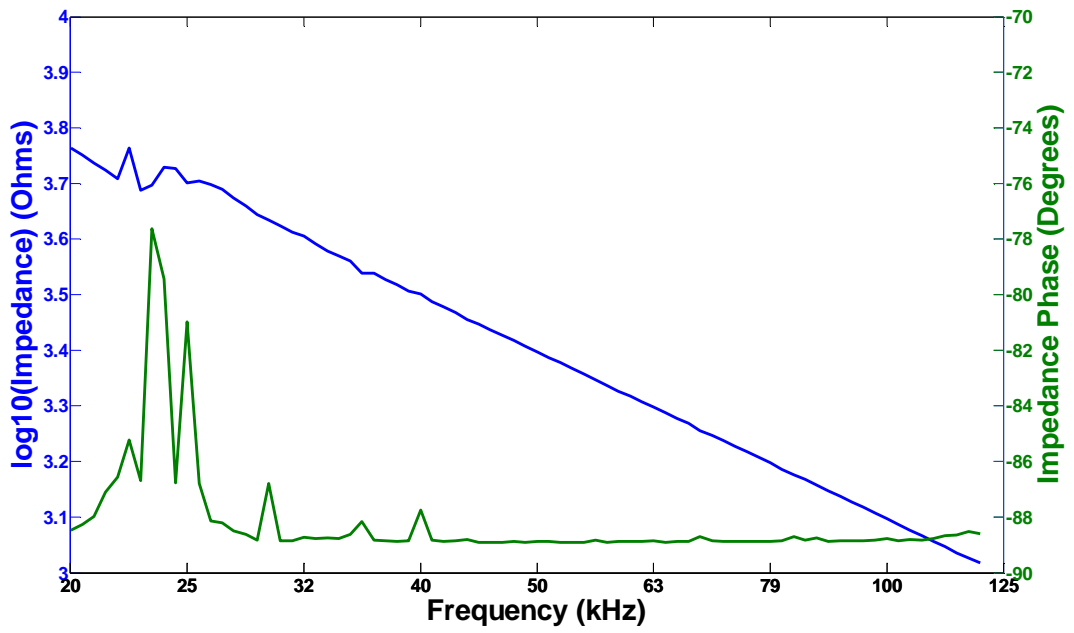


Figure F.16: Impedance characteristics of transducer under 325N load on Steel bar.

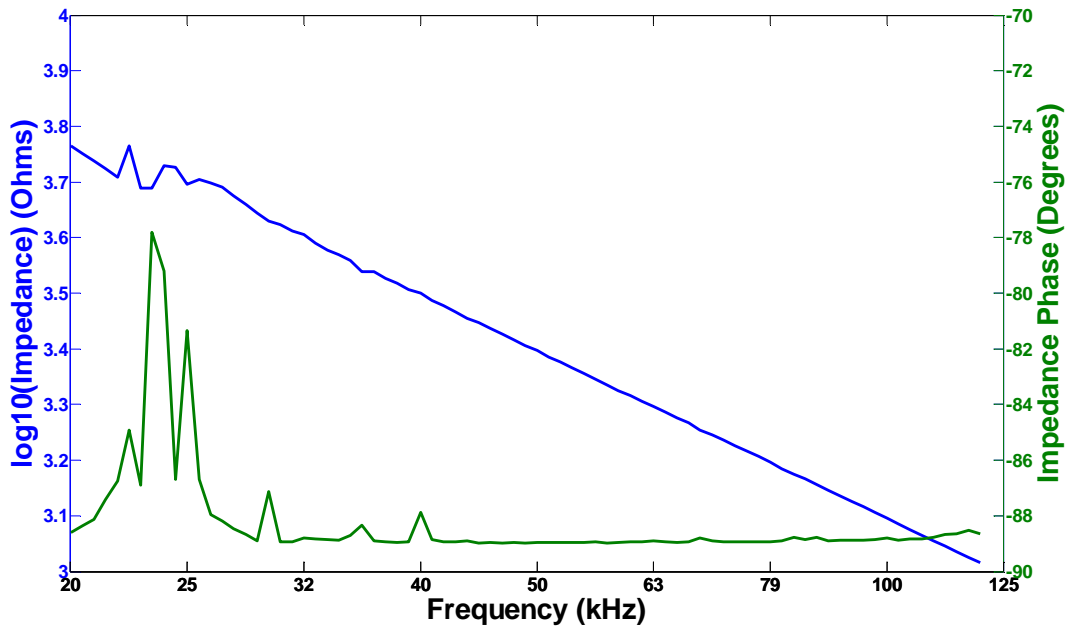


Figure F.17: Impedance characteristics of transducer under 350N load on Steel bar.

# **Appendix G – Laser Vibrometer Measurements of Mechanical Resonance in Transducer**

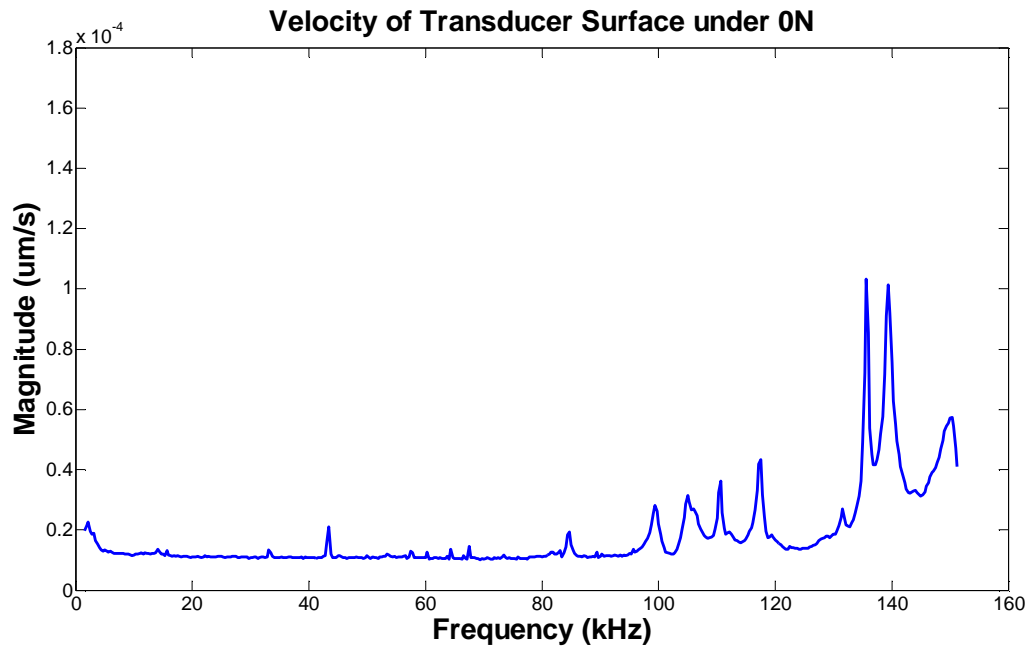


Figure G.1: Surface velocity of transducer excited within operating frequency range under 0N load.

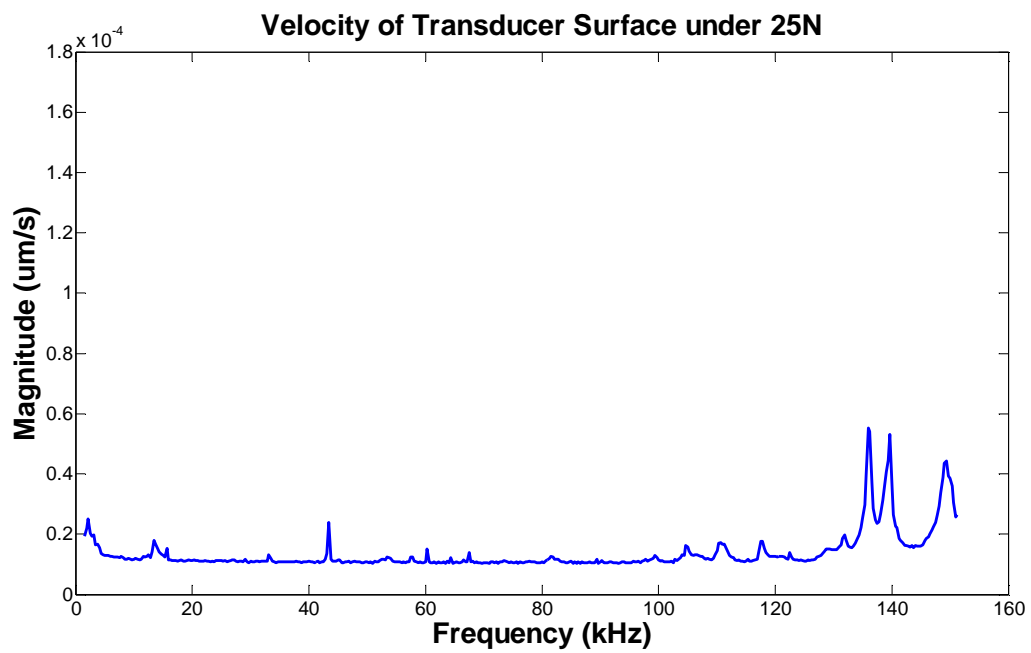


Figure G.2: Surface velocity of transducer excited within operating frequency range under 25N load.

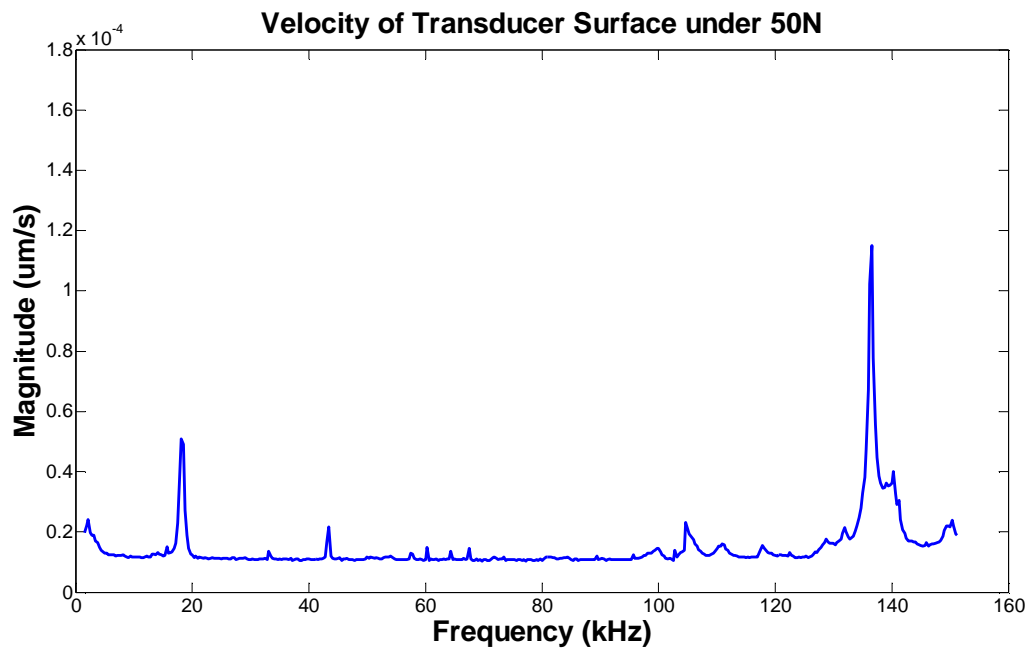


Figure G.3: Surface velocity of transducer excited within operating frequency range under 50N load.

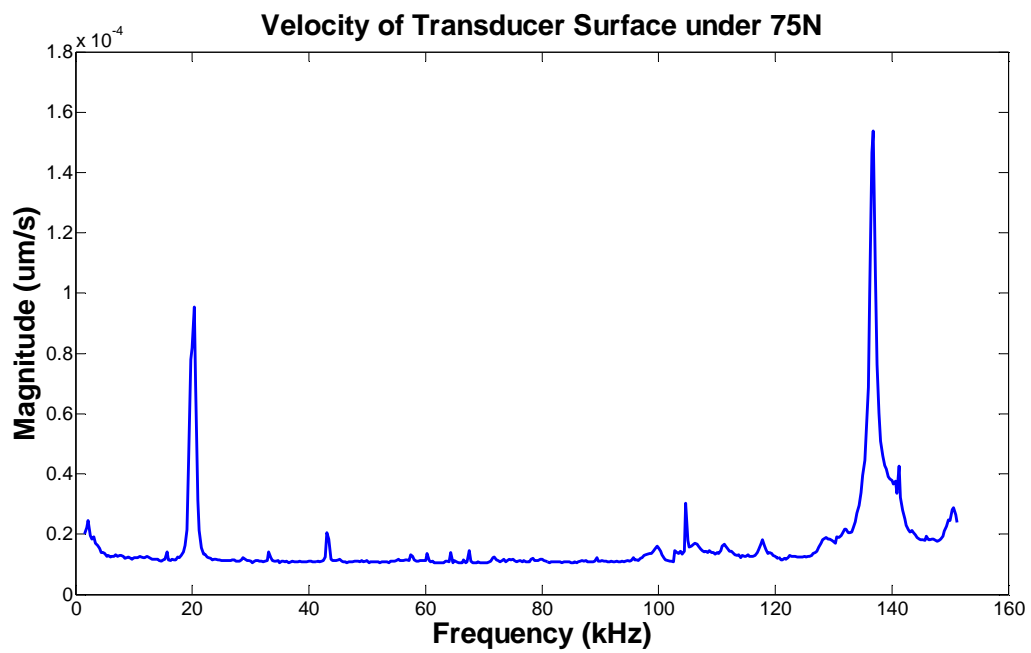


Figure G.4: Surface velocity of transducer excited within operating frequency range under 75N load.

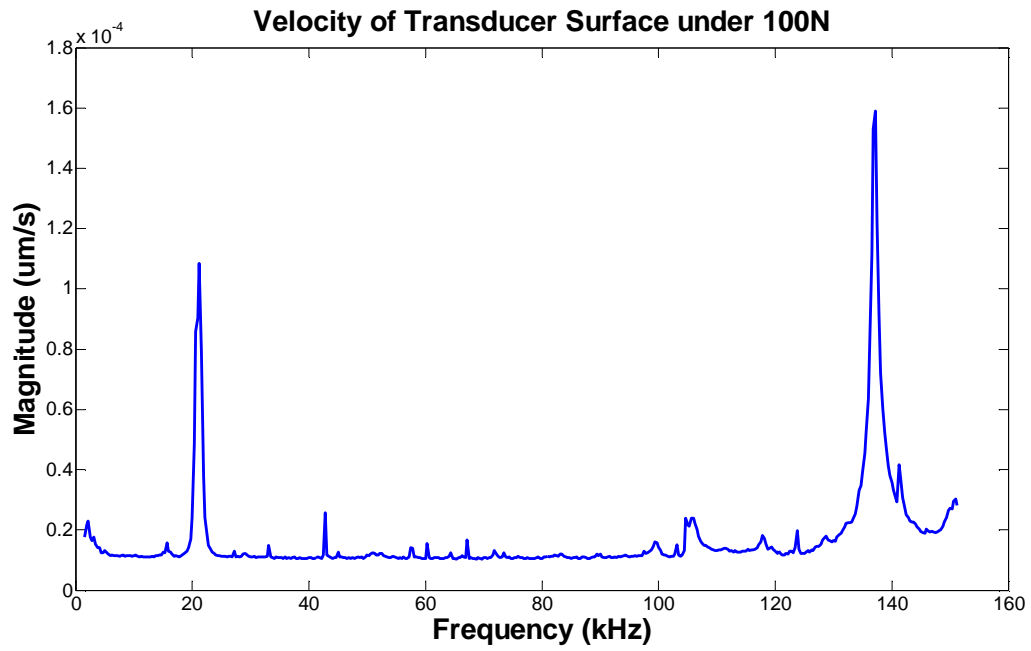


Figure G.5: Surface velocity of transducer excited within operating frequency range under 100N load.

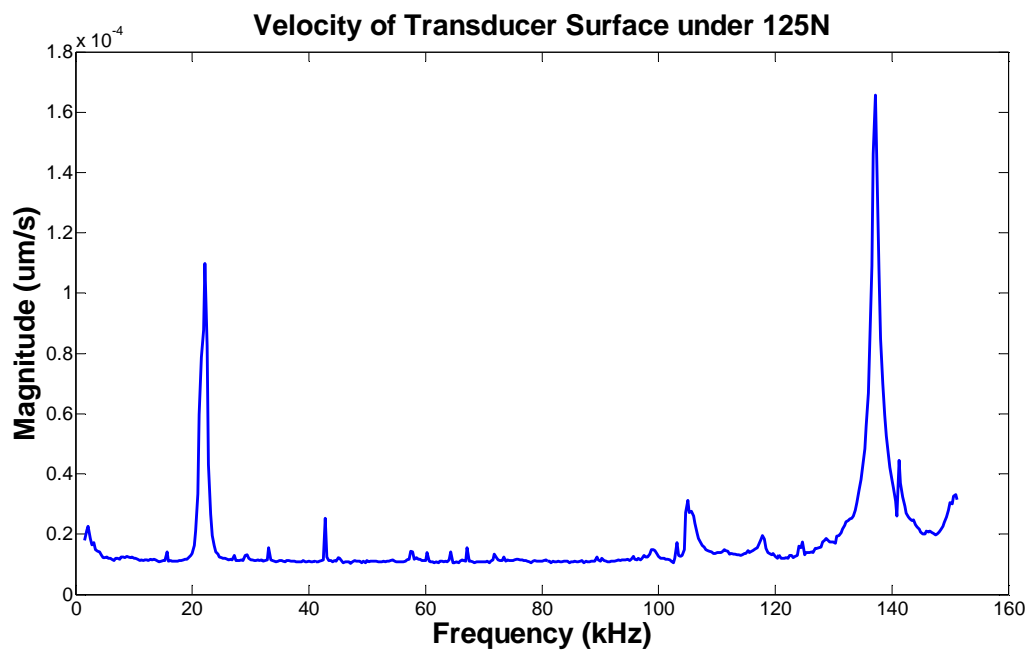


Figure G.7: Surface velocity of transducer excited within operating frequency range under 125N load.

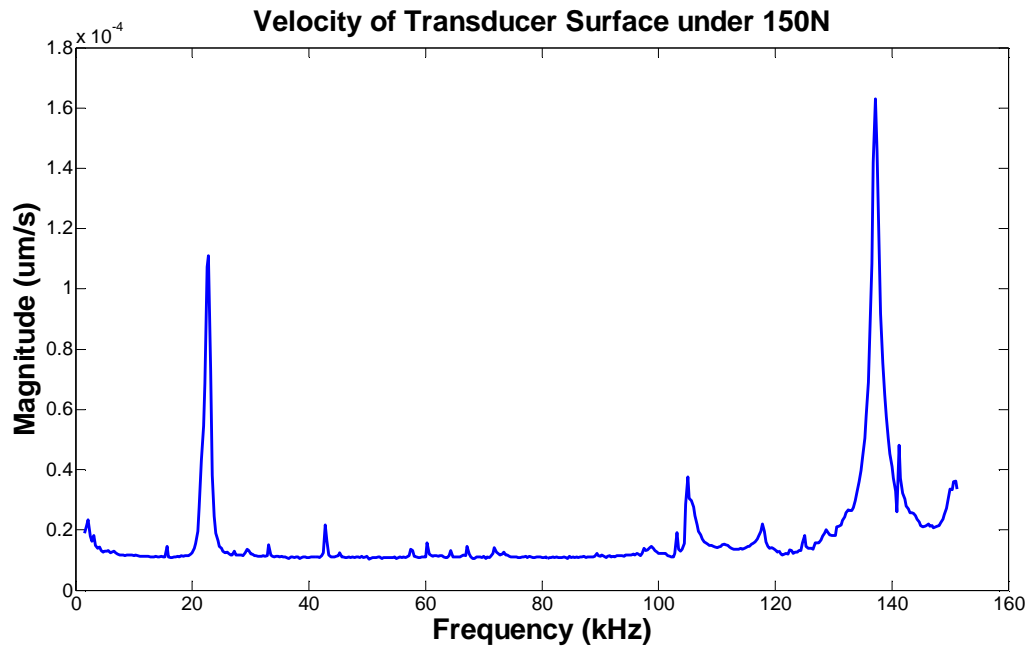


Figure G.8: Surface velocity of transducer excited within operating frequency range under 150N load.

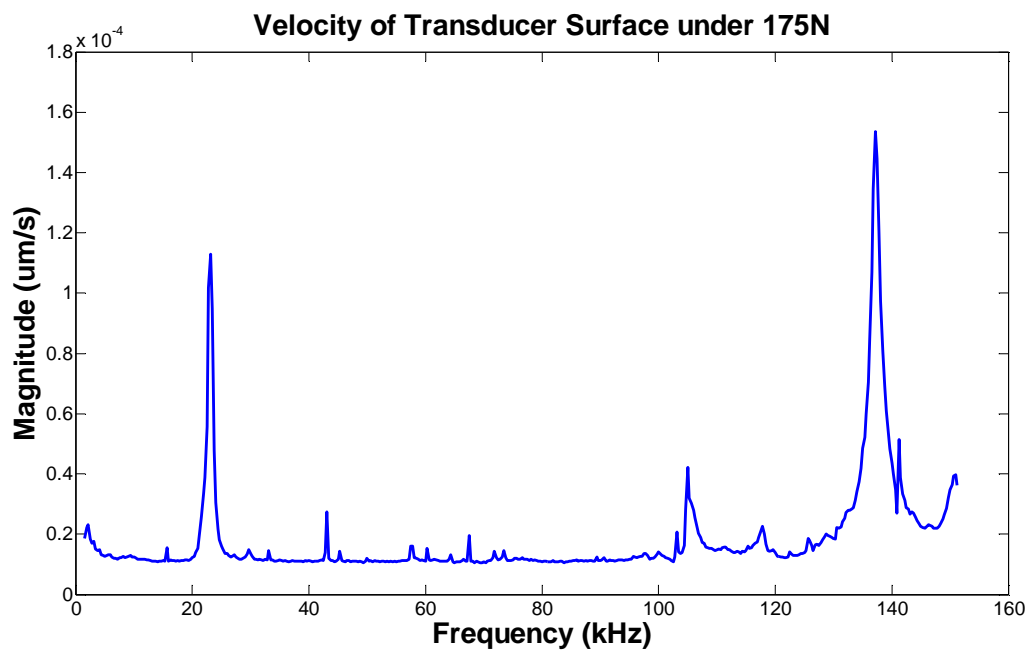


Figure G.9: Surface velocity of transducer excited within operating frequency range under 175N load.

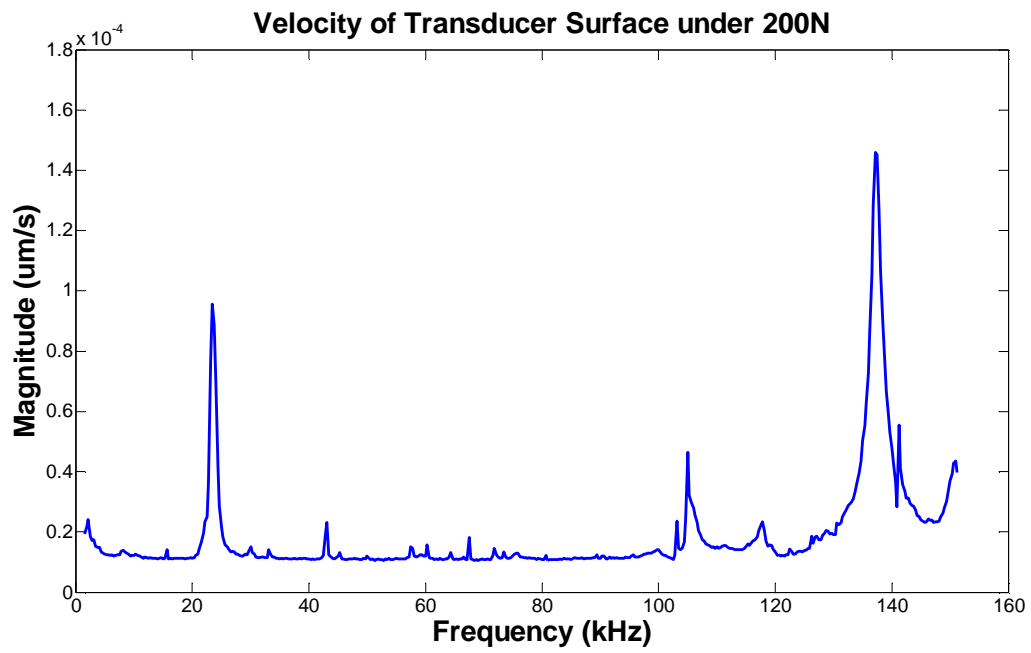


Figure G.10: Surface velocity of transducer excited within operating frequency range under 200N load.

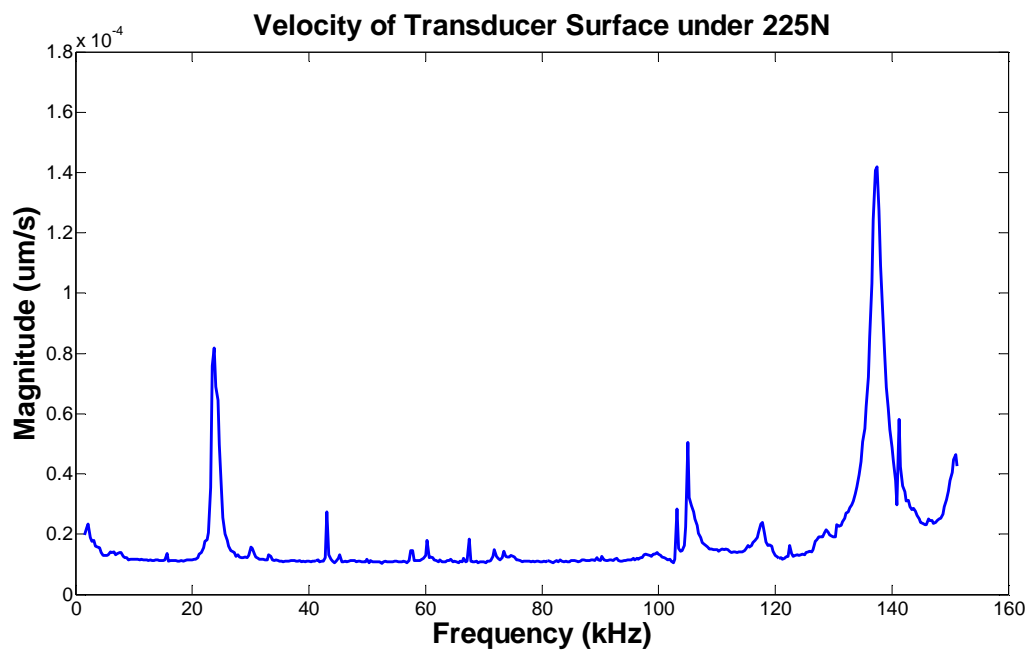


Figure G.11: Surface velocity of transducer excited within operating frequency range under 225N load.

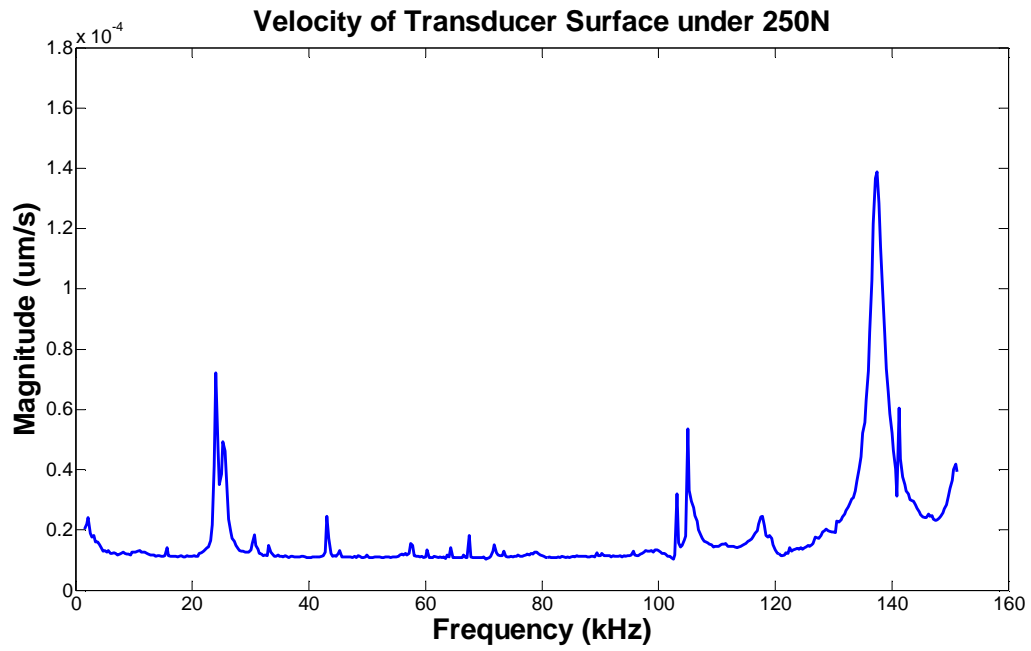


Figure G.12: Surface velocity of transducer excited within operating frequency range under 250N load.

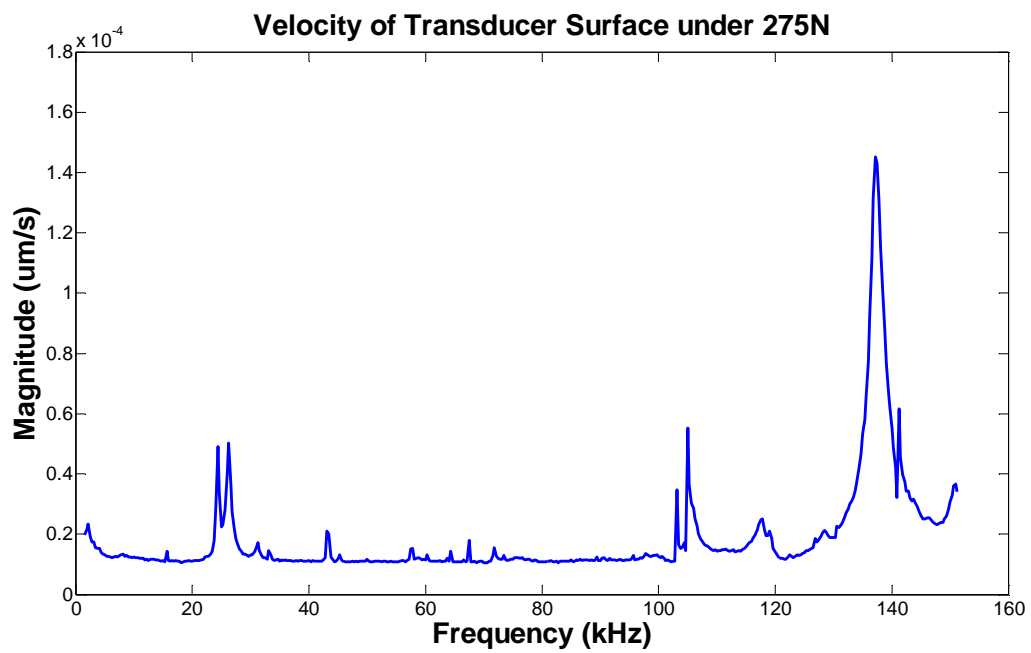


Figure G.13: Surface velocity of transducer excited within operating frequency range under 275N load.

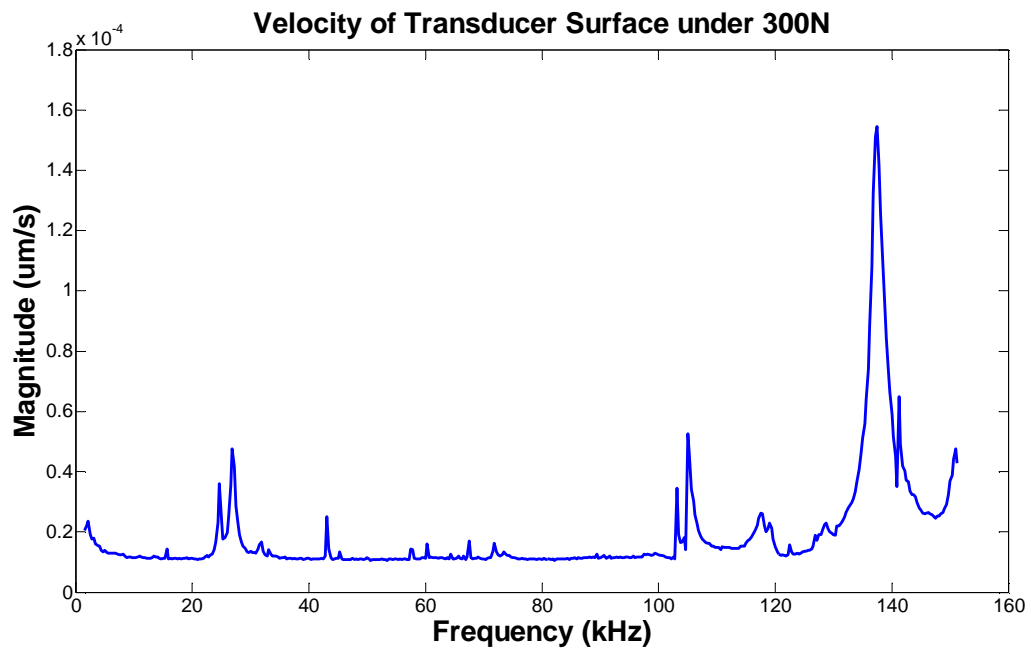


Figure G.14: Surface velocity of transducer excited within operating frequency range under 300N load.

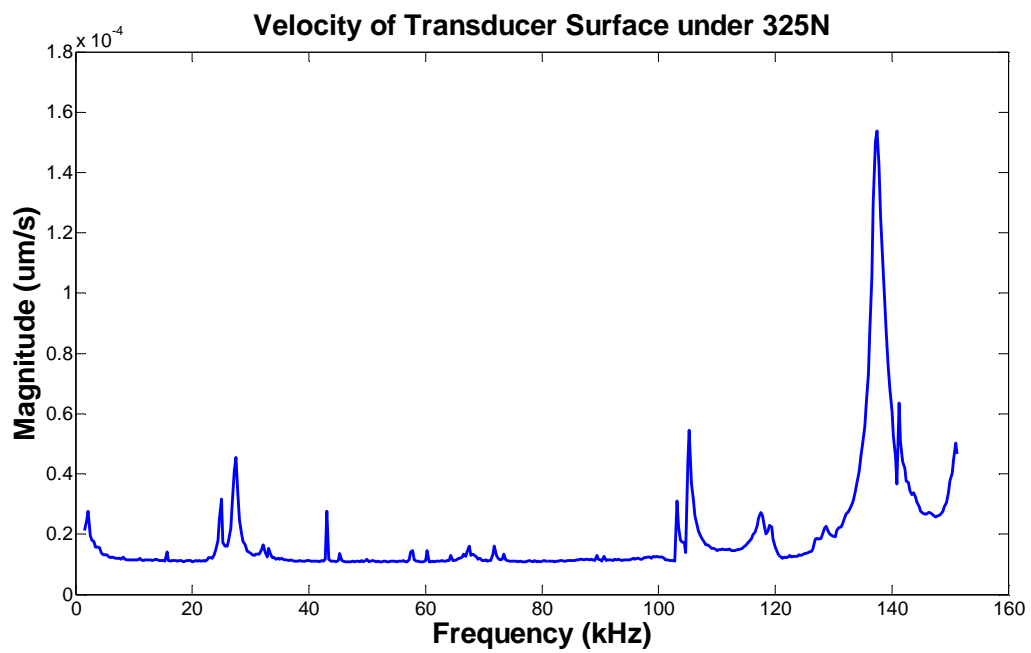


Figure G.15: Surface velocity of transducer excited within operating frequency range under 325N load.

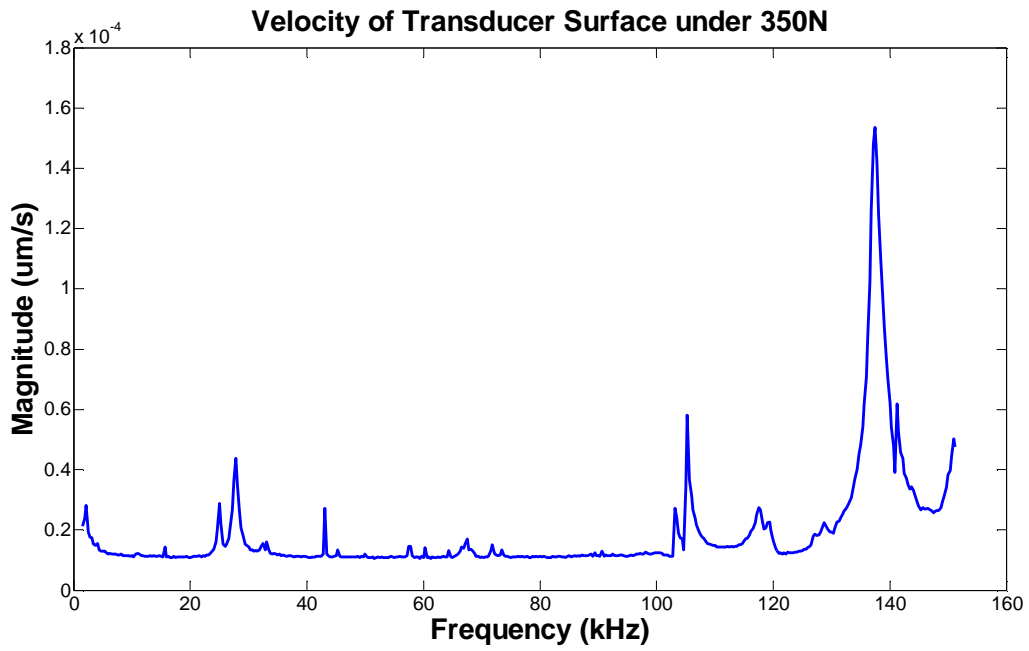


Figure G.16: Surface velocity of transducer excited within operating frequency range under 350N load.

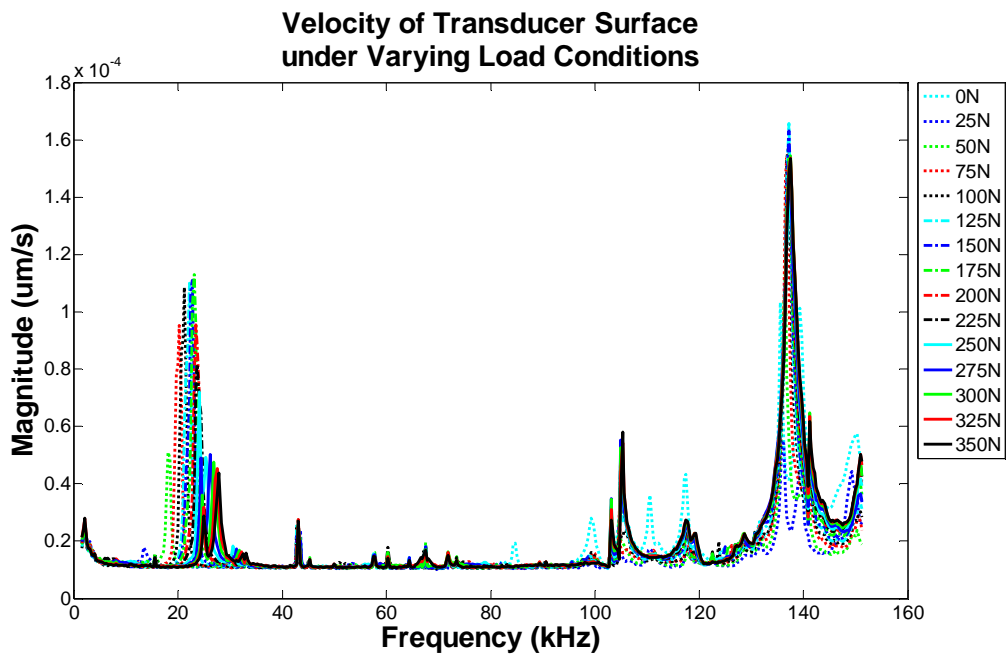
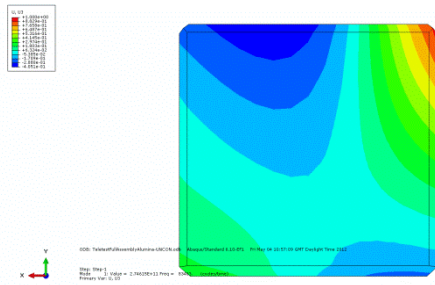
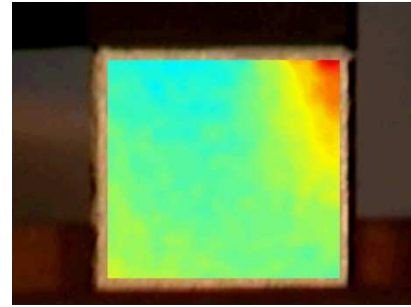


Figure G.17: Surface velocities of transducer excited within operating frequency range under varied load.

# **Appendix H – FEA Resonant Displacement Compared to Laser Vibrometer Measurement of Resonance in Transducers**

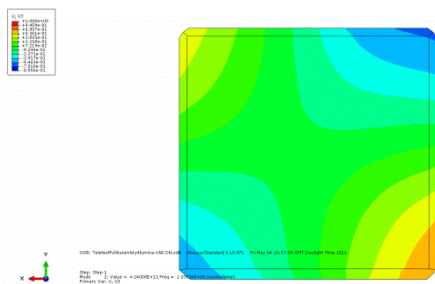


a)

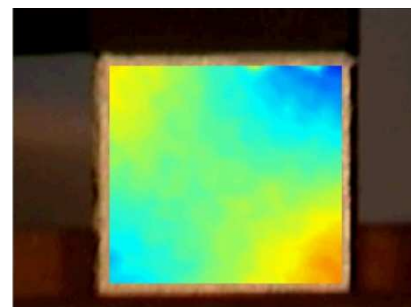


b)

**Figure H.1: Resonant displacement of transducer in free air at a) 83 kHz in FEA and b) 84 kHz by vibrometry.**

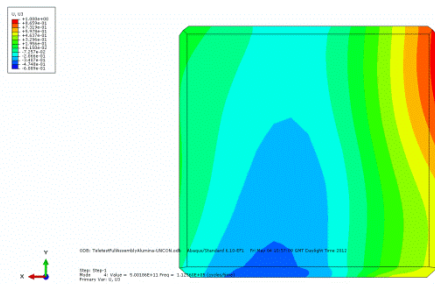


a)

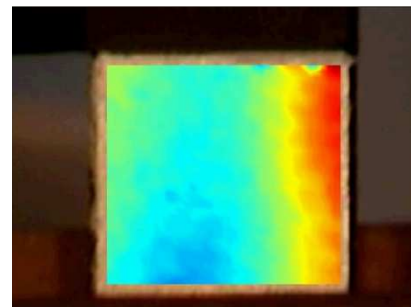


b)

**Figure H.2: Resonant displacement of transducer in free air at a) 103 kHz in FEA and b) 99 kHz by vibrometry.**

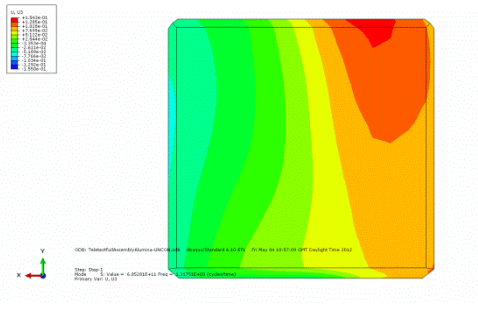


a)

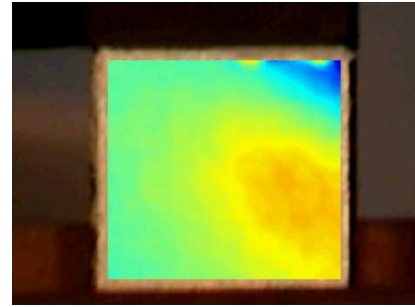


b)

**Figure H.3: Resonant displacement of transducer in free air at a) 112 kHz in FEA and b) 111 kHz by vibrometry.**

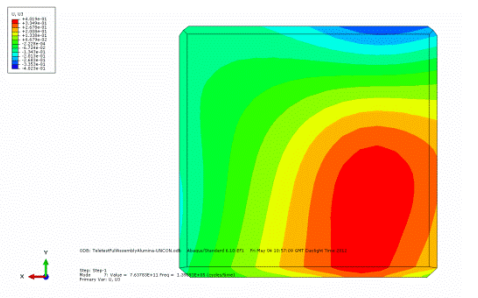


a)

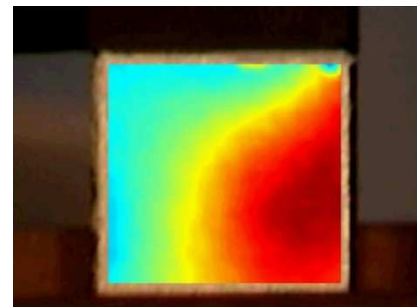


b)

**Figure H.4: Resonant displacement of transducer in free air at a) 132 kHz in FEA and b) 118 kHz by vibrometry.**

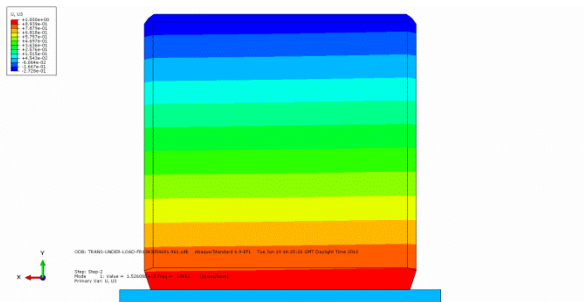


a)



b)

**Figure H.5: Resonant displacement of transducer in free air at a) 136 kHz in FEA and b) 139 kHz by vibrometry.**



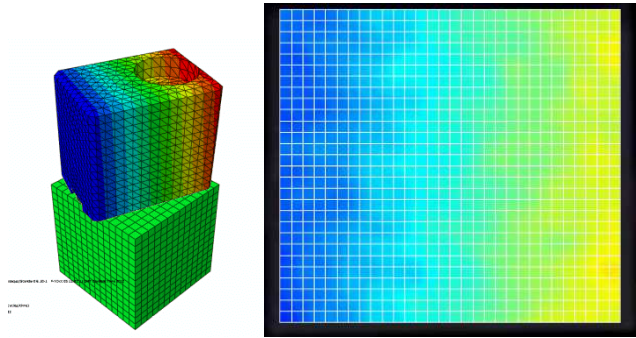
a)



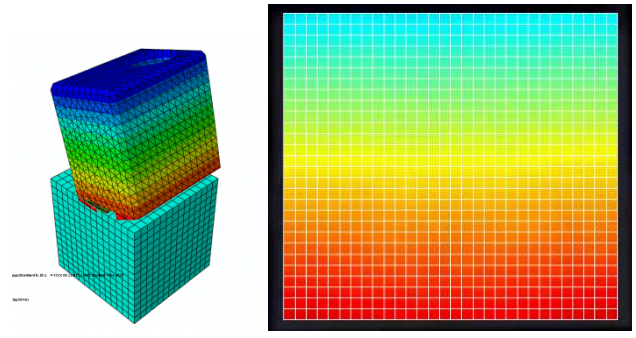
b)

**Figure H.6: Resonant displacement of transducer under 200N loading a) 19.6 kHz in FEA and b) 23 kHz by vibrometry.**

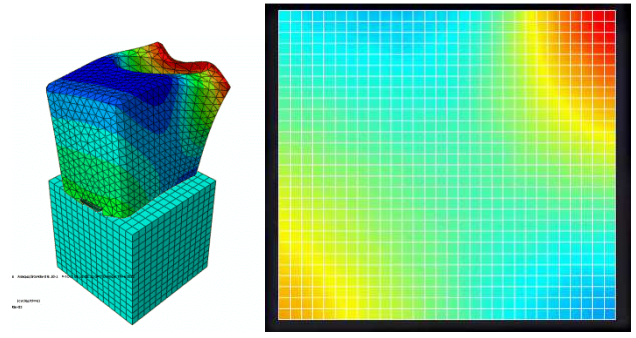




**a) Displacement in 11 kHz FEA model and measured displacement at resonance at 10 kHz**

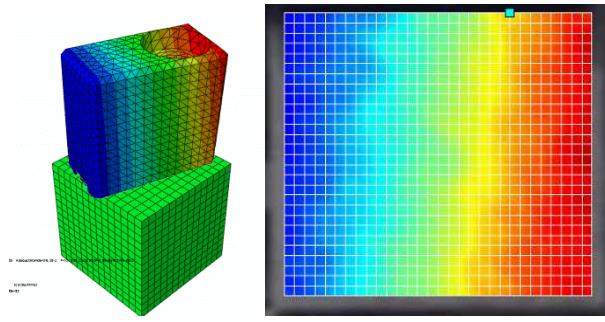


**b) Displacement in 23 kHz FEA model and measured displacement at resonance at 22.5 & 26 kHz**

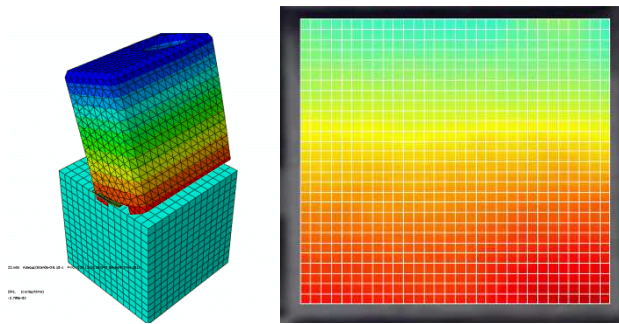


**c) Displacement in 80 kHz FEA model and measured displacement at resonance at 77 kHz**

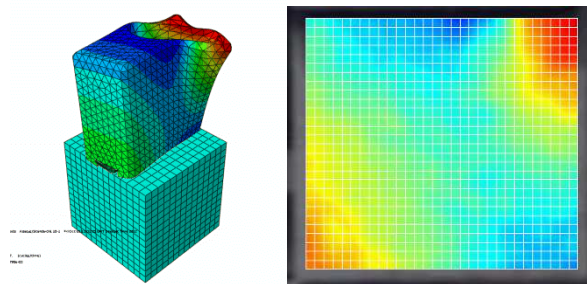
**Figure H.9: (a-c) Predicted displacements and measured displacements for transducer backing mass with 10mm width.**



a) Displacement in 14 kHz FEA model and measured displacement at resonance at 15 kHz

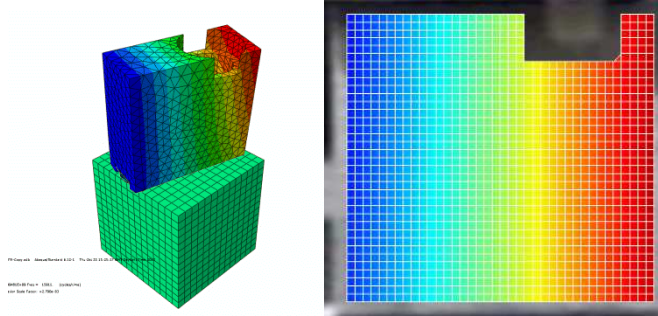


b) Displacement in 28.5 kHz FEA model and measured displacement at resonance at 24.5, 30.5, 34.5, 37.5 & 41 kHz.

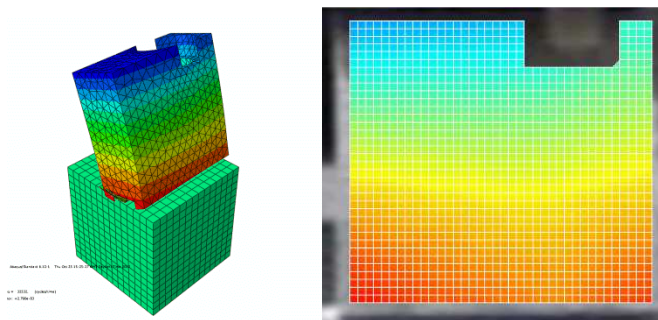


c) Displacement in 69 kHz FEA model and measured displacement at resonance at 63 & 69 kHz.

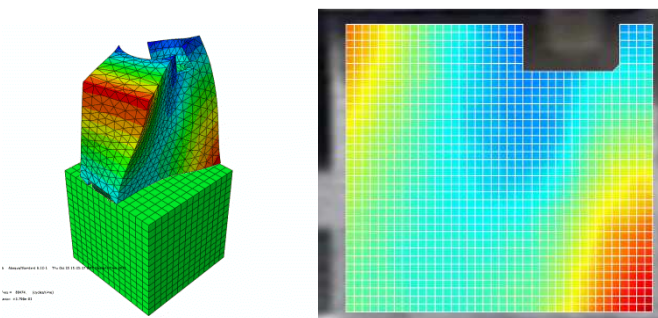
Figure H.10: (a-c) Predicted displacements and measured displacements for transducer backing mass with 7.5mm width.



**a) Displacement in 16 kHz FEA model and measured displacement at resonance at 16.5 kHz**



**b) Displacement in 32.5 kHz FEA model and measured displacement at resonance at 22, 24, 31 & 35 kHz**



**c) Displacement in 80 kHz FEA model and measure displacement at resonance at 58.5, 61.5, 76 & 87.5 kHz**

**Figure H.11: (a-c) Predicted displacements and measured displacements for transducer backing mass with 6mm width.**